Dissertation zur Erlangung des Doktorgrades der Naturwissenschaften

an der Fakultät für Geowissenschaften

der Ludwig-Maximilians-Universität München

Young tectonic evolution of the Northern Alpine Foreland Basin, southern Germany, based on linking geomorphology and structural geology

Markus Hoffmann

München, 15. März 2017

1. Gutachterin: Prof. Dr. Anke M. Friedrich

2. Gutachterin: Prof. Dr. Miriam Dühnforth

Tag der mündlichen Prüfung: 24. Juli 2017

Für

Horst† und Irene

Brick walls are there for a reason.

The brick walls are not there to keep us out,

they let us prove how badly we want something.

(Randy Pausch, 2012)

TABLE OF CONTENTS

List of Figures

List of Tables

Abstract

The Northern Alpine Foreland Basin (NAFB) formed as a result of alpine continental collision in Oligocene time. Tectonic shortening has been slow since the Miocene, implying that the NAFB subsidence has come to rest. The scope of this thesis is to find evidence that yield information regarding the recent vertical tectonic activity and a potentially ongoing basin inversion.

The identification of such an active inversion can be accomplished by studying the landscape evolution. This is possible, because the earth's surface contains information about tectonic and erosional processes. In order to understand and quantify the underlying mechanisms forming the landscape, both surface and subsurface information can be linked. Especially when geophysical or similar data are insufficient, geomorphological analyses provide new insights.

The NAFB is a low-strain sedimentary basin, where historic subsurface data confirm subsidence, while the present-day erosional relief indicates uplift. The basin has a long prospection history and geometries of basement faults are well known, but their link to topography is ambiguous and the landscape is regarded as climatically controlled. In this context, dense population and energy exploration call for a fundamental understanding, if the basin is uplifting and whether or not faults could potentially be reactivated.

This thesis aims at characterizing geomorphotectonic indicators of uplift, potentially indicating NAFB inversion. Related to this process, vertical motion of a few hundred meters to a few kilometers is expected to have been taking place during the Plio-Pleistocene. My study addresses the Quaternary geomorphology and distribution of sediments across the NAFB. To assess a potential link between asymmetric valleys and underlying basement faults in the NE portion of the basin (Tertiary Hills region), I analyzed high-resolution space-borne imagery and carried out geologic fieldwork.

Results in distinct geomorphological response of the NAFB are (a) regional scale erosion of sediments, (b) fluvial incision, (c) reactivation of documented faults and (d) regional scale tilting of paleo-geodetic markers.

In the NE portion of the NAFB, the geometry of a detected high-angle geologic subsurface contact associated with a surface escarpment, potentially originated from young surface faulting, while landscape morphology is intensely overprinted by climatic processes and anthropogenic land use.

The investigation of mid-Miocene coastal features of the Swabian Alb cliff line addresses the landscape evolution along the marginal area of the NAFB. The particular questions here are, if coastal outcrops are part of the same coast, and which mechanisms have caused their different present-day elevations. I investigated marine features in a geologic field survey and compiled stratigraphic data to infer the regional response to uplift. The results show that two sites represent temporally and spatially different coastal sections, and both have been intensely modified by multiple erosional processes. The data can be explained by invoking a combination of surface erosion and possible lithospheric scale uplift.

My study of well data and geomorphic markers, to infer NAFB Quaternary sediment budgets, yields a remarkable erosion of sediments along the central E-W basin axis and fluvial networks in disequilibrium. I examined erosion rates across different timescales, using sediment yields from NAFB catchments and basin sediment flux. On the Pleistocene timescale, geomorphic indicators of fluvial systems are investigated while for the Holocene, archeological data provide constraints on local erosion. The results of this study reveal a distinct oval-shaped erosion pattern across the NAFB, which can explain the modern erosional relief of the region, and further implies active inversion of the basin. Similar results are derived from drainage pattern and river steepness estimates.

The results of this thesis imply that the Quaternary landscape in the NAFB has been significantly influenced by tectonic activity. Further, the timing for the NAFB transition from subsidence to uplift is likely to originate at the Pliocene – Quaternary boundary, and continues. Therefore, the possibility of future fault reactivation, controlled by lithospheric scale uplift, cannot be ruled out.

Zusammenfassung

Das nördliche Alpenvorlandbecken (engl. abg. NAFB) entstand während des Oligozän durch die Kontinent-Kontinent Kollision der Alpen. Die Konvergenz dieser Region ist seit dem Miozän relativ gering. Dies deutet auf ein Ende der Beckensubsidenz hin. Der Zweck dieser Dissertation ist daher, neue Beweise für eine tektonisch bedingte, aktive, vertikale Deformation der Region zu finden. Außerdem soll eine mögliche Inversion des Vorlandbeckens untersucht werden.

Die Inversion eines Sedimentbeckens kann durch eine systematische Landschaftsanalyse untersucht werden. Diese Herangehensweise ist besonders geeignet, da die Erdoberfläche wichtige Informationen über Erosion und Tektonik enthält. Um die landschaftsformenden Mechanismen zu verstehen und zu quantifizieren, können Oberflächendaten mit Untergrunddaten verknüpft werden. Besonders im Falle unzureichender, geophysikalischer Daten können geomorphologische Studien diese Datenlücke füllen.

Das nördliche Alpenvorlandbecken repräsentiert ein Sedimentbecken mit geringer Deformationsrate. Vorhandene Untergrunddaten zeigen ein Absenkung; jedoch deutet die rezente Oberfläche mit ihrem erosiven Relief auf eine Hebung des Beckens hin. Da sich die Region durch eine lange Historie industrieller Prospektion und Exploration auszeichnet, ist eine große Zahl von Störungen im Grundgebirge des Beckens bekannt. Dennoch ist ein Zusammenhang dieser Störungen mit der heutigen Topographie ungeklärt und die Landschaftsentwicklung wird rein klimatischen Prozessen zugeschrieben. Es gilt jedoch auf Grund der dichten Besiedlung und der rezenten Exploration von Energiequellen und Rohstoffen in der Region zu klären, ob die vorhandenen Störungen durch eine Hebung des Beckens reaktiviert werden können und ob dies bereits während des Quartär der Fall war.

Das Ziel dieser Arbeit ist, tektonisch-geomorphologische Indikatoren, die auf eine potentielle Hebung bzw. Inversion des Vorlandbeckens hindeuten, zu bestimmen und zu untersuchen. Im Zusammenhang mit diesem Prozess ist eine Hebung von einigen hundert Metern bis hin zu einigen Kilometern zu erwarten. In meiner Arbeit werden u.a. die Geomorphologie und Verteilung quartärer Sedimente untersucht. Dabei analysiere ich den möglichen Zusammenhang zwischen asymmetrischen Tälern und Störungen im darunterliegenden Grundgebirge im nordöstlichen Vorlandbecken (Tertiäres Hügelland). Zu diesem Zweck habe ich hochauflösende, digitale

Satellitendaten untersucht und geologische Geländearbeiten durchgeführt. Die Ergebnisse zeigen, bezogen auf die geomorphologischen Prozesse, (a) regionale Erosion von Sedimenten, (b) lokal erhöhte Einschneidung von Flüssen, (c) Reaktivierung von Störungssystemen und (d) eine regionale Verkippung von paläogeodätischen Indikatoren.

Im nordöstlichen Teil des Beckens wurde ein geometrischer Zusammenhang zwischen einem geologischen Kontakt im Untergrund und einer Oberflächenstufe festgestellt. Dies deutet auf aktive Tektonik als Ursache hin, während die umgebende Landschaft zusätzlich durch klimatische und anthropogene Prozesse überprägt ist.

Die geologischen Prozesse am Rand des alpinen Vorlandbeckens wurden anhand von Küstenmarkern entlang der berühmten Klifflinie auf der Schwäbischen Alb untersucht. Die hier zu klärende Frage ist, ob die Aufschlüsse von mariner Fazies ein Bestandteil derselben Küste sind und wodurch die heutige Höhenlage der ehem. Küstenlinie kontrolliert wird.

Um eine mögliche Verbindung zu regionaler Hebung zu testen, habe ich Aufschlüsse mariner Fazies und lokale stratigraphische Zusammenhänge untersucht. Meine Ergebnisse zeigen dabei, dass die untersuchten Aufschlüsse sowohl zeitlich, als auch räumlich unterschiedliche Küstenpositionen darstellen. Außerdem wurden die Bereiche beider Aufschlüsse durch verschiedene Erosionsprozesse intensiv überprägt. Darüber hinaus sind in der Region Anzeichen für eine weiträumige Hebung zu erkennen, die möglicherweise durch einen Prozess auf der Lithosphärenskala kontrolliert wird.

Meine Untersuchungen quartärer Sedimentmengen und geomorphologischer Indikatoren im nördlichen Alpenvorlandbecken zeigen eine verstärkte Erosion der jungen Einheiten. Zudem offenbaren fluviatile Systeme der Region asymmetrische Drainagenetzwerke und übersteile Flussbett-Segmente. Die Analyse erfolgt auf Basis von Bohrdaten und prozess-geomorphologischen Analysen digitaler Höhenmodelle.

Die Erosion folgt dabei einem Ost – West orientierten Korridor durch das zentrale Becken. Die gestörten Flussnetzwerke befinden sich hauptsächlich im nordöstlichen Teil des Beckens. Ferner untersuche ich Erosionsraten über verschiedene Zeitskalen, basierend auf Sedimentations- und Transportraten der angrenzenden Einzugsgebiete. Für die Analyse pleistozäner Raten nutze ich geomorphologische Indikatoren von Flüssen. Die holozänen Raten basieren auf archeologischen Daten.

Anhand der Ergebnisse der Erosions- und Geomorphologiestudien kann hier erstmalig gezeigt werden, dass junge Erosionsmuster im gesamten Alpenvorlandbecken durch tektonische Aktivität und die Inversion des Beckens verursacht werden.
Die Ergebnisse meiner Dissertation implizieren außerdem, dass der Übergang des Beckens von Absenkung zu Hebung etwa an der Grenze Pleistozän – Quartär erfolgt ist und die Inversion auch weiterhin aktiv ist. Daher kann eine Reaktivierung von Störungssystemen nicht ausgeschlossen werden.

Acknowledgements

A long way has come to an end and it turns out, this is just the beginning. As many researchers did before when writing these final lines of their theses, I can say to have accomplished this milestone simply feels incredibly great. And now is the time to start something new. However, first I want to express my gratitude to a large number of people who travelled with me on this journey over the last years and made this time so valuable, intense and memorable to me.

First of all I like to thank my advisor Anke Friedrich for her strong support, inspiration and critics over the years. Thank you for providing the frame in which I learned to develop my own ideas and giving me the freedom and confidence to pursue those ideas to profundity. Your exhaustless motivation and expertise infected me with an enthusiasm for research problems already in my undergraduate times. I still remember the first chat we had in your office in Hannover and here we are now. Thank you also for the exceptional opportunity to work as the science coordinator at the chair of geology during the last three years. That was a unique experience and enabled me to further discover my leadership skills.
Further, I would like to thank my external advisor, Adelbert Niemeyer, for his great support during fieldwork, many enlightening discussions and his motivation and encouragement over the years. I also thank Miriam Dühnforth for her support, the continuous advice and the great discussions.

Over the years I also had the opportunity to discuss my research with many international colleagues. To name a few I like to thank Ryan Gold, Geoffrey King, Geoffrey Baily, Carry Johnson, Abbas Bahroudi, Mohammad Sharifi and Seth Stein. As part of this thesis, fieldwork in lower Bavaria and across Swabian Alb has been carried out almost every year, involving numerous Bachelor and Master students. I like to thank everybody who has helped in the field, preparing datasets and on one or the other way compiling this thesis. I will never forget these incredible days. You guys rock!

Danksagung

Besonders möchte ich mich bei der Betreuerin meiner Doktorarbeit, Anke Friedrich, für ihre Unterstützung, Inspiration und Kritik bedanken. Vielen Dank für den Rahmen, in dem ich lernen konnte, meine eigenen Ideen zu entwickeln und die Geduld, mich diese bis zum Ende verfolgen zu lassen. Ihre unerschöpfliche Motivation und große Expertise haben mich schon während meiner Studienzeit mit einem Enthusiasmus für wissenschaftliche Problemstellungen angesteckt. In Hannover fing alles mit einem kurzen Gespräch an und hier sind wir nun heute. Ich bedanke mich auch sehr für die außergewöhnliche Möglichkeit, während der vergangenen drei Jahre als wissenschaftlicher Koordinator des Lehrstuhls für Geologie tätig gewesen zu sein. Diese einzigartige Chance hat mir ermöglicht, meine Führungsqualitäten weiter zu entwickeln.
Ich danke auch meinem externen Betreuer, Adelbert Niemeyer, für seine große Unterstützung während der Geländearbeit, sowie für die vielen großartigen Diskussionen und seine fortwährende Motivation über die Jahre. Außerdem danke ich Miriam Dühnforth, für Ihre Unterstützung, Motivation und die vielen Ratschläge, sowie für unsere großartigen Diskussionen.

Mein großer Dank gilt meinen Kollegen, die mich während der letzten Jahre immer tatkräftig unterstützt haben. Allen voran bedanke ich mich bei Simon Kübler für sein unermüdliches Feedback und seinen fachlichen Rat, sowie die tatkräftige Unterstützung bei den vielen Geländetagen mit Bohrarbeiten und Geoelektrik. Danke für die großartigen Jahre in vielen gemeinsamen und benachbarten Büros, die wunderbare Zeit in der WG, die Hilfe bei der Überarbeitung aller Abbildungen und vor allem, danke für unsere großartige Freundschaft. Großer Dank gilt auch Ramona Baran und Stefanie Rieger, die im Gelände niemals überdrüssig wurden, die Geoelektrik wieder und wieder aufzubauen. Mit euch zusammen war es immer sehr lustig. Danke an Ramona Baran auch dafür, dass sie neben ihrem eng getakteten Beruf Zeit für fachliche Diskussionen und Ratschläge hatte. Großer Dank gilt auch meinem Kollegen Amir Abolghasem, für den gemeinsamen Aufbau des GPS-Projektes in Iran, sowie die gute Zeit in unserem gemeinsamen Büro.

Vielen Dank an meine internationalen Kollegen für die großartigen Diskussionen: Ryan Gold, Geoffrey King, Geoffrey Baily, Carry Johnson, Abbas Bahroudi, Mohammad Sharifi und Seth Stein. Außerdem danke ich alle weiteren Helfer an den Lehrstühlen für Geologie und Geophysik: Petra Veséla, Alessandro Verdecchia, Lorenzo Colli, Felix Fürgut and Elif Yldirim. Für die große Unterstützung während meiner administrativen Arbeit als Koordinator danke ich besonders: Rosa Susnjar, Rene Weiser, Michael Strauch und Angelika Doré.

Zum Schluss bedanke ich mich bei Sara. Danke, dass Du in den vielen stressigen Momenten immer eine große Stütze warst, für Deinen unermüdlichen Glauben an meinen Erfolg und die tatkräftige Hilfe beim finalen Korrekturlesen. Danke auch für Deine Geduld und Gelassenheit während der wochenlangen Reisen nach Iran und die große Freude zu Dir nach Hause zu kommen. Unsere gemeinsamen Stunden beim Arbeiten in den letzten intensiven Wochen waren großartig und dank Deines Humors haben wir immer sehr viel zu Lachen gehabt. Ohne Deine große Liebe und Motivation wäre das alles hier so nicht möglich gewesen.

Chapter 1

Introduction

The Northern Alpine Foreland Basin (NAFB) is a classic example of a peripheral basin (Allen and Homewood, 1986; Pfiffner, 1986). For centuries, geologists have studied the northern foreland of the Alps, but have not recognized its basin character until the late 19th century. First, it has been described as the *südbayerische Hochebene (southern Bavarian high plane)* (von Guembel, 1861), which refers to the high elevation and the characteristic erosional relief (Fig. 1.1). Indeed, the present-day elevation of the northern Alpine foreland is about 400 m – 500 m higher compared to the southern basin, the Po plane.

A decade later, the concept of the geosyncline, a depression that is filled with sediments, was introduced by Dana (1873) and Suess (1875), and the NAFB became recognized as an example. The geosyncline concept describes the area between a *Hinterland* (orogenic belt) and a craton as a *Vorlandbecken* (foreland basin). This specific area was later named an *Exogeosyncline* (Kay, 1951), based on the observation that material eroded from a mountain range is deposited in troughs along its margins. This concept has dominated geosciences until the 1960s. Later, the term 'foreland basin' has been re-introduced in the plate tectonic sense and eventually, it became established in the literature (e.g., Dickinson, 1974).

Two major types of basins are distinguished, the peripheral basin on the subducting plate and the retroarc basin on the overriding plate. This concept has been derived from the geometric and kinematic elements observed in various basin settings (DeCelles and Giles, 1996). The general geometry of a triangular wedge-shape that deepens towards the orogeny and tapers towards the craton, applies to the Alpine Foreland Basin. Regarding the fact that the NAFB is known as a sedimentary basin makes its present-day elevated erosional relief an unusual feature. The purpose of this thesis is to examine to what degree the two components of basin and surface are comparable.

For the Pliocene, Lemcke (1974) showed that the basin inverted, based on a proto-backstripping approach without considering the sediment compaction. A lithospheric controlled uplift across the Alps and the entire foreland, which is observed to be highest in the western and smallest in the eastern portion, has been proposed (Baran et

al., 2014). In summary, for the considered 5 Ma timescale, these observations actually point to an active basin system controlled by inversion. Nevertheless, the nature and origin of wide-area uplift across a sedimentary basin can be explained by a number of different processes, and in the context of the NAFB, differences between the eastern and western portion of the basin are significant.

Recent tomography and geological data suggest a switch in subduction polarity for the eastern Alps and the foreland at 20 Ma, when the Adriatic lithosphere started to subduct under continental Eurasia (Handy et al., 2014). For the western Alps and its foreland, recent geologic data indicate a decoupling of the Eurasian slab from the overlying orogen resulting in an overcompensated low topography of the western Alps (Kissling and Schlunegger, 2015). Studies on flexural modeling show that a late Cenozoic uplift across the German Molasse Basin is mainly controlled by a flexural process originating in, e.g., delamination of the lower Eurasian lithosphere accompanied by an unflexing of the Eurasian lithosphere (Andeweg and Cloething, 1998).

Indeed, these results imply the transition of the region north of the Alps, from a classic peripheral-type to a retroarc-type basin, which would result in late Cenozoic basin inversion, terminating subsidence. Further, if the lithospherically controlled mechanisms of basin uplift differ between east and west, a significant difference in the landscape evolution is expected, which is a key hypothesis to be explored in my study.

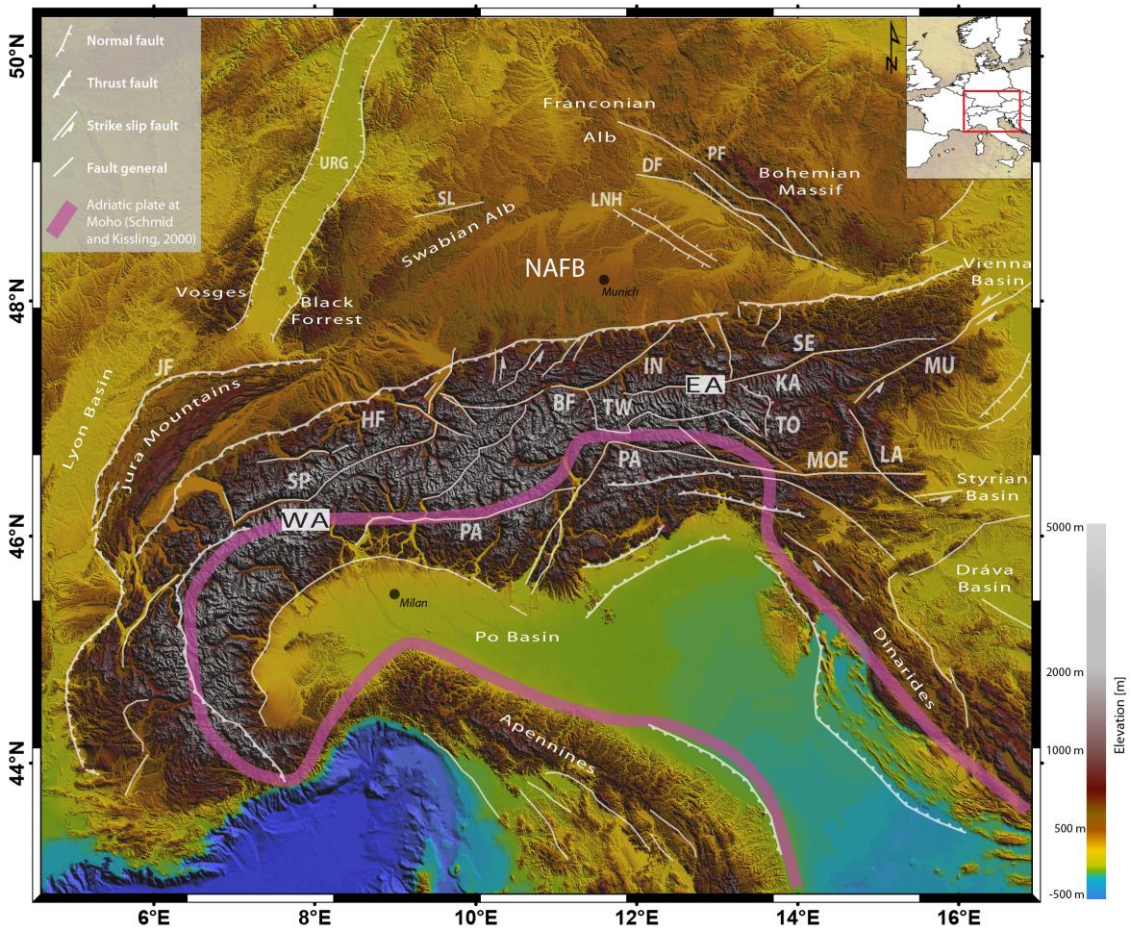

Fig. 1.1: Shaded relief map of the Alps and surrounding regions, showing major faults and basins. Note the difference in elevation between the southern (Po Plain) and the northern Alpine foreland. Background SRTM 1 arc second provided by NASA. Data compiled from Steininger and Wessely (1999). BF – Brenner fault, DF – Danube fault, EA – Eastern Alps, HF – Helvetic front, IN – Inn Tal fault, KA – Katschberg fault, LA – Lavanttal fault, LNH – Landshut-Neuoetting-High, NAFB – Northern Alpine Foreland Basin, JF – Jura front, MOE – Mölltal fault, MU – Mur-Muerz fault, TW – Tauern Window, PA – Periadriatic fault, PF – Pfahl fault, SE – Salzachtal-Ennstal fault, SL – Swabian Lineament, SP – Simplon fault, TO – Tauernostrand fault, URG – Upper Rhine Graben, WA – Western Alps.

The present-day elevation of the NAFB is high compared to the southern Alpine foreland and this could imply that the system is still active, but instead of active subsidence, here active inversion could be the predominant process.

A major focus of this thesis is to examine, if this is potentially ongoing today and my study specifically aims at pointing to the connection between subsurface data, which provide information on the early evolution of the NAFB and surface data, which provide constraints on the young basin evolution. I show how surface topography,

fluvial network and erosion pattern, as well as regional tilt and uplift in the basin and along its margin can be studied in context of an active foreland system. Here, the long history of NAFB research and exploration provides a fundamental database to address this problem.

Owed to the oil boom times in the early 20th century, a remarkable number of geophysical and geological industry data exist throughout the basin, which have been merged in a non-public basin model (GeoMol, 2015)[1]. Underlying data are mainly 2D seismic reflection and refraction lines as well as drill cores and subsidiary drilling data like sonic logs and geochemical analyses. The database also contains a large number of faults throughout the basin (Tab. 1.1). The NW-SE strike and the south-dip of predominant normal faults raise the question, whether those inherited faults have been reactivated or the basin remains inactive. In this context, new subsurface data and a rigorous analysis of surface topography that may connect to depth, can provide an answer.

Recent interest in sustainable alternative energy sources and prospects to store excess CO_2 resulted in renewed subsurface prospection. The prospection of subsurface heat-flow systems in the NAFB has led to the acquisition of numerous new 3D seismic and borehole data (e.g., Stadtwerke München). Due to hydrothermal pathways occurring along faults, the high-resolution imaging of tectonic structures is relevant to the scientific community.

However, the near surface trace of faults still remains unclear in most of the datasets, while another study suggests formation of new faults that appear to form within the sedimentary deposits by extensional faulting, independent of basement structures (von Hartmann et al., 2016).

[1] Note: The GeoMol database was not made available for this study.

Table 1-1: Summary of NAFB fault data

Location	Area covered [km^2]	Type of data	Resolution in depth [km below surface]	Fault dip [degree]	Number of faults	Youngest deposits offset by faults	Observation
East of Munich	~ 7,000	Reflection Seismic	0.8 - 3.5	50 - 60	53	Chatt sands [25 Ma]	Main reflectors are Chatt sands, Lithothamnian limestone. Oil and gas fields associated with fault traps: Velden, Dorfen, Isen, Weitermühle, Ampfing, Hohelinden, Anzing, Schaupping, Albaching, Ödgassen, Waldkraiburg, Mühldorf, Bierwang, Moosach, Wolfsberg, Assling, Höhenrain, Darching, Schnaitsee, Gendorf [1]
East of Munich	~ 7,000	Reinterpret Seismics and Well Data	0.8 - 3.6				Sequence stratigraphic analysis [2]
NAFB	> 25,000	Original and reinterpret Seismics and Well Data		60 - 75	> 200	Grimmelfing beds [17 Ma]	Basement faults [3, 4]
NAFB, eastern portion	~ 13,000		1.0 - 5.0		78	Aquitan sands [20 Ma]	Basement faults [5]
NAFB, eastern portion	~ 17,000	Reflection and Refraction Seismics plus Well Data	0.3 - 1.0	60 - 80	18	Helvet glaucinitic sand [18.5 Ma]	Surface mapping and seismic data combined for western basin (top to bottom). In the eastern basin, surface mapping was skipped and tectonic structures have been studied based on seismic data imaging the basement (bottom to top) [6]
NAFB, eastern portion (Ried)	~ 4,100	Reflection and Refraction Seismics plus Well Data	0.4 - 3.4	61 - 80	46		Confirmation of previously proposed strike-slip faults in the NAFB. Previous extensional faults (Oligocene) have been reactivated as thrust faults during the Miocene [7]

Notes: [1] Kraus, 1969; [2] Zweigel et al. 1998; [3] Janoschek 1961; [4] Unger 1999a, b, c; [5] Schwarzmeier 1981b; [6] Heermann 1954; [7] Wagner 1996a, 1998

Investigating geomorphology and connecting it with subsurface data can better address this problem. The knowledge of subsurface faults has been derived from industry prospection, and those data are isolated from the surface (see chapter II, Fig. 2.2 and Fig. 2.4). Generally, the subsurface data imply subsidence and deposition interrupted by phases of uplift and erosion often expressed in discordant contacts, while the surface data show deposition of Quaternary strata but dominantly uplift and erosion. Therefore, linking the two components is fundamental to figure out in what potential time range the transition to basin inversion occurred and what mechanisms were at play to possibly reactivate faults.

The landscape of the NAFB is characterized by a high plane (von Guembel, 1861), covered with Quaternary fluvial and lacustrine deposits, which are cut by erosional river valleys. Towards the NE portion of the basin, asymmetric valleys dominate the topography with a relief of tens of meters.
In order to collect data to identify Quaternary basin vertical surface motion and geomorphologic features from potential surface faulting, I have carried out remote sensing mapping on high-resolution digital elevation models (DEMs), extensive literature research to compile all available subsurface data and a field study to detect near-surface offset structures. In chapter II of this thesis, I test the hypothesis that the loess covered asymmetric topography of the Tertiary Hills region in the NAFB results from surface faulting, which produced escarpments where loess accumulated. In this context, I acquired new shallow geophysical and coring data to examine, to what degree those can be used to link geomorphic observations from high-resolution DEMs with subsurface data. This approach is then used to infer tectonic and erosional processes forming the landscape.

1. History of basin discovery and exploration

The NAFB is better known by the name *Molassebecken* (*Molasse Basin*) (e.g., Bachmann and Müller, 1991), which is a descriptive, stratigraphic term relating to the sedimentary fill of the basin. The fill consists of fine-grained marine, brackish and terrestrial deposits, recognized as a molasse type of material. Those deposits are covered by Pleistocene glacial and fluvial deposits (e.g., von Guembel, 1861; Penck

and Brückner, 1909; Füchtbauer, 1964). An early term, actually relating to the basin geometry, originates from Andrée (1937), where the region is named the *Tertiärbecken* (*Tertiary Basin*), pointing also to the time of formation and main depositional phase. Later, the basin name changed to a combination of a stratigraphic and a structural part of the term, *Molassetrog* (Bentz, 1949; Haus, 1951), named after the ancient farming-related German word for basin (*Trog*).

An early appearance of the name *Molassebecken* (*Molasse Basin*) can be found for the German portion in Haus (1952) and Heermann (1954), where fundamental mapping surveys and oil exploration of the NAFB are summarized. For the Austrian and Swiss portions of the NAFB, the term was introduced earlier (Kober, 1938; Rollier, 1904). The increased understanding of the geologic setting is the most likely reason for the final change in nomenclature.

The NAFB is well known as one of the most drilled and prospected basins in the world. The first oil was found in 1441, when monks near the village of Tegernsee discovered oil emerging from subaerially exposed shale layers (e.g., Kraus, 1969). The substantial content of hydrocarbons, mainly gas, coal and oil, led to establishing a professional exploration by the end of the 18th century. In 1792, the first coal beds where found near Penzberg (Wutz and Fohlmeister-Zach, 2010). Between 1910 and the 1930s the main exploration of gas and oil was initiated (Fig. 1.2). After the world market for oil collapsed in the late 1970s, the importance of the basin decreased significantly and production became unprofitable.

Fig. 1.2: Historical photo of oil drill rigs in the southern NAFB near the town of Bad Wiessee in 1911 (Photo: Gemeindearchiv Bad Wiessee).

2. Dynamic landscapes

This thesis examines the relationship between surface topography and subsurface faults in the NAFB and the evolution of vertical motion over time. Therefore, the temporal and spatial boundary conditions of landscape evolution are important. The earth's surface reacts to lithospheric, local tectonic and erosion processes with changing topographic relief (Burbank and Anderson, 2001). For an extended discussion on the evolution of the discipline of geomorphology, the reader is referred to Bishop (2007) and references therein, and Chorley et al. (1964).

Earth-surface processes balance and mask some relief by their compensational effects like e.g., hill slope diffusion. Therefore, surface imprints resulting from faulting and folding often remain unidentified, which is even more problematic in slowly deforming intracontinental regions (e.g., Braile, 1982) and humid climate zones (e.g., Bull, 2008), in which fault scarps are rapidly eroded (Fig. 1.3). In this context, geophysical subsurface data often are the only reliable source to identify tectonic structures. This requires datasets that show sufficient resolution near the surface, which are often not available, because industry data usually do not contain those

information, since they have been acquired for a different purpose (e.g., Kraus, 1969). Further, these geophysical analyses cannot be applied covering large regions, therefore the area of intended investigation has to be defined based on other geologic data. As recent studies have illustrated, the identification of faults in humid active low-strain regions is feasible by paleoseismologic trenching (e.g., Kübler et al., 2017; Vanneste et al., 2001). Limitations of those studies are the small spatial-scale as well as the financial and permission efforts, especially in populated areas like Central Europe.

The availability of new high-resolution airborne imagery (e.g., Google Earth Spot Imagery, TerraSAR-X DEM) provides an excellent low-cost alternative to investigate tectono-geomorphic features in apparent seismically extremely slow or inactive intracontinental and basin settings. This approach can be utilized to study tectonic geomorphology and link topography with subsurface data.

In addition, observations along the basin's margin yield information on uplift or subsidence of the foreland. The predicted stratigraphic response has been compared with models of flexural behavior, and the results have been found to be precise (Beaumont and Quinlan, 1984). The modeled geometry of a flexural foreland basin and its margin (forebulge) can be correlated with a distinct basal unconformity from early basin formation, and an onlap sequence. This configuration can be distinguished from eustatic variations by the geometry of the sedimentary contact, and therefore enables the detection of the forebulge in the geologic record, which further correlates with vertical motion of the plate (Crampton and Allen, 1995).

In the case of a basin with episodic marine conditions like the NAFB (Kuhlemann and Kempf, 2002), the modification of preserved coastal features provides an observational basis to study processes like erosion and tectonics. A coastline represents sea level at a specific point in time today or in the geologic past. If today the remnants of an ancient coast are found at elevations much higher than any inferred eustatic sea level, variations in the region (e.g., Haq et al., 1987; Miller et al., 2005), surface uplift from tectonics, erosion and lithospheric scale processes could be inferred.

In chapter III, I review the geomorphology and marine features of the mid-Miocene cliff coast along the northern margin of the NAFB. The famous cliff line (Lutzeier, 1922) has been used as a paleo-horizontal indicator to describe the eastward tilt of the Swabian Alb (Gall, 1969, 1974 a; Hofbauer, 2012). The coastal area has been uplifted

since the mid-Miocene and its present-day elevation ranges from c. 400 m to c. 800 m along strike. However, the causes of a tilt on a wavelength of 300 km remain unclear. Further, numerous local processes as erosion and faulting can equally explain the observed uplift. Therefore I examine, if the water level concept based on the ancient rocky shore, is applicable to infer a large-scale tilt of the region, and I discuss potential processes that additionally affected the region, located between the Alpine orogeny and the Rhine Graben rift.

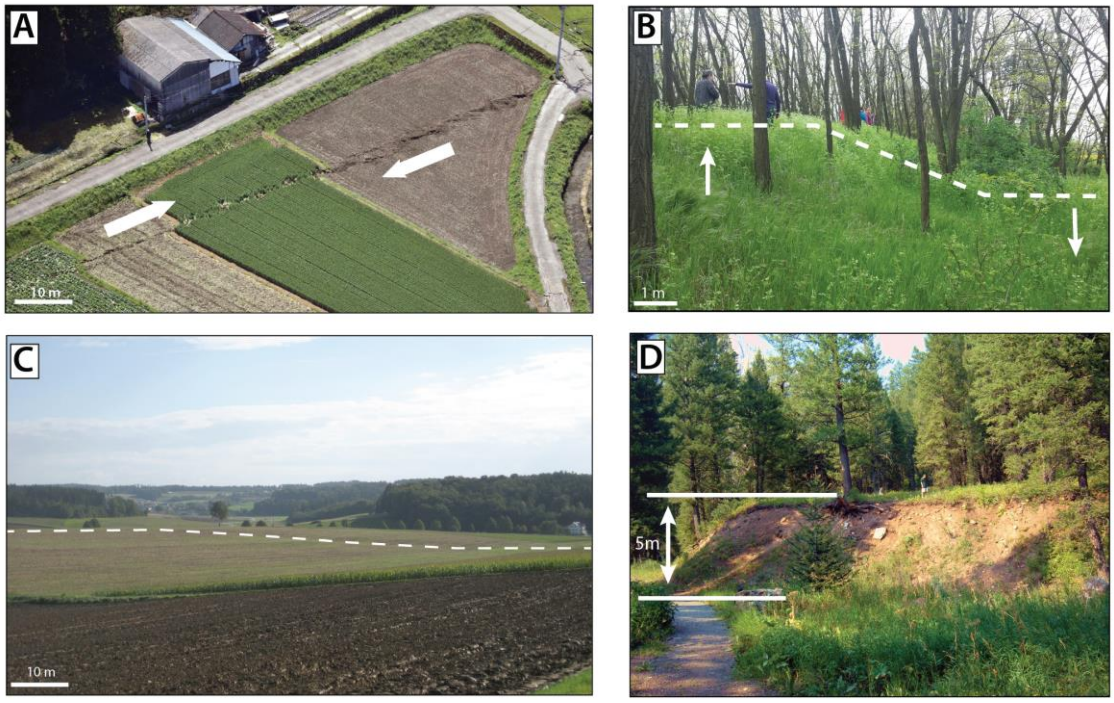

Fig. 1.3: Expressions and preservation of fault scarps in moderate to humid climatic conditions. A) Strike-slip fault scarp of the 2016, 7.3 Kumamoto earthquake in Japan, (Photo: Kyodo). B) Holocene normal fault scarp in the Vienna Basin, Austria, scarp height ~ 2 m, (Photo: Stephane Baize, 2016). C) Escarpment of unclear origin near Paindlkofen, southern Germany, height ~ 1.5 m (Photo: M.Hoffmann, 2012). D) Normal fault scarp of the 1959, 7.5 Hebgen Lake earthquake, Montana, USA (Photo: R.Losco, 2012). Examples A, B and D are related to regions of active seismicity, while C) is located in the northeast of the NAFB, where no active faulting is reported and no seismicity is recorded.

3. Paleo-coastal research and topography

The recognition and concept of ancient rocky shores has a long history starting with the first reports of De Maillet (1748). His observations of coastal morphology (notches) and marine bio-erosion have been derived from rocky shores along the Sinai peninsula in Egypt (Johnson, 1992). Later, similar observations of elevated coastal features were used to show that Scandinavia is actively uplifting by non-seismic processes (von Buch, 1810). These observations raised the attention of geoscientists to use coastlines as marker horizons for sea level changes and regional coastal uplift (e.g., Johnson, 1992). Compared to other methods, coastlines are a useful tool to infer regional evolution, especially vertical displacement, over great time and space ranges (Fig. 1.4).

The examples presented in chapter II and III emphasize the significance of understanding surface topography on multiple scales in order to detect a potential link to subsurface fault structures and their latest activity. Yet, there is another large-scale indicator of vertical surface motion to be applied in a foreland basin setting. Sediment budgets and erosion patterns are a well-established tool to infer dynamic vertical motion of a region (Baran et al., 2014; Hinderer, 2012; Kuhlemann and Kempf, 2002).

The erosional relief of the youngest deposits in the NAFB is investigated in chapter IV of this thesis, where I demonstrate the presence of enhanced basin axis parallel Quaternary erosion in the NAFB. These results point to an active basin inversion and also potential surface modification by local faulting. The results fit well in the context given in chapter II and III, demonstrating across multiple temporal and spatial scales that the NAFB is still active by inversion. Based on this I conclude, that the previously proposed uplift signal (Lemcke, 1974; Baran et al., 2014) ceased in the west by the end of the Pliocene, and migrated eastward along the transversal basin axis. The largest erosion in the Pliocene was observed for the western portion of the NAFB, while for the Quaternary, strongest erosion appears to be located in the eastern NAFB. This implies significant activity in the eastern foreland basin, therefore the assumption of a tectonically inactive eastern foreland basin is valid during the early phase of basin inversion in the west around 5 Ma. In contrast, this assumption does not hold for the Quaternary basin evolution. Hence, the contribution to basin

inversion during this time has to be identified in the geologic record on different spatial and temporal resolution.

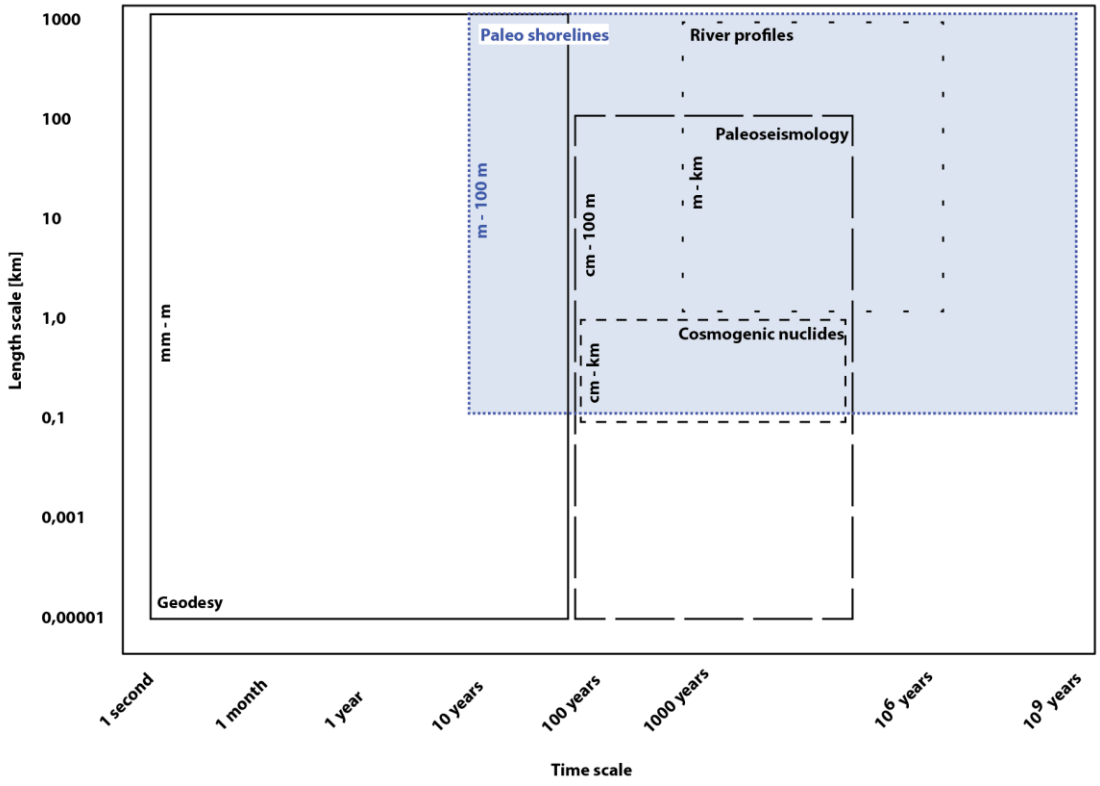

Fig. 1.4: Spatial and temporal scale of methods used to measure vertical displacement. Vertical numbers inside the boxes indicate the magnitude of each method. Paleo shorelines cover a wide range of time and space, making them a useful tool to extract dynamic earth surface and subsurface processes. Scale constraints are compiled from Massonnet and Feigl, 1998; Milne et al, 2001; McCalpin, 1996; von Blanckenburg, 2005; Norton et al, 2008; Sandiford, 2007; Roberts and White, 2010; Burbank and Anderson, 2001; Heller et al, 2003.

4. General remark

The major chapters of this thesis will be submitted to relevant peer-reviewed journals. For reasons of readability, the articles are presented in a modified format in this thesis. Some redundancies are a consequence of this formatting. The first four chapters were mentioned above. A fifth publication relates to work not otherwise presented in this thesis, describing the first southeast Iran - Makran permenant GPS backbone array developed and installed by the author of this thesis and collegues. The here presented articles for publication are:

Chapter II

Hoffmann M., Friedrich A.M., Niemeyer A. (in preparation for submission to International Journal of Earth Sciences): *Morphotectonic analysis of the asymmetric Tertiary Hills and possible connection to basement faults – Northern Alpine Foreland Basin, Germany*

Chapter III

Hoffmann M., Friedrich A.M. (in preparation for submission to International Journal of Earth Sciences): *Erosional and tectonic overprint of the mid-Miocene marine cliff line and its applicability as a paleo-geodetic marker of regional-scale tilting – Swabian Alb, southwestern Germany*

Chapter IV

Hoffmann M., Friedrich A.M., Dühnforth M. (in preparation for submission to Basin Dynamics): *Quaternary tectonic activity of the Northern Alpine Foreland Basin - Analysis of erosion patterns and geomorphic markers*

Appendix:

Hoffmann M., Abolghasem A.M., Bahroudi A., Sharifi M.A.; Friedrich A.M. (in preparation for submission to Journal of Geophysical Research: Solid Earth): *Installation of the New Geodetic Southeast Iran – Makran Backbone Array (SIMBAR) – Concepts, Challenges and First Results*

5. References

Allen, P. A., and Homewood, P., 1986, Foreland basins, Oxford, Blackwell Scientific Publications, Spec. Publ. Int. Ass. Sediment., 453 p. 3–11.

Andeweg, B. and S. Cloetingh (1998). "Flexure and 'unflexure' of the North Alpine German-Austrian Molasse Basin: constraints from forward tectonic modelling." Geological Society, London, Special Publications 134(1): 403–422.

Andrée, H., 1937, Das bayerische Tertiärbecken zum ersten Male durchbohrt: Gel und Kohle, v. 13, p. 1–5.

Bachmann, G. H., and Müller, M., 1991, The Molasse basin, Germany: evolution of a classic petroliferous foreland basin: Generation, accumulation, and production of Europe's hydrocarbons (ed. A.M. Spencer, Special Publication of the European Association of Petroleum Geoscientists, Oxford University Press, v. 1, p. 273–276.

Baran, R., Friedrich, A. M., and Schlunegger, F., 2014, The late Miocene to Holocene erosion pattern of the Alpine foreland basin reflects Eurasian slab unloading beneath the western Alps rather than global climate change: Lithosphere, v. 6.2, p. 124–131.

Beaumont, C., and Quinlan, G. M., 1984, Appalachian thrusting, lithospheric flexure, and the Paleozoic stratigraphy of the Eastern Interior of North America: Can. J. Earth Sci., v. 21, no. 9, p. 84–103.

Bentz, A., 1949, Bau und Erdölhöffigkeit des Molassetroges von Oberbayern und Oberschwaben: Erdöl und Kohle, v. 2, p. 41–52.

Bishop, P., 2007, Long-term landscape evolution: linking tectonics and surface processes: Earth Surface Processes and Landforms, v. 32, no. 3, p. 329–365.

Braile, L., 1982, An Ancient Rift Complex and its Relation to Contemporary Seismicity in the New Madrid Seismic Zone: Tectonics, v. 1, no. 2, p. 225–237.

Bull, W. B., 2008, Tectonic geomorphology of mountains: a new approach to paleoseismology, John Wiley & Sons, p. 311–324.

Burbank, D., and Anderson, R., 2001, Tectonic Geomorphology, p. 2–211.

Burbank, D., Beck, R. A., and Mulder, T., 1996, The Himalayan foreland basin: World and regional geology, p. 149–190.

Busby, C. J., and Ingersoll, R. V., 1995, Tectonics of sedimentary basins, 1–51.

Chorley, R. J., Dunn, A. J., and Beckinsale, R. P., 1964, The history of the study of landforms, or the development of geomorphology. Vol. 1, Geomorphology before Davis, Methuen, p.1–759.

Crampton, S. L., and Allen, P. A., 1995, Recognition of Forebulge Unconformities Associated with Early Stage Foreland Basin Development: Example from the North Alpine Foreland Basin: AAPG Bulletin, v. 79, no. 10, p. 1495–1514.

Dana, J. D., 1873, On some results on the Earth's contraction from cooling, including a discussion of the origin of mountains and the nature of the Earth's interior: American Journal of Science, v. 3, no. 5, p. 423–443.

De Maillet, B., 1748, Telliamed ou entretiens d'un philosophe Indien avec un missionaire Francois sur la diminution de la mer [A Telliamed or conversation between an Indian philosopher and a French missionary on the diminution of the sea]. Translated and edited by A.V. Carozzi, 1968, Urbana: University of Illinois Press, p. 1–58.

DeCelles, P. G., 2004, Late Jurassic to Eocene evolution of the Cordilleran thrust belt and foreland basin system, western USA: American Journal of Science, v. 304, no. 2, p. 105–168.

DeCelles, P. G., and Giles, K. A., 1996, Foreland Basin Systems: Basin Research, v. 8.2, p. 105–123.

Dickinson, W. R., 1974, Plate tectonics and sedimentation: Publ. Int. Ass. Sed. in Spec. Publ. SEPM 22, 1–27, v. 8, p. 77–90.

Füchtbauer, H., 1964, Sedimentpetrographische Untersuchungen in der älteren Molasse der Alpen.: Eclogae geol. Helv. Basel, v. 57, p. 157–298.

Gall, H., 1969, Geologische Untersuchungen im südwestlichen Vorries. Das Gebiet des Blattes Wittislingen: Dissertation Fakultät für Geowissenschaften der Ludwig-Maximilians-Universität München, p. 1–248.

-, 1974 a, Neue Daten zum Verlauf der Klifflinie der Oberen Meeresmolasse (Helvet) im südlichen Vorries: Mitteilungen der Bayersichen Staatssammlungen Paläontologie und historische Geologie, v. 14, p. 81–101.

GeoMol, 2015, GeoMol Project—assessing subsurface potentials of the Alpine Foreland Basins for sustainable planning and use of natural resources: Bavarian Environment Agency.

Handy, M. R., Ustaszewski, K., and Kissling, E., 2014, Reconstructing the Alps–Carpathians–Dinarides as a key to understanding switches in subduction polarity, slab gaps and surface motion: International Journal of Earth Sciences, v. 104, no. 1, p. 1–26.

Haq, B. U., Hardenbol, J., and Vail, P. R., 1987, Chronology of fluctuating sea levels since the Triassic: Science, v. 235, no. 4793, p. 1156–1167.

Haus, H. A., 1951, Zur paläogeographischen Entwicklung des Molassetroges im Bodenseegebiet während des mittleren Miozäns.: Mitt.-Bl. badischen geol. L.-Anst., Freiburg im Breisgau, p. 48–66.

-, 1952, Das Molassebecken im südwestdeutschen Gebiet: Bull. Ver. Schweizer. Petrol.-Geol. u.-Ing., v. 19, no. 57, p. 25–30.

Heermann, O., 1954, Erdölgeologische Grundlagen der Aufschlussarbeiten im Ostbayerischen Molassebecken: Bull. Ver. Schweiz. Petrol.-Geol. u. Ing., v. 21, no. 60, p. 5–22.

Heller, P. L., Dueker, K., and McMillan, M. E., 2003, Post-Paleozoic alluvial gravel transport as evidence of continental tilting in the US Cordillera: Geological Society of America Bulletin, v. 115, no. 9, p. 1122–1132.

Hinderer, M., 2012, From gullies to mountain belts: A review of sediment budgets at various scales: Sedimentary Geology, v. 280, p. 21–59.

Hofbauer, G., 2012, Jungtertiäre Talverschüttung und tektonische Verstellung entlang des Regnitz- Rezat-Tals: GDGH Berichte, v. 15, p. 1–16.

Janoschek, R., 1961, Über den Stand der Aufschlußarbeiten in der Molassezone Oberösterreichs: Erdöl-Zsch, v. 77, p. 161–175.

Johnson, M. E., 1992, Studies on Ancient Rocky Shores: A Brief History and Annotated Bibliography: Journal of Coastal Research, v. 8, no. 4, p. 797–812.

Kay, M., 1951, North American geosynclines: Geological Society of America Memoirs, v. 48, p. 1–132.

Kober, L., 1938, Die Molassebecken. Die tertiären Becken, in: Der Geologische Aufbau Österreichs, Springer Vienna, p. 157–178.

Kraus, L., 1969, Erdöl- und Erdgaslagerstätten im ostbayerischen Molassebecken: Erdoel-Erdgas-Zeitschrift, v. 85, p. 442–454.

Kübler, S., Streich, R., Lück, E., Hoffmann, M., Friedrich, A. M., and Strecker, M. R., 2017, Active Faulting in a Populated Low-Strain Setting (Lower Rhine Graben, Central

Europe) Identified by Geomorphic, Geophysical, and Geological Analysis: Geological Society of London, Special Publications, v. 432, p. 127–146.

Kuhlemann, J., and Kempf, O., 2002, Post-Eocene evolution of the North Alpine Foreland Basin and its response to Alpine tectonics: Sedimentary Geology, v. 152, p. 45–78.

Lemcke, K., 1974, Vetikalbewegungen des vormesozoischen Sockels im nördlichen Alpenvorland Perm bis zur Gegenwart?: Eclogae Geologicae Helvetiae, v. 67, no. 1, p. 121–133.

Lucchi, F. R., 1986, The Oligocene to Recent foreland basins of the northern Apennines, Foreland Basins, Volume 8, Special Publication of the International Association of Sedimentologists, p. 105–139.

Lüschen, E., Borrini, D., Gebrande, H., Lammerer, B., Millahn, K., Neubauer, F., and Nicolich, R., 2006, TRANSALP—deep crustal Vibroseis and explosive seismic profiling in the Eastern Alps: Tectonophysics, v. 414, no. 1–4, p. 9–38.

Lutzeier, H., 1922, Beiträge zur Kenntnis der Meeresmolasse in der Ulmer Gegend: Neues Jahrbuch für Geologie und Paläontologie, Beilagen Bände, Stuttgart, v. 46, p. 117–180.

Massonnet, D., and Feigl, K. L., 1998, Radar interferometry and its application to c hanges in the Earth's surface: Reviews of geophysics, v. 36, no. 4, p. 441–500.

McCalpin, J. P., and Nishenko, S. P., 1996, Holocene paleoseismicity, temporal clustering, and probabilities of future large (M> 7) earthquakes on the Wasatch fault zone, Utah: Journal of Geophysical Research: Solid Earth, v. 101, no. B3, p. 6233–6253.

Miller, K. G., Kominz, M. A., Browning, J. V., Wright, J. D., Mountain, G. S., Katz, M. E., Sugarman, P. J., Cramer, B. S., Christie-Blick, N., and Pekar, S. F., 2005, The Phanerozoic record of global sea-level change: Science, v. 310, no. 5752, p. 1293–1298.

Milne, G. A., Davis, J. L., Mitrovica, J. X., Scherneck, H. G., Johansson, J. M., Vermeer, M., and Koivula, H., 2001, Space-geodetic constraints on glacial isostatic adjustment in Fennoscandia: Science, v. 291, no. 5512, p. 2381–2385.

Norton, K. P., Blanckenburg, v., F., S., F., Schwab, M., and Kubik, P. W., 2008, Cosmogenic nuclide-based investigation of spatial erosion and hillslope channel coupling in the transient foreland of the Swiss Alps: Geomorphology, v. 95, no. 3, p. 474–486.

Penck, A., and Brückner, E., 1909, Die Alpen im Eiszeitalter, Tauchnitz, 1157 pp.

Pfiffner, O. A., 1986, Evolution of the north Alpine foreland basin in the Central Alps: In Foreland basins. Spec. Publ. Int. Ass. Sediment., v. 8, p. 219–228.

Roberts, G. G., and White, N., 2010, Estimating uplift rate histories from river profiles using African examples: Journal of Geophysical Research: Solid Earth, v. 115, no. B2.

Rollier, L., 1904, Die Entstehung der Molasse auf der Nordseite der Alpen: Vierteljahrsschr. naturf. Ges. Zürich, p. 159–170.

Sandiford, M., 2007, The tilting continent: a new constraint on the dynamic topographic field from Australia: Earth and Planetary Science Letters, v. 261, no. 1, p. 152–163.

Schwarzmeier, J., 1981b, Tektonik der Süddeutsches Großscholle.- In: Bayerisches Geologisches Landesamt [Hrsg.]: Erläuterungen zur Geologischen Karte von Bayern 1:500 000. – 3. Aufl., München, p. 97–101.

Steininger, F. F., and Wessely, G., 1999, From the Tethyan Ocean to the Paratethys Sea: Oligocene to Neogene stratigraphy, paleogeography and paleobiogeography of the circum-Mediterranean region and the Oligocene to Neogene Basin evolution in Austria: Mitteilungen der Österreichischen Geologischen Gesellschaft, v. 92, p. 95–116.

Suess, E., 1875, Die Entstehung der Alpen, W. Braumüller, p. 1–168.
Unger, H. J., 1999a, Die tektonischen Strukturen der bayerischen Molasse: Documenta naturae, v. 125, p. 1–16.
-, 1999b, Zur lithostratigraphisch-nomenklatorischen Verknüpfung von Ost-und Westmolasse in Bayern: Documenta naturae, v. 125, no. 17–45.
-, 1999c, Die Geisenfeld-Abfolge. Gedanken zur pliozänen ENtwässerung der bayerischen Molasse.: Documenta naturae, v. 125, no. 57–97.
Vanneste, K., Verbeek, K., Camelbeeck, T., Puaulissen, E., Meghraoui, M., Renardy, F., Jongmans, D., and Frechen, M., 2001, Surface-rupturing history of the Bree fault scarp, Roer Valley graben: Evidence for six events since the late Pleistocene: Journal of Seismology, v. 5, p. 329–359.
von Blanckenburg, F., 2005, The control mechanisms of erosion and weathering at basin scale from cosmogenic nuclides in river sediment: Earth and Planetary Science Letters, v. 237, no. 3, p. 462–479.
von Buch, L., 1810, Reise durch Norwegen und Lappland, Berlin, Nauck, p. 1–486.
von Guembel, C. W., 1861, Geognostische Beschreibung des bayerischen Alpengebirges und seines Vorlandes: J. Perthes, v. 1, p. 1–440.
von Hartmann, H., Tanner, D. C., and Schumacher, S., 2016, Initiation and development of normal faults within the German alpine foreland basin: The inconspicuous role of basement structures: Tectonics, v. 35, no. 6, p. 1560–1574.
Wutz, B., and Fohlmeister-Zach, K., 2010, Penzberg, Sutton Verlag GmbH, p. 7–127.
Zweigel, J., Aigner, T., and Luterbacher, H., 1998, Eustatic versus tectonic controls on Alpine foreland basin fill: sequence stratigraphy and subsidence analysis in the SE German Molasse: Geological Society of London, Special Publication, v. 134.1, p. 299–323.

Chapter 2

Morphotectonic analysis of the asymmetric Tertiary Hills and possible connection to basement faults – Northern Alpine Foreland Basin, Germany

Authors:
Hoffmann, M.[1]*, Friedrich, A.M.[1] Niemeyer, A.[2]

Affiliations
1. Department of Earth and Environmental Sciences, Ludwig-Maximilians University of Munich, Luisenstr. 37, 80333 München, Germany.
2. ERLUS AG, Hauptstr. 106, 84088 Neufahrn/NB, Germany.

*Corresponding author (e-mail: ma.hoffmann@lmu.de)

1. Abstract

The loess-mantled Tertiary Hills are well-known for their asymmetric surface morphology, which previously has been interpreted as a primary depositional feature that formed at times of westerly winds during the Pleistocene. The asymmetry occurs on scales of a few kilometers. This is similar to the spacing and orientation of well-known, but buried Tertiary high-angle fault systems of the North Alpine Foreland Basin (NAFB). The faults developed in Variscan basement and its Mesozoic to mid-Miocene cover. Their upper extent is uncertain, because the region is covered with Pleistocene loess deposits. To examine whether or to what degree the asymmetric hills may result from reactivation of Tertiary basement faults, we carried out a morphotectonic field study at two sites. There, we traced contacts between Tertiary gravel and Pleistocene loamy-loess deposits.

The *Paindlkofen* site lies c. 17 km NE of Landshut along the southern margin of the Dingolfing fault. The *Tunzenberg* site lies c. 20 km SW of Straubing along the southern margin of the Schierling fault. At the drill site *Paindlkofen,* geomorphic, geophysical and coring data reveal a sharp, steep NE-dipping contact associated with a 0.7 km long surface escarpment on cropland. Geomorphic and geologic mapping of a 20 m by 5 m open pit mine wall at *Tunzenberg* reveals cm-scale offsets of cross-

bedded fluvial deposits. Digital elevation model (DEM) remote sensing was used to map surface escarpments and shallow geophysics, and coring were utilized to detect geologic contacts at depth. Based on our results, surface morphology at both sites was modified by intense vegetation, anthropogenic activity and overprint from post-glacial soil mobilization. However, we interpret the geometry of the detected contact at *Paindlkofen* and the offsets at *Tunzenberg* to indicate a possible tectonic origin. Therefore, initial topography in the Tertiary Hills region likely existed before loess accumulated. Loess may have preferentially been deposited where pre-exisiting topography provided relief. Therefore, recent tectonic activity may have to be considered in understanding the erosion landscape of the NAFB, in particular the Tertiary Hills.

2. Introduction

Since the beginning of the 20th century, the NAFB has been known for its young, climatically controlled landscape (Penck and Brückner, 1909). The regional topography is locally subdued, due to the poorly consolidated fluvial deposits. In the northeastern portion of the NAFB, an area of gentle hills sticks out of the flat landscape. The Tertiary Hills topography, with its asymmetric valleys and loess accumulations, has been explained by climatic processes, where the landscape is controlled by runoff, freezing/ thawing, gravitational mass movement and lately agricultural land use (Leger, 1990; Wende, 1995), or by young surface uplift, forming an elevated erosional relief. In adjacent regions like the Swabian Alb and the Black Forest in southwestern Germany, the relationship between young relief and tectonics has been recognized, based on observations of enhanced fluvial incision, systematic dip of strata and steep valley flanks (Wagner, 1929). The general interpretation for those observations was that higher relief indicates younger surface uplift (Wagner, 1929, 1960).

During prospection of loess loam as raw material for brickworks in the Tertiary Hills, it has been observed that loess deposits are largest where high relief occurs along steep, NW-SE striking escarpments. Furthermore, NW-SE striking basement faults are known across the region from petroleum prospection (Tab. 2.1).

Some of those coincide with the asymmetric steep loess escarpments, permitting a tectonic interpretation (Fig. 2.1).

In this study, we aim to further explore whether faulting caused the present-day geomorphology and detected subsurface structures in the Tertiary Hills region of the NAFB. The results from previous work in adjacent regions (Tab. 2.2) suggest at least some Quaternary tectonics between the eastern Alpine thrust front and the Tertiary Hills region in the NE portion of the basin.

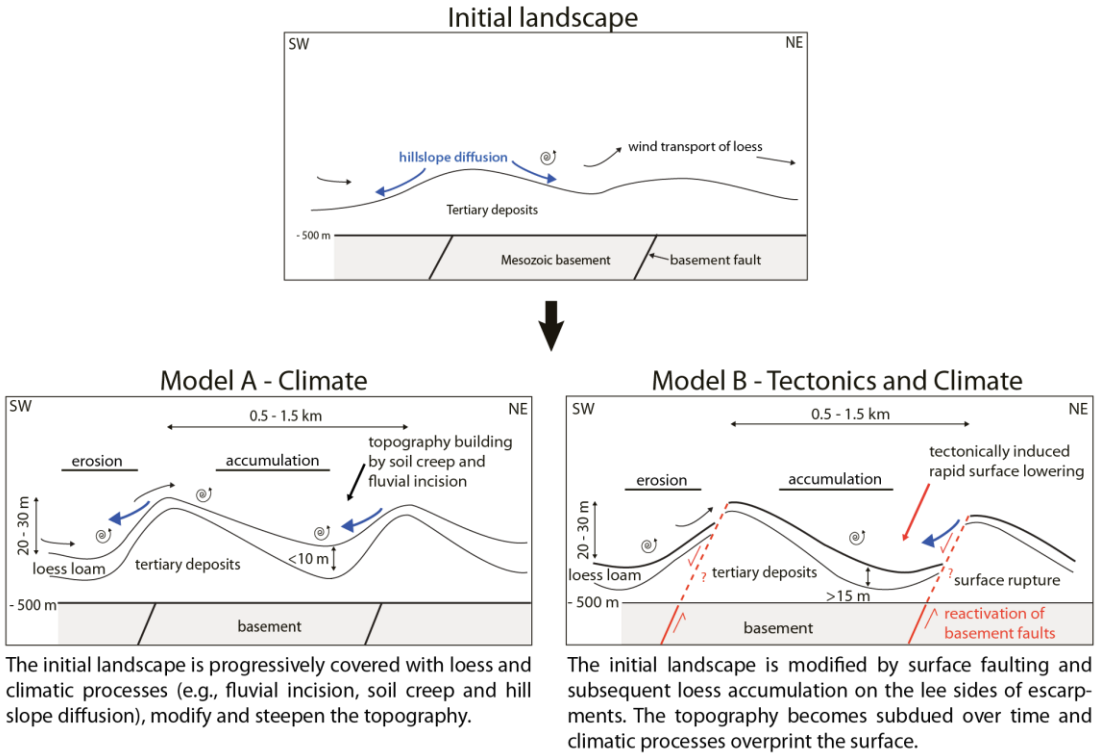

Fig. 2.1: Schematic models to explain the present-day topography of the Tertiary Hills region. Model A suggests geomorphology controlled by climate, while model B shows initial topography by active faulting and second order climatic overprinting. Not drawn to scale.

To test our hypothesis that active faulting contributed to the asymmetric topography, we examined available fault data for the NAFB from previous work (Tab. 1)[2]. The data come from geophysical industry exploration over the last six decades, incorporating 2D-, 3D-seismics and wells. The target areas of exploration covered only parts of the NAFB, where marine facies at depth have been identified as oil and gas host rocks (Kraus, 1969). In this context, a possible connection between the present-day landscape and the subsurface faults could improve the understanding of whether the NAFB is an active basin and in what sense activity is expressed.

The Oligo-Miocene basin fill reflects subsidence, while the stratigraphic record of the Pliocene (Lemcke, 1974) and the present-day elevated basin landscape (chapter I, Fig. 1) imply erosion.

For the NAFB, this scenario has been indirectly addressed by previous work and none of the published subsurface datasets show faults reaching the surface (Tab. 2.1).

[2] Note: The GeoMol database providing most of the existing seimsic and well data for the NAFB was not available to the authors of this study.

Table 2-1: Summary of NAFB fault data

Location	Area covered [km^2]	Type of data	Resolution in depth [km below surface]	Fault dip [degree]	Number of faults	Youngest deposits offset by faults	Observation
East of Munich	~ 7,000	Reflection Seismic	0.8 - 3.5	50 - 60	53	Chatt sands [25 Ma]	Main reflectors are Chatt sands, Lithothamnian limestone. Oil and gas fields associated with fault traps: Velden, Dorfen, Isen, Weitermühle, Ampfing, Hohelinden, Anzing, Schaupping, Albaching, Ödgassen, Waldkraiburg, Mühldorf, Bierwang,Moosach, Wolfsberg, Assling, Höhenrain, Darching, Schnaitsee, Gendorf [1]
East of Munich	~ 7,000	Reinterpret Seismics and Well Data	0.8 - 3.6				Sequence stratigraphic analysis [2]
NAFB	> 25,000	Original and reinterpret Seismics and Well Data		60 - 75	> 200	Grimmelfing beds [17 Ma]	Basement faults [3, 4]
NAFB, eastern portion	~ 13,000		1.0 - 5.0		78	Aquitan sands [20 Ma]	Basement faults [5]
NAFB, eastern portion	~ 17,000	Reflection and Refraction Seismics plus Well Data	0.3 - 1.0	60 - 80	18	Helvet glaucinitic sand [18.5 Ma]	Surface mapping and seismic data combined for western basin (top to bottom). In the eastern basin surface mapping was skipped and tectonic structures have been studied based on seismic data imaging the basment (bottom to top) [6]
NAFB, eastern portion (Ried)	~ 4,100	Reflection and Refraction Seismics plus Well Data	0.4 - 3.4	61 - 80	46		Confirmation of previously proposed strike-slip faults in the NAFB. Previous extensional faults (Oligocene) have been reactivated as thrust faults during the Miocene [7]

Notes: [1] Kraus, 1969; [2] Zweigel et al. 1998; [3] Janoschek 1961; [4] Unger 1999a, b, c; [5] Schwarzmeier 1981b; [6] Heermann 1954; [7] Wagner 1996a, 1999

Table 2-2: Summary of previous field observations used to infer Quaternary tectonic activity in the NAFB. Locations are shown in Fig. 2.2

Location	Observation	Reference
Graisbach	Surface lineaments in similar orientation with assumed faults	Mühlfeld (1968)
Passau	Surface lineaments in similar orientation with assumed faults	Streit (1979)
Traunstein	Tilted fluvial terraces, Quaternary deposits	Ganss (1968), Oeltzschner (1965), Schmidt-Thomé (1955)
Vilsbiburg	Tilted fluvial terraces, Pleistocene deposits	
Isar valley	Tilted fluvial terraces, Pleistocene deposits	
Inn valley	Tilted fluvial terraces, Pleistocene deposits	Ganns (1968), Mayr (1957)

Nonetheless, the problem of character and timing of basin activity is relevant, e.g., for the exploration of geothermal energy, CO_2 underground storage and potential earthquake hazards in the densely populated region.

On the short timescale, space-geodetic data across the Alps indicate N-S-directed convergence between Eurasia and the Adriatic plate, as well as counterclockwise rotation of ~ 20° of the two plates during the last ~ 5 Ma (Calais et al., 2003) (Tab. 2.3). The geodetic motion across the Alps indicates potential tectonic activity north of the Alps, where extensional strain would be expected for the western portion and its foreland, while N-S shortening would be expected for the eastern portion and foreland basin.

A compressional regime in the NAFB also has been deduced from borehole breakout data and fracture studies (Heidbach et al., 2008; Reinecker et al., 2010). This implies that current deformation occurring across the Alps and the foreland basin, can potentially reactivate faults. However, instrumental and historic seismicity in the German portion of the NAFB shows sporadic events with magnitudes of ~ 3.0, intensities > IV, respectively (Leydecker, 2011; NEIC, 2016) (Fig. 2.2).

Table 2-3: Summary of present-day geodetic signals across the Eurasia – Adriatic plate boundary

Location	Observation	Rate [mm/a]	Reference
Western Alps	Convergence Eurasia - Adriatic	0.5 - 1.0	Vrabec et al. 2006; D'Agostino et al. 2008
Eastern Alps	Convergence Eurasia - Adriatic	~ 2.0	Tesauro et al. 2005

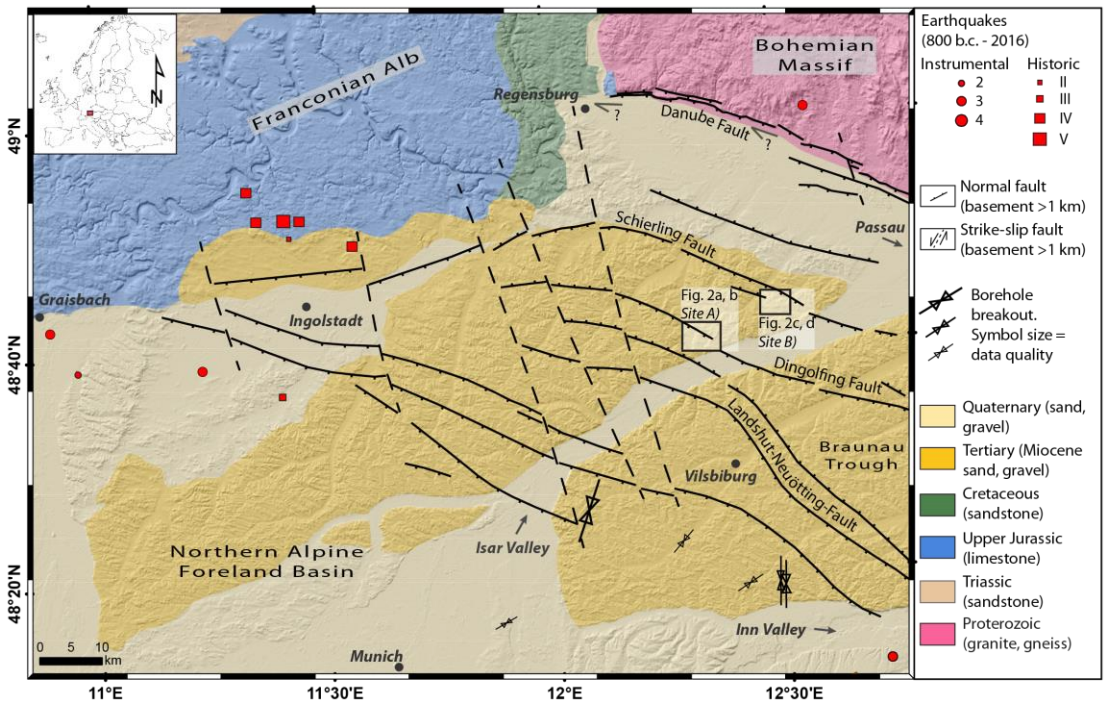

Fig. 2.2: Map of the Tertiary Hills region showing the relationship between major basement faults, surface geology and seismicity. Background SRTM 3 arc sec, provided by NASA. Surface geology simplified after geologic map of Bavaria, 1:500,000. Fault data compiled from Unger, 1999a. Borehole breakout data from Reinecker et al., 2010. Earthquake data from the NEIC data base; Leydecker, 2011 and the Bavarian seismic observation network: *BayWatch*.

The link between basement and surface is unclear, and if surface scarps have existed, the climatic overprint by loess accumulation and fluvial transport of glacial and interglacial periods has likely compensated and erased most of the initial topography. Therefore, we use new field evidence to shed light on this problem by linking subsurface data with geomorphologic observations.

3. Regional Setting

The NAFB initiated in the late Eocene, when the Eurasian plate margin subducted southwards (Genser et al., 2007; Schmid et al., 1996). The maximum depth was reached by mid-Miocene time with ~ 5 km at the northern Alpine front (Lemcke, 1974; Roll, 1952). The basin became filled with Oligocene to Miocene fluvial and marine sediments, and two major cycles of alternating marine and terrestrial sedimentation are reported (e.g., Füchtbauer, 1964).

3.1. Surface morphology and study site setting

The topographic expression of the NAFB shows flat-lying Quaternary fluvial deposits in the western portion, whereas only thin patches of Quaternary deposits and large portions of Tertiary sediments are exposed along gently elevated hills in the eastern portion (Tertiary Hills).

The Tertiary Hills topography is a unique feature of the NAFB. The area is located close to the northeastern margin of the German NAFB, about 90 km north of the Alpine thrust front and about 25 km south of the Bohemian Massif. It spans across about 3.500 km^2, with an average elevation of 420 m a.sl. The regional topography comprises a dense network of asymmetric gentle hills and valleys, locally interrupted by steep, mostly NW-SE striking escarpments. Our two study sites *Paindlkofen* and *Tunzenberg* are located in the Tertiary Hills area. The site *Paindlkofen* lies in the central part of the northern Tertiary Hills, while *Tunzenberg* is located closer to the northern margin about 10 km north of the Isar river valley (Fig. 2.2). Furthermore, the two study sites are situated above two well-known basement faults. *Paindlkofen* lies about 1 km south of the trace of the Dingolfing fault at depth. The site *Tunzenberg* lies 2 km south of the Schierling fault and about 1 km south of a second fault

structure, running parallel to the Schierling fault. Both faults are high angle normal faults at c. 1.5 km depth (Fig. 2.2).

In the region, unconsolidated late Miocene fluvial sand and gravel deposits are covered by up to 15 m thick Pleistocene loamy-loess deposits, as a remnant from the glacial/ interglacial periods over the last ~ 1.2 Ma (Jerz, 1993). The fertile soils, which developed on the loamy loess, have led to extensive agricultural land use since the Neolithic (e.g., Leopold and Völkel, 2007). Relative age control of the upper-most sediments is given by archeological findings. At the nearby sites Baierbach, Rohrberg and Reut, graves and stilt houses from the Bronze Age have been found (Erlus AG, Bayerisches Landesamt für Denkmalpflege). They are dated to 6,500 b.p. – 7,000 b.p. based on ceramics found at the sites. According to the fertile soils and the dense population, urban and agricultural land use is intense. The regional climate is humid with mean annual temperatures of 8 °C – 12 °C, and mean precipitation of 680 mm/a - 900 mm/a (German Weather Service 2016, Bayerisches Landesamt für Wasserwirtschaft, 1998). Therefore, the preservation potential of steep geomorphic features, such as faults scarps, is low.

3.2. Regional fault data

All available fault data are derived from previously published studies, which were designed to understand the deeper structure of the basin. Therefore, technical limitations emphasize the uncertainties regarding the connection to topography. For the available seismic data, the limit of resolution reached about 500 m below surface, due to the design of the 2D-reflection seismics (Bachmann et al., 1982; Kraus, 1969). The seismic array has been set to image the base of the Tertiary sediments (Lithotamnien limestone) and the Jurassic Malm limestone at depth > 1.5 km, which limits near surface resolution (Prinz and Strauß, 2012).

An additional limitation to detect fault offsets arises from the heterogeneous clastic sediment filling of the basin, because those deposits are poor reflectors. Accordingly, offsets have been derived mainly from the crystalline basement (e.g., Landshut-Neuöttinger-High) up to the base of the Burdigal (mid-Miocene), located at depths of > 500 m below surface in the eastern NAFB. For example, the Brackish Water Molasse (BM) and terrestrial sediments from Upper Freshwater Molasse (OSM) above do not provide strong reflectors, and no offsets of these younger deposits are observed. With the loss of resolution and strong reflectors in younger clastic

sediments, the upper temporal boundary for tectonic deformation has been set to the mid-Miocene (e.g., Unger and Schwarzmeier, 1982). However, the absence of record does not bear any information about younger tectonic activity.

New fault data are derived from high-resolution 3D-seismic campaigns from geothermal industry prospection. Based on these, von Hartmann et al. (2016) suggest that about 50 km southwest of Munich, the basin inherits a disconnected set of younger faults that developed in the middle and upper Miocene sediments independently from the basement structures. However, these faults also do not cut the surface. Finally, regional tectonics is expressed by alternating marine and terrestrial deposits of NAFB. Sequence stratigraphic studies attribute the transgressive – regressive cycles in the basin (Kuhlemann and Kempf, 2002) to tectonics (e.g., Jin et al., 1995; Zweigel et al., 1998), although climatic interpretations have also been proposed. Though, the temporal and spatial scale of these basin-wide studies is too large to infer local surface faulting. In summary, the NAFB appears to be highly dissected by numerous fault systems that are well documented. The degree to which these faults have influenced the present-day surface morphology is the focus of this paper.

4. Methods

Our geomorphologic study is based on geological principles that at the earth surface, sharp geologic contacts, i.e. topographic lineaments and geomorphologic steps, often relate to tectonic deformation. Detecting those features requires a clear exposure, but agricultural land use and urbanization of an area also midify tectonic landscape imprints (Almond et al., 2010). In regions with humid climate conditions and periglacial processes, tectonic surface features may be modulated by climatic processes such as fluvial erosion and vegetation (e.g., Bull, 2008). To overcome this problem in the study area, we applied a combination of remote sensing, shallow geophysics and coring, as well as field observations in order to detect any structures of shallow subsurface tectonic activity.

4.1. Geomorphic mapping

To identify surface lineaments that may correlate with subsurface faults, we utilized the new DEM from the TanDEM-X satellite mission (resolution of 12 m/pixel) and

local LiDAR (Light detection and ranging) data (resolution of 1 m/pixel). This dataset was available for 90 km^2. The data have been provided by the *Deutsches Zentrum für Luft- und Raumfahrt* (DLR). High-resolution LiDAR data also have been used for mapping. These data are based on the DGM1 (Digitales Geländemodell) subset with a ground resolution of 1 m/pixel. The data have been provided by the *Bayerisches Landesamt für Vermessung und Geoinfomation* (LVGM). We complemented remote sensing mapping with topographic reconnaissance mapping at the field sites (Fig. 2.3).

4.2. Shallow coring

We conducted two coring campaigns at *Paindlkofen,* using a motorized hand drill with a mud auger 4 cm in diameter and 8 m long rods for the first reconnaissance study. The survey was carried out by the ERLUS AG. They provided a driving core drill rig with rods of 30 cm in diameter and a maximum rod length of 20 m, operated by two tool pushers (Fig. 2.3, 2.4). For each core, the acquired material has been stored. The material has been analyzed using soil science principles and soil color matching based on the Munsell color chart. During drilling, soils and sediments on top of fluvial gravels were penetrated.
All drill cores terminated near the top of the gravels, penetrating those only in the upper centimeters. In total, 13 continuous cores have been drilled in 2007 and 2008 with a spacing of 8 m - 20 m across the suspected scarp (Fig. 2.3).

4.3. Resistivity tomography

Electric resistivity tomography is used to measure the chargeability and the resistivity of geologic units in the field (Prinz and Strauß, 2012; Scheffer and Schachtschabel, 2010). For the study site *Paindlkofen,* the resistivity data have been used to illustrate subsurface structures. The electrodes have been placed along the dirt road (Fig. 2.4). We used the standard four-electrode configuration to measure resistivity and conductivity of near surface sediments. Data were acquired with the Schlumberger array method and a Wenner configuration for cross testing (Fig. 2.5). The electrode spacing had to be dense in order to better resolve vertical structure (Daily et al., 2005). For large distances, the noise level of the Schlumberger array is higher

compared to the Wenner array, whereas the maximum depth is greater with the Schlumberger setting. The initial electrode spacing used at *Paindlkofen* was n = 1 m. The distance was gradually increased to n = 4 m. The Wenner configuration provides a more uniform ground coverage, while the Schlumberger approach produced a higher resolution by contemporaneous increase of the depth resolved. Data processing and visualization was carried out using the Geotomo *RES2DINV* software package.

4.4. Geologic field mapping

We have visited a quarry northeast of the study site *Paindlkofen*. The site *Tunzenberg* is located in a forested area outside the same village. The pit comprises an area of < 0.5 km^2. The site is excavated to a maximum depth of ~ 6 m into the gentle slope of a hill ridge. The pit mine is only temporarily active, resulting in colluvial wedges that cover the bottom exposure of sediments in several places. At both sites, we have mapped sedimentary and soil layers. At *Tunzenberg*, we have additionally carried out a clast habitus and lithology analysis to infer the provenance of the material (See appendix A1).

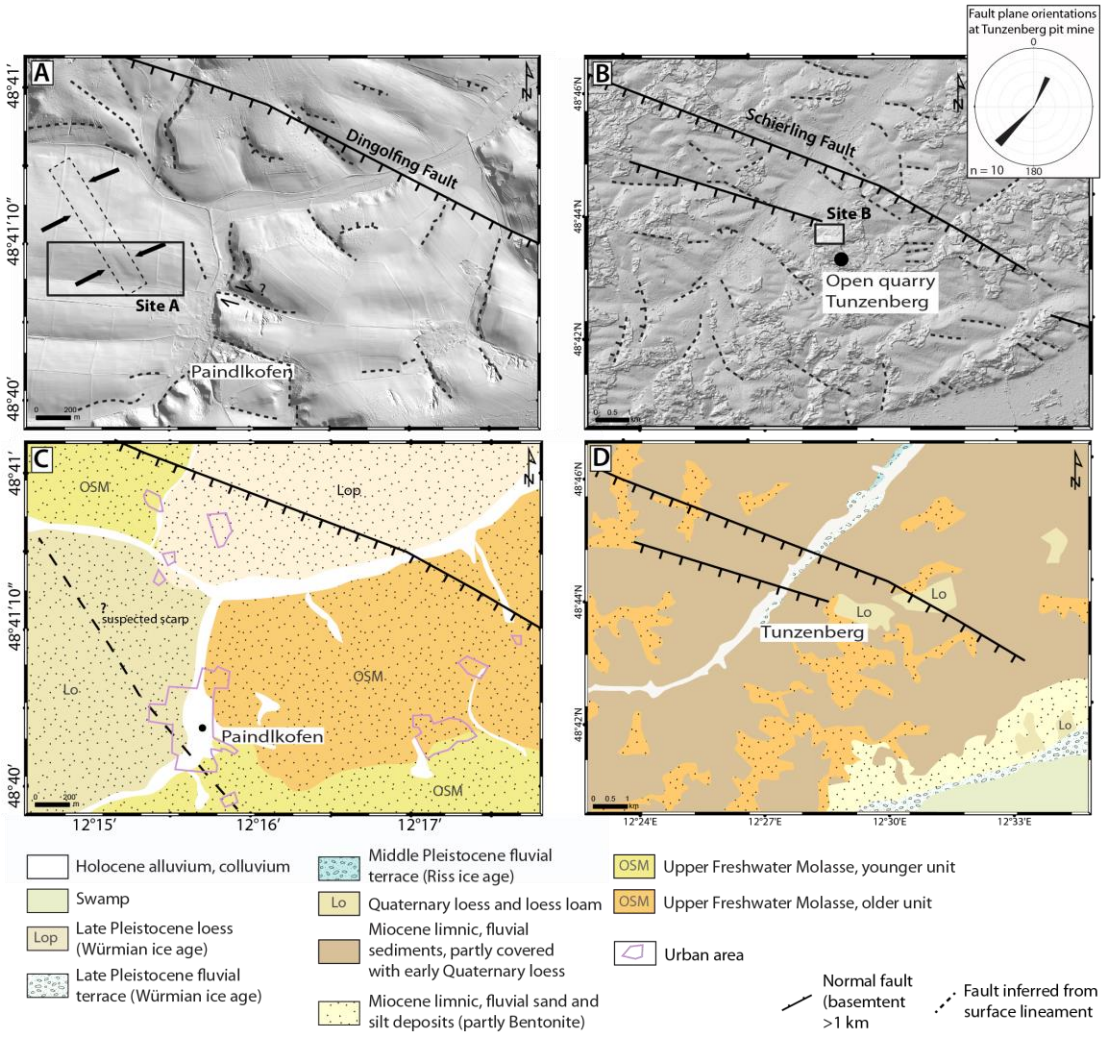

Fig. 2.3: Shaded relief map showing surface lineaments and simplified geology of the study sites *Paindlkofen* and *Tunzenberg*. A) Digital terrain model from LiDAR data, resolution is 1 m/pixel. Provided by the Bavarian Geodetic Service (LVG). The dashed box guided by arrows depicts the potential tectonic scarp. The stereonet inset indicates the orientation of normal fault planes measured at the outcrop. B) Digital terrain model derived from TanDEM-X data, resolution 12 m/pixel, provided by the DLR. C) and D) Geologic maps of the areas compiled from the Geologic maps of Bavaria 1: 500,000 and 1: 200,000, sheet 4.

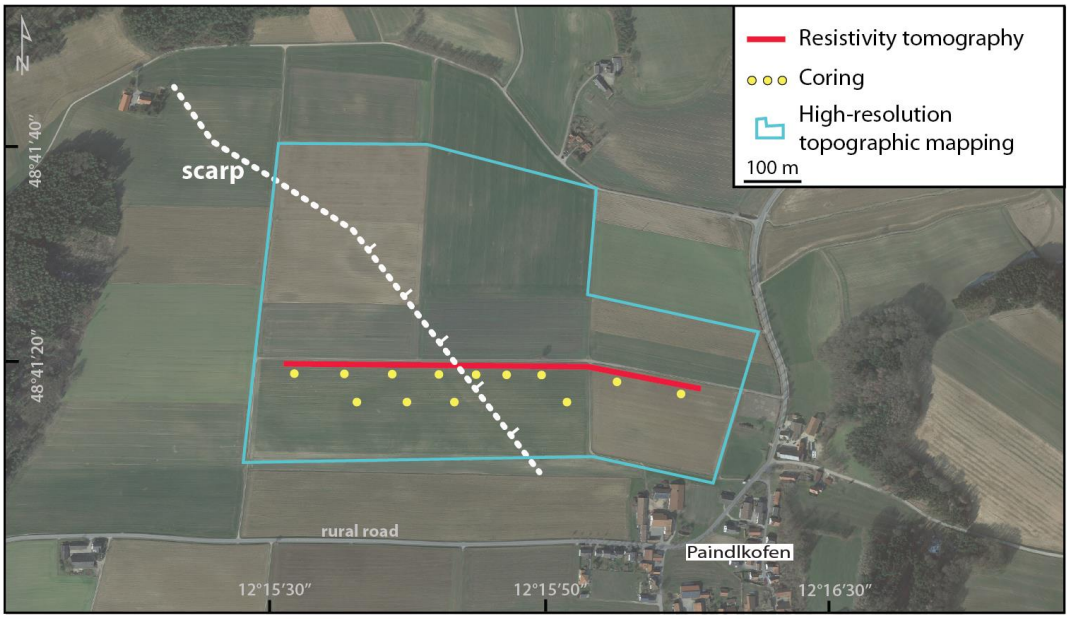

Fig. 2.4: Locations of geophysical and coring measurements at site *Paindlkofen*. White dashed line depicts the inferred scarp of NE dipping normal fault. Background satellite imagery: GeoBasis-DE/BKG, Digital Globe, 2016.

Fig. 2.5: Photo of the drill rig (A) used during the campaign and example of a core (B).

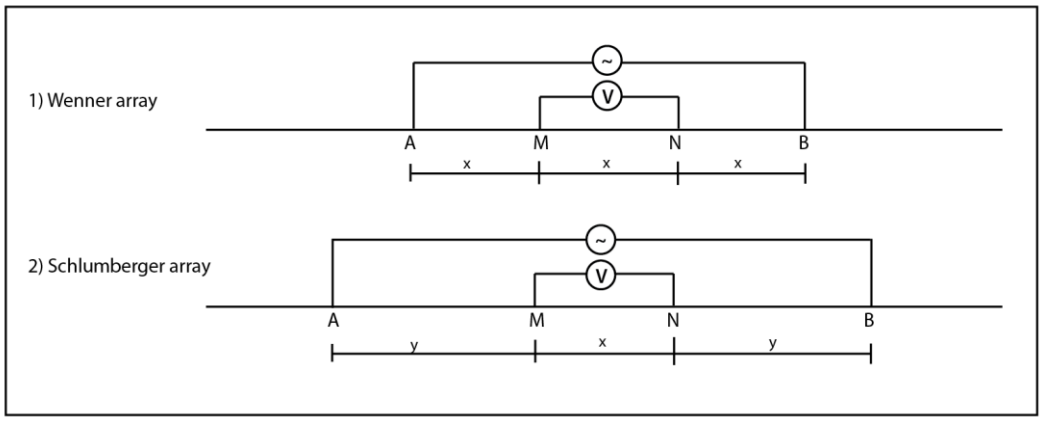

Fig. 2.6: Schematic setup of the Wenner (1) and Schlumberger (2) array in resistivity tomography. 1) A direct current is supplied at A and B, and the potential is measured at M and N. The interval (x) is keep identical when increasing the distance. 2) A direct current is supplied at A and B, and the potential is measured at points M and N. The interval (y) between the measure points increases symmetrically from the midpoint.

5. Results

Results are presented separately for the two sites. For site *Paindlkofen*, we provide data on shallow coring and geophysics, and we show regional observations on lithology. For site *Tunzenberg*, we show indicators of soft sediment deformation. At this site, no geophysical and coring survey has been conducted.

5.1. Study site Paindlkofen

5.1.1. Geomorphic analysis

The mapping based on high-resolution LiDAR imagery revealed a gentle NW-SE trending escarpment across a cropland area outside the village. The structure can be followed for about 0.5 km (Fig. 2.2, 2.7). Topographic field mapping confirms the remotely observed linear feature. In the vicinity, further lineaments are found (Fig. 2.2, 2.7).

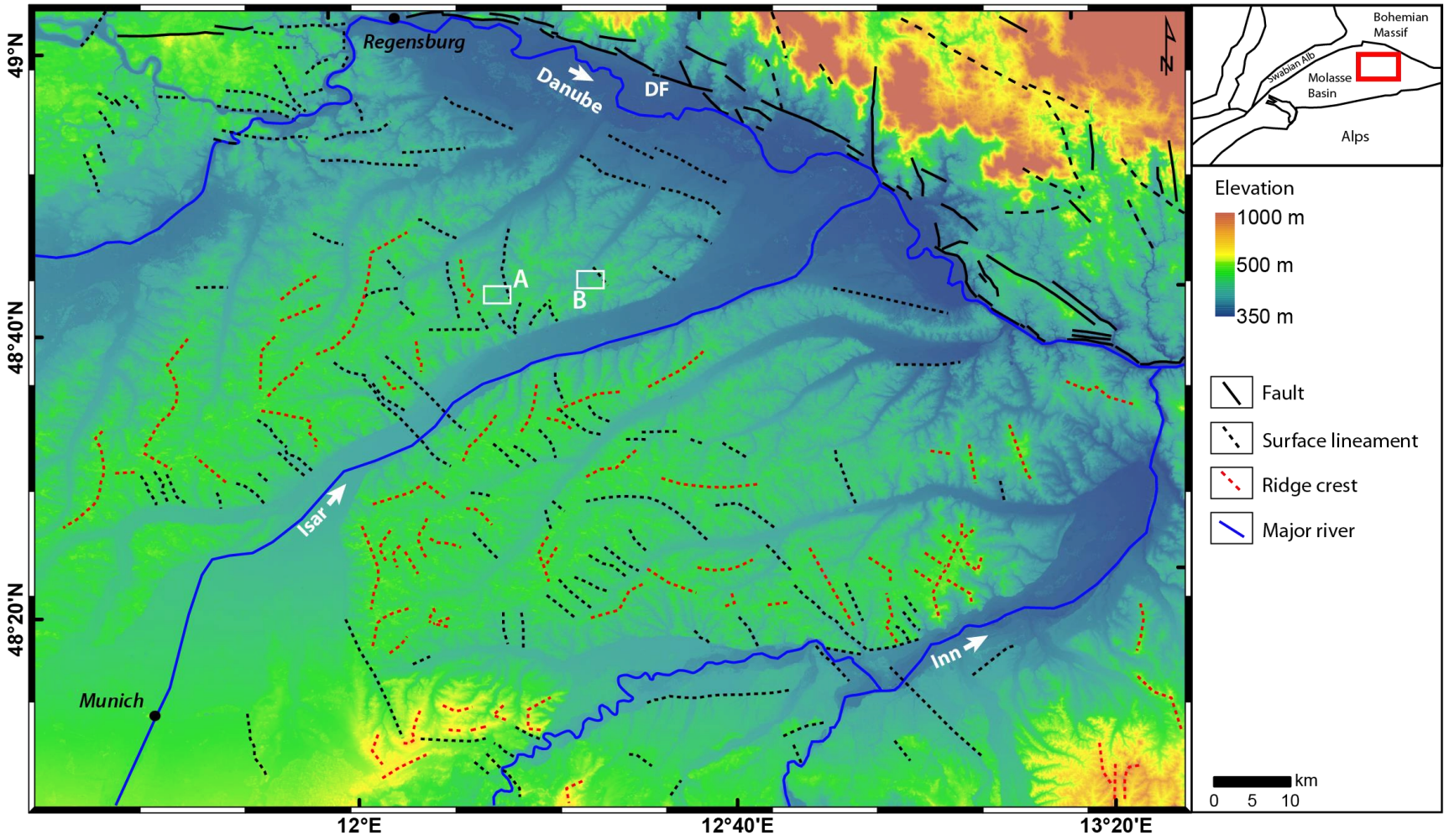

Fig. 2.7: Map showing the Tertiary Hills region and adjacent areas with mapped surface lineaments. Background DEM derived from TanDEM-X data, resolution 12 m/pixel. DF = Danube Fault. A) Study site *Paindlkofen*. B) Study site *Tunzenberg*.

5.1.2. Coring

The coring campaign revealed stratified layers east and west of the scarp. The cores west of the escarpment penetrate the gravel horizon at 5 m – 8 m depth, while the cores on the eastern side reach the gravel 20 m away from the scarp at 6.5 m depth (core B20) (Fig. 2.8, 2.9). In most of the cores, a 10 cm to 30 cm thick, brown-colored Ah horizon (Munsell color 10YR3/4) exists. The horizon consists of silt and clay with homogenously distributed organic material and shows typical color zonation from plowing. The plowing horizon is absent in the cores *2/3*, *6* and *10*. This horizon is underlain by 50 cm to 70 cm thick, silt-bearing loamy loess with calcite concretions. Downwards, the loess loam is decalcified and the silt content decreases to less than 0.5%. The contact to the underlying gravel horizon is gradual over ~ 10 cm, where single clasts mix with the loess loam. The grain size of the gravel horizon varies from coarse sand to gravel. The gravels are well rounded and dominantly consist of quartzite. The few feldspar-rich gravels are moderately to strongly weathered. The thickness of the loess loam deposit ranges from 2.8 m (core B3) west of the contact zone to over 11.8 m (core B2/3) east of it. Here, the gravel horizon has not been reached. The contact orientation is parallel to the inferred offset structure (Fig. 2.8).

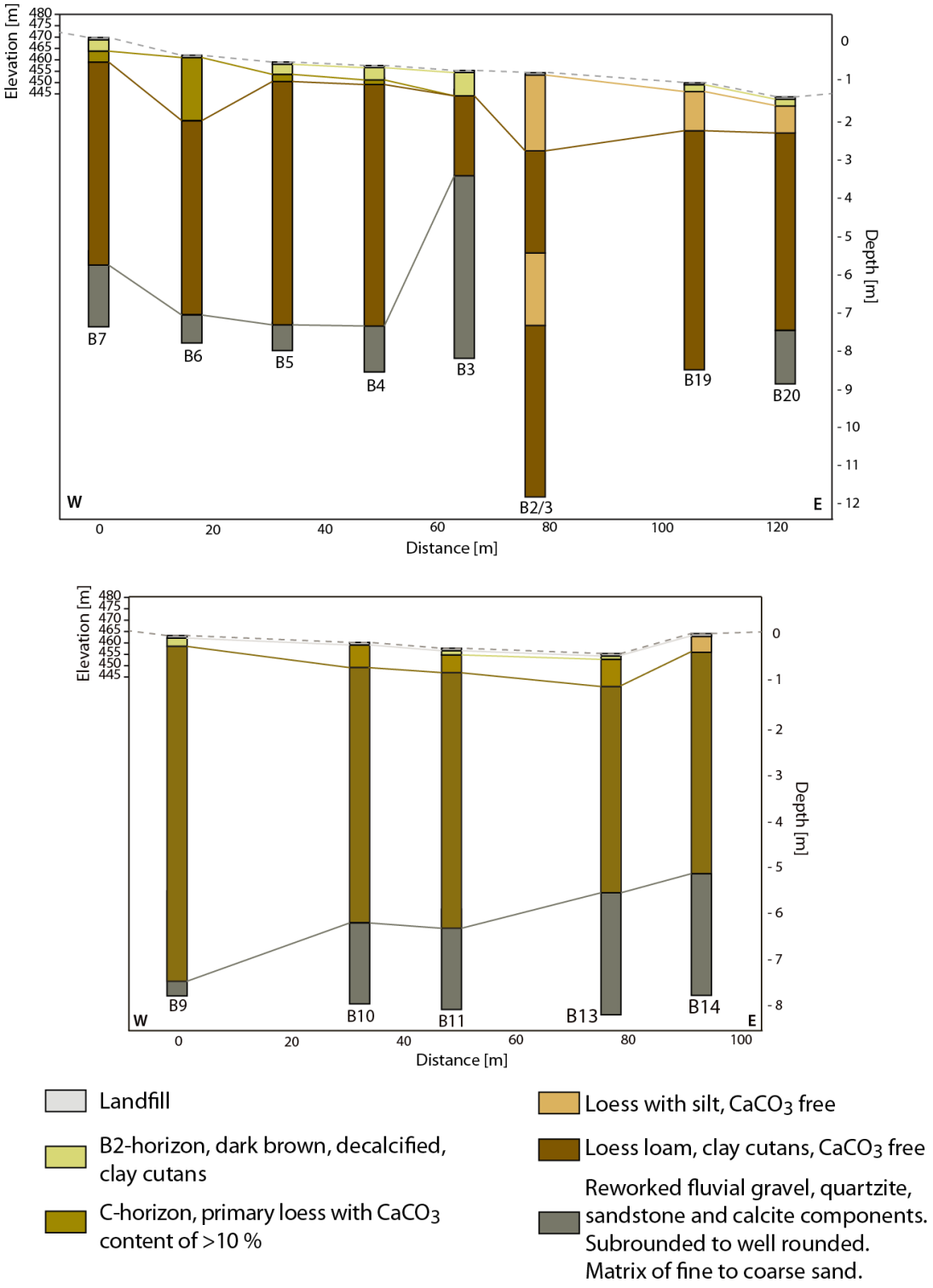

Fig. 2.8: Drill cores along the dirt road at site *Paindlkofen* with principle geology and topography (dashed line).

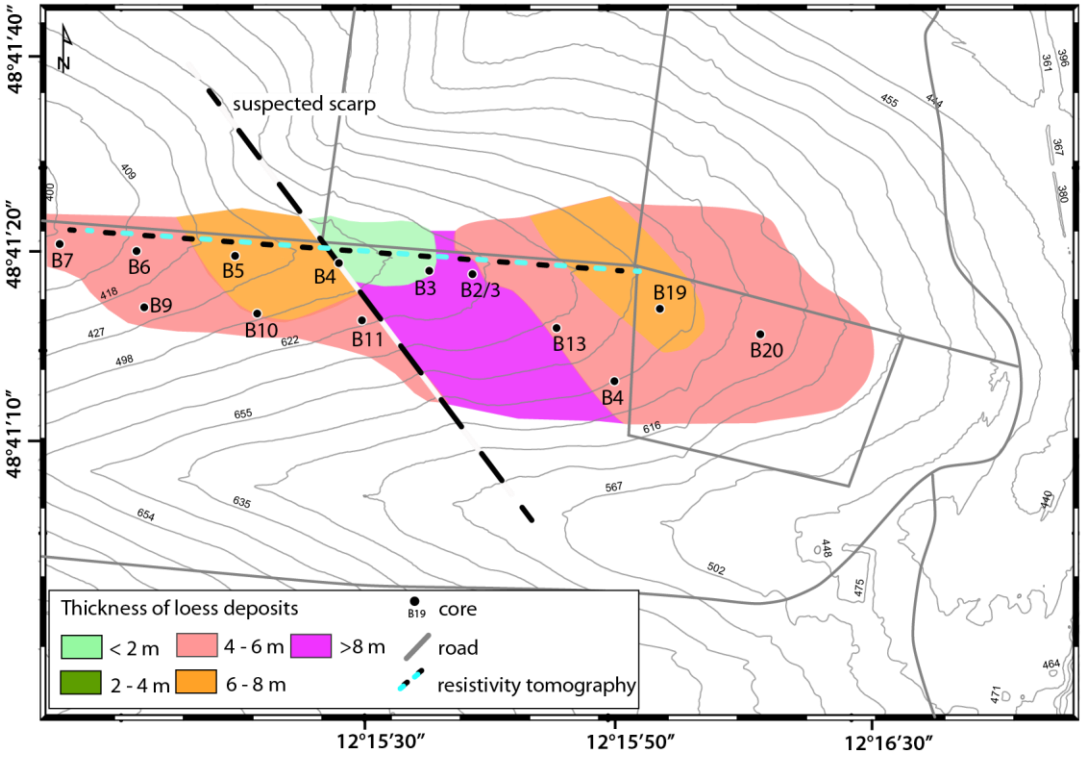

Fig. 2.9: Contour map showing the thickness of the loess loam deposit along the inferred tectonic scarp. Topographic data from the DGM, 1 m resolution, provided by the Bavarian Geodetic survey. Data are compiled from field records of the drill campaigns 2007 and 2008.

5.1.3. Resistivity Tomography

The resistivity tomography revealed a steep E-W-oriented offset of the contact between loess loam deposits and unconsolidated gravel (Fig. 2.10). The lithology has been verified with shallow coring at the site. Resistivity values (RMS: 16.2%) are generally low (40 Ω – 60 Ω, blue colors) at a depth of 10 m – 25 m. In the upper five meters below the surface, the resistivity is very low (5 Ω and 15 Ω). This can be explained by the thick, moist loess loam soils used as cropland described above. The thin layer of higher resistivity-values corresponds to the thin layer of landfill gravel distributed along the dirt road. An abrupt change in resistivity from about 300 Ω to 30 Ω occurs at 200 m on the profile. This is in agreement with the contact between loess loam and gravel deposits exposed in the drill cores.

Across the escarpment, the layers of loess loam (blue and turquoise colors) show an offset of 2 m – 4 m. East of the escarpment, also the gravel deposits (yellow colors) are present about 2 m – 4 m deeper compared to the western side. The eastern end of

the profile is marked by an ancient loess loam pit used by local farmers. Therefore, data closer to the pit are regarded as potentially disturbed and have been excluded.

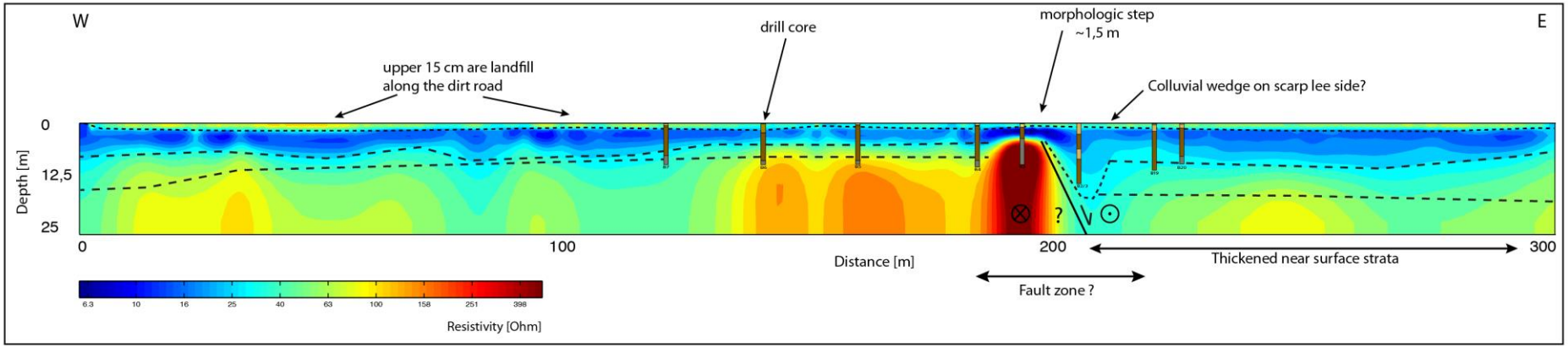

Fig. 2.10: Resistivity tomography (Schlumberger array) and drill cores for reference at site *Paindlkofen*. The inferred geologic layers are indicated by the dashed lines.

5.2. Study site Tunzenberg

5.2.1. Geomorphic analysis

Our mapping shows a general geomorphic trend, where the topographic orientation of individual valleys and ridge crests is oriented in two main strike directions. The direction ~ 300° is parallel to the strike of basement faults in the region, while orientations of ~ 50° – 90° reflect escarpments perpendicular to the basement faults (Fig. 2.2). The drainages along the ridge flanks are about 1 km long.

5.2.2. Geologic field mapping

The investigated outcrop is a small, temporary active pit mine of about 50 m in diameter. It exposes steep, 70° – 85°, mining faces of up to 6 m in height consisting of poorly consolidated sedimentary layers. The gravel pit mine exposes several sedimentary layers that show cm-scale offsets and disturbed wavy layers. The upper-most cover of loess loam comprises an Ah horizon up to 20 cm thick. Below the soil horizon, distinct oxidized remnants of roots are found in almost vertical lines reaching a depth of 1.0 m – 1.5 m. The layers below the root-bearing horizon exhibit an alternating sequence of loess loam and fine-grained sands with coarser, medium to well-rounded clasts of crystalline rocks.

Especially in one area of the pit location, the disturbed bedding of sedimentary layers can be identified (Fig. 2.11). The flame structures truncate the original horizontal sedimentary layering in the upper part of the outcrop. The clast orientation and ripple marks show an eastward direction. In the lower portion of the outcrop, cross-bedding size increases from 10 cm to 30 cm (Fig. 2.11). On the eastern side of the exposed section, an offset of about 3 cm is visible across a 75 cm long cross-bedding structure. Along the offset, the long axis of clasts (diameter 1 cm – 3.5 cm) aligns with the vertical fault offset. A few centimeters away from the fault core, the clasts still show a dip down towards the fault. In the undisturbed parts of the layer, clasts show sub-horizontal bedding. The lithologies and abundance of the fluvial clasts have been analyzed with a raster counting method over several, 1 m^2 wide rectangles along the trench walls. The observed rock units are mainly metamorphic basement rocks (Quarzite, Lydite and Diorite). The clast rounding is medium to good. We compared

the lithological abundance of metamorphic and crystalline rocks with the clasts observed in the drill cores at site *Paindlkofen*. Both show strong similarities and almost no calcareous rocks. The mapping results at *Tunzenberg* show small-scale extensional offsets of fine to coarse-grained silt and sand deposits, about 4 m below surface.

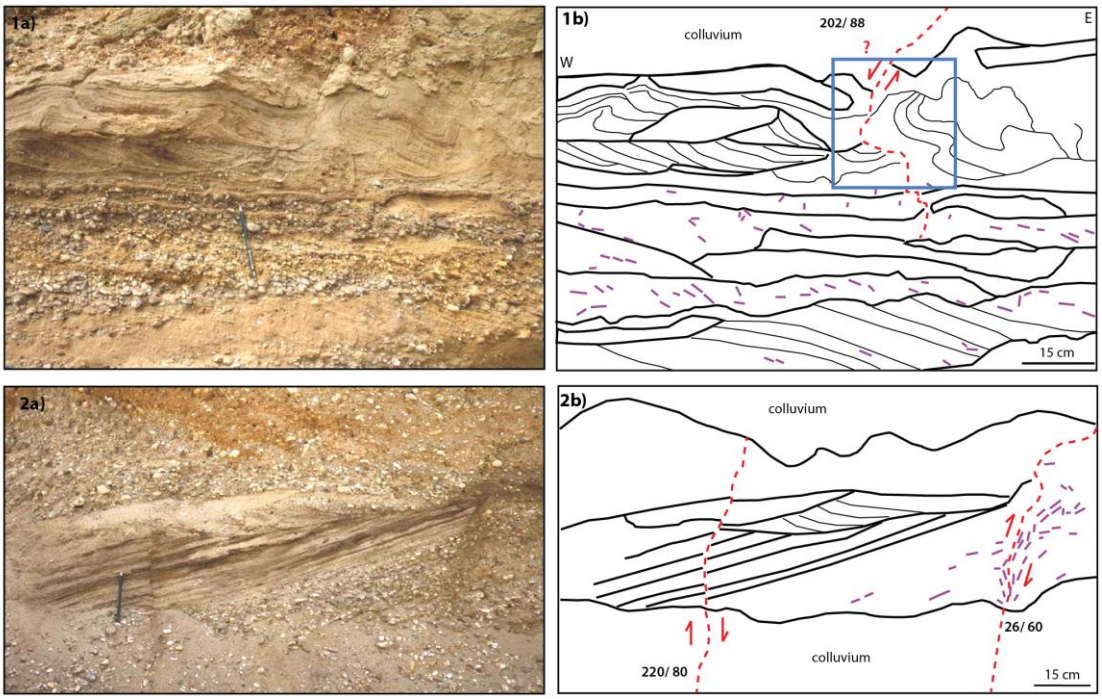

Fig. 2.11: Photo panel showing offset and disturbed sediment structures at site *Tunzenberg*. 1a) Miocene fluvial gravel, and coarse to fine sand deposits are exposed below reworked loess loam and an active soil horizon. 1b) In the mapped section, the central part showing a vertical flame like structure is highlighted by the blue box. Here, sediment bedding is modified and inclined. 2a) Miocene cross-bedded fine sand with overlain by Miocene fluvial coarse sand and gravel. 2b) The mapped section reveals ~ 3 cm offsets of the layers. The upper and lower most parts of the outcrop are covered with a colluvial wedge. Both outcrops reveal Calcite and Quartzite clasts of diameters between 2 cm and 6 cm. The clasts are digitally mapped by their longitudinal axis (1b, 2b). The orientation of the line (purple) indicates the clast orientation embedded in the sedimentary layer. Outcrop 1) reveals normal stream controlled bedding. At outcrop 2), the clast orientation has been secondary aligned to the fault, visible by the dipping downward orientation.

6. Interpretation

The results from mapping of the TanDEM-X and LiDAR datasets reveal numerous asymmetric valleys and lineaments in the surface morphology of the Tertiary Hills region. The strike directions of the surface lineaments agree with the basement fault orientation (Fig. 2.1), which we interpret as an indicator of tectonic activity.

At *Paindlkofen,* the observed structure turned out to be a likely candidate to result from active tectonics. For the site *Tunzenberg,* the identification of linear escarpments was limited by the technical details of the TanDEM-X dataset, which images buildings and forested areas, masking potential small-scale structures of < 10 m, especially in forested areas. However, we interpret the vertical alignment of clasts observed at Tunzenberg (Fig. 2.11) as fault related.

The investigated offset at *Paindlkofen* lies close to the Dingolfing fault (Fig. 2) and dips towards the NE with c. 70°. About 5 km south of the Dingolfing fault, another basement structure dipping to the NE marks the southern end of a small graben in the area. Our geophysical, shallow coring and geologic field mapping results at site *Paindlkofen* suggest a fault-related offset of the gravel layers. The conductivity and the core data match a steep linear scarp structure striking ~ 318° NW, which coincides with the main strike direction of the major fault systems of the Landshut-Neuötting-Fault and the Dingolfing Fault.

The northeastern side of the detected structure appears to be the hangingwall of the that dips with about 75° - 80° towards 48° NE. The corresponding footwall on the western side is characterized by the shallower depth of the gravel horizon. However, the resistivity approach does not exactly image the real structures at depth. The RMS of 16.2% for the Schlumberger array changes for different settings, and we also had to deal with variations in ground coupling due to different soil moisture and pore space. The scarp visible in the topography has been modified by intense land use and might not reflect the initial morphology, and although high-resolution LiDAR data have been used, no additional surface structure has been identified. Finally, the coring we carried out at the site turned out to deliver the most reliable data to infer an offset of unconsolidated loess, sand and gravel deposits. In this context, the main marker horizon which can also be identified in the changing resistivity, is the gravel unit forming the base of the coring data. We attribute the strong deepening of the contact between the loess loam and gravel deposits within < 5 m to tectonics.

The coring results are essential to locate the offset zone and differentiate near- and far-field zones of the potential scarp at site *Paindlkofen*. The locally increased content of silt found in drill core B2/3 right at the hangingwall of the escarpment indicates that fluvial surface deposits of silt and sand have been eroded and re-deposited as colluvium. The sediments above and below the silty section are uniformly composed of loess and loess loam. Gravel deposits with a sandy matrix are below the depth of coring at this position.

Both examples suggest surface faulting of late Miocene age for site *Tunzenberg* and early Pliocene to Quaternary for site *Paindlkofen*. The upper part of the accumulated loess loam at site *Paindlkofen* is most likely of Quaternary age, and the thickest deposit of > 8 m occurs on the lee side of the detected escarpment. Therefore, the escarpment has either formed before the loess accumulated, which could be late Miocene according to the offsets in the gravel deposits, or it has formed by renewed Quaternary tectonic activity, which has also offset the loess deposit. However, the deposits lack absolute radiocarbon dating, and paleo soil horizons are too sparsely distributed to infer a precise age for the site. Based on archeological data from the region, the uppermost meters of loess loam deposits are 6,500 – 7,000 years old. However, this does not necessarily reflect the age of the deposits found here. At the archeological sites, a soil erosion of at least c. 2 m has been inferred since c. 7,000 b.p. We could not determine whether erosion has affected our two study sites similarly, because of lacking age constraints. Though, if the potential local erosion at Tunzenberg was higher, the deposits could be older.

7. Discussion

For the observed structures at the two study sites, we consider an overprint by climatic processes like soil creep. The effect of soil creep is significant in permafrost settings, where during warm periods the water-saturated soils on the southwestern side (northern hemisphere) get mobilized by thawing and gravitational sliding. On the sun-averted site, the frozen ground remains mostly undisturbed. For the Tertiary Hills region, permafrost and the described mobilization has been reported (Jerz, 1993). The study site *Paindlkofen* shows an increase in loess loam thickness at the northeastern side of the small hill. If the climatically controlled hillslope diffusion would be the only factor controlling the morphology at the site, the northeastern hill flank should be less affected. This is opposite to our observation. Therefore, we rule out to observe only soil creep here, but an erosional overprint from mobilization by snow accumulation on the colder, sun-averted side still has to be expected (Wende, 1995).

The loess sediments are thickest right at the contact with > 8 m, but the mean thickness on the hangingwall (east) and the footwall (west) is almost uniform between 4 m and 6 m. The increase in sediment thickness is sharply bound by the scarp. A solely climatic formation, where loess is distributed in e.g., former fluvial channels and on shallow initial topography by wind deposition and 2nd order soil mobilization, would show more homogeneous thicknesses (Leger, 1990), and cannot explain the offset in the gravel layer. Therefore, based on the steep and narrow contact zone, we rule out to only observe a climatic effect of loess deposition. However, climatic processes and regional soil erosion have overprinted the original topography, as seen by numerous fluvial channels and swamps in the area. The dimensions of the modern channels at the narrow valley floors do not exceed widths of 5 m – 10 m and a depth of > 3 m.

Channel systems, which show a similar strong linear and parallel pattern, have been observed in the vicinity of Paindlkofen. However, local mapping reveals that the inferred fault is oriented oblique to fluvial channels nearby. We therefore rule out to simply observe remnants of a large fluvial system. The present-day topography of the site on a shallow hill is unlikely part of a large and deep channel that was occupying the region. From our geomorphic mapping, we do not see evidence for this scenario.

At site *Tunzenberg*, the dense vegetation and the therefore unclear topographic situation prevented a detailed geophysical and coring based analysis. The exposed offsets in the quarry, however, revealed a tectonic history of the Miocene fluvial sediments. The strongly weathered and gravitationally modified upper part of the pit mine prevented us from observing offsets in the Pleistocene and Holocene sediments.

Our study revealed fluvial sand and gravel-deposits, with material that has been transported from the Bohemian Massif (see A1) into the basin in the latest Miocene, before the Danube was occupying the region. The observed sand and gravel lenses with offsets on the order of 2 cm – 5 cm and flame-like structures at the same scale could result from co-seismic or non-seismic origin (Obermeier, 1996). The fault planes strike 220° to 250° NE-SW. This is about the Riedel angle relative to the main fault orientation of the Schierling fault (striking 100° - 115° NW-SE, Fig. 2.2). However, a permafrost overprint is capable of producing similar flame structures by soil creep and freezing and thawing (Obermeier, 1996). The Tertiary Hills have been part of the periglacial region of the Alpine foreland basin with distributed permafrost (Jerz, 1993).

However, the small-scale extensional offsets ~ 4 m below surface are not anywhere near a local ice wedge or sagging structures. We therefore rule out to observe simple soil disturbance based on climatic variations at this location.

The lithological composition of the gravel deposits at both sites indicates a source area in the Bohemian Massif, since crystalline metamorphic rocks dominate against only three limestone pebbles found during our campaign. This provides an age control of the deposits, because fluvial transport with headwaters in the Bohemian Massif area reached the Tertiary Hills region only until the late Miocene (Bader, 1982a; Lemcke, 1988; Villinger, 1989). After the late-Miocene deposition, the fluvial deposits could have also been reworked into younger terraces. Therefore, the offsets at *Paindlkofen* and *Tunzenberg* could be younger than late Miocene.

Furthermore, the observed lineaments in late Miocene and Quaternary sediments are consistent with a tectonic origin, which is supported by the investigated high-angle offsets in aeolian and fluvial sediments. Both indications of active tectonics are located in the vicinity of the projected surface traces of normal faults documented at a depth of ~ 1 km (Unger, 1999a; Unger and Schwarzmeier, 1982).

Based on our results, we suggest that the landscape of the Tertiary Hills is best described as a tectonically active composite landscape (Fig. 2.13) that is a composition of the climatically controlled surface evolution (Fig. 2.12) with tectonic activity. The composite nature in our case includes tectonic surface modification as well as climatic overprint. The schematic, step-wise evolution of the Tertiary Hills based on tectonic surface shaping, is illustrated in Fig. 2.13. Here, the data from the two study sites show how the composite landscape evolves over time and its complexity increases. This enables us to suggest surface faulting and masking by climatic overprint for post Miocene tectonics in the Tertiary Hills (Fig. 2.13).

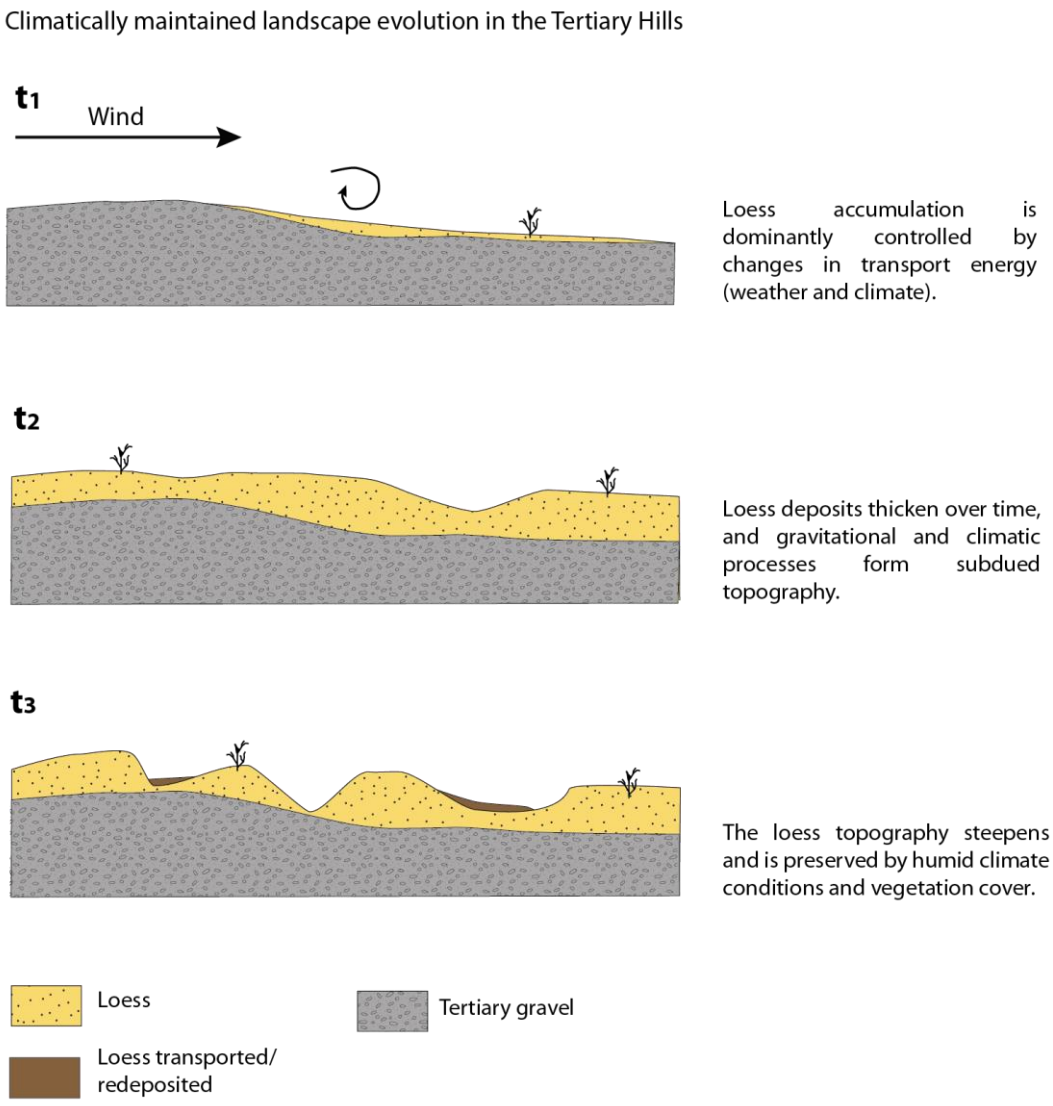

Fig. 2.12: Schematic sketch of principle features of a climatically controlled loess landscape. The landscape is characterized by ongoing deposition of loess that is later reworked and transported by fluvial and gravitational processes.

7.1. Composite climatic landscape (Fig. 2.12):

The currently accepted model of landscape evolution in the Tertiary Hills is based on climatic drivers. Here, the initial landscape inherits smooth variations due to gravitational and fluvial reworking of sand and gravel (t_1). The wind-transported loess is deposited by changes in wind transport energy, and the loess cover thickens over time (t_2). Then, ongoing surface processes from fluvial transport, land sliding and precipitation modify the landscape producing asymmetric valley flanks. However, the subsurface remains undisturbed by this process.

7.2. Composite tectonic landscape (Fig. 2.13):

An alternative explanation for the present-day landscape in the Tertiary Hills is presented here. In our model, multiple factors contribute to shaping the asymmetric landscape. At time t_1, an initial scarp forms, which has been formed by surface faulting. The scarp acts as a new barrier to loess-transport by wind that accumulated on the lee side. At the time t_2, loess has accumulated to form a horizon and the surface is characterized by a smoothed topography typical for loess landscapes e.g., the chinese loess plateau (Liu et al., 1991). The preexisting fault scarp is inherited without any surface modification. At step t_3, the formation of topsoil and growing vegetation stabilizes the loess landscape, and precipitation enhances the decalcification of the upper loess layers. Enrichment of calcite nodules and manganese groundwater horizons can now be observed. At time t_4, the fault system is reactivated and produces a new surface scarp, offsetting the accumulated loess deposits. This escarpment is now prone to enhanced erosion, which is accelerated in unconsolidated loess deposits. The scarp, rapidly degrades and erosion products of fluvial silt and sand deposits are trapped in the zone of the colluvial wedge. The material above the offset gravel deposit is uniform resulting in footwall, hangingwall and colluvial wedge consisting of a similar lithology. At time t_5, the degradation of the fault scarp has acted to completely level the escarpment. The new surface has reached steady state conditions that effectively mask the fault event. In general, the degradation of surface escarpments in moderate to humid climate zones is a fast process acting on the decadal time scale (Wallace, 1977). In our opinion, the

tectonically controlled composite landscape model (Fig. 2.13) is consistent with the largest number of available observations.

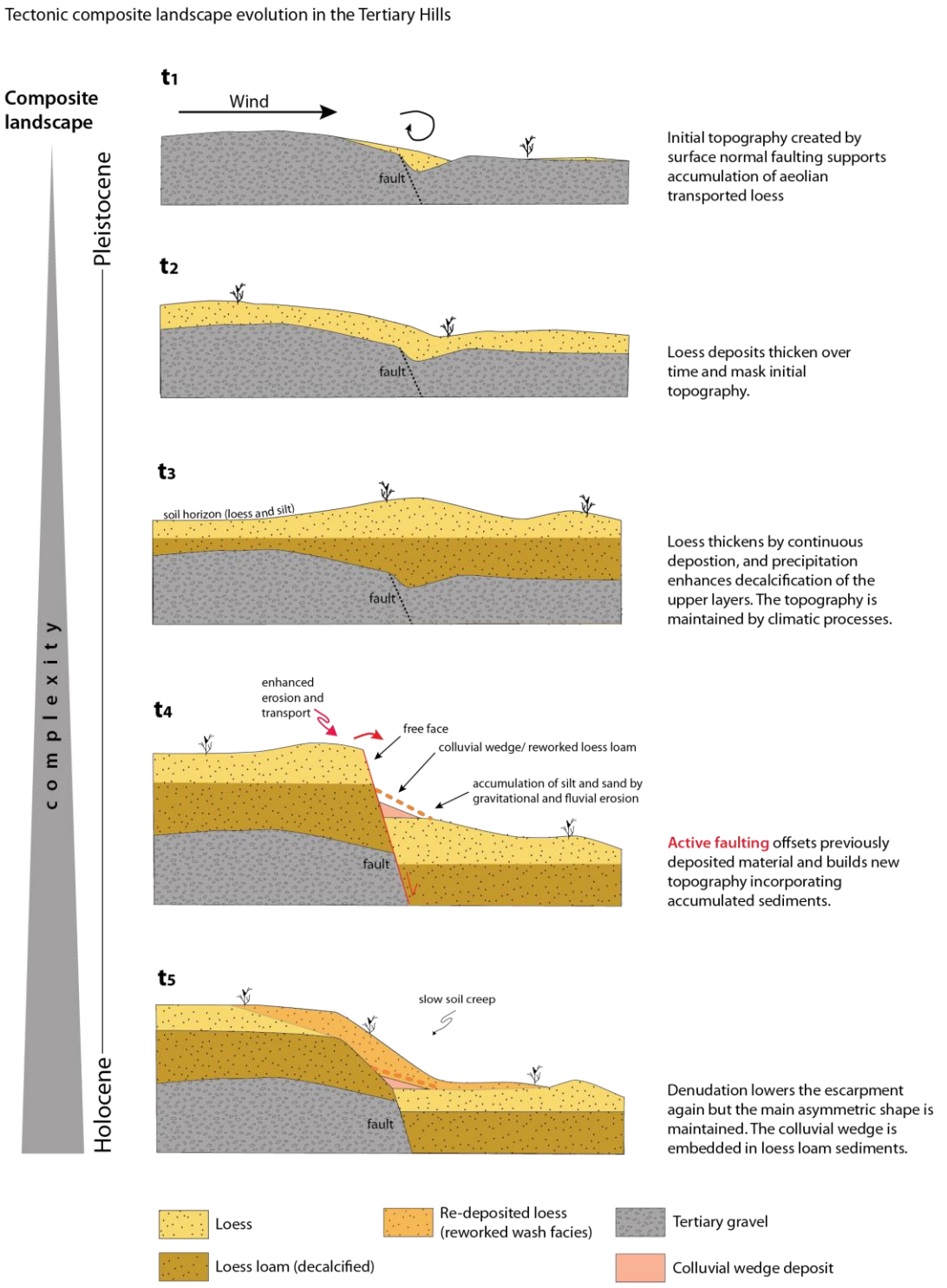

Fig. 2.13: Schematic sketch of principle features in a tectonically controlled landscape with inherited topography. The landscape is characterized by ongoing deformation of multiple tectonic overprints. Loess accumulates along the surface escarpments.

The Tertiary Hills are likely to be influenced by young tectonics. The strike of the lineaments and the surface escarpment at site *Paindlkofen* is oriented parallel to the direction of the geodetic velocity field across the Alps and the foreland basin (Tab. 2.3).

The observed normal fault offsets at *Tunzenberg* only show a small vertical component of several centimeters. A lateral component cannot be deciphered from the observations. The strike of the fault offsets is about perpendicular to the Schierling normal fault, located c. 1.5 km north of the site (Fig 2.2). There is no evidence that the documented normal fault 2 km northwest is extending into the area of the quarry. Therefore, the offsets cannot be linked directly to one of the basement structures and could potentially result from a near surface fault that is undocumented.

Moreover, gravitational processes along the hill flank where site *Tunzenberg* is located, can potentially be responsible for the extensional offsets detected. Therefore, we cannot completely rule out a sedimentary origin by e.g., gravitational subsidence.

The contribution from preexisting topography within the gravel layer cannot be deciphered by our data. If the initial topography accounts for parts of the offset > 4-m-offset, the contribution from faulting would be less, accordingly. However, a tectonic shaping of the surface could still be inferred. For example, a strike-slip regime that produces very small offsets (Wallace, 1977) could possibly explain the inferred tectonic regime in the Tertiary Hills region (Unger, 1999a; Unger and Schwarzmeier, 1982, 1987). This is again in agreement with the expected deformation pattern in the present-day oblique, NW directed eastern Alps GPS velocity field (D'Agostino et al., 2008; Tesauro et al., 2005; Vrabec et al., 2006; Tab. 2.3).

The present-day geodetic signal across the Eurasia-Adriatic plate boundary indicates shortening. Simultaniously, the NAFB basement faults are regarded as inactive since the Miocene, based on the youngest detected subsurface offsets (Unger, 1999a; Unger and Schwarzmeier, 1982, 1987). If shortening occurs at the southern basin margin, potential deformation could also be absorbed by the structures of the Northern Calcareous Alps. This might have caused the documented young displaced deposits (Tab. 2.1).

However, deformation may also be accommodated by faults in the Tertiary Hills. The fact that the Tertiary Hills currently appear to be aseismic can also result from very long recurrence intervals, as observed in intraplate settings (e.g., Braile, 1982).

Although numerous faults and current plate motion are known, still the connection between the existing faults and the present-day topography is uncertain in the NAFB. Furthermore, the observed > 4 m offset of unconsolidated loess loam against fluvial gravel is unlikely to be the result of a single event. The required minimum moment magnitude to rupture the near surface strata would have to be on the order of > 6.5 for a normal fault and > 6.9 for a strike slip fault (Wells and Coppersmith, 1994). The corresponding rupture length would exceed 30 km. This is a structure length that could only be reached if multiple surface lineaments in the area would be connected to a continuous fault plane. We do not have clear evidence for this assumption, even though some of the mapped lineament structure suggests this (Fig. 2.3, 2.7). A 4-m-offset can also form by gravitational mass movement and hillslope diffusion processes (Burbank and Anderson, 2001). We consider these processes as likely to have contributed during the formation of the surface escarpment. Since the unconsolidated loess loam and gravel deposits are not layered, colluvial deposist of non-tectonic origin are potentially present.

Our preferred explanation for the displaced loess loam and gravel deposit here is a cumulative offset (Fig. 2.12), like observed for other tectonic systems in similar humid climate conditions (Vanneste et al., 2001). However, since the region is composed of homogeneous Pleistocene and Quaternary loess loam deposits underlain by fluvial gravel, the identification of a tectonic contact at depth remains challenging, because of the limited reflectors in shallow geophysics.

8. Conclusions

We found numerous geomorphic features, which formed by a combination of tectonic and climatically-induced processes. In the Tertiary Hills region, the observed asymmetric loess deposits can be explained by accumulation along pre-existing fault scarps. Also, surface lineaments detected on high-resolution DEMs match the geometry of basement faults, and the subsurface offsets we detected at the study sites *Paindlkofen* and *Tunzenberg* can be linked to inferred faults by the similar geometry.

The dominating mechanism that shaped the late Quaternary landscape evolution in the Tertiary Hills is likely tectonics. While the regional landscape evolution is overprinted by climatically influenced base-level lowering and consequent head ward erosion of river systems, the local scale tectonic activity mainly contributed to the asymmetric Tertiary Hills. In this context, our new data help to locate and link topography with basement faults in the NAFB.

However, to strengthen this hypothesis, detailed studies are required in order to precisely image the surface and subsurface connection. Promising results are expected from new high-resolution seismic campaigns, supplemented by drilling.

Our approach of utilizing the new TanDEM-X data to study lineament orientations and additional low cost field surveys help to locate the target areas for further research. Once a fault has been identified, paleoseismological studies will enable quantification of timing and magnitudes of events. Clearly more mapping, synthesis and seismic campaigns are needed – unless industry-based data recently compiled in GeoMol (2015) do contain better data.

9. Acknowledgements

MH acknowledges salary from the Helmholtz Alliance Project - HGF, Remote sensing and Earth System Dynamics, WPG9 – Geological context of tectonically active but seismically inactive regions, awarded to AMF. The authors acknowledge LMU for financial support of field work.

10. References

Almond, A., Whitman, Z., Cockcroft, M., Wilson, T., Eger, A., Nobes, D., Shanhun, F., and Moot, D., 2010, Agricultural land rehabilitation following the 2010 Darfield (Canterbury) Earthquake: a preliminary report: Bulletin of the New Zealand Society for Earthquake Engineering, v. 43, p. 432.

Bachmann, G. H., Dohr, G., and Müller, M., 1982, Exploration in a Classic Thrust Belt and Its Foreland: Bavarian Alps, Germany: AAPG Bulletin, v. 66, no. 12, p. 2529–2542.

Bader, K., 1982a, Die Verbauung von Ur-Isartälern durch die Vorlandvergletscherung als Teilursache der anomalen Schichtung des Quartärs in der Münchener Ebene.: Mittl.Geograph.Ges. München, v. 67, p. 5–20.

Braile, L., 1982, An Ancient Rift Complex and its Relation to Contemporary Seismicity in the New Madrid Seismic Zone: Tectonics, v. 1, no. 2, p. 225–237.

Bull, W. B., 2008, Tectonic geomorphology of mountains: a new approach to paleoseismology, John Wiley & Sons, p. 311–324.

Burbank, D., and Anderson, R., 2001, Tectonic Geomorphology, p. 2–211.

Calais, E., DeMets, C., and Nocquet, J. M., 2003, Evidence for a post-3.16-Ma change in Nubia–Eurasia–North America plate motions?: Earth and Planetary Science Letters, v. 216, no. 1–2, p. 81–92.

D'Agostino, N., Avallone, A., Cheloni, D., D'anastasio, E., Mantenuto, S., and Selvaggi, G., 2008, Active tectonics of the Adriatic region from GPS and earthquake slip vectors: Journal of Geophysical Research: Solid Earth, v. 113, no. B12, p. 1–19.

Daily, W., Ramirez, A., Binley, A., and LaBrecque, D., 2005, Electrical resistance tomography–theory and practice: Near-Surface Geophysics, Investigations in Geophysics, v. 13, p. 525–550.

Füchtbauer, H., 1964, Sedimentpetrographische Untersuchungen in der älteren Molasse der Alpen.: Eclogae geol. Helv. Basel, v. 57, p. 157–298.

Ganss, O., 1968, Erläuterungen zur Geologischen Karte von Bayern, 1:25k, Blatt Traunstein: Bayerisches Geologisches Landesamt, p. 9–337.

Genser, J., Cloething, S. A. P. L., and Neubauer, F., 2007, Late orogenic rebound and oblique Alpine convergence: New constraints from subsidence analysis of the Austrian Molasse basin: Global and Planetary Change, v. 58, p. 214–223.

Heermann, O., 1954, Erdölgeologische Grundlagen der Aufschlussarbeiten im Ostbayerischen Molassebecken: Bull. Ver. Schweiz. Petrol.-Geol. u. Ing., v. 21, no. 60, p. 5–22.

Heidbach, O., Tingay, M., Barth, A., Reinecker, J., Kurfeß, D., and Müller, B., 2008, The World Stress Map database release 2008: GFZ Potsdam, p. 3–15.

Janoschek, R., 1961, Über den Stand der Aufschlußarbeiten in der Molassezone Oberösterreichs: Erdöl-Zsch, v. 77, p. 161–175.

Jerz, H., 1993, Das Eiszeitalter in Bayern - Erdgeschichte, Gesteine, Wasser, Boden, Stuttgart, E. Schweizerbart'sche Verlangsbuchhandlung, Geologie von Bayern II.

Jin, J., Aigner, T., Luterbacher, H. P., Bachmann, G. H., and Müller, M., 1995, Sequence stratigraphy and depositional history in the south-eastern German Molasse Basin: Marine and Petroleum Geology, v. 12, no. 8, p. 929–940.

Kraus, L., 1969, Erdöl- und Erdgaslagerstätten im ostbayerischen Molassebecken: Erdöl-Erdgas-Zeitschrift, v. 85, p. 442–454.

Kuhlemann, J., and Kempf, O., 2002, Post-Eocene evolution of the North Alpine Foreland Basin and its response to Alpine tectonics: Sedimentary Geology, v. 152, p. 45–78.

Leger, M., 1990, Loess landforms: Quaternary International, v. 7, p. 53–61.

Lemcke, K., 1974, Vetikalbewegungen des vormesozoischen Sockels im nördlichen Alpenvorland Perm bis zur Gegenwart?: Eclogae Geologicae Helvetiae, v. 67, no. 1, p. 121–133.

-, 1988, Das bayerische Alpenvorland vor der Eiszeit, p. 1–175.

Leopold, M., and Völkel, J., 2007, Quantifying prehistoric soil erosion—A review of soil loss methods and their application to a Celtic square enclosure (Viereckschanze) in Southern Germany: Geoarchaeology, v. 22, no. 8, p. 873–889.

Leydecker, G., 2011, Erdbebenkatalog für Deutschland mit Randgebieten für die Jahre 800 bis 2008, Geologisches Jahrbuch Reihe E, Volume Band E59, p. 1–198.

Liu, D., Ding, Z., and Guo, Z., 1991, Loess, environment, and global change. Science, Science Press, p. 1–288.

Mayr, M., 1957, Geologische Untersuchungen in der ungefalteten Molasse im Bereich des unteren Inn: positionsblätter Simbach a. Inn 653 und Julbach 652 Ostteil.

Mühlfeld, R., 1968, Photogeologische Beobachtungen zum Sedimentaufbau und zur Tektonik im ostbayerischen Molassebecken zwischen Landshut und Eggenfelden: Geol. Jb., v. 85, p. 285–298.

Obermeier, S. F., 1996, Use of liquefaction-induced features for paleoseismic analysis — An overview of how seismic liquefaction features can be distinguished from other features and how their regional distribution and properties of source sediment can be used to infer the location and strength of Holocene paleo-earthquakes: Engeneering Geology, v. 44, no. 1–4, p. 1–76.

Oeltzschner, H., 1965, Geologische und sedimentpetrographische Untersuchungen auf Blatt Vilsbiburg 7540 (Niederbayern): Univ. München, 101 S., 39 Abb. p. 1–101.

Penck, A., and Brückner, E., 1909, Die Alpen im Eiszeitalter, Tauchnitz, p. 1–1157.

Prinz, H., and Strauß, R., 2012, Ingenieurgeologie, Springer Verlag, p. 1–650.

Reinecker, J., Tingay, M., Müller, B., and Heidbach, O., 2010, Present-day stress orientation in the Molasse Basin: Tectonophysics, v. 482, no. 1–4, p. 129–138.

Roll, A., 1952, Der unmittelbare Nachweis des Vindelizischen Rückens unter der süddeutschen Molasse: Geologische Rundschau, v. 40, no. 2, p. 243–248.

Scheffer, F., and Schachtschabel, P., 2010, Lerhbuch der Bodenkunde, Spektrum Akademischer Verlag Heidelberg, v. 16. Auflage, 1–481.

Schmid, S. M., Pfiffner, O. A., Froitzheim, N., Schönborn, G., and Kissling, E., 1996, Geophysical-geological transect and tectonic evolution of the Swiss-Italian Alps: Tectonics, v. 15, p. 1036–1064.

Schmidt-Thomé, P., 1955, Zur Frage quartärer Krustenbewegungen im Alpen-und Voralpengebiet des Isartalbereichs: Geologische Rundschau, v. 43, no. 1, p. 144–158.

Schwarzmeier, J., 1981b, Tektonik der Süddeutsches Großscholle.- In: Bayerisches Geologisches Landesamt [Hrsg.]: Erläuterungen zur Geologischen Karte von Bayern 1:500 000. – 3. Aufl., München, p. 97–101

Streit, R., 1979, Fig. 10.

Tesauro, M., Hollenstein, C., Egli, R., Geiger, A., and Kahle, H.-G., 2005, Continuous GPS and broad-scale deformation across the Rhine Graben and the Alps: International Journal of Earth Sciences, v. 94, no. 4, p. 525–537.

Unger, H. J., 1999a, Die tektonischen Strukturen der bayerischen Molasse: Documenta naturae, v. 125, p. 1–16.

-, 1999b, Zur lithostratigraphisch-nomenklatorischen Verknüpfung von Ost-und Westmolasse in Bayern: Documenta naturae, v. 125, no. 17–45.
-, 1999c, Die Geisenfeld-Abfolge. Gedanken zur pliozänen Entwässerung der bayerischen Molasse.: Documenta naturae, v. 125, no. 57–97.
Unger, H. J., and Schwarzmeier, J., 1982, Die Tektonik im tieferen Untergrund Ostniederbayerns: Bayerisches Geologisches Landesamt.
-, 1987, Bemerkungen zum tektonischen Werdegang Südostbayerns: Geol. Jb., v. A105, p. 3–23, p. 197–220.
Vanneste, K., Verbeek, K., Camelbeeck, T., Puaulissen, E., Meghraoui, M., Renardy, F., Jongmans, D., and Frechen, M., 2001, Surface-rupturing history of the Bree fault scarp, Roer Valley graben: Evidence for six events since the late Pleistocene: Journal of Seismology, v. 5, p. 329–359.
Villinger, E., 1989, Zur Fluss-und Landschaftsgeschichte im Gebiet von Aare–Donau und Alpenrhein: Jahresh. Ges. Naturkd. Württembergs, v. 144, p. 5–27.
von Hartmann, H., Tanner, D. C., and Schumacher, S., 2016, Initiation and development of normal faults within the German alpine foreland basin: The inconspicuous role of basement structures: Tectonics, v. 35, no. 6, p. 1560–1574.
Vrabec, M., Preseren, P. P., and Stopar, B. O. J. A. N., 2006, GPS study (1996–2002) of active deformation along the Periadriatic fault system in northeastern Slovenia: tectonic model: GEOLOGICA CARPATHICA-BRATISLAVA, v. 57/1, p. 57.
Wagner, G., 1929, Junge Krustenbewegungen im Landschaftsbilde Süddeutschlands, F. Rau, p. 274–292.
-, 1960, Einführung in die Erd-und Landschaftsgeschichte: mit besonderer Berücksichtigung Süddeutschlands., Verlag der Hohenlohe'schen Buchhandlung, Rau, p. 1–664.
Wagner, L. R., 1996, Stratigraphy and hydrocarbons in the Up- per Austrian Molasse Foredeep (active margin): Eur. Assoc. Geosci. Eng. Spec. Publ., v. 5, p. 217–235.
-, 1998, Tectono-stratigraphy and hydrocarbons in the Molasse Foredeep of Salzburg, Upper and Lower Austria - in: Mascle, A. et al (eds.): Cenozoic Foreland Basins of Western Europe: Geological Society of London, Special Publication, v. 134, p. 339–369.
Wallace, R. E., 1977, Profiles and ages of young fault scarps, north-central Nevada: Geological Society of America Bulletin, v. 88, no. 9, p. 1267–1281.
Wells, D. L., and Coppersmith, K. J., 1994, New Empirical Relationships among Magnitude, Rupture Length, Rupture Width, Rupture Area, and Surface Displacement: Bulletin of the Seismological Society of America, v. 84, no. 4, p. 974–1002.
Wende, R., 1995, Drainage and valley asymmetry in the Tertiary Hills of Lower Bavaria, Germany: Geomorphology, v. 14, p. 255–265.
Zweigel, J., Aigner, T., and Luterbacher, H., 1998, Eustatic versus tectonic controls on Alpine foreland basin fill: sequence stratigraphy and subsidence analysis in the SE German Molasse: Geological Society of London, Special Publication, v. 134.1, p. 299–323.

11. Appendix

A1) Sample photos.

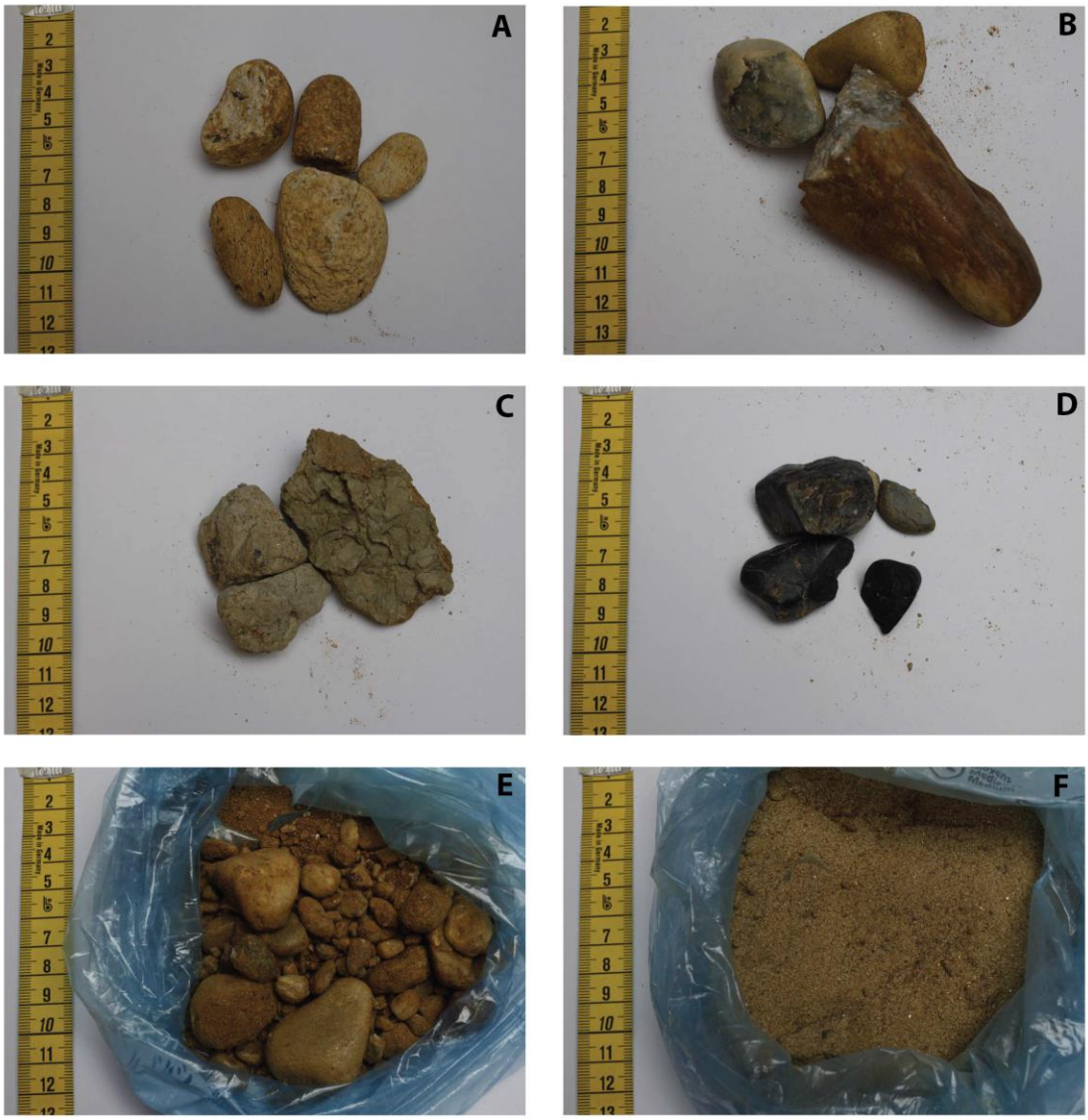

Fig. 2.14: Overview of lithologies and grain size analysis at site *Tunzenberg*. A) Granite. B) Quarzite. C) Marlstone. D) Lydite. E) Grainsize 0.5 cm - 7 cm (gravel). F) Grainsize < 0.1 cm (sand and silt). Photos by C. Zausinger.

Chapter 3

Erosional and tectonic overprint of the mid-Miocene marine cliff line and its applicability as a paleo-geodetic marker of regional-scale tilting, Swabian Alb, southwestern Germany

Authors:
Hoffmann, M.[1]* and Friedrich, A.M.[1]

Affiliation
1. Department of Earth and Environmental Sciences, Ludwig-Maximilians University, Luisenstraße 37, 80333 Munich, Germany

*Corresponding author (e-mail: ma.hoffmann@lmu.de)

1. Abstract

A prominent mid-Miocene coastal landscape is exposed for about 300 km along the Swabian Alb in southern Germany. This feature, known as the *cliff line*, yields an elevation difference of ~ 500 m along strike. Its age is mid Miocene, implying a narrow feature which may be used as a paleo-geodetic marker. Alternatively, the features may belong to a wider coastal zone that contains the incremental uplift history of the zone since their formation in mid-Miocene time. To test the usefulness of the cliff line as a paleo-geodetic tilt marker, we synthesized published results and conducted geological and geomorphological field studies based on remotely sensed data. We then analyzed coastal features in terms of their coevalness, linerarity and distribution. Our results cast doubt on the linearity of the marine coastline. It is better characterized as a broad paleo-coastal region that was affected regionally by deformation and erosion, as well as locally by a ballistic impact. Coastal features are exposed at two well-known sites *Heldenfingen* and *Burgmagerbein*. Analyses of these paleo-coastal sites reveal substantial differences among the marine features, such as size of bio-erosion traces from rock-boring organisms.

These findings indicate temporal and spatial differences of the sites along the mid-Miocene coast. We estimate the individual surface uplift of the two sites as < 0.1

mm/a and quantify contributions from erosion, local tectonics and Rhine Graben rift flank uplift.

Furthermore, the cliff line coastal area may have marked the northern boundary of the Northern Alpine Foreland Basin NAFB. We examined potential paleo-positions of the forebulge related to the NAFB. We found a match of coastal facies mapped for the region and different sea level stage of marine occupation from our sites investigated. The results are based on analysis of marine and terrestrial facies, showing a late-Miocene caliche horizon and a plaeo-fluvial system, matching time and position of the inferred forebulge zone.

2. Introduction

Paleo-geodetic markers are useful tools to study vertical motion of the earth surface. Corals are one example of a sensitive marker to estimate relative vertical motion of a reef associated with regional tectonics (e.g., Sieh et al, 1999). Particular marker horizons, covering both large spatial and temporal scales, are also ancient coastlines (see also chapter I, Fig. 1.4).

2.1. History of ancient rocky shore research

The oldest ancient rocky shores in Barberton Mountain, South Africa, are dated to ~ 3.5 Ga (Byerly et al., 1986; Johnson, 1992). Shoreline scarps were noticed first by De Maillet (1748) in Egypt. Later, Lyell (1845) and De La Beche (1846) investigated shorelines in North America and Great Britain. Besides the successions of coastal marine facies, the major coastal features that prevail are traces of rock-boring and brazing organisms (lithophocoenose), as well as wave cut rock platforms (Grabau, 1913, 1940; Radwanski, 1970).

The cliff line (Fig. 3.3) defines the Burdigalian sea level high-stand of the Miocene ocean at c. 17.5 Ma – 17.6 Ma (Gall, 1969, 1971a, b, 1974 a; Kuhlemann et al., 2001; Lutzeier, 1922; Schetelig, 1962). The cliff line's biostratigraphic age is based on the occurrence of the late Tertiary representative of the oyster *Crassostrea* at some of the cliff outcrops (Gall, 1969; Kirby, 2000; Lutzeier, 1922). The cliff line is a product of collected field observations along the Swabian Alb, and the different courses of the cliff line drawn by previous authors (Fig. 3.2) result from the scattered appearance of

those coastal features. These features are mostly small holes drilled into the micritic limestone substrate by marine bivalves, here *Pholas desmoulinsii* (Lutzeier, 1922) and sponges, here *Cliona* (Grant, 1826). The cliff line shows more bends at its eastern extent, where more outcrops have been reported. Towards the western portion of the Swabian Alb, in the vicinity of the Black Forest, the published line straightens, but fewer sites are documented along this segment (Tab. 3.1; Fig. 3.2).

Along the northwestern margin of the NAFB (Fig. 3.1a), such a coastal area is known as the mid-Miocene cliff line (Lutzeier, 1922). The entire cliff spans about ~ 300 km in an E-W-direction and its elevation changes by about 500 m (800 m in the west to ~ 350 m in the east), implying large-scale tilt of the region. This tilt has been so far attributed to the uplift of the Black Forest (e.g., Hofbauer, 2012).
The ancient coast has been studied by previous authors based on field observations (Tab. 3.1; Fig. 3.2) and the relative position of the sites was utilized to infer a ~ 300 km long cliff line (e.g. Gall, 1969). This is based on the exposures of marine features following the gentle topographic step between the Kuppenalb in the north and the more subdued Flächenalb to the south of the Swabian Alb high plain (Fig. 3.1a) (e.g., Hüttner, 1958; Kiderlen, 1931).

Table 3-1: Summary of previously studied cliff sites along the Swabian Alb. For locations see Fig. 3.2.

No.	Location	Observation	Age	Reference
1	**Tuttlingen**	Holes from rock-boring organisms (Bivalves and sponges)	-	Gall 1969
2	Gammertingen	Holes from rock-boring organisms (Bivalves and sponges)	-	Gall 1974 a; Gall 1974 b
3	Münsingen	Holes from rock-boring organisms (Bivalves and sponges)	-	Hüttner 1961; Nathan 1955; Schalk 1957
4	Laichingen	Holes from rock-boring organisms (Bivalves and sponges)	-	Lutzeier 1922
7	**Heldenfingen**	Holes from rock-boring organisms (Bivalves and sponges)	-	Hüttner 1961; Nathan 1955; Schalk 1957; Lutzeier 1922; Gall 1969; Reiff 1958
8	Scheuenberg	Holes from rock-boring organisms (Bivalves and sponges)	-	Hüttner 1961; Nathan 1955; Schalk 1957; Lutzeier 1920; Gall 1969; Reiff 1958
9	Staufen	Distributed boulders of micritic Jurassic limestone drilled by *Lithophaga*	Miocene	Gall 1974 a; Gall 1974 b
10	Bachhagel	Fine-grained coastal sediments with shell fragments have been found in a drilling in 1955 (Bayerisches Landesamt für Umwelt)	Miocene	Gall 1971a
11	Zöschingen	Fine-grained coastal sediments with shell fragments have been found in a drilling in 1955 (Bayerisches Landesamt für Umwelt)	Miocene	Hüttner 1961
12	Ballmertshofen	Fine-grained coastal sediments with shell fragments have been found in a drilling in 1955 (Bayerisches Landesamt für Umwelt)	Miocene	Hüttner 1961

13	**Dischingen**	Fine-grained coastal sediments with shell fragments have been found in a drilling in 1955 (Bayerisches Landesamt für Umwelt)	Miocene	Moos 1925; Hüttner 1961
14	**Dattenhausen**	Fine glauconitic sand deposits overlain by volcanic breccia (*Bunte Breckzie*) sediments from the Ries	Miocene	Gall 1974 a; Gall 1974 b
15	Eglingen	-	-	Hüttner 1961
19	**Amerdingen**	Fine-grained coastal sediments with shell fragments have been found in a drilling in 1955 (Bayerisches Landesamt für Umwelt)	Miocene	Nathan 1955
21	Bissingen	Distributed boulders of micritic Jurassic limestone drilled by *Lithophaga*	-	Lutzeier 1922
22	**Burgmagerbein**	Fine glauconitic sand deposits overlain by volcanic breccia (*Bunte Breckzie*) sediments from the Ries. Oyster shells.	Miocene	Geyer and Gwinner 1991; Gall 1974a
23	Kesselostheim	Fine-grained coastal sediments with shell fragments have been found in a drilling in 1955 (Bayerisches Landesamt für Umwelt)	Miocene	Lutzeier 1922
24	Mauren	Fine-grained coastal sediments with shell fragments have been found in a drilling in 1955 (Bayerisches Landesamt für Umwelt)	Miocene	Gall 1971
25	Ebermergen	Fine-grained coastal sediments with shell fragments have been found in a drilling in 1955 (Bayerisches Landesamt für Umwelt)	Miocene	Gall 1974 a; Gall 1974 b

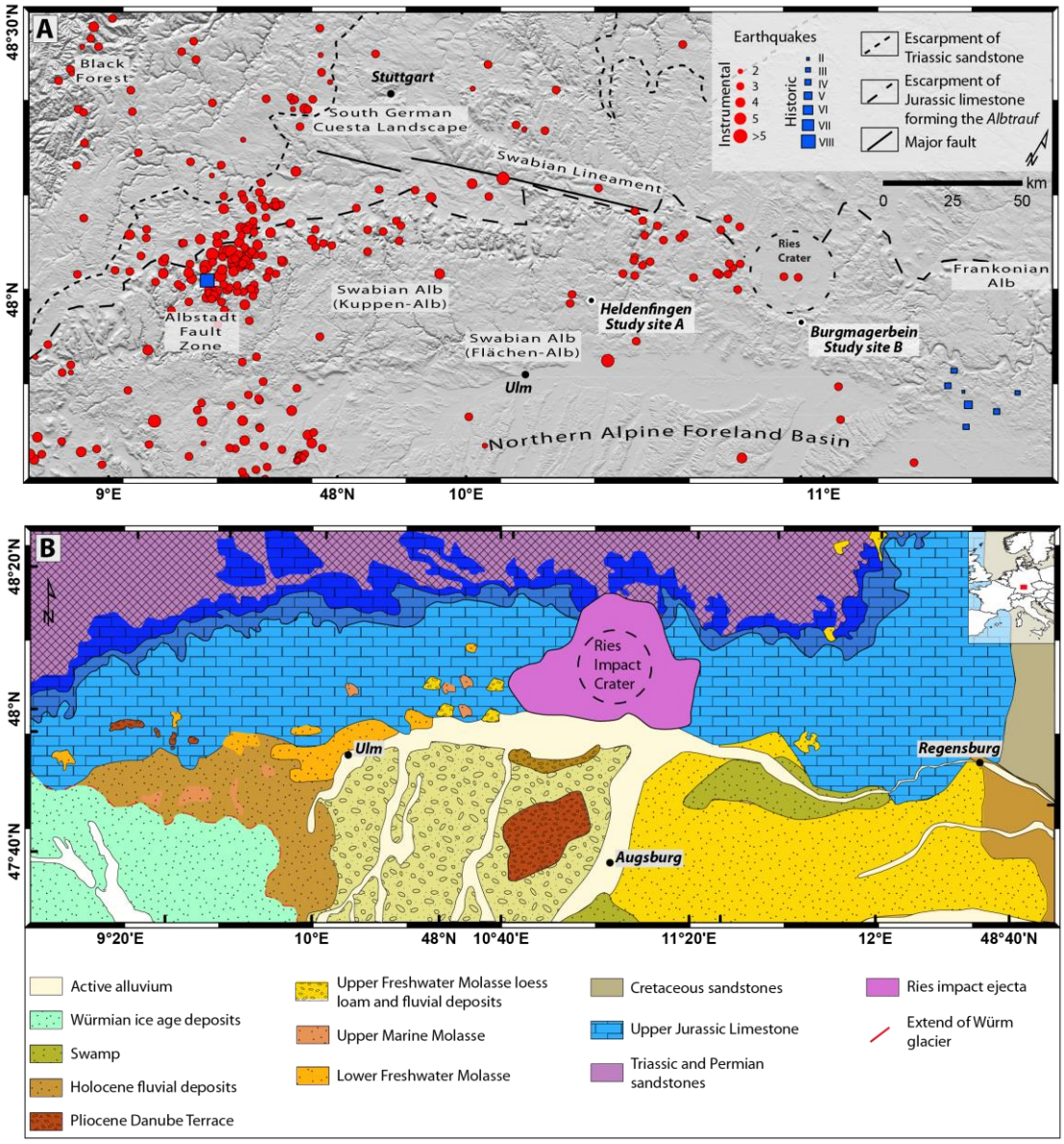

Fig. 3.1: Shaded relief map of the Swabian Alb and adjacent regions showing regional seismicity and geology. Background SRTM (Shuttle radar topography mission) digital elevation model, 30 m resolution, provided by NASA. A) Earthquakes compiled from NEIC catalog and Bavarian Seismic Observatory (BayWatch). B) Simplified geologic map of the Swabian and Frankonian Alb. Modified from the geologic map of Bavaria, 1 : 500,000; geologic map of Germany, 1 : 200,000; Scheuenpflug (1976), Ufrecht (2009).

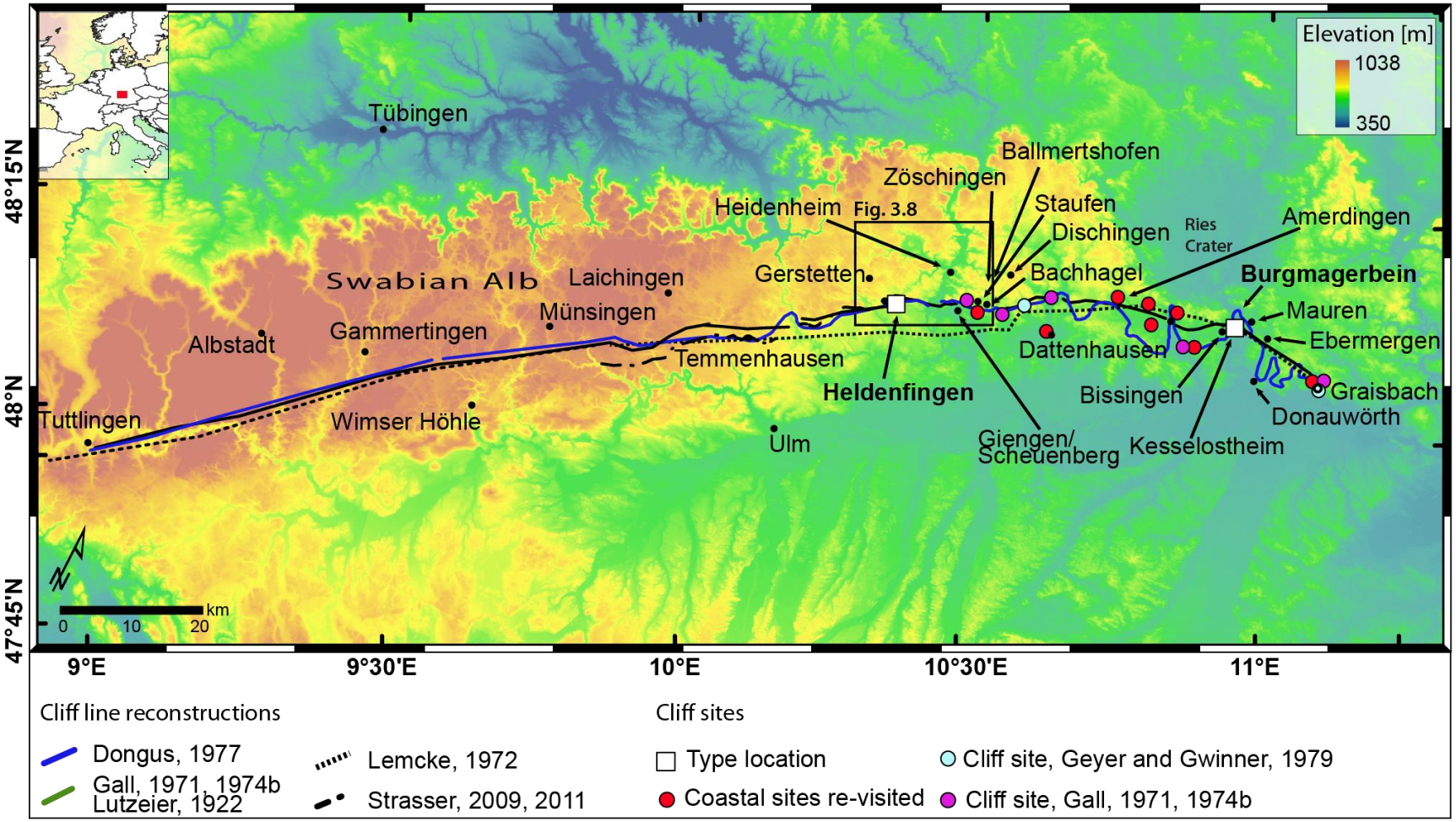

Fig. 3.2: Tectono-geomorphic map of the cliff line trace along the Swabian Alb. The base dataset is the TanDEM-X intermediate DEM (Digital elevation model), 12 m resolution, provided by DLR. Colored dots depict outcrops of marine Miocene facies.

The inferred cliff is interpreted to show a coastal spray zone that was dominantly controlled by tidal effects (Fig. 3.3) (e.g., Lambeck and Chappel, 2001; Winker and Howard, 1977). Whether the previously investigated sites along the Swabian Alb cliff line all reflect coeval marine occupation at similar water depth remains unclear. Previous authors have documented marine features based on bio-erosion and shells that were found in the vicinity of cliff line outcrops (e.g., Gall, 1974 a; Kiderlen, 1931; Lutzeier, 1922). However, potential differences in water depth have not been addressed.

This is particularly relevant, because regional uplift may only be inferred, if these features belong to the same ancient coast. However, temporally and spatially different remnants of a coast may still be used to deduce regional uplift, since they still reflect past sea level. Therefore, if the narrow cliff line could be extended into a wider coastal zone, additional signals of surface uplift might be identified in the region.

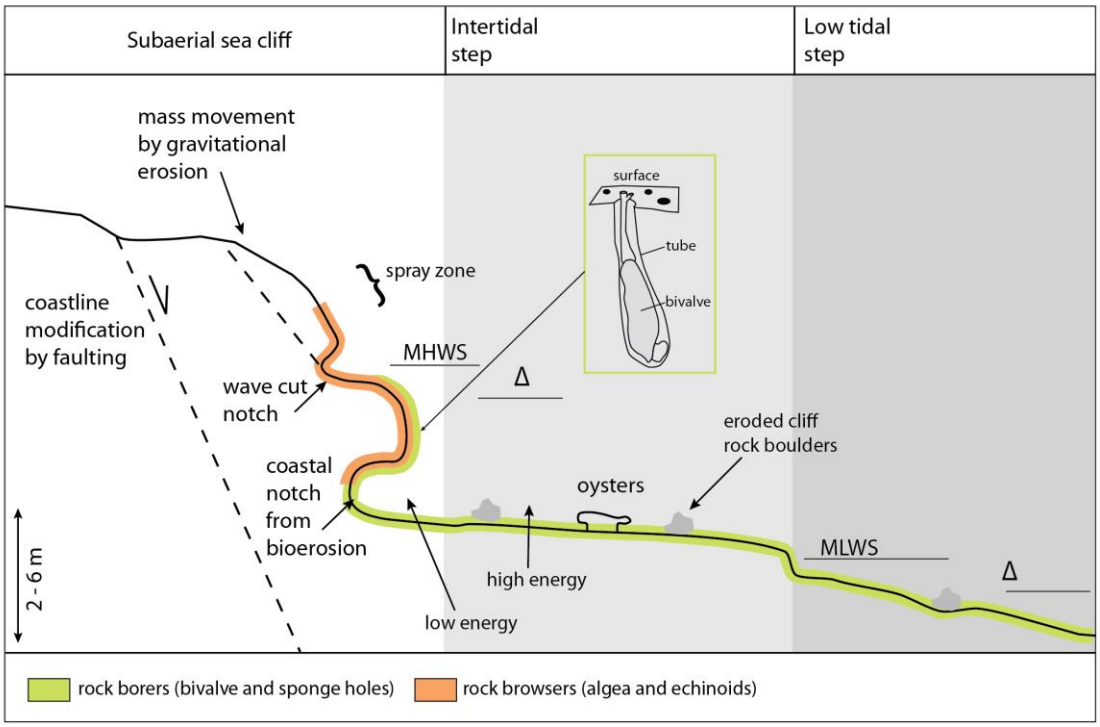

Fig. 3.3: Schematic cross section of a cliff coast and the distribution of bio-erosive organisms along the shore platform. MHWS = Mean high-water spring, MLWS = Mean low-water spring. Delta indicates the eustatic sea level variations and coastline migration. The inset illustrates the living tube of the bivalve *Pholas dactylus*. Modified after Healy (1968), Neumann (1966) and Pinn et al (2005).

The elevation of a coastline changes with global sea level variations, but may also vary regionally by surface uplift (e.g., England and Molnar, 1990). Therefore, utilizing coastal data to derive uplift rates can be difficult, if eustatic sea level change is not well known (e.g., Miller et al., 2005). Furthermore, variations in subsidence and sediment supply also control coastline positions, and these processes do not directly depend on eustatic sea level variations. Assigning coastal details to related water depth can provide the required precise information on the position of a coastal area, because the context of facies and sequences indicates the coast more reliable (Miller et al., 2005).

The reconstruction of sea level variations (e.g., DeConto and Pollard, 2016; Haq et al., 1987; Miller et al., 2005), continent-scale uplift (Burke, 1996), paleogeographic reconstructions (e.g., Blakey et al., 1983) and local tectonics have been tied to coastlines as a reference line (e.g., Pirazzoli, 1988; Pirazzoli et al., 1996).

The displacement of coastal features along faults additionally modifies the original coastal topography and can lead to both spatial and temporal uncertainties in reconstructing, whether the coastline was reaching the present-day elevation of the features, or the land surface rested at lower elevations during marine (Fig. 3.3). Also, transgression acts as a prime mechanism to modify or erase traces of previous coastlines (Cawthra et al., 2016). Finally, the morphology of the coast may be misleading, because various marine species build morphologic features similar to coastal notches by bio-erosion processes (e.g., Healy, 1968; Kelletat, 1997). This can lead to an underestimation of water depth, since the bio-erosion can take place off-shore, several meters below the wave-cut platform (Fig. 3.3).

In order to shed light on this problem, we examined and compared two prominent cliff sites to assess, whether and to what degree coastal features are usable to infer regional uplift and tilt.

3. Regional Background and Stratigraphic Setting

The Swabian Alb cuesta landscape exposes Mesozoic sedimentary rocks gently dipping to the southeast with ~ 0.4° - 9.0° (Fig. 3.1b). Here, Jurassic limestone is subaerially exposed, while at c. 5 km depth close to the Alpine range front (e.g., Lüschen et al., 2004). On the Swabian Alb, the Triassic sedimentary rocks reach a

thickness of up to 1-km-thick in areas where they cover the crystalline basement of the Black Forrest (Carlé, 1955), and about 1.6 km across the rest of the Swabian - Franconian Alb (Geyer and Gwinner, 1991). On the northern margin, Triassic and Jurassic sandstone and limestone form several escarpments up to 100 m each. The most prominent of which, the so-called Albtrauf, forming the top part of the stacked Jurassic limestone (Wagner and Koch, 1961) (Fig. 3.1a). The rapid erosion along the northern escarpment has been explained by the base level lowering of the Rhine and its tributaries. The head ward erosion of Rhine and Neckar tributaries started to cut southward into the Swabian Alb cuesta since the late Eocene, when the Rhine graben started to open and lowered the Rhine base level (e.g., Rosendahl et al., 2006).

Remnants of two depositional mega cycles of the foreland basin are preserved on the Swabian Alb. In this paper, we use the German abbreviations for the NAFB sedimentary cycles by convention of Matter et al. (1980). The Upper Marine Molasse (OMM) and Brackish Water Molasse (BM) represent the youngest cycle of depositional environment with shallow marine conditions, and the Upper Freshwater Molasse (OSM) represents the last cycle of terrestrial conditions (e.g., Doppler, 1989; Füchtbauer, 1964; Schlunegger et al., 2001). OMM and OSM sparsely cover the Swabian Alb plateau. OMM sediments only occur as isolated patches, while in contrast the OSM has covered up to 50% of the plateau, persisting approximately until the late Miocene with a thickness of ~ 250 m that have been eroded since then (Dongus, 1977; Hüttner, 1958; Rosendahl et al., 2006). A thicker initial cover of Miocene basin sediments and an even higher erosion of up to 450 m that also extended into the limestone, is suggested by Bergerat (1994).

The youngest deposits on the Swabian Alb are thin Quaternary loess loams. Further, alteration products of iron oxide concretions in calcitic rocks mixed with Quaternary loess loam fill the numerous karst caves in wide areas across the region (*Bohnerz* deposits). In those deposits, fossils can be found providing relative age control. Based on this, most of the cave deposits are dated to be Pliocene to Pleistocene (e.g., Abel et al., 2006). The *Bohnerz* is a product from tropical laterite alteration, originating from the clay rich *Bankkalk* formation (Reicherter et al., 2008). This material has been widely reworked and re-deposited during the Quaternary. It contains up 50% of iron in places (Rosendahl et al., 2006). The age of the *Bohnerz* is suggested to range from Miocene to Pliocene (e.g., Reicherter et al., 2008; Ufrecht, 2008), but it is found mainly in contact with karst fillings from the early Oligocene to mid Miocene

(Ufrecht, 2008), suggesting a potential wider age range. During the Oligocene, karstification of the exposed Jurassic limestone has started and increased during the Miocene. During the onset of karstification, the Paleogene and Cretaceous sediments were already removed from the Swabian Alb and the surrounding regions. Today, karst caves from enhanced surface erosion are also found in the Jurassic limestone at depth of 3 km close to the Alpine front (Doppler and Schwerd, 1996), which shows that karstification existed prior to Alpine orogeny. The strongest karstification into the Jurassic of the Swabian Alb has reached its peak by the beginning of the Pliocene (Villinger, 1986).

Furthermore, the central Swabian Alb is cut by about 350 small volcanoes. The volcanic cones are mainly composed of olivine-rich melinitic and nephelinitic rocks (Mäussnest, 1982; Wilson and Downes, 2006). Their K/Ar ages range from 16 Ma – 11 Ma (Lippolt et al., 1973). Their appearance is correlated with the Urach through syncline, which has been active since the Triassic. The upwelling of hot mantle material has potentially supplied the volcanic system (Glahn et al., 1992). On the other hand, local generation of magma in a chamber underneath the Swabian Alb from decompression melting due to lithospheric flexure along the NAFB forebulge has been proposed to explain the local volcanism (Wilson and Downes, 2006).

3.1. Fault Systems and Seismotectonics

The Swabian Alb is an area of continuous moderate seismicity (Fig. 3.1a). Compared to the Rhine Graben area and the Alps, earthquakes cluster only in small areas mostly in the southwest. This area is characterized by sinistral strike-slip deformation in the N-S striking Albstadt fault zone as well as the Hohenzollern Graben and the Lauchert Graben (Reicherter et al., 2008; Reinecker and Schneider, 2002). The largest event of the Hohenzollern Graben region occurred on November 16, 1911, M_L 6.1. The first instrumentally recorded earthquake of the Hohenzollern Graben system occured on September 03, 1978, M_L 5.7, near Albstadt. The focal depths of events range from 6 km to 11 km (Grünthal and Wahlström, 2003a). Adjacent to the Hohenzollern Graben, the Lauchert Graben is located in the southeast. It strikes about N-S with an angle of ~ 45° relative to the Hohenzollern Graben. At the Lauchert Graben neither significant historic, nor instrumental seismic activity has been reported (Fig. 3.1a).

3.2. The mid-Miocene coast

The ancient rocky shore studied here is a remnant of the Paratethys ocean and formed during the mid-Miocene at its northern margin along the south German cuesta landscape (Fig. 3.5) (Kuhlemann and Kempf, 2002; Steininger and Wessely, 2000). The marine climax occured during the Eggenburgian (e.g., Doppler and Schwerd, 1996; Kuhlemann and Kempf, 2002; Schetelig, 1962), when it covered parts of the Swabian Alb and cut into the subaerially exposed Jurassic limestone (Rosendahl et al., 2006).

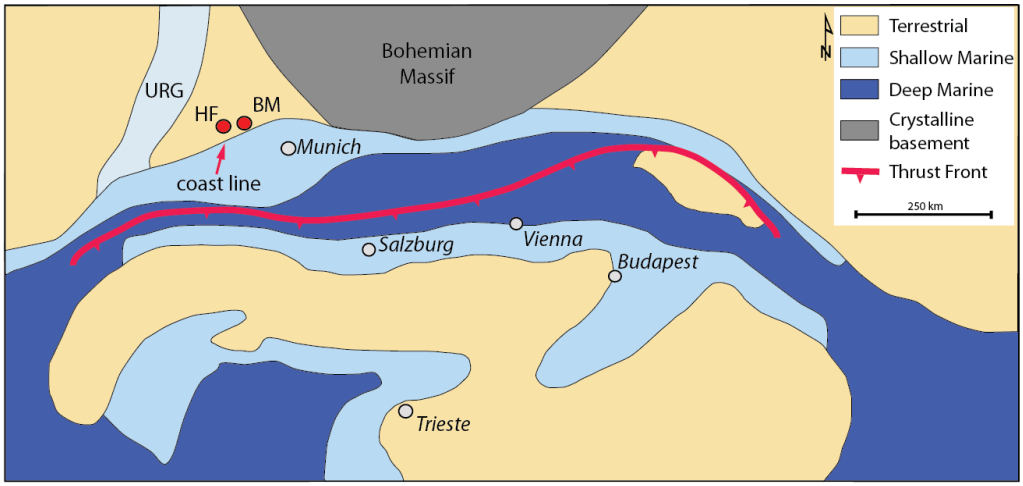

Fig. 3.4: Plate reconstruction of the northwest Europe during the early Miocene (20 Ma - 18 Ma), indicating the paleo coastline and the present-day position of two cliff outcrops. HF = *Heldenfingen*; BM = *Burgmagerbein*; URG = Upper Rhine Graben. Modified after Wagner (1996), Steininger and Wessely (1999).

Prior to the mid-Miocene, the Swabian cuesta landscape was subject to erosion of at least 250 m (Hüttner, 1961), contemporaneous with a general marine regression phase (Kuhlemann and Kempf, 2002). During the time of OSM-deposition, the erosion in the Alps accelerated resulting in a high sediment flux into the proximal and distal basins (Kuhlemann and Kempf, 2002). Subsequently, the abandoned cliff became buried by southerly-derived OSM sediments. This rapid coverage with terrestrial sediments in the late Miocene is regarded as a prerequisite for the preservation of the cliff (Dongus, 1977; Gall, 1974 a). The re-exhumation and uplift of the cliff coast has later been explained by (1) increased climatically driven erosion after 17.5 Ma (Gall,

1974 a, 1974 b), or (2) eustatic sea-level lowering and increased erosion of the OSM coverage at around 14.5 Ma (e.g. Birzer, 1969; Dongus, 1977; Hüttner, 1958). In the late Miocene (14.9 Ma e.g., Storzer et al., 1995), the impact of the Ries meteorite locally swiped away up to 100 m of sediment and covered parts of the Swabian Alb and the foreland basin with scraped off Jurassic limestone boulders (Brockhorizont). This has most likely also overprinted coastal features, providing an upper-bound on erosion in this region.

The outburst later was reworked and transported westward in fluvial systems of the Alpine Foreland Basin, mainly in the river system of the Graupensandrinne (Pohl et al., 1977). Therefore, the extent of the cliff line in the larger vicinity of the impact crater remains difficult to reconstruct. East of the impact site, the cliff line remains untraced.

The coastline morphology is regarded as fault- and joint-controlled in several places along the Swabian Alb (Dehm, 1962; Moos, 1925; Roll, 1935). The authors proposed that several steep escarpments potentially result from faulting during and after the marine occupation, based on marine features that have been likely offset by the faults.

3.3. The Heldenfingen study site (A)

The study site is situated on the eastern part of the Swabian Alb about 30 km west of the Ries impact crater (Fig. 3.2). The site has been excavated as a gravel pit mine in the 1940s - 60s. Later the quarry has been abandoned. The geology of the area is dominated by Jurassic limestone (Oberer Massenkalk) building up the gentle topography. About 300 m to the south, an in-situ isolated patch of OMM can be found. The area is also partly covered with sediments from the OSM, and the surrounding small valleys and gentle depressions are filled with Quaternary loess loam and alluvial deposits (Fig. 3.5). The region is intensively farmed as cropland and has also been agriculturally consolidated in the 1950s and 60s. Further, numerous small concentric depressions from karst cave collapses are found in the forested areas north of the cliff site.

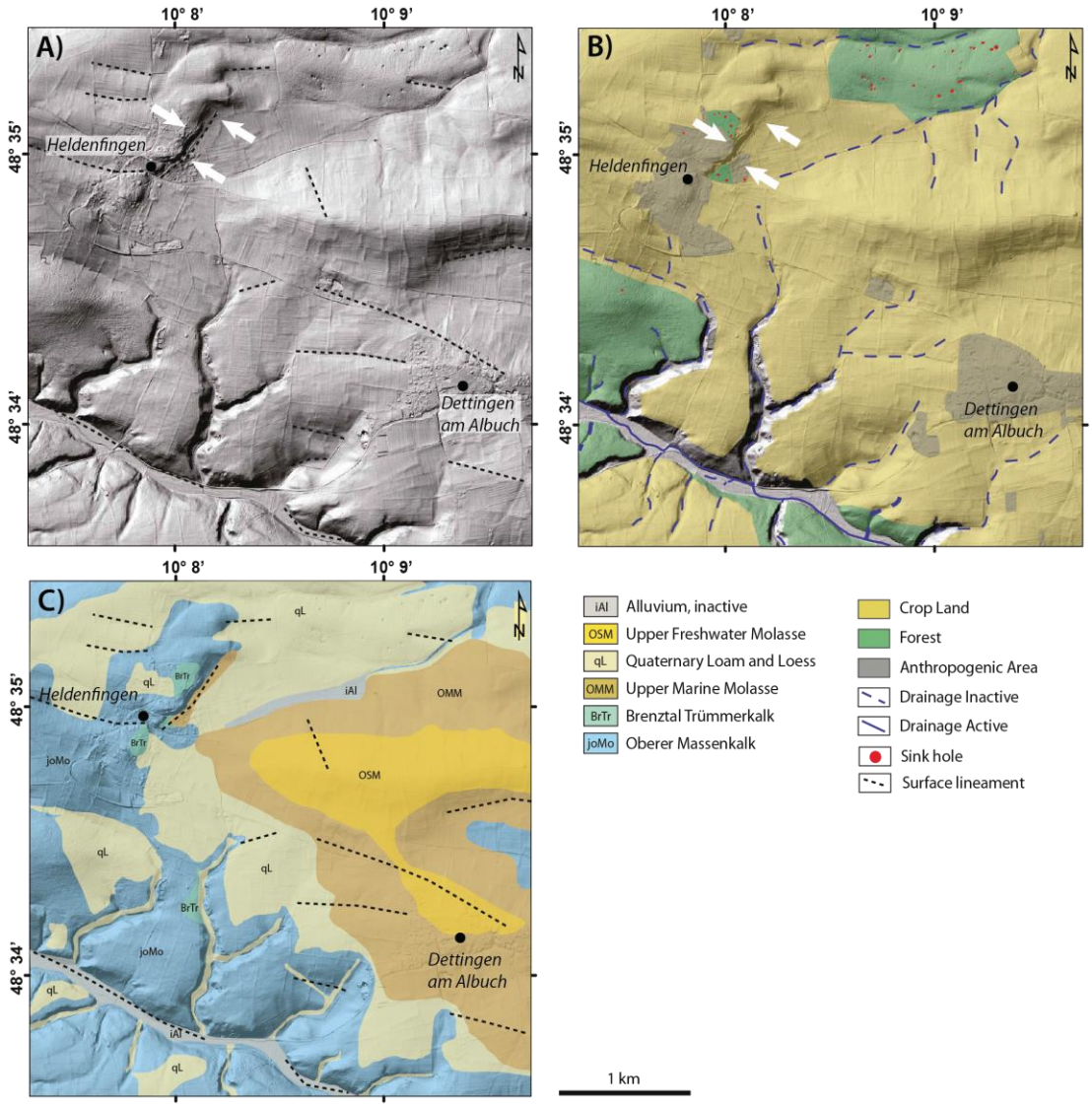

Fig. 3.5: Geomorphologic and geologic setting of the cliff site *Heldenfingen*. A) Hillshade DEM based on airborne LiDAR data, provided by the Landesamt für Vermessung und Geoinformation. White arrows depict the scarp of the cliff outcrop along the western wall of the abandoned pit mine. B) Geomorphologic features of the cliff site. C) Simplified geologic map of the *Heldenfingen* site. Modified after the geologic map of Bavaria, 1 : 25,000, sheet 7428 Heidenheim a.d.B.

3.4. The Burgmagerbein study site (B)

The study site is situated on the eastern part of the Swabian Alb about 3 km south of the Ries impact crater rim (Fig. 3.1a). The cliff site lies at ~ 200 m elevation south of the village of *Burgmagerbein*. The site has been excavated during the occupation as gravel pit mine in the 1970s - 90s. The pit mine is abandoned today, owned by the company Ulbricht & Tannhauser. The gravel pit has been declared as national geo heritage site by the Bavarian Geologic Survey.

The geology of the area is dominated by Upper Jurassic limestone overlain by several meter thick ejecta Suevit from the Ries impact. Patches of allochthone Jurassic rocks are scattered across the area. Around the gravel pit, OMM facies occurs as joint and karst filling. In these sediments Pliocene mammal bones and teeth have been found (Hüttner, 1961). The entire area is covered by a ~ 2-m-thick impact breccia horizon (Suevit, Brockhorizont). To the S-W, an in-situ patch of OSM is found. The gentle slopes and valleys are covered with Quaternary loess loam and alluvium deposits, which are often modified by agricultural land use.

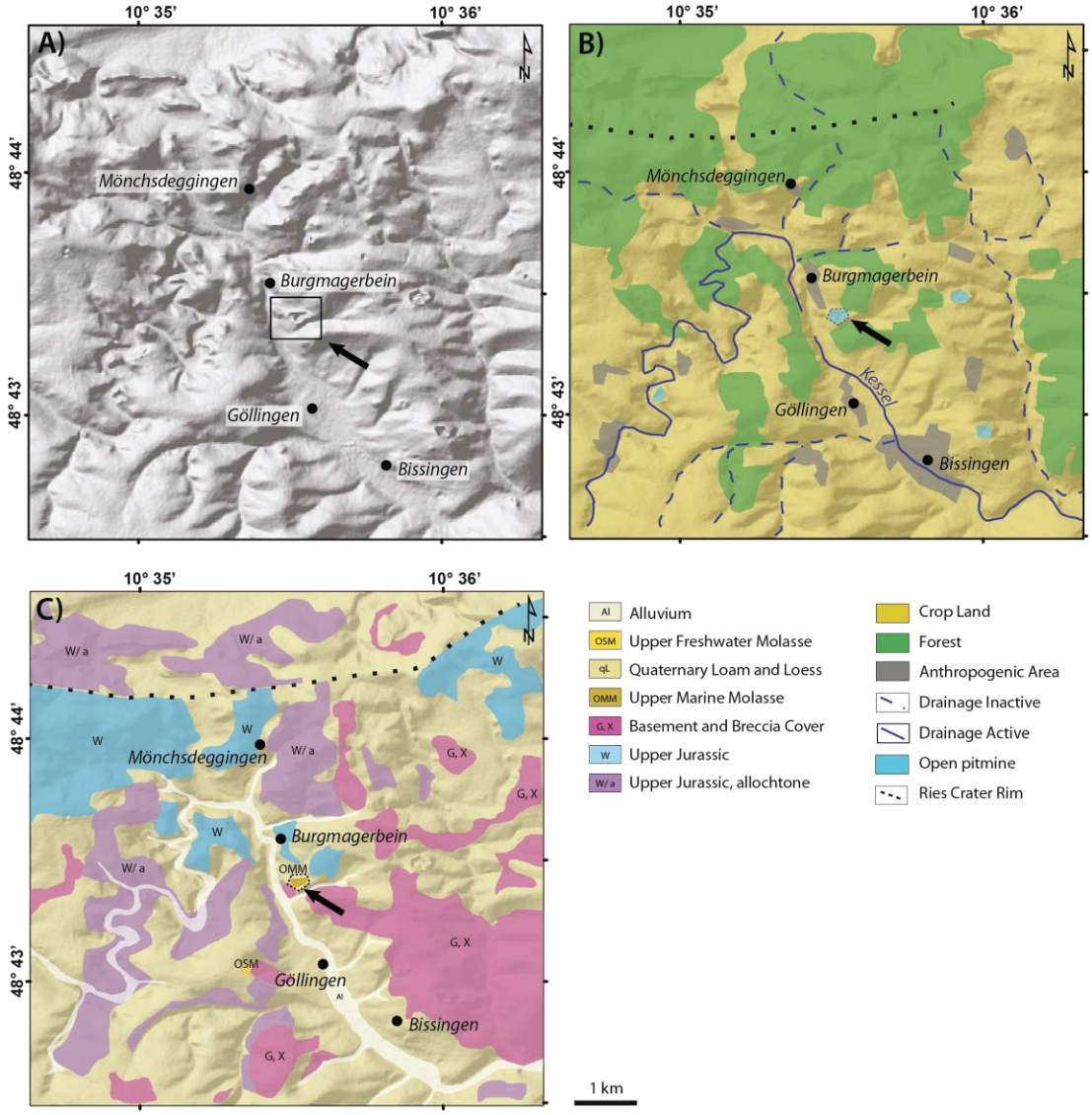

Fig. 3.6: Geomorphologic and geologic setting of the cliff site *Burgmagerbein*. A) Hillshade DEM based on airborne LiDAR data, provided by the Landesamt für Vermessung und Geoinformation. The black arrow depicts the abandoned pit mine. B) Geomorphologic features of the cliff site. C) Simplified geologic map of the *Burgmagerbein* site. Modified after the geologic map of Bavaria, 1 : 50,000, sheet Ries.

4. Methods

In this study, we utilize a combination of remote sensing and field mapping techniques to recognize tectono-geomorphic features across the Swabian Alb. The data are supplemented by geologic field mapping at the two sites *Heldenfingen* and *Burgmagerbein, respectively*. Additionally, historic cliff sites have been compiled from previously published studies and we have re-visited documented sites in several field campaigns. However, after six decades many of the described locations are not accessible since they have become parts of urban areas. In case of former open pit mine outcrops, most of those have been backfilled. At the remaining sites, we investigated characteristics and distribution of traces from rock-boring organisms.
We have focused on the two sites *Heldenfingen* and *Burgmagerbein,* providing the largest range of features.
In order to quantify surface uplift of the Swabian Alb region, we estimate the paleo-coastal position of the two sites and synthesize the results with previously published uplift and erosion rates. In order to infer the potential position and migration of the NAFB forebulge area, we conduct a facies and onlap analysis based on geologic maps of the region. We finally compare the results with a conceptional facies distribution in a forebulge setting to test our hypothesis.

4.1. Geomorphic mapping

We used the digital elevation model (DEM) derived from the TanDEM-X intermediate data provided by the *Deutsches Zentrum für Luft- und Raumfahrt* (DLR). The resolution is 144 m^2/pixel. This dataset was available for most of the Swabian Alb. Missing parts towards the western most extend have been subsidized by the SRTM 1 arc second enhanced elevation model, provided by NASA. The data have been mapped in hillshade view as well as in a colored scheme to enhance optical contrasts of linear features using ArcGIS V. 10.3.

4.2. Field mapping and analysis of bio-erosion features

During several field surveys, we have revisited and mapped the cliff sites, where marine coastal facies and features such as traces of rock-boring organisms, are exposed. The distribution and position of boreholes have been mapped. We also

measured their diameter and depth and applied an area based counting procedure, where holes across a raster of squares with a size of 1600 cm^2 each have been documented at the outcrops.

For the statistical analysis of the coastal features at both sites, we recorded the spatial pattern and the dimensions of bivalve boreholes by defining 5 major classes of borehole diameters ranging from < 0.4 cm to > 2 cm and counting the holes in the defined squares. Also the position of holes of different sizes relative to each other has been recorded. The results have then been compared to recent rock-boring observations from southern Spain and literature data, in order to verify that we observed real bio features instead of erosional pattern like limestone typical honeycomb weathering. Furthermore, joint orientations at both sites *Heldenfingen* and *Burgmagerbein* have been recorded and plotted in rose diagrams.

4.3. Estimating local surface uplift

From observation at the two cliff sites, we estimated the total surface uplift of the study sites *Heldenfingen* and *Burgmagerbein*. The general concept is based on the approach by Abbott (1997), which was developed for mountainous regions. In this study, we apply the calculation to estimate the individual surface uplift of the two sites *Heldenfingen* and *Burgmagernbein*. The input parameters used in this preliminary calculation are listed in Tab. 3.2, and for the calculation we use the formula:

$$U_{ti} = (Z_i - Z_{ii}) + E_i + SL_i - U_{EI} \quad (1)$$

$$U_i = U_{ti} / t \quad (2)$$

where U_i is the total bedrock uplift in mm/a; Z_i is the present-day topographic elevation (m); Z_{ii} is the initial elevation (m); E_i is the thickness of eroded material (m); SL_i is the change in sea level (m); t is the time of deformation (Ma) and U_{EI} is the isostatic component of uplift by erosion (80% of the eroded material). The input parameters compiled from literature and our field measurement (Tab. 3.2) are used to solve equation (1) and (2). In the calculation, we incorporate the isostatic component of 80% from material eroded (e.g., Champagnac et al., 2007), based on the amount of

minimum erosion (Tab. 3.2, column I, J). This value is assumed to be uniform over the area investigated (Hüttner, 1958). However, an error estimate is not given in the publication. In agreement with general sediment budget calculations, the estimated average error is on the order of 50% (Hinderer, 2001). We recognize the variations of the calculated signals are influenced by the error from sediment budget analysis, but this does not affect the overall pattern of relative regional surface uplift.

4.4. Onlap and facies analysis

The geologic map of Germany 1 : 200,000 (BGR; Zitzmann, 2003) and local geologic maps at 1 : 25,000 (Bayerisches Landesamt für Umwelt) have been used to digitize areas, where the deposits of UMM (Untere Meeres Molasse), USM (Untere Süßwasser Molasse), OMM and OSM are in contact with the underlying Mesozoic limestone (Jurassic Malm). When stratigraphic units are missing in the chronologic sequence, a hiatus is defined. The temporal hiatus length has been defined using the geologic maps. From the contact lines, we have mapped the area of unconformal contact to infer the erosional history at the location (Yldirim, 2016). This concept can further be utilized to estimate the area of the potential NAFB forebulge.

The forebulge is defined as an area of non-deposition and/ or erosion (e.g., DeCelles and Giles, 1996). Therefore, the local hiatus record across the marine and terrestrial units provide a first order estimate of a distal elevated zone along the northern margin of the basin. In order to visualize changes in peripheral bulge position, we synthesized the geologic data in three maps, showing the basin setting during deposition/ erosion of USM, OMM and OSM.

The analysis of regional geologic maps reveals several unconformable contacts along the Swabian Alb. These contacts are 1) OSM – Jurassic, 2) OMM – Jurassic and 3) USM – Jurassic. We have traced the contact lines of different facies along the Swabian Alb and converted those to a facies and hiatus map.

Based on the assumption that the forebulge is represented by erosion and onlap structures in the geologic record relative to their surrounding (e.g., DeCelles and Giles, 1996; Quinlan and Beaumont, 1984), the observations from mapping are utilized to infer potential positions of this erosional forebulge region.

The cross section (Fig. 3.13) reveals small patches of OMM between the cliff site and the basin. At the base of the Albstein carbonate caliche horizon, an erosional truncation to the underlying USM, OMM and OSM sediments is detected.
The facies model (Fig. 3.14) summarizes the described erosional and depositional zones in the near- and far-field of a forebulge. Based on the onlap data (Fig. 3.13) and the forebulge depo-zone concept (Fig. 3.14), we have compiled three maps showing the depositional paleo-environment during the Miocene (Fig. 3.15).

5. Results

5.1. Site Heldenfingen (A)

5.1.1. Geomorphology

Mapping on the high-resolution TanDem-X DEM reveals several fault and surface lineaments in the area of coastal sites along the Swabian Alb. The structures are oriented parallel and perpendicular to the cliff line (Fig. 3.8 and 3.9). For example, in the area of the site *Heldenfingen*, several faults and surface lineaments are observed, like a ~ 1.0 km long, NE-SE striking lineament about 500 m NE of the outcrop (Fig. 3.9). Another 500 m in the same direction, a ~ 1.0 km long, NW dipping normal fault has been documented on the geologic map (Landesamt für Geologie und Rohstoffe, Baden-Württemberg). The largest fault of the area is located about 6 km northwest of the village *Heldenfingen*. Here the NW-SE striking sinistral Heidenheim fault offsets Jurassic limestone over few hundred meters. About 6 km east of Heldenfingen, the Mergelstetten Fault offsets rocks of the Brockhorizont over several tens of meters (Geologic map of Baden-Württemberg, sheet 7326 Heidenheim a.d.B.). At the Steinheim meteorite crater, the Heidenheim fault potentially extends NW-ward across the crater, as inferred by a left lateral offset of the outer crater rim. In general, numerous surface lineaments are observed and many of those show topographic escarpments that strike at similar orientations as the escarpments invoked to explain the cliff line.

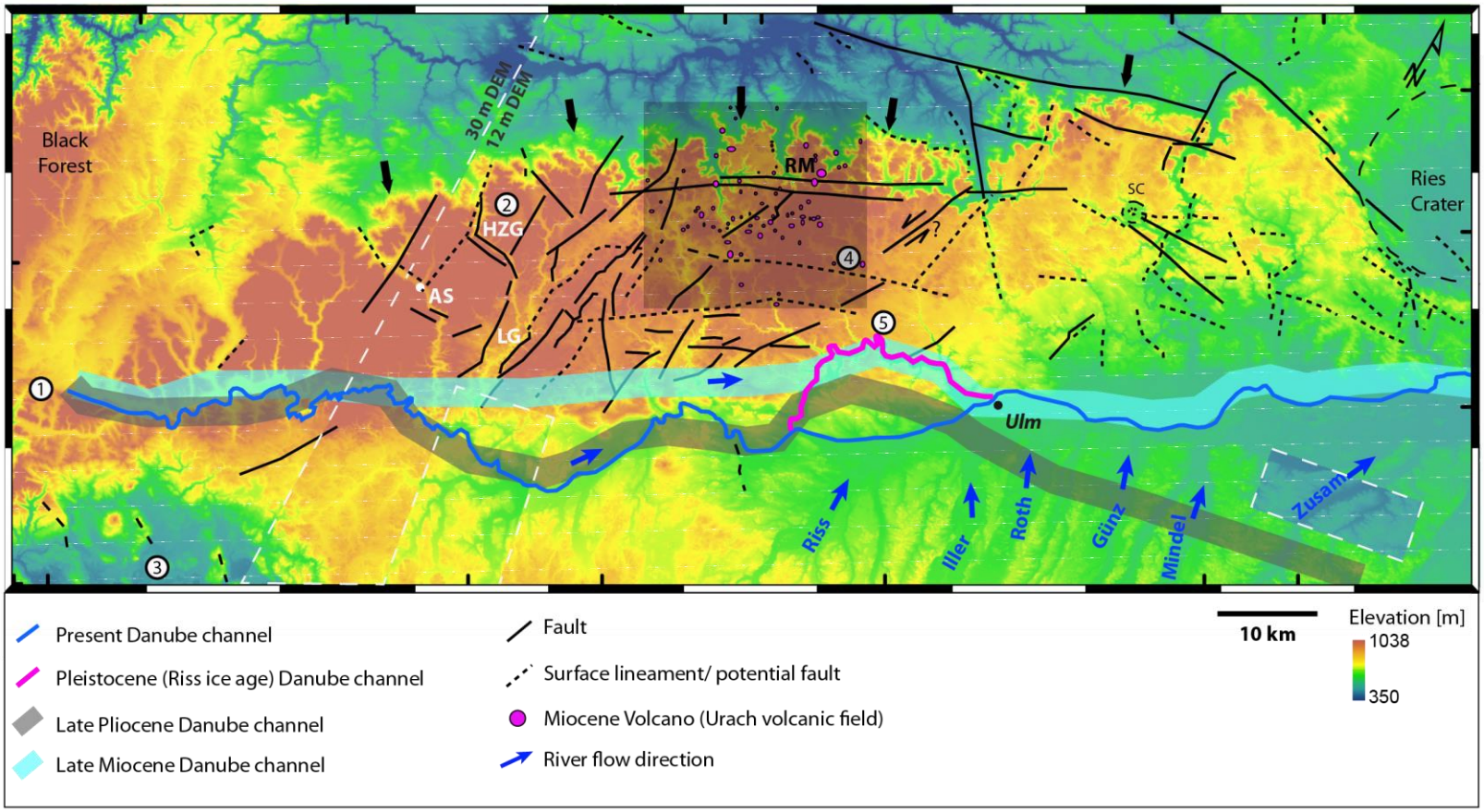

Fig. 3.7: Shaded relief map of the geomorphic and tectonic features along the western Swabian Alb. Background: TanDEM-X intermediate DEM, 12 m resolution, provided by DLR. Black arrows trace the escarpment of the Upper and Lower Jurassic and the underlying Permian (Albtrauf). 1) Danube source, 2) Hohenzollern Graben, 3) Lake Constance, 5) Laichinger cave, 6) Blautopf cave system with early Neanderthal settlements. AS = Albstadt, LG = Lauchert Graben, HZG = Hohenzollern Graben, U = Ulm, RM = Randecker Maar. Historic Danube river bed data compiled from Landesamt für Geologie, Rohstoffe und Bergbau, Baden-Württemberg; Villinger (2005); Scheuenpflug (1976).

5.1.2. Coastal features

The ~ 10 m long and 3 m high outcrop is divided into two parts. In the upper part, numerous boreholes from bivalves are homogenously distributed. The lower part shows significantly less holes. The analysis of borehole dimensions reveals three different types of rock-boring trace fossils. The large holes (> 1 cm) dissect smaller ones (~ 0.8 cm) and both types are penetrated with a dense network of micro holes (< 0.5 cm) (Fig. 3.9a). The small holes are concentrated in the central part of the outcrop, near the small flat surface. On the surface, as well as below the flat part, almost no boreholes are observed. The outcrop also shows several joints sets, striking NNE and E-W respectively (Fig. 3.10a). On the surfaces of the NNW striking joints, the same range of boreholes sizes is found, while in the E-W joint only the micro holes are found.

5.2. Site Burgmagerbein (B)

5.2.1. Geomorphology

At the site, the overprint from the Ries impact and its ejecta cover the entire area, and therefore no potential faults or lineaments at the surface have been detected. However, from the TanDEM analysis, we recognize several fault structures along the crater rim and inside the impact crater (Fig. 3.8).

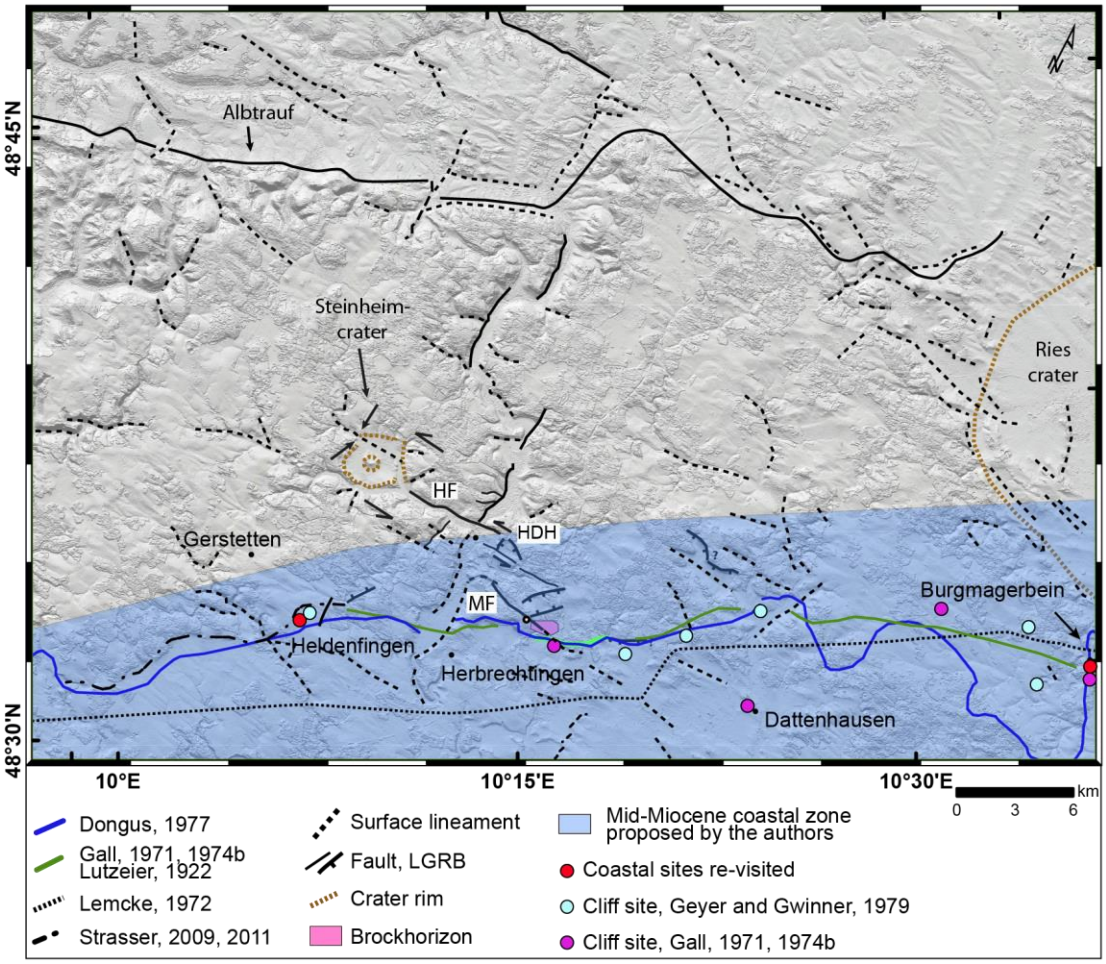

Fig. 3.8: Tectono-geomorphic map of the Swabian Alb in the area between Heidenheim a.d.B. and the Ries impact crater. The colored lines depict cliff lines published by previous authors. HF = Heldefingen Fault, MF = Mergelstetten Fault. Fault data are compiled from the tectonic map of Baden-Württemberg, LGRB, online data viewer, 2016.

5.2.2. Coastal features

The outcrop is divided into several sections of a few square meters, inside the open pit mine. The marine features are found at edges and turns of the quarry walls at the upper two levels. The distribution of marine features across the outcrop is similar. On the upper most level, lithified oyster shells are attached to the Jurassic limestone rock. The borehole-bearing horizons occur below the oyster level. The analysis of boreholes reveals two generations of holes with diameters > 1 cm and small holes of ~ 0.5 cm. The highest number of holes has been detected for the 0.4 cm – 1 cm range (Fig. 3.9b). The boreholes are mainly adjoined.

Joints in the outcrop dominantly strike NW-SE (Fig. 3.10b). This direction coincides with the observed main fault and lineament directions on the Swabian Alb (Fig. 3.7,

3.8). Inside the pit mine most of the steep west and northeastward facing planes represent artificial surfaces due to mining activity.

A) Heldenfingen

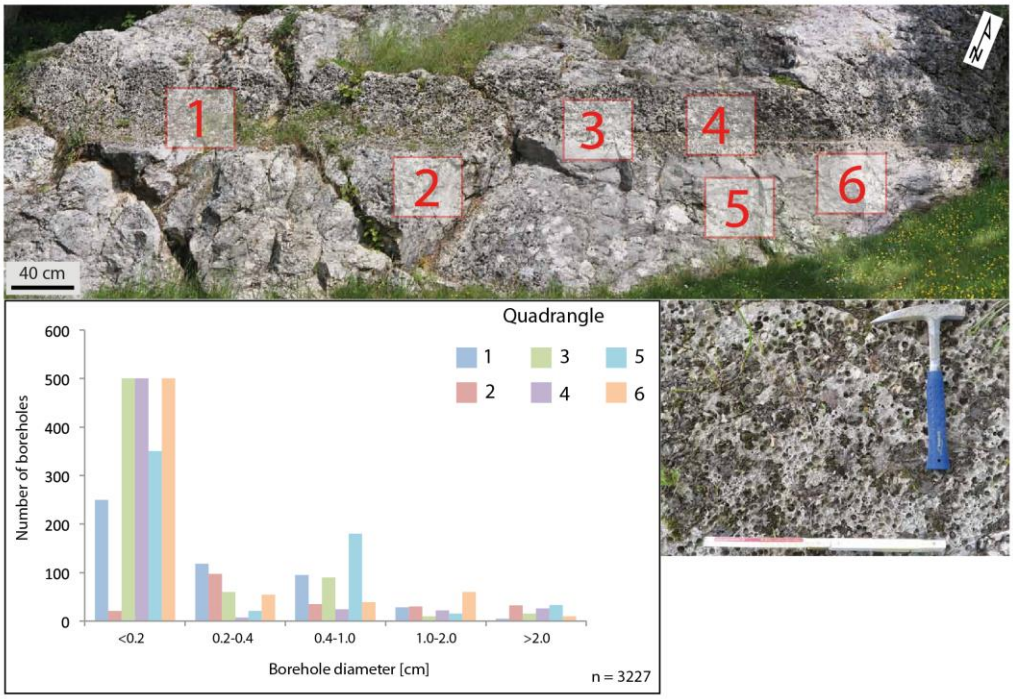

B) Burgmagerbein

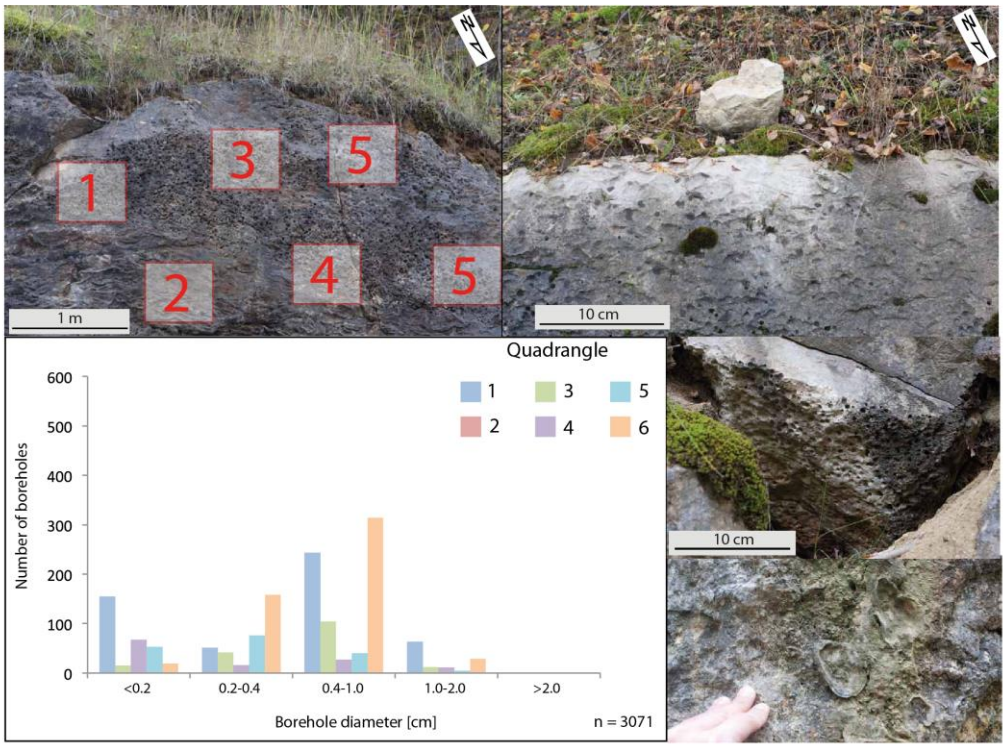

Fig. 3.9: Previous page: Photo panel of the marine bio-features at the two cliff sites investigated. The bar plots show measured sizes of boreholes at the sites *Heldenfingen* (A) and *Burgmagerbein* (B). The numbered boxes in both panels depict examples of the counting quadrangles used at both sites. The common reference square size is 1,600 cm^2 for both datasets. Note the remarkable higher number of small-sized holes at *Heldenfingen*.

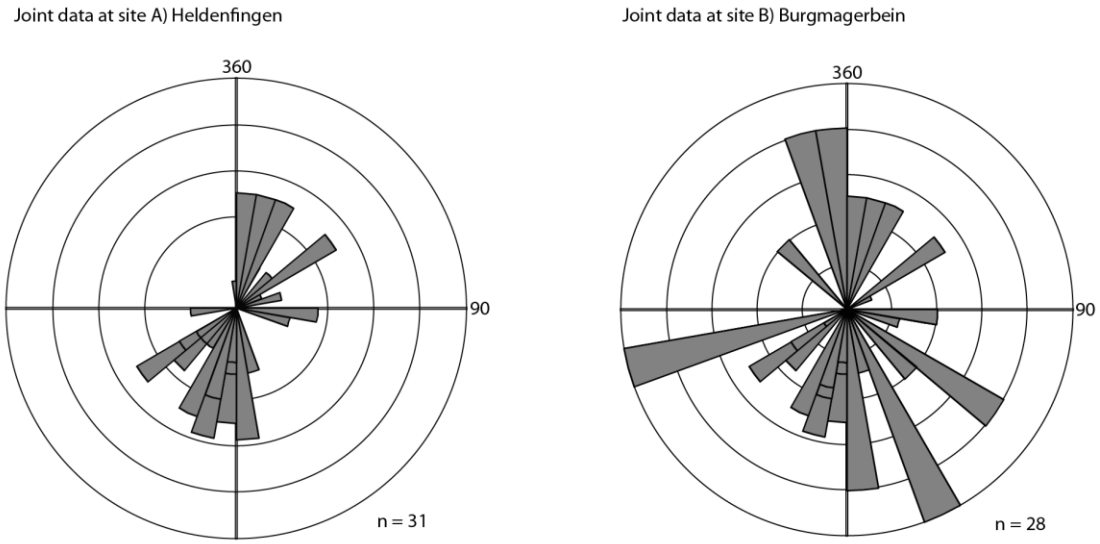

Fig. 3.10: Rose plot of joint orientation at the sites *Heldenfingen* and *Burgmagerbein* (plot: lower hemisphere).

5.3. Uplift estimates for the sites Heldenfingen and Burgmagerbein

Our calculation of relative surface uplift is based on the geologic observations at the two sites investigated in our study and the interjacent reference site *Dattenhausen* (Gall, 1969) (Fig. 3.11; Tab. 3.1). We have compiled literature data to calculate uplift and erosion rates in the area (Tab. 3.1). By calculating the uplift based on the uplift formula (Abbott, 1997), we obtain long-term average uplift rates for the last 17.5 Ma of (0.05 ± 0.022) mm/a for the site *Heldenfingen* and (0.03 ± 0.016) mm/a at the site *Burgmagerbein*, respectively. The rate at site *Dattenhausen* is (0.04 ± 0.018) mm/a, (Tab. 1, column K). The results clearly show a higher uplift rate at site *Heldenfingen* which is about 25% increased relative to site *Burgmagerbein* and reference site *Dattenhausen.*

The mapping of geologic contact within the deposits of the Swabian cuesta landscape provides an additional control on the surface tilt (Fig. 3.12). In the western portion of the Swabian Alb, around Tuttlingen, the strata dip with angles between 2° and 9° towards the SE. The general dip of the sedimentary layers decreases towards the E. In the area of the Ries impact crater dip, values of ≤ 1° are observed. The majority of the exposed strata are bedded horizontal to sub-horizontal.

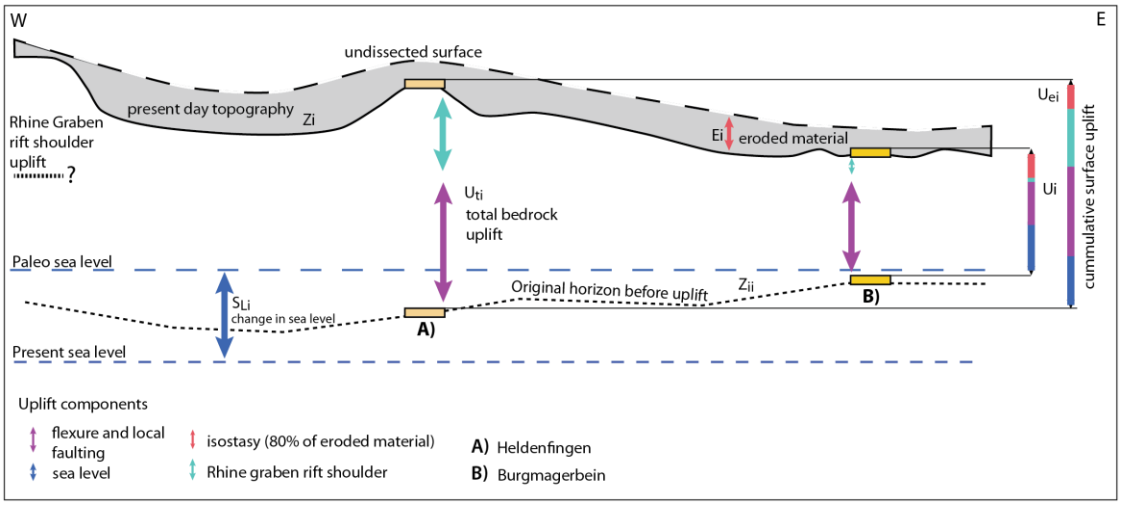

Fig. 3.11: Schematic summary of dynamic processes acing during the uplift of coastal sites along the Swabian Alb. A) *Heldenfingen* and B) *Burgmagerbein*. Modified after Abbott, 1997; Burbank & Anderson, 2001. For calculation see the methods section. Not drawn to scale.

Table 3-2**:** Calculation of relative surface uplift at sites *Heldenfingen*, *Burgmagerbein* and *Dattenhausen*.

A) Site	**B) Present-day elevation of site[1] [m.a.sl.]**	**C) Estimated initial topographic elevation[1] [m.a.s.l]**	**D) Range of paleo water depth[2] [+/- m]**	**E) Late Miocene sea level[3] [m]**	**F) Relative eustatic uplift [m]**	**G) Erosion rate[4] [km/Ma]**	**H) Swabian Alb uplift rate[5] [mm/a]**	**I) Min. sediment yield eroded[4] [km]**	**J) Isostatic compensation [km]**	**K) Caculated long-term uplift rate [mm/a]**
A) Heldenfingen	643.25	- 30	2	- 30	613	0.015	0.013	0.255	0.113	**0.05**
B) Burgmagerbein	456.71	- 1	2	- 30	426	0.015	0.013	0.255	0.113	**0.03**
C) Dattenhausen	465.63	- 50	2	- 30	435	0.015	0.013	0.255	0.113	**0.04**
Parameter in calculation (3.4.)	Z_i	Z_{ii}	-	SL_i	-	-	-	E_i	U_{EI}	U_i

1) This study, 2) Pinn et al, 2005, 3) Kominz et al, 2008; Miller et al, 2005, 4) Dongus 1972, Hüttner 1958, 5) Strasser et al, 2009. Time of deformation (t): 17.5 Ma (Hüttner, 1961).

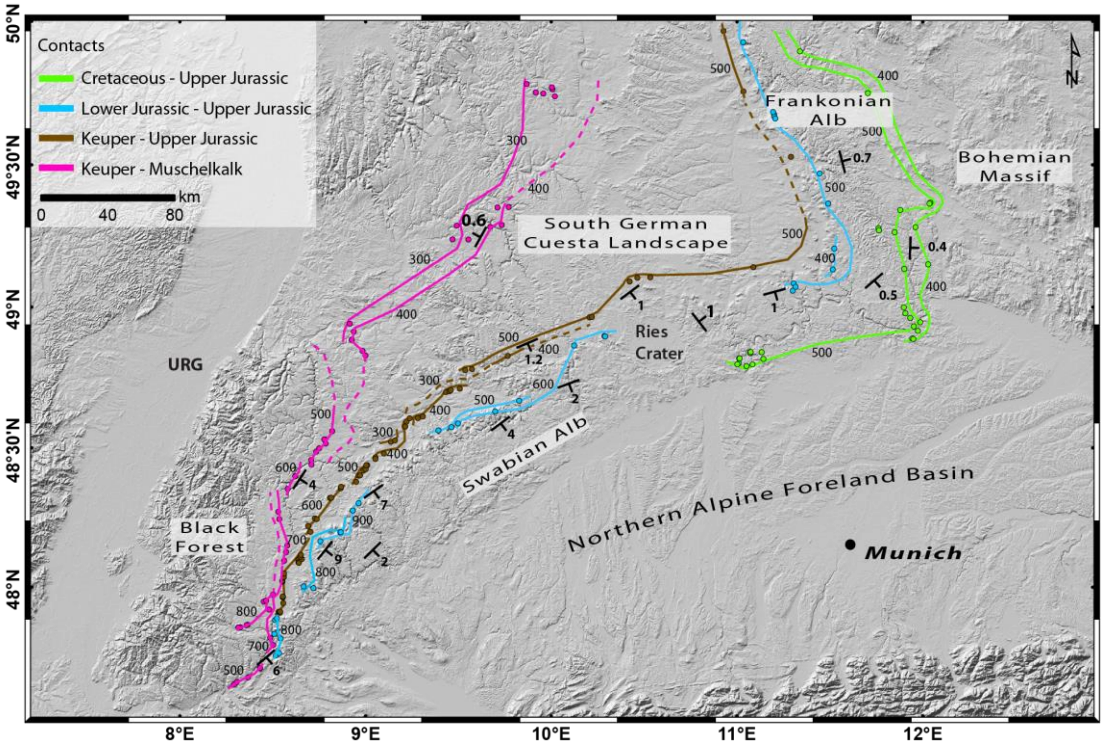

Fig. 3.12: Shaded relief map showing strike lines and regional dip of Mesozoic strata along the Swabian Alb. Data compiled from the Geologic map of Germany, 1 : 200,000 and regional geologic maps, LGRB data viewer, 2016. Additional strike and dip measurements are complied from Peterek and Schröder (2010); Roll (1935).

5.4. Sequence stratigraphic analysis

Results of the facies analysis are shown in Fig. 3.13 and Fig. 3.16. The coastal area investigated in this study represents an angular unconformity (onlap) of marine strata (coastline) onto the Jurassic limestone of the Swabian Alb during the Eggenburgian. Based on geologic maps, further onlaps are present south of *Heldenfingen*.

We observe basin parallel contacts of different marine facies along the Swabian Alb. A NE-SW striking corridor from the fluvial Graupensandrinne (GSR) covers these facies and further to the S, the caliche platform of the Albstein swell can be found in parallel orientation. The underlying sediments of the OSM, OMM and USM are also exposed on the Swabian Alb, N of the GSR.

As indicated in the cross section (Fig. 3.13), the boundary zone between the Swabian Alb and the NAFB shows an erosional relief with truncating the onlapping sediments. The onlaps of sediments of the two marine-terrestrial mega cycles run parallel to the basin boundary along the Swabian Alb, except for the SBM (Fig. 3.13).

Fig. 3.13: Next page: Shaded relief map showing the distribution and onlaps of late Miocene sediments along the boundary zone between the NAFB and the Swabian Alb. The simplified cross section below illustrated the sequence stratigraphic structures along the southern rim of the Swabian Alb. The dashed line indicates potentially missing OMM sediments between the cliff site *Heldenfingen* and the marine sediments in the basin. Background SRTM enhanced digital elevation model, resolution 90m/pixel, provided by NASA. T = Tuttlingen; H = Heldenfingen; D = Dattenhausen; B = Burgmagerbein; URG = Upper Rhine Graben.

Lower Miocene 20 - 16 Ma

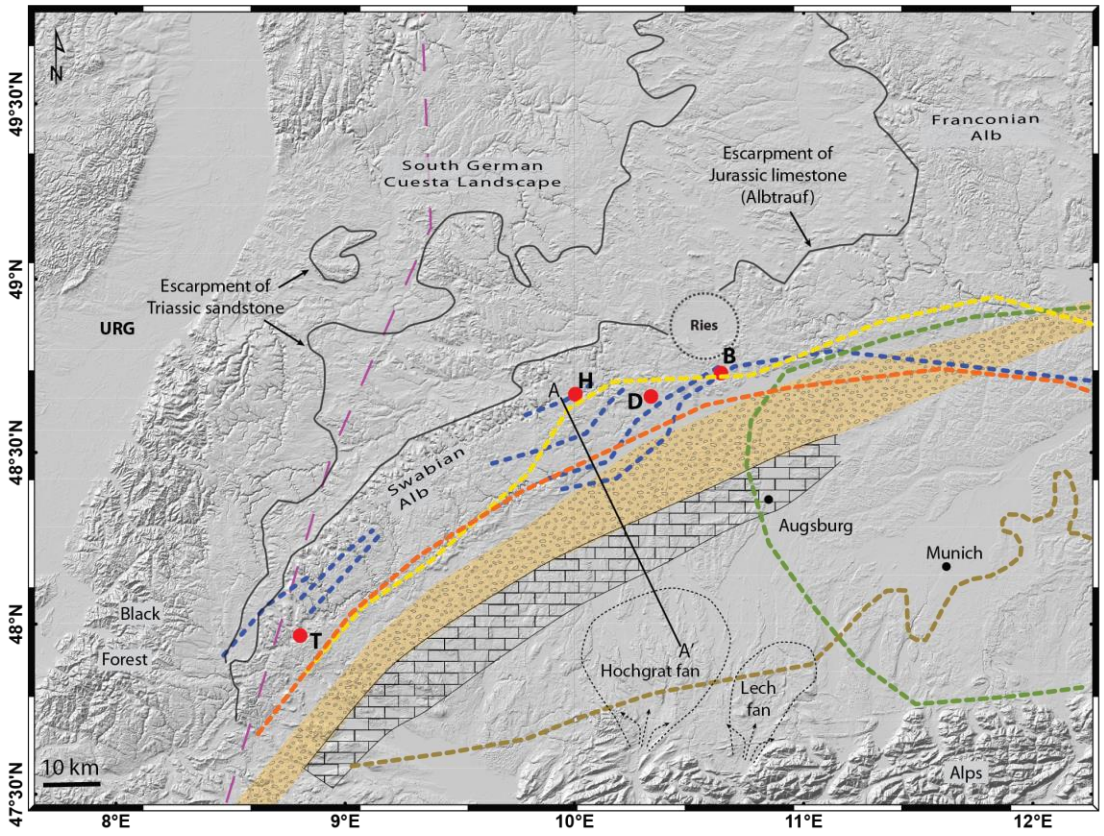

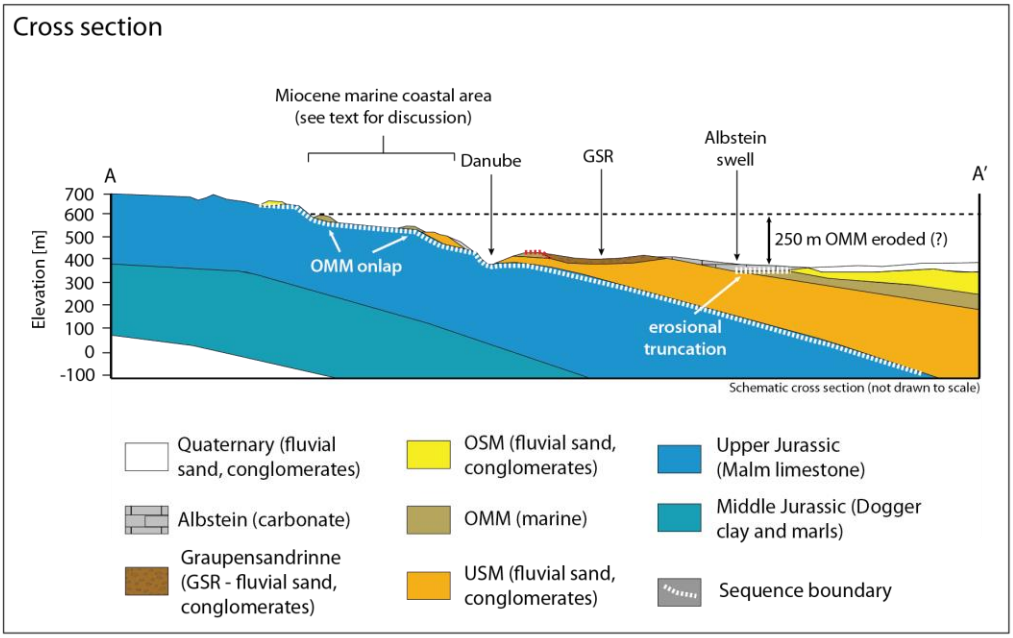

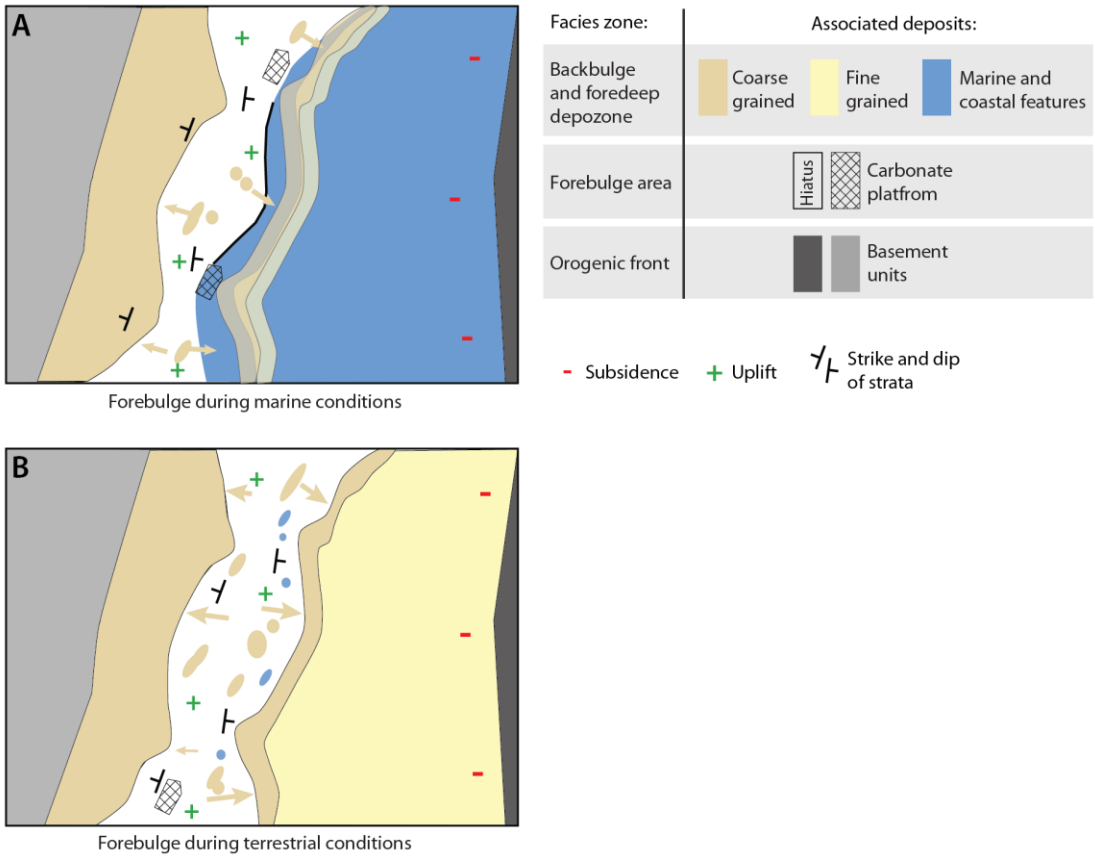

Fig. 3.14: Schematic map showing the concept of facies distribution and transport environments in a forebulge zone. The erosional area separates a foreland basin from the craton/ back bulge region (Giles and DeCelles, 1996).

6. Interpretation

At its western most extent, the cliff line has been documented only by isolated coastal facies and sporadic topographic relief along the Swabian Alb. Therefore, a distinct cliff in the proper sense is not preserved. Towards the E, in the vicinity of both coastal sites investigated, we observed faults and surface lineaments that resulted in N-exposure of coastal features. Vertical offsets appear as a cliff. Further, in the area of the Ries impact crater, the paleo-coast has been additionally erased and modified by the impact itself and ejecta material that has removed parts of the landscape (Schalk, 1957; Schetelig, 1962).

The cliff site *Burgmagerbein* south of the crater is potentially not contemporaneous with site *Heldenfingen* and may represent part of a younger coast. A southward bend of the proposed cliff line around the Ries crater may be an erroneous simplification, which lacks any support, because the coast is most likely older.

A tectonic control, or at least a primary modification of the ancient coastline, is evident from the boreholes, observed on the joint surfaces at site *Heldenfingen*. This shows, the surface must have existed during the marine occupation. The strike of most of the joints correlates with the NE-SW orientation of tectonic structures in the region. Regarding the timing of the tectonic activity, an estimate is derived from faults near Mergelstetten that offsets rocks from the Ries impact. Therefore, the fault is younger than ~ 14.9 Ma and thus was active after the cliff line has formed. The maximum offsets can be estimated to be several tens of meters. A similar result comes from the suggested ~ 200 m offset at the Steinheim impact crater, which formed contemporaneously with the Ries (Heizmann et al., 2002). We interpret the younger fault activity as an indicator for the cliff line's secondary overprint by tectonic activity, masking the original coast.

Both cliff sites show a similar pattern of bivalve boreholes, but only at the site *Heldenfingen*, the larger holes are penetrated by another set of smaller holes. The variation of detected borehole sizes is generally greater at the site *Burgmagerbein*. At the site *Heldenfingen*, the amount of the smallest holes is significantly higher, while the other sizes are less represented compared to site *Burgmagerbein*. The greatest number of holes can be found among diameters of 2 mm - 3 mm (Fig. 3.9a and b).

The marine features of site *Heldenfingen* suggest a greater water depth compared to site *Burgmagerbein*. The significant overprint of bivalve boreholes (large holes) by

rock-boring sponges (micro holes) indicates a water depth below the spray and high energetic tidal zone (> 10 m) at site *Heldenfingen* (Fig. 3.1).

We did not observe a similar pattern of overprinted rock-boring trace fossils at site B). Here, the bivalve borehole size distribution is more uniform and no second occupation of other species is observed. We interpret the findings at site *Heldenfingen* as a flat coastal regime followed by a phase of deeper marine conditions during a transgressive stage, where the middle Miocene coast moved northward onto the Swabian Alb Jura landscape.

Therefore, the analysis of the coastal features, distributed marine sediments and tectonic surface lineaments suggests that the cliff outcrops are part of a widespread coastal zone. This zone is characterized by several coeval depositional facies, as also seen in other coastal settings today (e.g., Goldstein et al., 2012). The along-strike variations in secondary overprint limit the applicability of the cliff line as a linear paleo-geodetic water level. However, the present-day elevation of the former coastal and near coastal sites reflects surface uplift that affected the entire Swabian Alb and surroundings after the mid-Miocene.

In the western most portion of the Swabian Alb, this uplift appears to be controlled at least in part by the mid-Miocene rift flank rise of the Rhine graben. Furthermore, our results indicate a potential contribution to late Miocene uplift of the Swabian Alb by the NAFB forebulge. The spatial and temporal evolution is summarized in Fig. 3.15.

Fig. 3.15: Next page: Panels showing the facies environment in the NAFB and along the northern margin for three time steps during the Miocene. The individual time steps indicate the relevant hiatuses and transport systems related to the basin and forebulge evolution (see also Fig. 3.14 for the schematic model to identify a forebulge area).

Plate A

Early Miocene (~21 Ma).

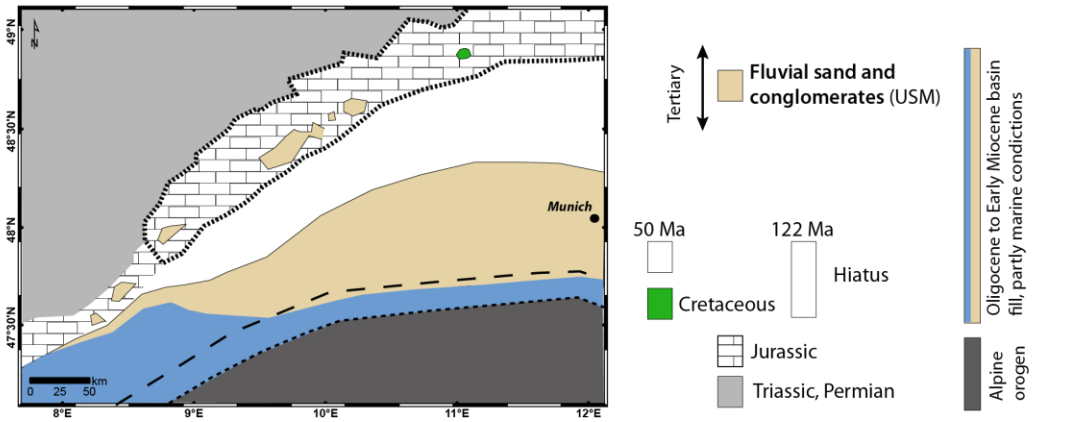

Plate B

Middle Miocene (~17 Ma). OMM is eroded from the Jurassic base

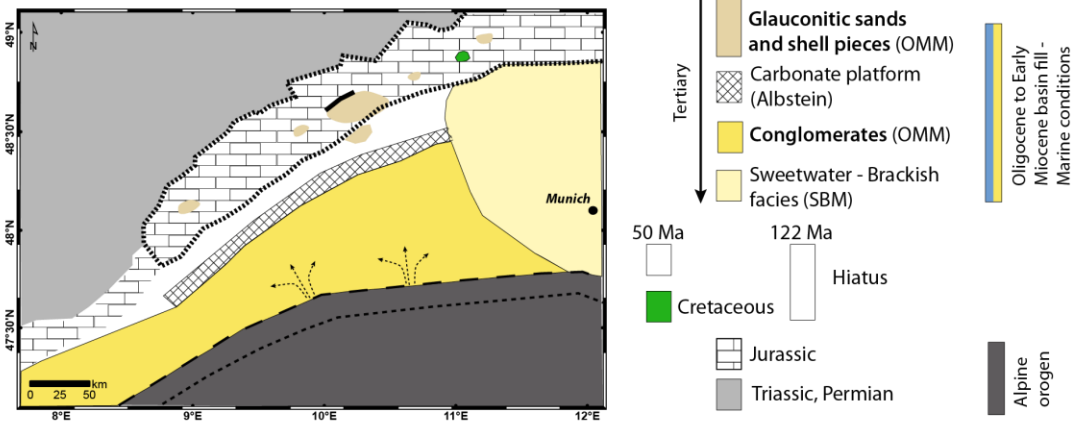

Plate C

Late Miocene (~12 Ma). OSM is eroded down to Jurassic

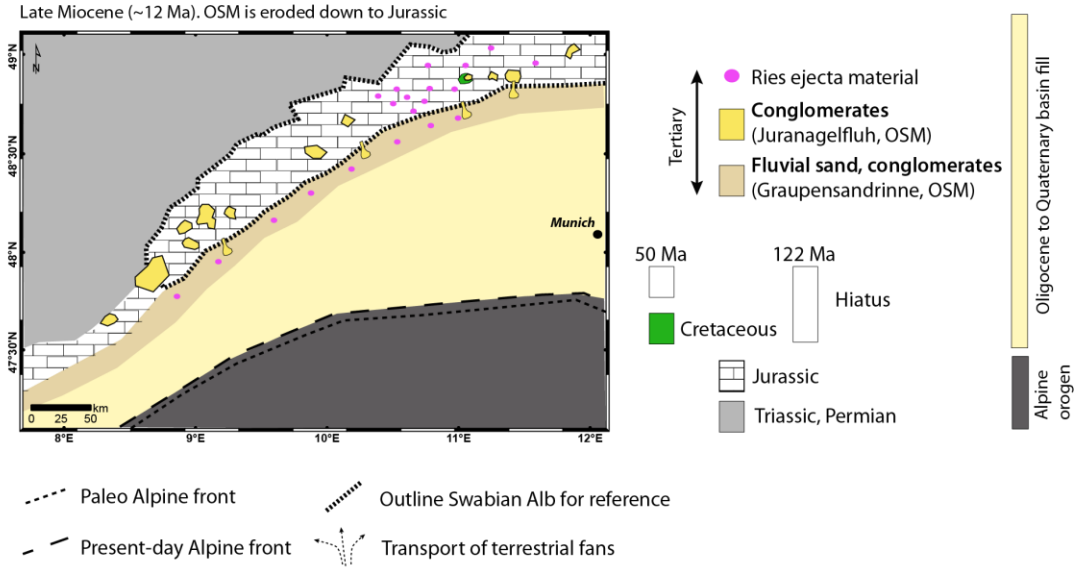

7. Discussion

7.1. Evolution of the coastal region along the northern margin of the NAFB

In all maps compiled in Fig. 3.15, we recognize a zone of erosion and transport, which is progressively shifting northward between the early and late Miocene. The facies compiled from the regional geologic maps indicate the different depositional zones along the northern rim of the eastern foreland basin. The observations match the depositional units of the predicted forebulge concept quite well (Fig. 3.14).

A) Early Miocene

During this time, fluvial sand and conglomerates are deposited on the Jurassic limestone of the Swabian Alb. The same sediments are also found in the southern part of the basin. Terrestrial sediments are missing along a 50 km - 60 km wide, E-W axis north of Munich.

B) Mid-Miocene

During this time, the shallow ocean flooded most of the Swabian Alb. This is evident from coastal marine facies of glauconitic sands and coastal debris sediments. Also the observed traces from rock-boring organisms indicate the coastal environment. Further to the south, fine-grained marine sediments are found in drill cores, indicating an offshore depositional zone.

C) Late Miocene

On the Swabian Alb, conglomerates (Juranagelfluh) formed by erosional transport from the northern rim of the Alb. The material was transported southward into a fluvial system that existed along the southern rim of the Swabian Alb (Graupensandrinne) (Doppler and Schwerd, 1996; Kiderlen, 1931). North of the Albtrauf, none of these Miocene sediments have been deposited. When the Ries meteorite impacted on the Swabian Alb at ~ 14.9 Ma (Storzer et al., 1995), the ejecta material became incorporated into the terrestrial transport systems existing at that time. This provides an additional age control of the sediments, because Ries ejecta are found along the aforementioned fluvial system.

The paleo-shoreline of the Miocene ocean has left coastal remnants that are modified by surface erosion, local tectonics and the Ries meteorite impact. Its present-day elevation is therefore a combination of dynamic processes along the southern German cuesta landscape. We suggest that the previously established cliff line is not preserved in-situ and therefore reflects significant overprinting by surface processes, which limits the applicability as a paleo-geodetic water level. However, the coastal area along the Swabian Alb still reflects surface uplift, which can be correlated with potential local tectonics and uplift of the entire region. Therefore, cliff sites are affected by local tectonics and erosion, while the coastal area can still be well used to study regional uplift of the Swabian Alb and adjacent areas after the mid-Miocene.

In the NAFB, additional geologic observations possibly indicate the forebulge area. In the northwestern portion of the NAFB, the formation of a basin-axis-parallel caliche horizon with limestone pebbles (Albstein barrier) south of the Graupensandrinne, is dated to be late Burdigal in age (Geyer, 2011; Zöbelein, 1985a). These deposits potentially mark the onset of the northward shift of the peripheral high, since they indicate shallow brackish or fluvial-lacustrine conditions. By the onset of the Burdigal, these deposits did not yet exist (Doppler and Schwerd, 1996).
However, Buchner et al (2003) showed based on Ar^{39}/Ar^{40} ages, that the sediments associated with the fill of the GSR are much younger (14.4 Ma) than previously thought (Reichenbacher et al., 1998). If this area is indicative for the forebulge zone, it would have been exposed about 3 Ma after the last marine cycle in the basin, which likely flooded the previously existing peripheral high. Subsequently, the bulge was located roughly along the Swabian Alb during the late Miocene. The transport of conglomerates (Juranagelfluh) into the Graupensandrinne indicates the higher elevation in the north, which caused the south-directed transport of terrestrial detritus. After the Ries impact, the ejecta material was also transported into the west-draining fluvial systems, along the northern margin of the foreland basin (Fig. 3.14, 3.16).
Furthermore, the timing of the Urach volcanics (11 Ma – 14 Ma, Lippolt et al., 1973), that have been attributed to forebulge activity (Wilson and Downes, 2006), match the timing and position of the suggested passage of the peripheral high during the late Miocene.
Lastly, the late Miocene to Pliocene enhanced karstification along the Swabian Alb, as evident from e.g., the Laichingen cave and Bear cave (Strasser, 2011; Strasser et

al., 2009; Ufrecht, 2008), reflects subaerial exposure. The oldest caves on the central Swabian Alb (Laichinger cave, Falkenstein cave, Blautopf cave) presumably already existed 14 Ma – 20 Ma ago (Hasenmayer, 1985, 1996). This would confirm the subaerial exposure of the region controlled by uplift of the forebulge.

The detected scale of surface uplift across the Swabian Alb shows a wavelength of ~ 300 km and an amplitude ≥ 500 m. This wide-area signal is difficult to explain by upper crustal structures. More likely, it may be regional-scale uplift drawn by upper mantle or asthenospheric processes. For northwestern Europe, the arrival of the Island mantle plume has been linked to uplift and hiatuses at c. 55 Ma (Friedrich et al 2016, in review, Gondwana Research). For the Swabian Alb and the northern half of the NAFB, the mostly missing Paleocene and Cretaceous sediments are likely the result of large-scale uplift that led to enhanced erosion. This could reflect a dynamic topography signal. Therefore, the region might be overprinted by this large-scale mantle process.

The coastal features at site *Heldenfingen* do not necessarily reflect a wave based coastal notch as inferred from the bio-erosion traces. The analysis of the lithophocoenose reveals the presence of sponges after the rock was colonized by rock-boring bivalves. Sponges are morphology controlling organisms by building notches due to bio-erosion at rates between 1.0 mm/a and > 1 cm/a (Healy, 1968; Kelletat, 1997; Neumann, 1966). Their habitat optimum ranges from a few meters below water level down to several tens of meters. Recently, shelf sponge colonies have been observed in water depths > 1,000 m (Lundsten et al., 2014). These findings indicate that site *Heldenfingen* likely experienced a higher water depth.
This is in agreement with observations of neritic marine facies to the west between Ulm and Herbrechtingen. Here, marine sands and clay overlain by terrestrial conglomerates (Jura-Nagelfluh) have been documented at an elevation of > 700 m southeast of Albstadt (Roll, 1935). The deposits are in contact with the Jurassic limestone and the type of contact has been interpreted as a transgressive onlap. This would confirm the inferred deeper marine conditions at *Heldenfingen* further to the east. The marine transgression causing the local features potentially has covered larger areas of the Swabian Alb, which has been previously suggested for other segments of the cliff (Gall, 1975). After the occupation by marine sponges, the

following regression must have been rapid and did not allow a new coastal occupation by other shallow water rock-browsers. However, such a rapid coastline migration seems unlikely and therefore a possible mechanism to explain the change from submarine to subaerial is vertical displacement from coseismic uplift, as for example observed along the southern coast of Crete with coseismic uplift of up to nine meters (e.g., Pirazzoli, 1988; Pirazzoli et al., 1996).

The observed faults and lineaments, associated with the cliff line, indicate horizontal offsets from several tens up to a hundred meters. Vertical scarps of a similar scale are not detected. The observed faults are younger than the coastal features, because they offset Ries ejecta deposits, indicating that tectonics modified the coastal region after it became abandoned.

The eastern most coastal location *Burgmagerbein* yields different bio-erosion features and sediment records. Since the site is located close to the Ries impact carter, it is overprinted by impact related transport of material (Gall, 1974 a; Kiderlen, 1931). However, the coastal features are exposed at locations several meters below the present-day surface and the massive limestone sequence, outcropping in the pit mine, does not show any evidence for a large-scale mass transport. Only the upper 2 m - 3 m thick Suevite horizon reveals the impact related surface erosion. Furthermore, the set of marine bio-features shows a different paragenesis compared to site *Heldenfingen*, with only large bivalve boreholes and oyster shells. This implies that the *Burgmagerbein* site potentially formed under shallower marine conditions, or it could be also significantly older and does not belong the mid-Miocene coastal area.

The fact that the site is situated right at the southern margin of the younger Ries impact crater could reflect a very wide coastal area, whose northern extend has been erased by the Ries impact. Alternatively, the site could reflect an exposure of an earlier marine transgression, which only reached the southernmost tip of the Swabian Alb. However, the linear extend of a wide coastal zone across the Ries area during the mid-Miocene is the favored explanation here, because east of the Ries crater, a continuation of the cliff line at a roughly similar latitude has been suggested. This would confirm the Ries crossing geometry of the original coast (Bausch, 2000).

The age of both sites is constrained by sparse fossil assemblages (Geyer, 2011; Rosendahl et al., 2006), which are not necessarily reflecting the youngest or oldest marine phase. The oyster shells found at the two sites provide an age estimate of c.

mid-Miocene, but since each site still shows different species that are not only reflecting different water depth, the sites are potentially not coeval.

Besides the uncertainties in site age, their elevation reflects regional uplift. The western most part of the cliff coast is likely to be influenced by the rift flank uplift of the Rhine Graben that accelerated in the Miocene (Hinsken et al., 2007). Upwelling of hot buoyant mantle material underneath the flanks of the Rhine Graben rift reaching up 50 km eastward (Ziegler, 1990), could be responsible for wide-ranging surface tilt. However, the dip of strata towards the south and southeast is restricted to the area closest to the Black Forest toe. The uplift history along the rift flanks has been studied based on syn-rift sedimentation data (Hinsken et al., 2007). The results suggest that uplift is potentially older than the cliff coast along the Swabian Alb. During the Burdigalian, the forebulge uplift of the western NAFB might have caused uplift of the Upper Rhine Graben and adjacent regions.

Therefore, we suggest the cliff line has recorded a localized rift flank uplift coupled with the western forebulge uplift instead of a coeval long-distance tilt of the entire Swabian Alb. Furthermore, the central and eastern Swabian Alb seems to be unaffected by the Rhine Graben rift flank uplift, since we observe a significant decrease in the regional dip of strata. The reason for this could be that the rift flank uplift is simply older than the marine features investigated here. For uplift of those, a more widespread, uniform process is held responsible for the present-day elevation. Growing evidence from our investigation suggests that the region has experienced moderate uplift caused by the passage of the NAFB flexural bulge. One indicator is the gentle and uniform southward dip of Mesozoic strata across the central Swabian Alb.

In addition, the onlaps of mid-Miocene sediments onto the Swabian Alb Jurassic limestone reveal erosion of OMM sediments in this area after the Eggenburgian (Fig. 3.13). Between the OMM and the Jurassic, a sequence boundary is identified whose northern most extend is represented by the *Heldenfingen* coastal site.

Towards the basin, the sediments are erosionally truncated by the incision of the mid-Miocene (Badenian; Graupensandrinne - GSR). This fluvial system has eroded most of the OMM deposits by enhanced incision (e.g., Doppler and Schwerd, 1996). A possible reason for the basin axis parallel incision could be uniform uplift due to the position close to the NAFB forebulge. The last phase of the fluvial and limnic deposits of the BM has extended from east to west only up to the area of Augsburg

(Fig. 3.13). Here, also the conglomerates of the Hochgrat and Lech fans have been transported in a NE direction (Doppler, 1989; Doppler and Schwerd, 1996), and these sediments did not cross the Albstein barrier, which emphasizes the assumed uplift of the western basin part and the bounding contact zone along the Swabian Alb as the forebulge.

Based on the paleo shoreline position of the two sites, the surface uplift for the area is estimated to be 0.05 mm/a – 0.09 mm/a. A fraction of this signal results from response to isostatic uplift of (0.03 ± 0.0013) mm/a – (0.04 ± 0.0013) mm/a, caused by local erosion of at least 250 m of sediments (Champagnac et al., 2007; Hüttner, 1958).

This estimate is one order of magnitude greater than the late Miocene 0.005 mm/a – 0.017 mm/a uplift reported from cave levels across the Swabian Alb (Strasser, 2009). Both estimates indicate a slow, wide-area uplift along the marginal region of the NAFB. However, our inferred relative surface uplift might suffer from two major uncertainties. The amount of erosion across the Swabian Alb is not well constraint (Hüttner, 1958). Further, the relative coastal position of the two sites has been derived from their bio-features and the comparison to other coastal environments (e.g., Kelletat, 1997). This extrapolation is not nessecarily the only scenario for the region. Especially the lack of precise radiometric age constraints in addition to the biostratigraphic correlation is a source of ambiguity. Nevertheless, the proposed rates based on geologic observations confirm an uplift of the marginal area relative to the NAFB since the mid-Miocene that likely reflects a combination of local tectonics and underlying large scale processes.

The results from additional facies and hiatus mapping suggest a contribution from the NAFB forebulge during the Miocene. Forebulge identification in terms of timing and geometry has to be conducted by studying related geologic observations (Tab. 3.3). An additional approach to detect a forebulge is derived from modeling. However, in this context a mismatch of the modeled dimensions and the geologic observations can occur (Crampton and Allen, 1995). This is because models often assume simple plate configurations and do not account for secondary overprint. The model of e.g., Crampton and Allen (1995) suggests a wavelength of both basin and forebulge zone that is equal, and only the amplitude of the bulge is estimated to be 40 times smaller than the basin’s one. This can be regarded as a first estimate but only geologic data

can provide sufficient information to infer the potential forebulge position. Based on data from our study and supported by geologic maps, we locate a potential forebulge area of the NAFB.

In the early Miocene (lower Egerian), an erosional or non-depositional corridor extended just north of the central basin axis from east to west (Kuhlemann and Kempf, 2002). This is regarded as the position of the forebulge at that time.

When a flexure, forming the forebulge, starts to decrease, the bulge accounts for that by backward migration towards the thrust front (e.g., Crampton and Allen, 1995). Similarly, the suggested eastern Alps slab break-off at ~ 20 Ma (Handy et al., 2014) possibly has resulted in the migration of the peripheral bulge basin-ward (Fig. 3.16). During the mid-Miocene, when OMM was deposited on the Swabian Alb, the previously existing central basin forebulge zone most likely was flooded, because marine facies are widely distributed in the area (Kuhlemann and Kempf, 2002). The shallow ocean prograded onto the Swabian Alb and deposited shallow coastal sediments is this area. It cannot be determined, whether the forebulge has remained stable during this time or it moved further north- or southward, because no submarine sediment transport systems have been detected that could show corresponding transport directions.

In the Ottnagian, a fluvial system (Graupensandrinne – GSR; Fig. 3.4), about 10 km - 15 km wide, extended along the boundary between the elevated Swabian Alb and NAFB. Material in this system has been transported southwestward. During this time, sediments of the OMM have been widely eroded, down to the top of the USM and replaced by conglomerates and sands. We suggest that this fluvial system has developed right along the southern margin of the forebulge zone.

A similar setting is known from the western Alpine foreland in Switzerland, where a river system developed on top of the buried forebulge during the Oligocene (Schlunegger et al., 1997). Another example is reported from the Himalaya foreland basin, where the present-day Ganges river flows on the southern (distal) side of the forebulge and young strata are overlapping the actual forebulge area (Karner and Watts, 1983).

Table 3-3: Geometries and key observations of forebulge areas in flexural basins and depressions

Region	Age	Wavelength [km]	Amplitude [m]	Mechanism of formation	Basin depth [km]	Key observations	Reference
Gulf of Maine	Holocene	5 - 10	20 - 25	Deglaciation	0.2 - 0.3	Sedimentary structure: foresets	Barnhardt et al, 1995
Western interior basin	Jurassic	300	200	Cont. Collision	4	Erosional truncation of surfaces, notches tilted away from the bulge, transgressive onlaps	Plint et al, 1993; Busby and Ingersoll, 1995,
Western Taiwan basin	Pliocene	50	200	Cont. Collision	5	Basal unconformity and positive Bouguer anomaly	Busby and Ingersoll, 1995; Ho-Shing Yua and Ying-Wei Choub, 2001
NAFB	Eocene	40	200	Cont. Collision	5	Basal unconformity and onlap of strata	Crampton and Allen, 1995
Fennoscandia	Holocene	300	60	Deglaciation	-	Tilt of paleo shorelines	Fjeldskaar, 1994
Karoo basin	Permian	450	400	Cont. Collision	6	Onlaps, transgressive and regressive horizons	Catuneanu et al, 2002
Himalaya foreland basin	Paleocene	300	500	Cont. Collision	5.5	Angular uncoformity with fluvial conglomerates	Singh, 2003; Burbank et al 1996

8. Conclusions

The mid-Miocene cliff line along the Swabian Alb has been significantly overprinted by erosion, tectonics and a meteorite impact. The coastal features of the two outcrops *Heldenfingen* and *Burgmagerbein* show different paragenesis of marine, rock-boring species. Based on these results, both sites most likely are not coeval and formed at different water depths. Therefore, the marine cliff along the Swabian Alb is better characterized as a wide coastal region instead of a narrow cliff line.

The previously deduced east-tilt of the Swabian Alb is not necessarily a continuous, regional process. The present-day elevation of mid-Miocene coastal features rather reflects episodic and local displacement, bound to the individual history of coastal outcrops.

When using the ancient coast as a paleo-geodetic marker, it has to be corrected for the local modifications and only outcrops reflecting the same age and water depth are robust to infer a surface uplift or tilt between those. The previously inferred Swabian Alb east-tilt by uplift of the Rhine Graben rift flanks (Black Forest) could be older than the marine features.

Most of the late Miocene and Pliocene vertical motion is likely caused by a northward migration of the NAFB forebulge, supplemented by an additional uniform uplift signal. In this context, we detected an uplift signal on the order of 0.05 mm/a for the region since the mid-Miocene. This signal across the region could also result from an underlying process, e.g., dynamic topography, which has additionally uplifted the Swabian Alb. However, further studies in adjacent regions are necessary to deduce evidence for this scenario.

Finally, the exact timing of formation and uplift of the features documented here cannot be resolved, because the features lack precise age constraints. Therefore, radiometric dating is necessary to gain better temporal constraints.

9. References

Abbott, L. D., Eli A. Silver, Robert S. Anderson, Randall Smith, James C. Ingle, Stanley A. Kling, David Haig, Eric Small, Joseph Galewsky, and William S. Sliter, 1997, Measurement of tectonic surface uplift rate in a young collisional mountain belt: Nature, v. 385, p. 501–507.

Abel, T., Harlachr, C., and Ufrecht, W., 2006, Zur Verkarstung der Bären- und Karlshöhle bei Erpfingen (Schwäbische Alb) im Plio-Pleistozän unter Berücksichtiugng von SInterchronologie und Paläontologie: Jber. Mitt. Oberrhein. Geol. Ver., N.F., v. 88, p. 9–51.

Bachmann, G. H., and Müller, M., 1991, The Molasse basin, Germany: evolution of a classic petroliferous foreland basin: Generation, accumulation, and production of Europe's hydrocarbons (ed. A.M. Spencer, Special Publication of the European Association of Petroleum Geoscientists, Oxford University Press, v. 1, p. 273–276.

Barnhardt, W. A., Gehrels, W. R., and Kelley, J. T., 1995, Late Quaternary relative sea-level change in the western Gulf of Maine: Evidence for a migrating glacial forebulge: Geology, v. 23, no. 4, p. 317–320.

Bausch, W. M., 2000, Die Albüberdeckung auf den Blättern Schamhaupten und Riedenburg: Erlanger Beiträge zur Petrologie und Mineralogie, v. 10, p. 53–60.

Bergerat, F., 1994, From inversion methods to paleostress field reconstructions in platforms, chains and basins: an overview. Some examples in Western and Central Europe. In: Roure, F. (ed.) Peri- Tethyan Platforms Paris: Editions Technip., p. 159–178.

Birzer, F., 1969, Molasse und Ries-Schutt im westlichen Teil der südlichen Frankenalb: Geologische Blätter für Nordost-Bayern, v. 19, p. 1–28.

Blakey, R. C., Peterson, F., Caputo, M. V., Geesaman, R. C., and Voorhees, B. J., 1983, Paleogeography of Middle Jurassic continental, shoreline, and shallow marine sedimentation, southern Utah: Rocky Mountain Section (SEPM).

Burbank, D., and Anderson, R., 2001, Tectonic Geomorphology, p. 2–211.

Burbank, D., Beck, R. A., and Mulder, T., 1996, 9 The Himalayan foreland basin, 149–190.

Burke, K., 1996, The African Plate: S.Afr.J.Geol., v. 99, no. 4, p. 341–409.

Busby, C. J., and Ingersoll, R. V., 1995, Tectonics of sedimentary basins, p. 1–51.

Byerly, G. R., Lowe, D. R., and Walsh, M. M., 1986, Stromatolites from 3,300–3,500 Myr Swaziland Supergroup, Barberton Mountain Land, Sotuh Africa: Nature, v. 319, p. 489–491.

Carle´ , W., 1955, Bau und Entwicklung der Süddeutschen Großscholle: Beihefte zum Geologischen Jahrbuch, v. 16, p. 128–149.

Catuneanu, O., Hancox, P. J., Cairncross, B., and Rubidge, B. S., 2002, Foredeep submarine fans and forebulge deltas: orogenic off-loading in the underfilled Karoo Basin: Journal of African Earth Sciences, v. 35, no. 4, p. 489–502.

Cawthra, H. C., Compton, J. S., Fisher, E. C., MacHutchon, M. R., and Marean, C. W., 2016, Submerged shorelines and landscape features offshore of Mossel Bay, South Africa: Geological Society, London, Special Publications, v. 411, no. 1, p. 219–233.

Champagnac, J. D., Molnar, P., Anderson, R. S., Sue, C., and Delacou, B., 2007, Quaternary erosion-induced isostatic rebound in the western Alps: Geology, v. 35, no. 3, p. 195.

Crampton, S. L., and Allen, P. A., 1995, Recognition of Forebulge Unconformities Associated with Early Stage Foreland Basin Development: Example from the North Alpine Foreland Basin: AAPG Bulletin, v. 79, no. 10, p. 1495–1514.

De La Beche, H. T., 1846, On the formation of the rocks of south Wales and south western England.: Memoirs of the Geological Survey of Great Britain, v. 1, p. 238–296.

De Maillet, B., 1748, Telliamed ou entretiens d'un philosophe Indien avec un missionaire Francois sur la diminution de la mer [A Telliamed or conversation between an Indian philosopher and a French missionary on the diminution of the sea]. Translated and edited by A.V. Carozzi, 1968, Urbana: University of Illinois Press, p. 1–58.

DeCelles, P. G., and Giles, K. A., 1996, Foreland Basin Systems: Basin Research, v. 8.2, p. 105–123.

DeConto, R. M., and Pollard, D., 2016, Contribution of Antarctica to past and future sea-level rise: Nature, v. 531, no. 7596, p. 591–597.

Dehm, R., 1962, Das Nördlinger Ries und die Meteortheorie: Mitt. Bayer. Staatssamml. Paläont. hist. Geol., v. 2, p. 69–87.

Dongus, H., 1972, Schichtflächenalb, Kuppenalb, Flächenalb (Schwäbische Alb): Zeitschrift für Geomorphologie, v. 16, p. 374–392.

-, 1977, Die Oberflächenformen der Schwäbischen Alb und ihres Vorlandes: Selbstverlag des Geographischen Institutes der Universität Marburg, v. 72, p. 8–29

Doppler, G., 1989, Zur Stratigraphie der nördlichen Vorlandmolasse in Bayerisch-Schwaben: Geologica Bavarica, v. 94, p. 83–133.

Doppler, G., and Schwerd, K., 1996, Faltenmolasse, Aufgerichtete Molasse und westliche Vorlandmolasse, *in* Freudenberger, W., and Schwerd, K., eds., Erläuterungen zur Geologischen Karte von Baysrn 1: 500,000, Volume 4: München, Bayersiches Geologisches Landesamt, p. 150–168.

England, P., and Molnar, P., 1990, Surface uplift, uplift of rocks, and exhumation of rocks: Geology, v. 18, no. 12, p. 1173–1177.

Fjeldskaar, W., 1994, The amplitude and decay of the glacial forebulge in Fennoscandia: Norsk Geologisk Tidsskrift, v. 74, no. 1, p. 2–8.

Füchtbauer, H., 1964, Sedimentpetrographische Untersuchungen in der älteren Molasse der Alpen.: Eclogae geol. Helv. Basel, v. 57, p. 157–298.

Gall, H., 1969, Geologische Untersuchungen im südwestlichen Vorries. Das Gebiet des Blattes Wittislingen: Dissertation Fakultät für Geowissenschaften der Ludwig-Maximilians-Universität München, p. 5–140

-, 1971a, Geologische Karte von Bayern 1: 25000, Erläuterungen zum Blatt Nr. 7328 Wittislingen: Bayerisches Geologisches Landesamt München, p. 186.

-, 1971b, Obere Süßwassermolasse (Hangendserie) über Riestrümmermassen bei Graisbach (südöstliches Vorries) und ihre Bedeutung für die Landschaftsgeschichte des Schwäbisch-Fränkischen Alb: Mitteilungen der Bayersichen Staatssammlungen Paläontologie und historische Geologie, v. 11, p. 295–326.

-, 1974 a, Neue Daten zum Verlauf der Klifflinie der Oberen Meeresmolasse (Helvet) im südlichen Vorries: Mitteilungen der Bayerischen Staatssammlungen Paläontologie und historische Geologie, v. 14, p. 81–101.

-, 1974 b, Geologischer Bau und Landschaftsgeschichte des südöstlichen Vorrieses zwischen Höchstädt a. d. Donau und Donauwörth: Neues Jahrbuch der Geologischen und Paläontologischen Abhandlungen, Stuttgart, v. 145, no. 1, p. 58–95.

-, 1975, Der III. Zyklus der Oberen Meeresmolasse (Helvet) am Südrand der Schwäbisch-Fränkischen Alb: Mitteilungen der Bayerischen Staatssammlung für Paläontologie und historische Geologie, v. 15, p. 179–205.

Geyer, O. F., and Gwinner, M. P., 1979, Die Schwäbische Alb und ihr Vorland: Slg. Geol. Führer, v. 67, p. 271.

Geyer, O. F., Gwinner, M.P., Geyer, M., Nitsch, E. and Simon, T., 2011, Geologie von Baden-Württemberg, 627 p.

Glahn, A., Sachs, P. M., and Achauer, U., 1992, A teleseismic and petrological study of the crust and upper mantle beneath the geothermal anomaly Urach/SW-Germany: Physics of the earth and planetary interiors, v. 69, no. 3–4, p. 176–206.

Goldstein, R. H., Franseen, E. K., Dvoretsky, R. A., and Sweeney, R. J., 2012, Controls on focused-flow and dispersed-flow deepwater carbonates: Miocene Agua Amarga Basin, Spain: Journal of Sedimentary Research, v. 82, no. 7, p. 499–520.

Grabau, A. W., 1913, Principles of Stratigraphy. New York: A.G. Seiler & Co, v. 1, p. 185p.

-, 1940, The Rhythm of the Ages. Peking, Henri Vetch, 561p.; 2nd printing in 1978 with an introduction by A.V. Carozzi: Huntington, N.Y., Krieger, p. 561p.

Grant, R. E., 1826, Notice of a New Zoophyte (Cliona celata Gr.) from the Firth of Forth.: Edinburgh New Philos. J., v. 1, p. 78–81.

Grünthal, G., and Wahlström, R., 2003a, An Mw based earthquake catalogue for central, northern and northwestern Europe using a hierarchy of magnitude conversions: Journal of seismology, v. 7, no. 4, p. 507–531.

Handy, M. R., Ustaszewski, K., and Kissling, E., 2014, Reconstructing the Alps–Carpathians–Dinarides as a key to understanding switches in subduction polarity, slab gaps and surface motion: International Journal of Earth Sciences, v. 104, no. 1, p. 1–26.

Haq, B. U., Hardenbol, J., and Vail, P. R., 1987, Chronology of fluctuating sea levels since the Triassic: Science, v. 235, no. 4793, p. 1156–1167.

Hasenmayer, J., 1985, Blautopf - Blauhöhle, Schlüssel für ein neues Verkarstungsbild des Schwäbischen Juras: Blaubeurer Heimatbuch, p. 19–50.

-, 1996, Das Geheimnis des Blautopf. – GEO 5: 10–38: GEO, v. 5, p. 10–38.

Healy, T. R., 1968, Bioerosion on shore platforms developed in the Waitemata Formation, Auckland: Earth Science Journal, v. 2, no. 1, p. 26–37.

Heizmann, E. P., Reiff, W., and Steinheim, A., 2002, Der Steinheimer Meteorkrater, München, Friedrich Pfeil Verlag, Führer durch das Meteorkratermuseum, einer von der Gemeinde Steinheim am Albuch betriebenen Zweigstelle des Staatlichen Museums für Naturkunde in Stuttgart, 167 p.

Hinderer, M., 2001, Late Quaternary denudation of the Alps, valley and lake fillings and modern river loads: Geodinamica Acta, v. 14, no. 4, p. 231–263.

Hinsken, S., Ustaszewski, K., and Wetzel, A., 2007, Graben width controlling syn-rift sedimentation: the Palaeogene southern Upper Rhine Graben as an example: International Journal of Earth Sciences, v. 96, no. 6, p. 979–1002.

Hofbauer, G., 2012, Jungtertiäre Talverschüttung und tektonische Verstellung entlang des Regnitz- Rezat-Tals: GDGH Berichte, v. 15, p. 1–16.

Hüttner, R., 1958, Geologische Untersuchungen im SW-Vorries auf Blatt Neresheim und Wittislingen: Dissertation Universität Tübingen, p. 1–347.

-, 1961, Geologischer Bau und Landschaftsgeschichte des östlichen Härtsfeldes (Schwäbische Alb): Jahrbuch geologisches Landesamt Baden Württemberg, v. 4, p. 49–125.

Johnson, M. E., 1992, Studies on Ancient Rocky Shores: A Brief History and Annotated Bibliography: Journal of Coastal Research, v. 8, no. 4, p. 797–812.

Karner, G. D., and Watts, A. B., 1983, Gravity anomalies and flexure of the lithosphere at mountain ranges: Journal of Geophysical Research: Solid Earth, v. 88, no. B12, p. 10449–10477.

Kelletat, D. H., 1997, Mediterranean coastal biogeomorphology: processes, forms and sea-level indicators, in: Transformations and evolution of the Mediterranean coastline: Bulletin de l'institut oceanographique, Monaco, v. 18, no. 3, p. 209–226.

Kiderlen, H., 1931, Beiträge zur Stratigraphie und Paläographie des süddeutschen Tertiärs: Neues Jahrbuch der Geologischen und Paläontologie, Beilagen Bände, Stuttgart, v. 66, no. Abt. B, p. 215–384.

Kirby, M. X., 2000, Paleoecological Differences Between Tertiary and Quaternary Crassostrea Oysters, as Revealed by Stable Isotope Sclerochronology: Palaios, v. 15, no. 2, p. 132–141.

Kominz, M. A., Browning, J. V., Miller, K. G., Sugarman, P. J., Mizintseva, S., and Scotese, C. R., 2008, Late Cretaceous to Miocene sea‐level estimates from the New Jersey and Delaware coastal plain coreholes: An error analysis: Basin Research, v. 20, no. 2, p. 211–226.

Kuhlemann, J., Frisch, W., Dunkl, I., and Székely, B., 2001, Quantifying tectonic versus erosive denudation by the sediment budget: the Miocene core complexes of the Alps: Tectonophysics, v. 330, p. 1–23.

Kuhlemann, J., and Kempf, O., 2002, Post-Eocene evolution of the North Alpine Foreland Basin and its response to Alpine tectonics: Sedimentary Geology, v. 152, p. 45–78.

Lambeck, K., and Chappel, J., 2001, Sea level change through the last glacial cycle: Science, v. 292.5517, p. 679–686.

Lemcke, K., 1974, Vetikalbewegungen des vormesozoischen Sockels im nördlichen Alpenvorland Perm bis zur Gegenwart?: Eclogae Geologicae Helvetiae, v. 67, no. 1, p. 121–133.

Lemcke, K., Engelhardt, W. V., and Füchtbauer, H., 1953, Geologische und sedimentpetrographische Untersuchungen im-Westteil der ungefalteten Molasse des süddeutschen-Alpenvorlandes, p. 19–128.

Lippolt, H. J., Todt, W., and Baranyi, I., 1973, K-Ar ages of basaltic rocks from the Urach volcanic district, SW Germany: Fortschr. Mineral., v. 50, p.101–102.

Lundsten, L., Reiswig, H. M., and Austin, W. C., 2014, Four new species of Cladorhizidae (Porifera, Demospongiae, Poecilosclerida) from the Northeast Pacific: Zootaxa, v. 3786, p. 101–123.

Lüschen, E., Lammerer, B., Gebrande, H., Millahn, K., and Nicolich, R., 2004, Orogenic structure of the Eastern Alps, Europe, from TRANSALP deep seismic reflection profiling: Tectonophysics, v. 388, no. 1–4, p. 85–102.

Lutzeier, H., 1922, Beiträge zur Kenntnis der Meeresmolasse in der Ulmer Gegend: Neues Jahrbuch für Geologie und Paläontologie, Beilagen Bände, Stuttgart, v. 46, p. 117–180.

Lyell, C., 1845, Travels in North America: New York, Wiley & Putnam, 231 p., v. 1.

Matter, A., Homewood, P., Caron, C., Rigassi, D., Van Stujivenberg, J., Weidmann, M., and Winkler, W., 1980, Flysch andMolasse of western and central Switzerland, Geology of Switzerland, a Guidebook, Part B, Excursions (Ed. by R.Trümpy), Schweizer. Geol.Komm., p. 261–293.

Mäussnest, O., 1982, The Volcanic Phenomena in the Urach Region, *in* Haenel, R., ed., The Urach Geothermal Project (Swabian Alb, Germany): Stuttgart, Schweizerbart' sche Verlagsbuchhandlung, p. 157–163.

McCalpin, J. P. E., 2009, Paleoseismology (Vol. 95), Academic press, p. 497–598.

Miller, K. G., Kominz, M. A., Browning, J. V., Wright, J. D., Mountain, G. S., Katz, M. E., Sugarman, P. J., Cramer, B. S., Christie-Blick, N., and Pekar, S. F., 2005, The Phanerozoic record of global sea-level change: Science, v. 310, no. 5752, p. 1293–1298.

Moos, A., 1925, Beiträge zur Geologie des Tertiärs im Gebiet zwischen Ulm a. D. und Donauwörth: Geogn. Jh., v. 37, p. 167–252.

Nathan, H., 1955, Das Tertiär im südlichen bayerischen Vorries, in: Erläuterungen zur Geologischen Übersichtskarte der Süddeutschen Molasse 1:300 000, Geologische Karte, p. 42–55.

Neumann, A. C., 1966, Observations on coastal erosion in Bermuda and measurements of the boring rate of the sponge, Cliona lampa: Limnology and Oceanography, v. 11, no. 1, p. 92–108.

Peterek, A., and Schröder, B., 2010, Geomorphologic evolution of the cuesta landscapes around the Northern Franconian Alb – review and synthesis: Zeitschrift für Geomorphologie, v. 54, no. 3, p. 305–345.

Pinn, E. H., Richardson, C. A., Thompson, R. C., and Hawkins, S. J., 2005, Burrow morphology, biometry, age and growth of piddocks (Mollusca: Bivalvia: Pholadidae) on the south coast of England: Marine Biology, v. 147, no. 4, p. 943–953.

Pirazzoli, P. A., 1988, Sea-level changes and crustal movements in the Hellenic arc (Greece). The contribution of archaeological and historical data. - In: Archaeology of Coastal Changes., Raban A. ed., BAR Int. Ser.: Oxford, Oxford Univ. Press, v. 404, p. 157–184.

Pirazzoli, P. A., J., L., and Stiros, S. C., 1996, Coastal Indicators of Rapid Uplift and Subsidence Examples from Crete and other Mediterranean Sites: Z. f. Geom. NF Suppl. Bd., v. 102, p. 21–35.

Plint, A. G., Hart, B. S., and Donaldson, W. S., 1993, Lithospheric flexure as a control on stratal geometry and facies distribution in Upper Cretaceous rocks of the Alberta foreland basin: Basin Research, v. 5, no. 2, p. 69–77.

Pohl, J., Stöffler, D., Gall, H., and Ernstson, K., 1977, The Ries impact crater: Impact and Explosion Cratering, Pergamon Press, New York, p. 343–404.

Quinlan, G. M., and Beaumont, C., 1984, Appalachian thrusting, lithospheric flexure, and the Paleozoic stratigraphy of the Eastern Interior of North America: Canadian Journal of Earth Sciences, v. 21, no. 9, p. 973–996.

Radwanski, A., 1970, Dependence of rock-borers and burrowers on the environmental conditions within the Tortonian littoral zone of Southern Poland. In: Crimes, T.P. and Harper, J.C. (eds.), Trace Fossils. Liverpool: Seel House Press, p. 371–390.

Reichenbacher, B., Böttcher, R., Bracher, H., Doppler, G., von Engelhardt, W., Gregor, H. J., Heissig, K., Heizmann, E. P., Hofmann, F., Kälin, D., and Lemcke, K., 1998, Graupensandrinne–Ries-Impakt: Zur Stratigraphie der Grimmelfinger Schichten, Kirchberger Schichten und Oberen Süßwassermolasse (nördliche Vorlandmolasse, Süddeutschland): Zeitschrift der deutschen geologischen Gesellschaft, v. 149, no. 1, p. 127–161.

Reicherter, K., Froitzheim, N., Jarosinski, M., Badura, J., Franzke, H. J., Hansen, M., and Stackebrandt, W., 2008, Alpine tectonics north of the Alps: The Geology of Central Europe. Volume 2: Mesozoic and Cenozoic, p. 1233–1285.

Reiff, W., 1989, Das Kliff in Heldenfingen und die Klifflinie auf der Heidenheimer Alb: Jahrbücher und Mitteilungen des oberrheinischen geologischen Vereins 71, p. 467–482.

Reinecker, J., and Schneider, G., 2002, Zur Neotektonik der Zollernalb: Der Hohenzollerngraben und die Albstadt-Erdbeben: Jahresberichte und Mitteilungen des oberrheinischen geologischen Vereins, p. 391–417.

Roll, A., 1935, Beobachtungen lämgs der Küste des burdigalen Meeres auf der schwäbischen Alb: Zeitschrift der Deutschen Geologischen Gesellschaft, p. 281–307.

Rosendahl, W., Junker, B., Megerle, A., and Vogt, J., 2006, "Schwäbische Alb." Wanderungen in die Erdgeschichte, Volume 18, p. 160.

Schalk, K., 1957, Geologische Untersuchungen im Ries. Das Gebiet des Blattes Bissingen: Geologica Bavarica, 107 p.

Schetelig, K., 1962, Geologische Untersuchungen im Ries: das Gebiet der Blätter Donauwörth und Genderkingen: Geologica Bavarica, v. 47, p. 98 S., 25 Abb., 91 geol. Karte.

Scheuenpflug, L., 1976, Erste Hinweise auf eine pliozäne Donau in der östlichen Iller-Lech-Platte (Bayerisch Schwaben), p.26–29.

Schlunegger, F., Jordan, T. E., and Klaper, E. M., 1997, Controls of erosional denudation in the orogen on foreland basin evolution: The Oligocene central Swiss Molasse Basin as an example: Tectonics, v. 16, no. 5, p. 823–840.

Schlunegger, F., Melzer, J., and Tucker, G., 2001, Climate, exposed source-rock lithologies, crustal uplift and surface erosion: a theoretical analysis calibrated with data from the Alps/North Alpine Foreland Basin system: International Journal of Earth Sciences, v. 90, no. 3, p. 484–499.

Sieh, K., Ward, S. N., Natawidjaja, D., and Suwargadi, B. W. (1999): Crustal deformation at the Sumatran subduction zone revealed by coral rings. Geophysical Research Letters, 26 (20), p. 3141–3144.

Singh, B. P., 2003, Evidence of growth fault and forebulge in the Late Paleocene (~ 57.9–54.7 Ma), western Himalayan foreland basin, India: Earth and Planetary Science Letters, v. 216, no. 4, p. 717–724.

Steininger, F. F., and Wessely, G., 2000, From the Tethyan Ocean to the Paratethys Sea: Oligocene to Neogene stratigraphy, paleogeography and paleobiogeography of the circum-Mediterranean region and the Oligocene to Neogene Basin evolution in Austria: Mitteilungen der Österreichischen Geologischen Gesellschaft, v. 92, p. 95–116.

Storzer, D., Jessenberger, E. K., Kunz, J., and Lange, J.-M., 1995, Synopsis von Spaltspuren- und Kalium-Argon-Datierungen an Ries-Impaktgläsern Graupensandrinne - Ries-Impakt 161 und Moldaviten.: Exkursionsftihrer Veröff. GGW, v. 195, p. 79–80.

Strasser, M., 2011, Höhlen der Schwäbischen Alb als Pegelschreiber für Flussgeschichte und Tektonik in Südwestdeutschland seit dem Miozän [Ph.D. Dissertation]: Universtität Stuttgart, 109 p.

Strasser, M., Strasser, A., Pelz, K., and Seyfried, H., 2009, A mid Miocene to early Pleistocene multi-level cave as a gauge for tectonic uplift of the Swabian Alb (Southwest Germany): Geomorphology, v. 106, no. 1–2, p. 130–141.

Ufrecht, W., 2008, Evaluating landscape development and karstification of the Central Schwäbische Alb (Southwest Germany) by fossil record of karst fillings: Zeitschrift für Geomorphologie, v. 52, no. 4, p. 417–436.

Villinger, E., 1986, Untersuchungen zur Flussgeschichte von Aare-Donau/Alpenrhein und zur Entwicklung des Malm-Karsts in Südwestdeutschland: Jh. geol. Landesamt Baden-Württemberg, Freiburg, v. 28, p. 297–362.

Wagner, G., and Koch, A., 1961, Raumbilder zur Erd-und Landschaftsgeschichte Südwestdeutschlands: Spectrum Verlag, 32 p.

Wagner, L. R., 1996, Stratigraphy and hydrocarbons in the Up- per Austrian Molasse Foredeep (active margin): Eur. Assoc. Geosci. Eng. Spec. Publ., v. 5, p. 217–235.

Wilson, M., and Downes, H., 2006, Tertiary-Quaternary intraplate magmatism in Europe and its relationship to mantle dynamics. In: Gee, D.G. and Stephenson, R. (eds.) European lithosphere dynamics.: Geological Society of London, v. 32, p. 147–166.

Winker, C. D., and Howard, J. D., 1977, Correlation of tectonically deformed shorelines on the southern Atlantic coastal plain: Geology, v. 5, p. 123–127.

Yldirim, E. C., 2016, Reconstructing basin evolution through unconfomities: Hiatus mapping across the Northern Alpine Foreland Basin, unpublished Master Thesis, Ludwig-Maximilians Universtität München, 118 p.

Ziegler, P. A., 1990, Geological Atlas of Western and Central Europe Shell Int. Petrol. Maatschap: Geological Society of London, 239 p.

Zitzmann, A., 2003: Die Geologische Übersichtskarte 1:200 000 – von der Karte bis zur Sachdatenbank. Zeitschrift der Deutschen Geologischen Gesellschaft, Band 154/1, E. Schweizerbart´sche Verlagsbuchhandlung Stuttgart, p. 121–139.

Zöbelein, H. K., 1985a, Helicidenschichten und Albstein in der miozänen Vorlandmolasse Südwestdeutschlands: Jh. geol. Landesamt Baden- Württemberg, Freiburg, v. 27, p. 41–92.

Chapter 4

Quaternary tectonic activity of the Northern Alpine Foreland Basin - Analysis of erosion patterns and geomorphic markers

Authors
M. Hoffmann[1]*, A.M. Friedrich[1], M. Dühnforth[1]

Affiliation
1. Department of Earth and Environmental Sciences, Geology, Ludwig-Maximilians University of Munich, Germany

*Corresponding author (e-mail: ma.hoffmann@lmu.de)

1. Abstract

The low-strain Northern Alpine Foreland Basin (NAFB) exposes an elevated, erosional relief landscape, with asymmetric fluvial systems and minor Quaternary sediments. Climatic processes have so far been used to explain these features, but this does not address the pronounced elevated relief of the basin. An alternative explanation can be given by introducing Quaternary tectonics and potential basin uplift.

We examine Quaternary deposits and tectono-geomorphic features of the NAFB on timescales from $10^6 – 10^3$ years. Regional synthesis of well data is used to estimate the amount and distribution of Quaternary erosion across the basin. In addition, we assess the shape and stream characteristics of fluvial systems, to infer geometries and river steepness, which possibly express river response to surface uplift.

Sediment yield estimates reveal an average Quaternary thickness of c. 60 m across the NAFB, which is minor compared to the net sediment influx and sediment thickness in other circum-Alpine basins. The thinnest Quaternary cover follows an oval shaped E-W-pattern, along the central basin axis. We infer basin uplift from observed erosion, showing an average rate of c. 0.68 km/Ma since c. 35 Ma. Fluvial systems show asymmetric networks, stream capture and locally high channel-steepness indices (*KSN*), which all concentrate in the eastern portion of the NAFB. These results

suggest, that Quaternary erosion and stream features of young rivers correspond to basin inversion and possibly local tectonics in the eastern NAFB.

2. Introduction

Foreland basins are recorders of the tectonic processes along collisional orogenic plate boundaries. In particular, a basins' stratigraphy and geometry is useful in reconstructing its vertical motion history (Allen and Homewood, 1986; Quinlan and Beaumont, 1984). The NAFB in central Europe (Fig 4.1a and b), which evolved over Oligocene and Miocene time, is mainly regarded as a contemporaneously inactive basin system, based on stress-field and seismicity data (e.g., Heidbach et al., 2008; Reicherter et al., 2008).

If so, a change in the vertical motion from subsidence to uplift (inversion) of the basin must have occurred between late Miocene and present-day. A prominent Pliocene hiatus has been observed in bore-hole data across the whole basin and a proto-backstripping analysis implied westward-increasing basin uplift of a few tens of meters to over 2 km (Lemcke, 1974). The presence of a Pliocene hiatus may imply renewed basin uplift, but the overlying Quaternary record may be dominated by higher erosion rates during the Quaternary glacial and interglacial cycles. Thus, it has been uncertain if this late Miocene- to Pliocene-uplift continued during Quaternary time. We address this problem by providing new data and examining the Quaternary landscape in the NAFB, with focus on erosion patterns and fluvial geomorphic markers.

Indicators for the basin's vertical motion can be found at different time scales. While short-term data (seconds to decades), like space-geodetic measurements and instrumental and historic seismicity might indicate low activity of a region, long-term geologic and geomorphic data (centuries to millennia) can show increased activity by erosion and displacement of deposits. In this context, reviewing each dataset and comparing the time dependent rate, can provide better constraints of active vertical motion.

The geodetic velocities across the Alps show a slow NNW directed convergence between Eurasia and the Adriatic plate across the Alps (Fig. 4.1; Tab. 4.1).

In the NAFB and adjacent regions, numerous seismometer stations are recording earthquakes (Bavarian Seismic Survey), showing that seismicity is concentrated in the central Alps and the western foreland basin in Switzerland. Further areas of frequent seismicity are the Albstadt region at the Swabian Alb, as well as the Rhine Graben Rift (Fig. 4.2). For the central NAFB in Germany, documented earthquakes are sparse, showing magnitudes below 4.0 and intensity V, respectively (Leydecker, 2011; NEIC data base, 2016).

To detect possible basin inversion and tectono-geomorphic features, the considered timescale has to be enlarged. This can be accomplished by studying active river systems (Schumm, 1986) and sediment budgets (Hinderer, 2001; Hinderer, 2012).

In this study, we present a new tectono-geomorphic analysis of the German portion of the NAFB, with results from Quaternary erosion estimates, remote sensing mapping and digital drainage pattern analysis. The results imply that the NAFB is subject to continuous slow uplift, which has potentially also reactivated preexisting faults in the northeastern portion of the basin.

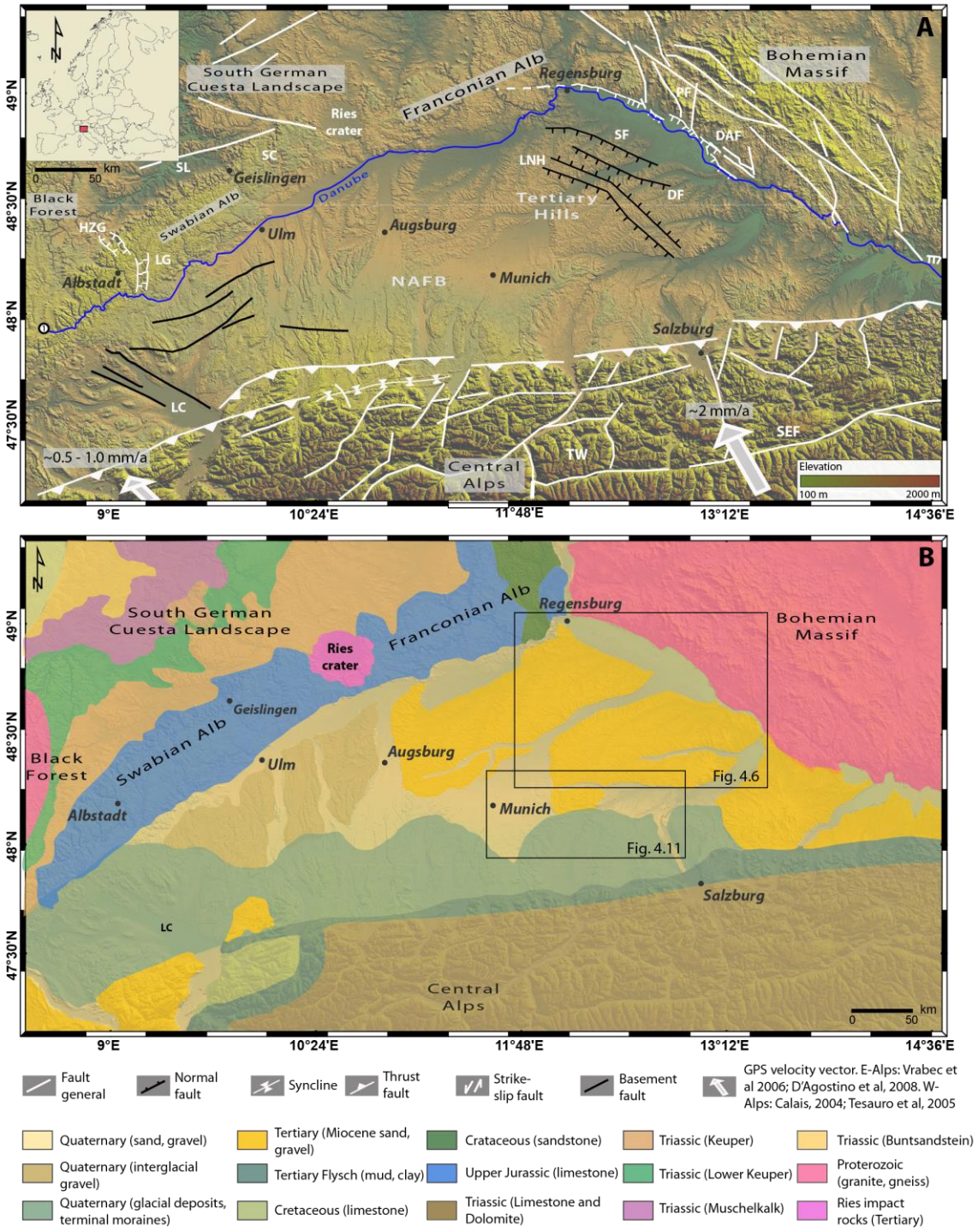

Fig. 4.1: Shaded relief map of the NAFB, German portion. A) Map of major fault systems. Background SRTM 3 arc sec. Arrows indicate the direction of the present-day GPS velocity field (EUREF network, Tesauro et al, 2005). Fault data from Bachmann and Müller, 1987; Unger, 1999; Schmid and Kissling, 2000. LC = Lake Constance, SL = Swabian Lineament Fault, SC = Steinheim Crater, LNH= Landshut-Neuoettinger-High, DAF = Danube Fault, DF = Dingolfing Fault, PF = Pfahl Fault, TW = Tauern Window, SF = Schierling Fault, SEF = Salzach-Ennstal-Fault, HZG = Hohenzollern Graben, LG = Lauchert Graben. B) Simplified geologic map of the NAFB. Data are compiled from the Geologic map of Bavaria, 1 : 500,000 and the Geologic map of Germany, BGR, 1 : 200,000.

Table 4-1: Summary of present-day geodetic signals across the Eurasia – Adriatic plate boundary

Location	Observation	Rate [mm/a]	Reference
Western Alps	Convergence Eurasia - Adriatic	0.5 - 1.0	Vrabec et al. 2006; D'Agostino et al. 2008
Eastern Alps	Convergence Eurasia - Adriatic	~ 2.0	Tesauro et al. 2005

3. Regional background

3.1. Geological setting

The NAFB is regarded as a peripheral foreland basin that developed on the subducting European plate (Bachmann and Müller, 1991; DeCelles and Giles, 1996). Today, the basin covers an area of ~ 55,000 km^2 with a width varying from ~ 10 km in western Switzerland and lower Austria to about 140 km in the central German part (Fig. 4.1a). The basin formed in the late Eocene, when the Eurasian continental margin started to collide and subduct under the Adriatic plate, forming the accommodation space on the Eurasian crust (Genser et al., 2007; Pfiffner, 1986; Schmid et al., 1996). Prior to formation of the NAFB, the plate convergence between Eurasia – Adriatic plate collision in the Cretaceous was followed by the collision in the late Eocene (Schmid et al., 1996). A slab break-off occurred most likely between 34 Ma and 29 Ma (Davies and von Blanckenburg, 1995), resulting in the detachment of the dense European oceanic plate from the upper buoyant part (e.g., Regard et al., 2008).

The continuing collision after 32 Ma is expressed in thrusting along the Periadriatic line and the Helvetic nappes propagation (32 Ma - 19 Ma) (Schmid et al., 1996). The crustal thickening and loading of the European plate led to the formation of two basins on the northern NAFB and southern side (Po basin) of the rising Alpine orogeny (e.g., Andeweg and Cloetingh, 1998). For the NAFB, the maximum basin depth was reached during the Miocene with > 5 km at the northern Alpine front (Lemcke, 1974).

The Adriatic-Eurasia continental collision gradually slowed down from > 8 mm/a at the onset of basin formation, to ≤ 2 mm/a today (D'Agostino et al., 2008; Schlunegger

and Kissling, 2015; Vrabec et al., 2006). Compared to other sedimentary basins, the NAFB can be considered as rather small (Tab. 4.2). Recently, a switch in subduction polarity in the eastern Alps has been suggested, using mantle tomography data (Handy et al., 2014). This presumably changed at least the eastern portion of the foreland basin from a peripheral to a retroarc stage, when the Adriatic slab started to subduct underneath the Eurasian continental lithosphere.

Table 4-2: Summary of characteristics of different collisional basins

Location	Basin type	Age of formation [Ma]	Max depth [km]	Max. width [km]	Paleo convergence rate [mm/a]	Present day convergence rate [mm/a]	Modern climate	Paleo climate	Drainage orientation	Reference
Adriatic Foreland Basin (Po Basin)	Peripheral	~ 30	5 - 8	120	-	5	Warm, medium dry	Sub-tropical to warm	Longitudinal	Lucchi, 1986; Busby and Ingersoll, 1995; Royden et al, 1987; Handy et al, 2014; Devoti et al, 2008
Alberta Basin	Retroarc	~ 500	~ 5	800	-	-	Continental	-	-	Bachu, 1995; Busby and Ingersoll, 1995
Appalachian Foreland Basin	Peripheral	~ 460	< 2	300	19 - 33	-	Cold humid to continental	Tropical	-	Busby and Ingersoll, 1995; Allen and Homewood, 1986
Himalayan Foredeep	Peripheral	90 - 45	5.5	500 (northwest end)	East ~ 10, West ~ 20	~ 18	Sub-tropical to warm, desert	Sub-tropical	Longitudinal	Busby and Ingersoll, 1995; Wesnousky et al, 1999; Larson et al, 1999; Burbank et al, 1996
North American Cordillera Foreland Basin	Retroarc	155 - 110	6	500 (E-W) at center	140 - 240	10	Continental dry	-	-	DeCelles, 2004; Busby and Ingersoll, 1995; Sella et al, 2002
Northern Alpine Foreland Basin	Post peripheral	40 - 35	5	140 (N-S) at center	Western Alps: Late Eocene to mid-Miocene: 2 - 3 Eastern Alps: 1.7 - 3.5 (30 Ma – 10 Ma)	Western Alps: 0.3 - 1 Eastern Alps: ~ 2	Moderate humid	Sub-tropical	West: Transversal; East: Longitudinal	Lüschen et al 2006; Handy et al, 2014; Pfiffner 1986; Trümpy, 1973; Busby and Ingersoll, 1995; Lammerer et al, 2008; Vrabec et al, 2006; D'Agostino et al, 2008
Persian Gulf	Peripheral	270	12	1,500	-	23	Arid, desert and partly submarine	Tropical, later submarine	-	Konyuhov and Maleki, 2006; Sella et al, 2002

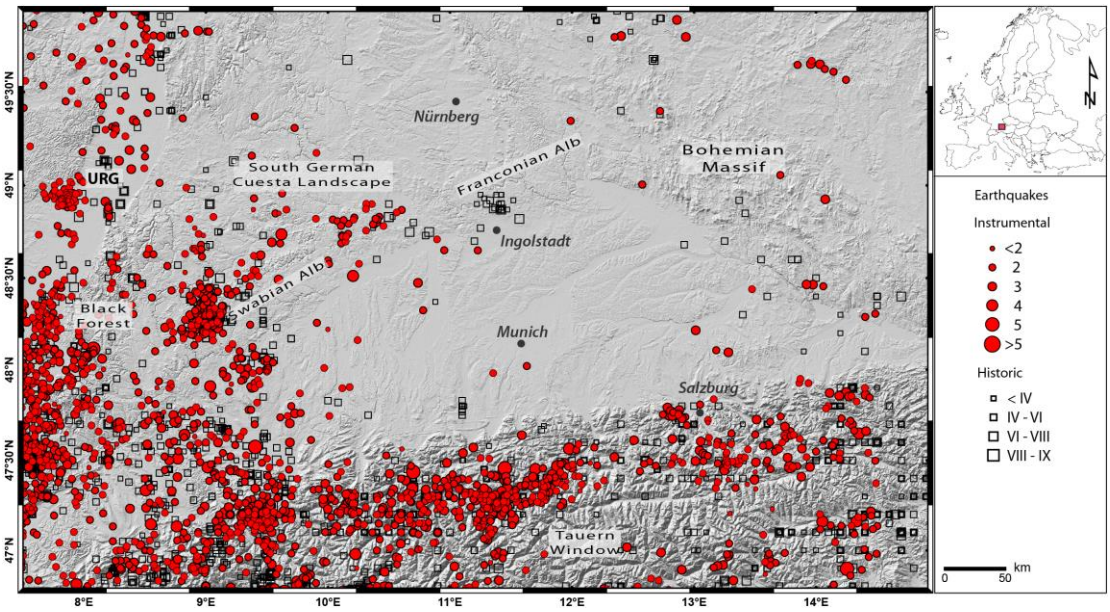

Fig. 4.2: Seismicity map of the NAFB and adjacent regions. Background: Digital elevation model (DEM) based on SRTM, 1 arc sec data, provided by NASA. URG = Upper Rhine Graben. Seismicty data compiled from the NEIC catalog and the seismic catalog for the European Union (479 B.C. - 1960; van Gils and Leydecker, 1991).

The basin is filled with Eocene to Miocene clastic and marine sediments (Fig. 4.1, Fig. 4.3), and two depositional mega cycles of alternating marine and terrestrial sedimentation are recognized (Füchtbauer, 1964). In this paper, the conventional German abbreviations are used for the depositional mega sequences (von Guembel, 1861). During the Oligocene, deep marine conditions of the Lower Marine Molasse (UMM) predominated with mainly shelf slope deposits, so-called ‘Flysch’ (Hesse, 1975; Sinclair, 1997). The second marine stage occurred in the lower Miocene with the Upper Marine Molasse (OMM). The marine stages were interrupted by terrestrial sedimentation in the early Oligocene (Lower Freshwater Molasse, USM) and again in the late Miocene (Upper Freshwater Molasse, OSM) (e.g., Doppler, 1989; Schlunegger et al., 2001). Those sedimentary sequences are directly linked to the orogenic advance rate and flexural changes of the basin geometry. The orogenic advance accompanied by topographic rise of the mountain range, results in enhanced erosional flux of terrestrial material into the basin. This is often expressed in large fan deposits that can widely prograde across the basin (Burbank, 1992; Kuhlemann and Kempf, 2002; Quinlan and Beaumont, 1984; Schlunegger and Simpson, 2002).

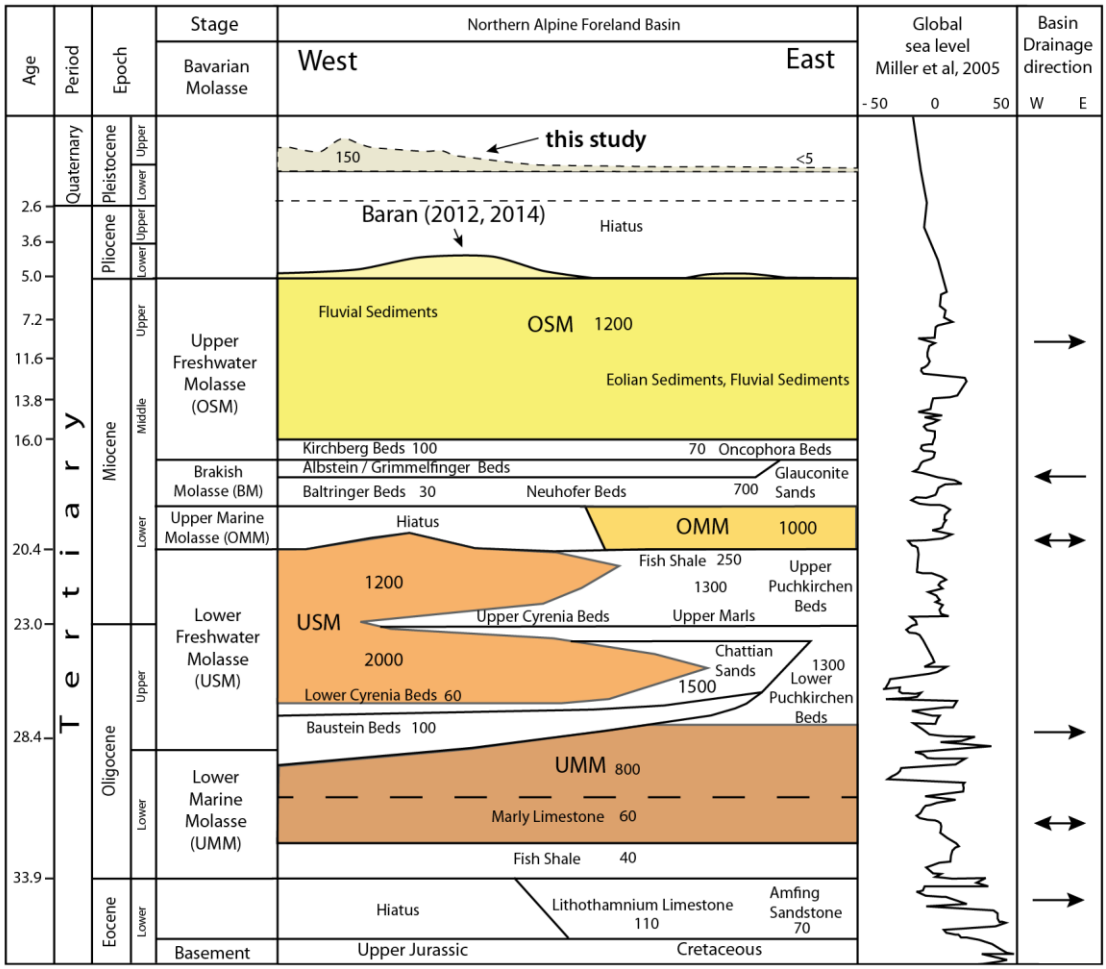

Fig. 4.3: Schematic stratigraphy of the NAFB (Austria, Germany, Switzerland). Data for the Pliocene and Quaternary have been added. Modified after Lemcke 1974, 1988; Bachmann & Müller 1992; Unger 1997, Kuhlemann und Kempf, 2002. Numbers in east - west section refer to the average thickness of sediments in meters. Quaternary data from this study. Global sea level curve after Miller et al, 2005. Not drawn to scale.

The sedimentation ceased between 8.5 Ma and 4.5 Ma (e.g., Bernet et al., 2009). During this time, the deposits along the southern margin became incorporated into the northward advancing thrust sheets, resulting in exhumation and reworking since the late Miocene (e.g., Kuhlemann et al., 2001). The youngest depositional units are Quaternary glacial and interglacial sediments that also contain reworked older Molasse material (Jerz, 1993). These deposits are thickest near the Alpine front in the south, becoming progressively thinner toward the northern basin margin.

The early dynamic reconstructions of the basin evolution have been carried out on broad scales (e.g. Ziegler, 1990). Later, new integrated, localized studies have been proposed to better understand the evolution between 30 Ma and 5 Ma (Kuhlemann and Kempf, 2002). The youngest dynamic change and reorganization of the western foreland basin in Switzerland from about 5 Ma on, has been linked to lithospheric unloading by Baran et al. (2014). The authors suggest that basin uplift and enhanced erosion since 5 Ma originates in the western Alps as a result from unloading of the Eurasian lithosphere slab, which significantly contributed to the postulated erosion increase around 5 Ma (Zhang et al., 2001). Prior, the climate change to warm and humid conditions at ~ 8 Ma (Böhme et al., 2008), had already changed the erosional flux and the surface morphology of the basin. To explain the present-day topography in the eastern basin other than by tectonics, numerous studies have suggested that climate change around 8 Ma and 5 Ma led to enhanced erosion that controlled the landscape evolution (Hay et al., 1992; Herman et al., 2013).

The effects of the Last Glacial Maximum (LGM), with the formation of thick Pleistocene loess loam soils as a remnant from interglacial periods during the Quaternary (Jerz, 1993) cover most of the initial topography. The long-term natural denudation rates of the basin range on the order of ~ 0.1 mm/a averaged over 5 Ma (Baran et al., 2014). Superimposed is the glacial isostatic rebound since the LGM (Würmian ice age), with uplift rates of ~ 0.3 mm/a for glaciated areas in the Alps and their northern front, and < 0.1 mm/a in the foreland (Norton and Hampel, 2010; Stocchi et al., 2005).

3.2. Basement fault data

Numerous basement faults in the NAFB have been documented over the last decades, derived from hydrocarbon industry prospection (Tab. 4.3; Fig. 4.4). Based on the number and orientation of the faults, a potential reactivation could be expected (for a detailed discussion on potential fault reactivation, see also chapter II of this thesis, Hoffmann et al., 2016a). In fact, it has been proposed that faults in the NAFB have been reactivated after the late Miocene, based on observations of tilted terraces and lineament mapping (Ganss, 1968; Mayr, 1957; Oeltzschner, 1965; Penck, 1922; Schmidt-Thomé, 1955; Unger and Schwarzmeier, 1982, 1987). These observations

are spatially limited to the immediate Alpine range front, for example along the banks of the early Pleistocene lake Rosenheim, southeast of Munich (Ganss, 1968).

In order to estimate possible fault reactivation, subsurface information can be very helpful. Seismic imaging campaigns like the TransAlp (Gebrande et al., 2006) and other local studies have shown in depths of > 500 m, that the youngest sediments offset by detected basement faults are late Miocene in age (Gebrande et al., 2006; Heermann, 1954; Lüschen et al., 2006; Lüschen et al., 2004). Potential offsets in younger sediments above have not been resolved. One of the main reasons for this is the design of previous geophysical studies, where data from shallower depths have been erased due to the intense noise level from the seismic reflection and refraction line setup (Knödel et al., 2013; Prinz and Strauß, 2012). Especially the hydrocarbon industry exploration campaigns have been used to target hydrocarbon host rocks, like the Jurassic limestone (Malm) and source rocks, like the Jurassic Purbeck, in depths of > 2 km (Kraus, 1969). Therefore, the methodological limit of the data due to acquisition and processing methods so far prevented detecting offsets near the surface. This argument however, cannot be quoted to simply rule out ongoing deformation in the NAFB, and other indicators of activity have to be considered.

Table 4-3: Summary of previously published observations related to active tectonics in the NAFB

Location	Observation	Reference
Graisbach	Surface lineaments in similar orientation with known basement faults. Asymmetric patterns of fluvial systems correlating with inferred fault locations	Mühlfeld (1968)
Passau	Surface lineaments in similar orientation with assumed faults	Streit (1979)
Traunstein	Tilted fluvial terraces, Quanternay deposits	Ganns (1968), Oeltzschner (1965), Schmidt-Thomé (1955)
Vilsbiburg	Tilted fluvial terraces, Pleistocene deposits	
Isar valley	Tilted fluvial terraces, Pleistocene deposits	
Inn valley	Tilted fluvial terraces, Pleistocene deposits	Ganss (1968), Mayr (1957)

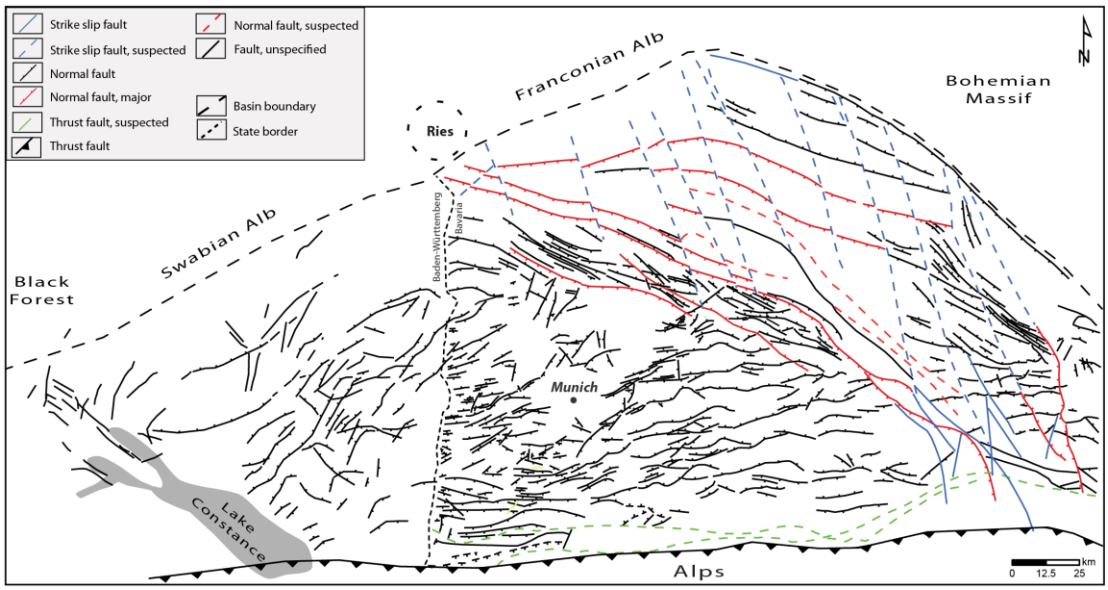

Fig. 4.4: Simplified tectonic map of basement faults in the NAFB. Compiled from Unger 1999; Kraus 1969; LGRB; Schwarzmeier, 1981b; Ziegler, 1992.

3.3. Fluvial systems

After the last marine cycle in the NAFB at c. 17 Ma (Kuhlemann and Kempf, 2002), a fluvial system (Graupensandrinne) developed on the northern margin of the basin, draining the basin and surrounding areas of the Bohemian Massif, the Franconian and Swabian Alb in a westward direction (Doppler and Schwerd, 1996; Reichenbacher et al., 1998). The successor of this system is the modern river Danube, which represents the main discharge system in the NAFB, as the drainage area comprises most of the basin and large tributaries, having their headwaters in the central Alps. The drainage divide between the Danube and the Rhine extends between Lake Constance and the Black Forest. The western Alps' drainages flow into the Rhine river and the distal North Sea basin. Central and eastern Alps' drainages flow towards the Danube ending in the distal Black Sea basin. Other pre-Danube fluvial systems existed along the northwestern and southern rim of the basin since the mid- and late Miocene (Zöbelein, 1995). The earliest signs of a west flowing Danube are dated to about ~ 9 Ma (Kuhlemann and Kempf, 2002; Rutte, 1987). After 8 Ma, the flow direction changed from west to east, which has been attributed to a base level lowering in the east (Lindner, 2011 and references therein; Lóczy, 2007). In fact, during the Pliocene,

a rapid subsidence of the distal basin, the Black Sea, has been observed (Nikishin et al., 2003).

Today, the NAFB is mainly drained by the rivers Iller, Riss and Lech in the west and rivers Isar, Vils, Rott, Inn and Salzach in the east. Western rivers are north - south oriented, while eastern rivers are oriented northeast - southwest to straight east - west. The orientation of the tributaries has changed several times during the last 30 Ma, which has been attributed to dynamic reorganizations of the basin controlled by the subduction (Fig. 4.3) (Kuhlemann and Kempf, 2002; Lemcke, 1984; Unger, 1999c; Villinger, 1989). The reconstruction of the drainage systems in the eastern NAFB has been carried out based on gravel distributions from large Alpine fans. The sedimentary composition indicates the source area, used to back-trace the paleo channel path. However, a basin-wide drainage reconstruction is hampered by sorting and erosion effects, limiting the validity of the provenance analysis (Brügel, 1998; Kuhlemann and Kempf, 2002; Lemcke, 1984). The slower erosion of limestone, compared to feldspar rich crystalline rocks, produces a biased lithological composition. For the rivers Danube and Inn, terrace correlations are used to reconstruct their paleo channel location in the central and eastern foreland (Lemcke, 1984; Mayr, 1957; Villinger, 1989). Results show, the Inn has moved progressively away from the Alpine front northward during the Pleistocene. The Danube undulated north - south over a distance of ~ 50 km between the Pliocene and late Pleistocene. For the western basin in Switzerland, the reconstruction of fluvial/ fan systems has been used to show surface response to lithospheric slab roll back and coupled mountain range uplift (Schlunegger and Kissling, 2015). Along the southern margin of the Jura Mountains, Schlunegger et al. (1997) showed the evolution of a basin parallel drainage system, which developed on the buried stationary basin forebulge during the late Oligocene.

4. Methods

In this study, we utilize a combination of (1) remote sensing mapping to identify potential tectonic lineaments, (2) geomorphologic markers to study river network geometry and channel steepness and (3) geologic well- and field data synthesis to estimate erosion rates and pattern on long ($\geq 10^6$ a), medium ($10^5 – 10^4$ a) and short ($\leq 10^3$ a) time scales.

4.1. Geomorphic mapping

For the geomorphic mapping of the NAFB, we used the digital elevation model (DEM) derived from the TanDEM-X intermediate data, provided by the *Deutsches Zentrum für Luft- und Raumfahrt* (DLR). The resolution is 144 m^2/pixel. This dataset was available for 90,000 m^2, while data limits occur at the Alpine front due to processing errors of the high topography. The mapping has been further subsidized by the ASTER DEM 1 arc second, enhanced elevation model, provided by NASA.

4.2. Stream order analysis

The shape of fluvial systems is a prime indicator of tectonic processes as well as changes in sediment yield and transport characteristics in basin settings (Beaumont et al., 1992; Burbank, 1992; Burbank and Anderson, 2001; Kirby and Whipple, 2012; Tucker and Slingerland, 1997; Whipple and Tucker, 1999). Therefore, the dynamic behavior of a river system can reflect the systems' response to tectonically induced surface deformation (Burbank and Anderson, 2001 and references therein) (Fig. 4.5). The interplay of river dynamics involving grain size, sediment load, stream velocity and gradient controls the overall channel pattern (e.g., Schumm, 1986). The classic river form shows a steeper gradient in the upstream part, resulting in braided or straight systems. This pattern changes downstream to a meandering system, when sediment load and steepness decrease (Burbank and Anderson, 2001).

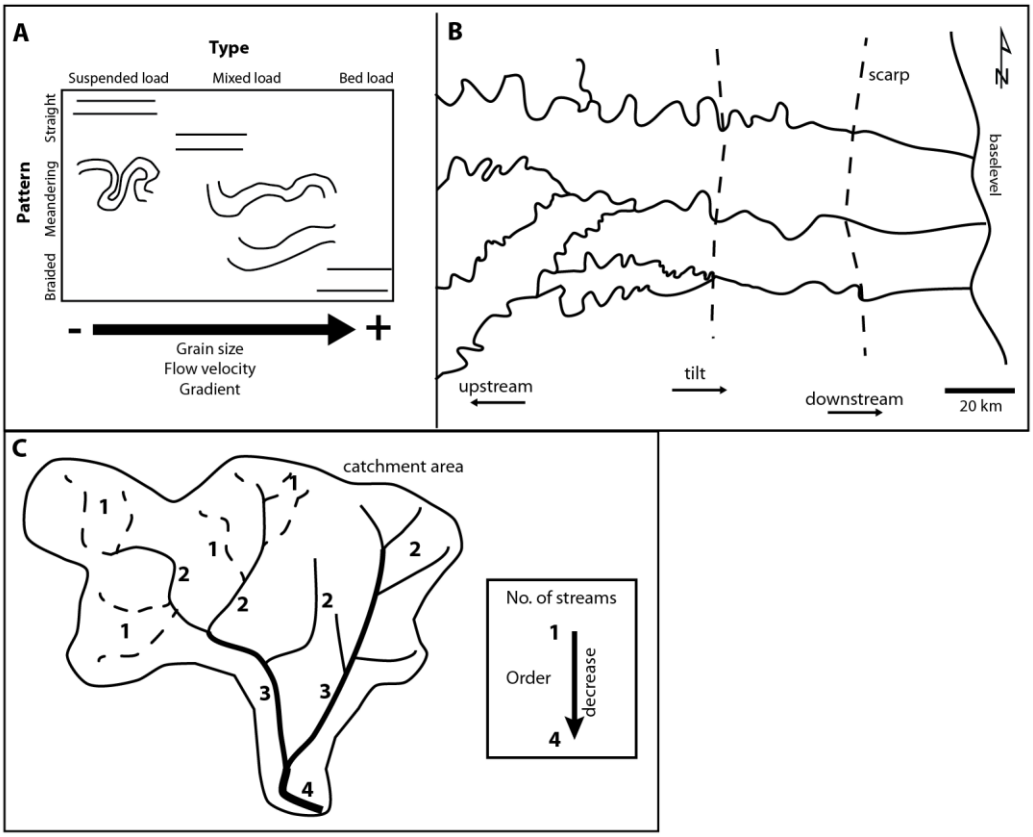

Fig. 4.5: Principle dependencies of geomorphology and fluvial systems. A) Variations in fluvial channel pattern as a response to changes in sediment load, grain size, flow gradient and flow velocity (after Burbank and Anderson, 2001). B) River network changes from meandering in the west to straight on the eastern side where the gradient is lower. The region is tilting to the east. The rivers cross scarps where they show sidestepping. C) Stream order concept of a river network (simplified after Strahler, 1954a). Small tributaries (1st order) connect to the next larger channel (2nd order) and so forth. The order only increases, when two tributaries of the same order interconnect.

For the statistical analysis of the stream networks in the NAFB, we used the *Strahler* stream-order-method (Strahler, 1957a). This analysis is a quantitative method that numbers individual streams by their size from tributaries to main fluvial channels. The number of hierarchy only increases, when two streams of the same order intersect. A higher total number reflects the size of the drainage. This approach can be used to assess the symmetry of a fluvial network, where asymmetric shapes indicate active reorganization.

We have computed the stream order based on the TanDEM-X and ASTER DEM datasets using Esri ArcGIS, version 10.3, software. The results are visualized as a network of connecting lines (Fig. 4.5c).

The results are used to evaluate the pattern of the rivers and their tributaries concerning stream length and distribution, in order to identify an equilibrium or disequilibrium stage (Willett et al., 2014). The total area analyzed comprises about 54,000 km^2. Prior to the GIS based calculation, the DEMs have been prepared by a bi-cubic resampling and gap interpolation to avoid bias from data gaps and false pixel values, using the software Global Mapper (Version 17).

4.3. Normalized steepness index

The pattern of stream steepness along the river channel can be utilized to extract river segments that are actively deforming (Kirby and Whipple, 2012). The MatLab codes from the *TopoToolbox* (Schwanghart and Scherler, 2014) have been used to extract channel profiles based on the 30 m ASTER DEM (NASA). Based on the channel extraction we have calculated the normalized steepness index *KSN* (Schwanghart and Scherler, 2014) (see Appendix A of this chapter), to conduct a slope vs. area analysis with a well-established standard reference concavity of - 0.45 (Kirby and Whipple, 2012), and an increased concavity of - 0.5 to address the low relief loess landscape of the Tertiary Hills. The output of the calculation is shown as a set of connecting lines with colored segments, indicating the relative local steepness. The results of the steepness index are used to determine, if the steepness of a channel slope is in equilibrium relative to its size, its position along the entire stream profile and the drainage area. In cases of over-steepened channel segments a vertical, non-climatic deformation is inferred (Kirby and Whipple, 2012).

4.4. Calculation of Quaternary erosion rates

For the erosion estimates we synthesized publically available well data of 346 wells, derived from the database of the geologic survey of Bavaria (LfU), and a map of Quaternary deposits in the western portion of the NAFB provided by the geologic survey of Baden-Württemberg (LGRB). The data have been used to digitally construct surfaces representing (1) the basal topography of the Quaternary sediments in the NAFB (German part) and (2) the thickness of Quaternary sediments. To build the mesh surfaces, we have used the software Global Mapper (Version 17) and the final visualization was carried out using Esri ArcGIS V10.3.

In a later step, we automatically constructed erosion contour lines from the data, indicating the regional pattern of eroded Quaternary sediments, and integrated those with information from regional and local geologic maps, 1 : 200,000, 1 : 50,000 and 1 : 25,000. To finally calculate the amount of Quaternary erosion, we followed four calculation steps (see appendix of this chapter and Tab. 4.4 – 4.10).

In order to identify young tectonic activity, we convert the erosion into an uplift rate for eight test sites across the basin, and compare those results with published data (Lemcke, 1974; Strasser, 2011; Strasser et al., 2009). For the short time scale erosion estimates, archeological data (Fig. 4.18) are derived from two ancient gravesites and stilt house findings in the Tertiary Hills region. The grave depths found in the region are c. 0.2 m, which is about 1.8 m shallower than the original burial depth. For the stilt houses a similar value has been detected. This is used to infer a removal of sediments of 1.8 m in 6,500 – 7,000 years (Bayerisches Landesamt für Denkmalpflege).

5. Results

5.1. Tectono-geomorphic map

The remote sensing mapping reveals a preferentially NE-SW oriented pattern of surface lineaments (Fig. 4.6). The linear features associated with asymmetric valleys also show a striking NW-SE, while the adjacent ridge crests show a more random range of orientations. In several locations, the course of present-day river channels follow the trace of the mapped lineaments e.g., for the Inn river east of Munich and the Danube river southwest of Regensburg (Fig. 4.6).

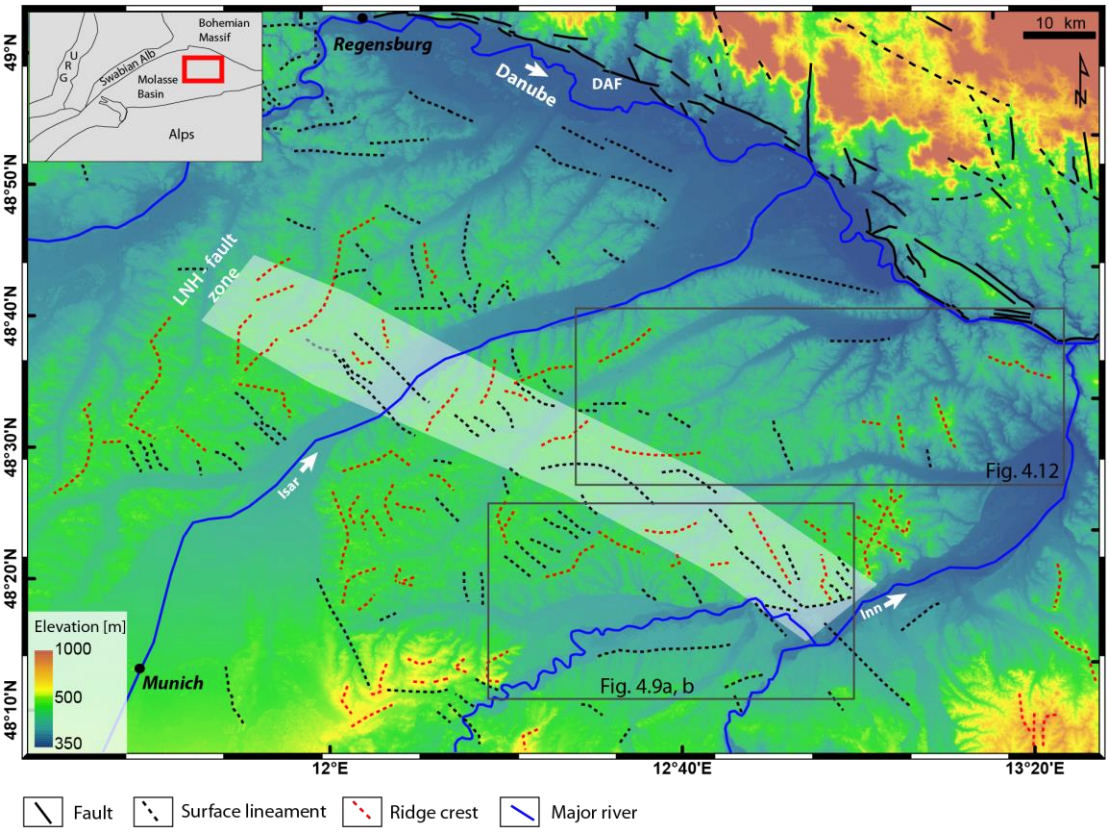

Fig. 4.6: Shaded relief map of the Tertiary Hills region. Mapped tectonic structure from this study. Background TanDEM-X elevation model, resolution 12 m/pixel. DAF = Danube Fault, URG = Upper Rhine Graben. White marked area corresponds to Landshut-Neuötting fault system.

5.2. Stream orientation and river terraces

The orientation of rivers in the NAFB reveals a change in orientations of major rivers from west to east. In the western part, fluvial systems are oriented perpendicular to the basin axis, flowing almost straight north, while in the eastern portion the river systems are oriented preferentially parallel to the basin axis, flowing northeastward. The drainage divide strikes north - south at the longitude of Augsburg (Fig. 4.7). The boundary of the river network pattern is located in the area of the Landshut-Neuötting-High (LNH). Also, the increase in NW-SE oriented lineaments matches the extend of the LNH basement structure. The major rivers, indicated by the highest stream order, show a clear change from longitudinal to transversal orientation from west to east (Fig. 4.8). In the area of the Iller, Riss and Lech rivers, the dominating orientation of channels with the highest order 10 to 12 (main drainages) is N-S. For

these rivers, also a general minor meandering is observed. In the eastern section, the major channels of the orders 10 to 12 are oriented preferentially eastward and northeastward. The higher order tributaries (values 10 to 12) form an irregular pattern across the area. There is almost no meandering observed and the overall channel pattern is straight (Fig. 4.7).

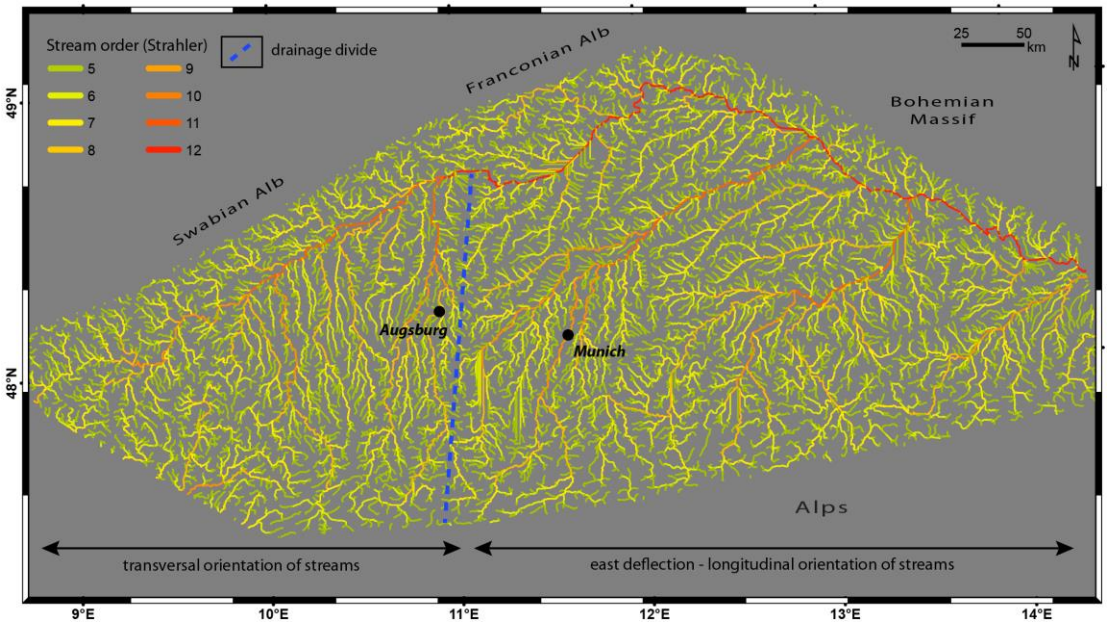

Fig. 4.7: Map showing the stream order of the NAFB (Strahler method). The drainage area threshold has been set to > 10 km^2.

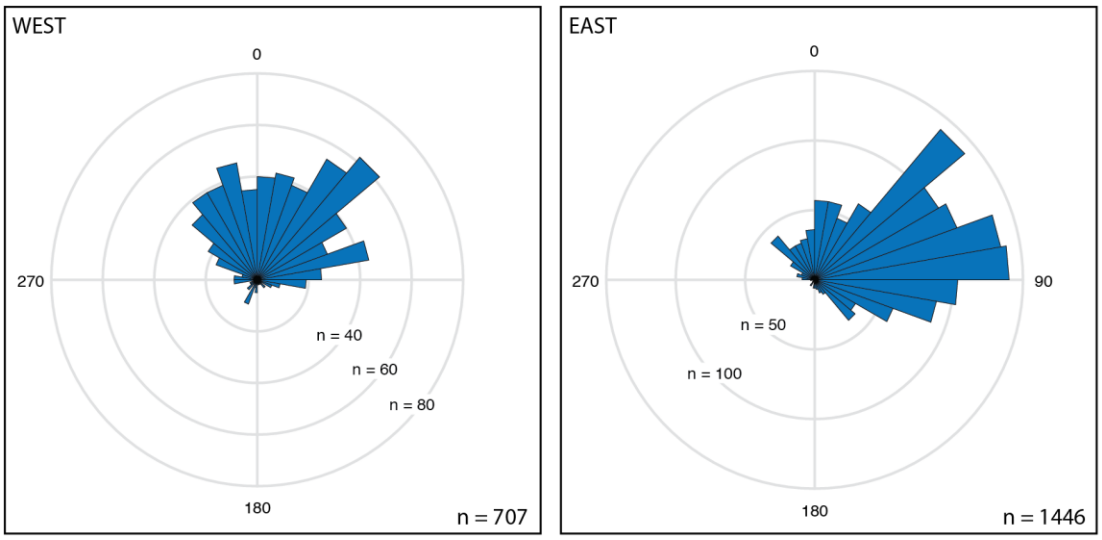

Fig. 4.8: Rose plots of stream orientation in the NAFB derived from Strahler stream order calculations.

Further to the east, the Inn river crosses several normal and dextral strike slip basement faults. This coincides with a sharp, southeastward bend of the river (Fig. 4.6). The fluvial channel shows an increased meandering and large terraces between Wasserburg am Inn and Marktl am Inn (Fig. 4.9). At Marktl, the river is deflected southeast by about 90° for a distance of ~ 10 km, until it reaches the topographic southernmost tip of the Tertiary Hills. Downstream, it shifts back to its previous northeast direction and the channel becomes straightened with increased incision. Further downstream, only small abandoned terraces occur, continuing until the river reaches the base level of the Danube at Passau.

The river segment with large meanders and young, abandoned cut terraces can be found between Waldkraiburg and the southeastern boundary of the hangingwall from the LNH near Marktl (Fig. 4.9).

Upstream, both rivers Inn and Salzach show increased incision crossing an east-west oriented axis between the Alpine range front and the onset of the Tertiary Hills. In this area, both rivers incise into terraces composed of poorly consolidated glacial fine to coarse-grained sand and gravel deposits. The deposists are of Pleistocene to Holocene age (Unger, 1978b).

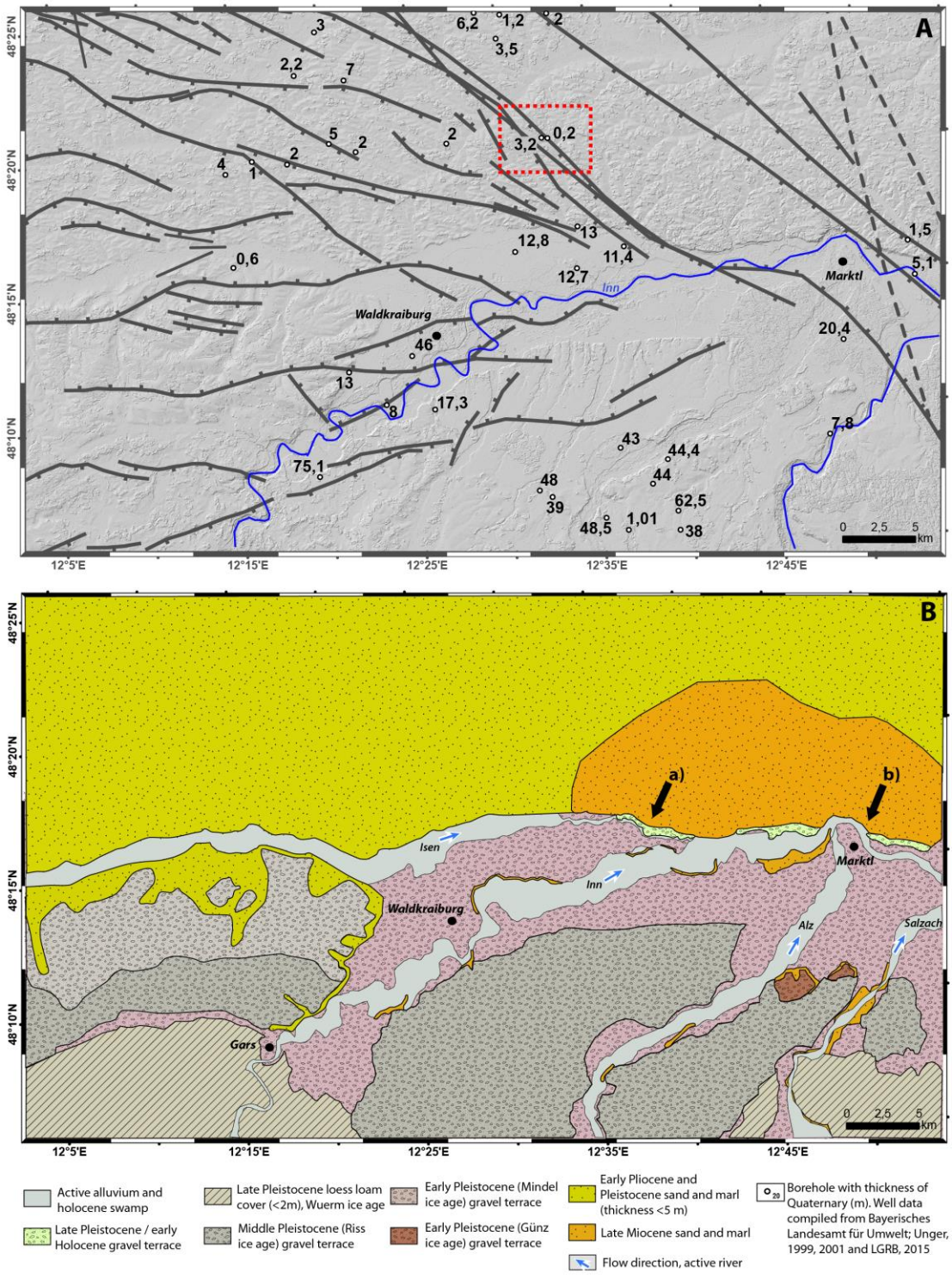

Fig. 4.9: Map showing the geologic setting in the area of *Waldkraiburg*. A) Map of basement faults. Background TanDEM-X digital elevation model, resolution 12 m/pixel. The red dashed box indicates an offset of Quaternary sediments above a set of normal faults. B) Simplified geologic map compiled from the Geologic Map of Bavaria, 1 : 50,000, sheet L7740 - *Mühldorf am Inn* and the Geologic Map of Germany, 1 : 200,000, BGR, Hannover

The rivers Vils and Rott (stream orders 10, 11), cross the Tertiary Hills region in a similar NE orientation, having their source close to the southwestern margin of the Tertiary Hills. The drainage basin of the Rott is narrow and elongated in a NE-SW direction, while the basin of the Vils river is generally wider, but shows a pronounced narrowing where it comes close to the Rott headwaters. Their channels show an increased steepening along the main drainage channel and their tributaries (Fig. 4.12). The elevation and steepness of the Vils tributaries is lower compared to the Rott. In the Rott headwaters, we identify a c. 10 km long channel that shows a northward orientation towards the Vils in its upstream portion, but is deflected by about 85° eastward into the Rott direction (marked by number 1 in Fig. 4.12).

5.3. Normalized steepness index KSN

The calculated normalized steepness index (*KSN*) across the NAFB shows distinct zones of steep river- and tributary segments, with generally steeper river segments in the eastern part of the basin (Fig. 4.10). For the rivers Inn and Salzach, the steepest segments with *KSN* values > 2,000 (Fig. 4.11) are observed between the Alpine range front and the southeastern extend of the Tertiary Hills region.
For the river Isar, the segment with the highest steepness values is found in the Tertiary Hills region, between Landshut and Deggendorf (Fig. 4.10).

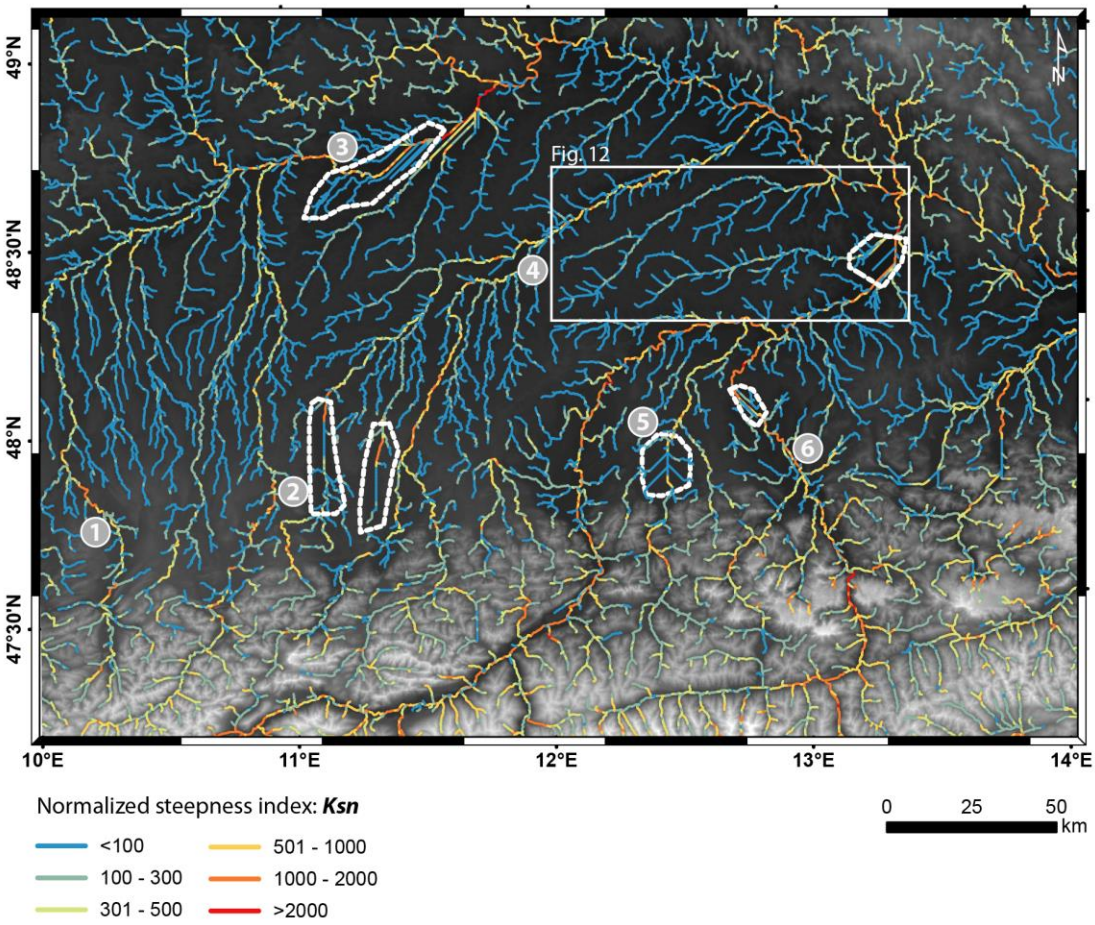

Fig. 4.10: Map showing the normalized steepness index (*KSN*) for major rivers in the NAFB and adjacent areas in the Alps. Background ASTER DEM 1 arc sec. White dashed lines indicate lake and swamp areas, resulting in artificial linear flow paths. Rivers: 1 = Iller; 2 = Lech; 3 = Danube; 4= Isar; 5= Inn; 6= Salzach.

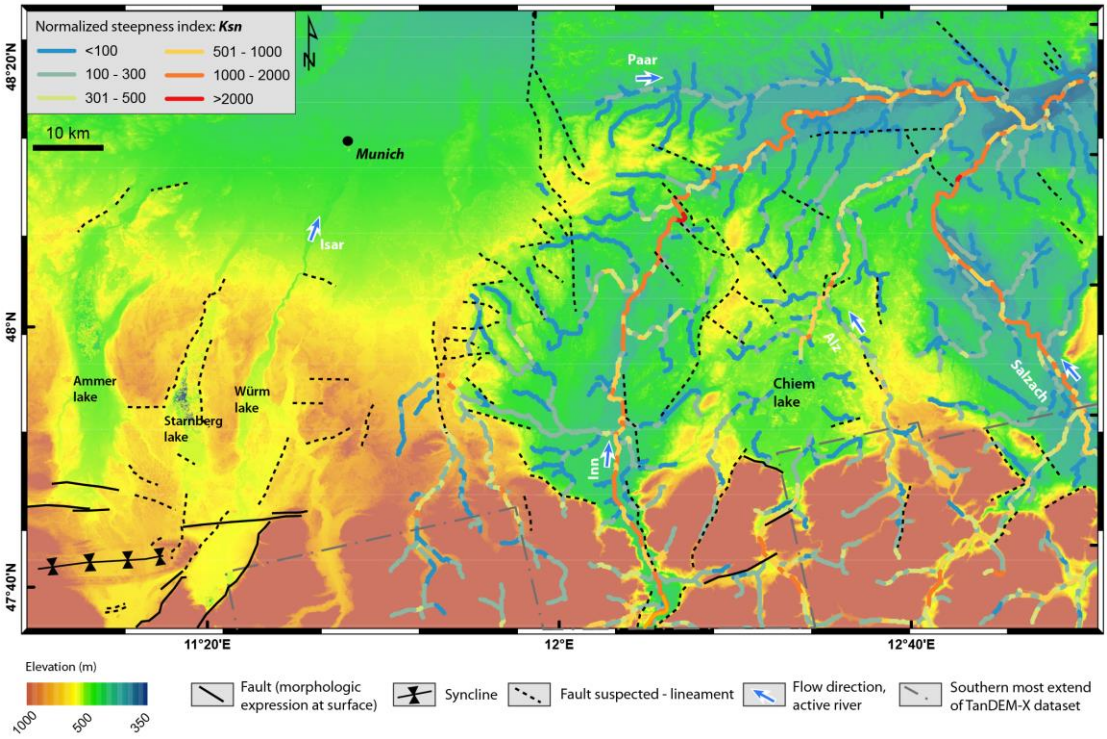

Fig. 4.11: Map showing the region along the Alpine range front and the foreland basin between the Ammer lake and Chiem lake. *KSN* values are shown for the Inn-Salzach river systems. Background TanDEM-X elevation model, resolution 12m/pixel. The Würm lake is a dry lake since the Würm ice age.

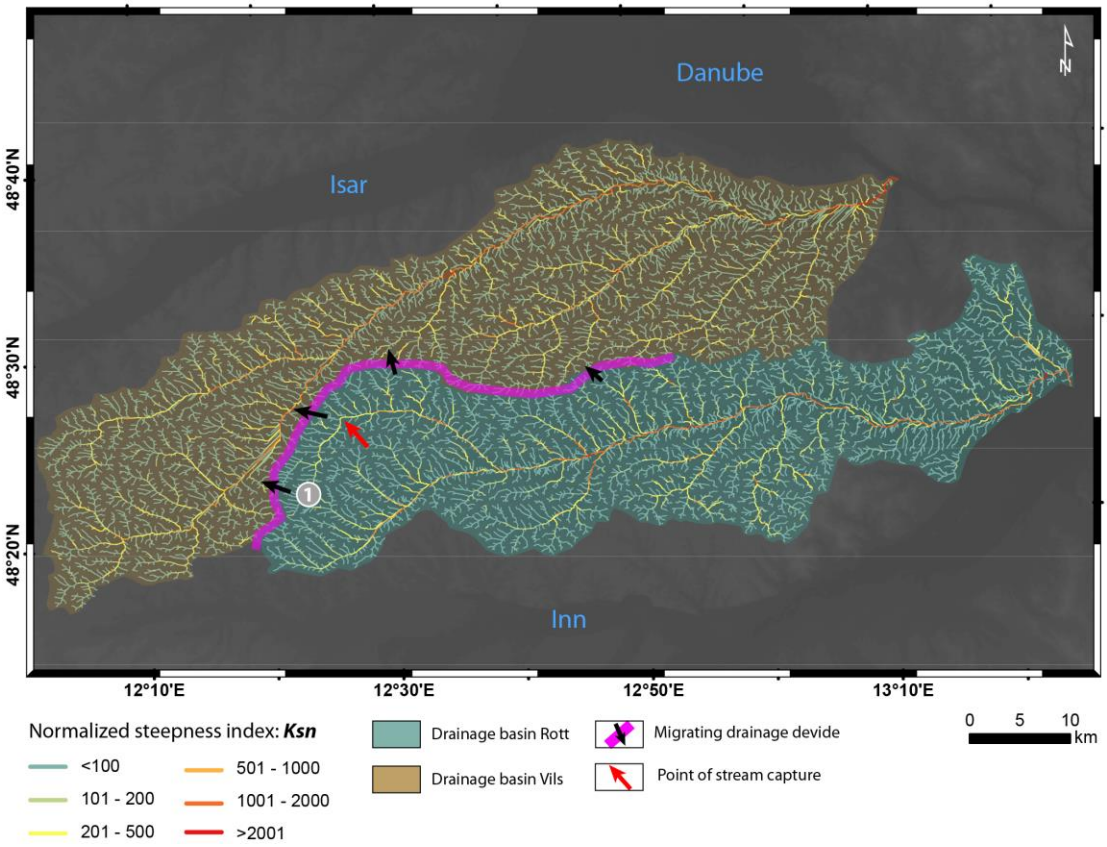

Fig. 4.12: Map showing the normalized steepness index of the rivers Vils and Rott in the southeast Tertiary Hills loess region. Background, TanDEM-X digital elevation model, resolution 12 m/ pixel. 1 = stream captured by the Rott. Both rivers show steepening in their central parts indicated by high *KSN* values. The rivers common drainage divide appears to migrate north - westward into the headwaters of the Vils river. The Rott river has a lower steady-state steepness at its channel heads, which drives the divide towards the steeper Vils.

5.4. Quaternary erosion pattern

The analysis of borehole data across the German part of the NAFB reveals an oval shaped pattern of Quaternary sediment thicknesses. We identified a narrow bounded zone of steep, vertical relief in the basal surface of the Quaternary sediments in the southern Tertiary Hills region (Fig. 4.13). This Quaternary basal surface also shows topographic steps of up ~ 100 m, and these locally coincide with the extend of basement fault structures, close to the LNH normal fault (Figs. 4.1a and 4.13).

The analysis of Quaternary sediments reveals a thin average cover of ~ 60 m in the NAFB (Fig. 4.14).

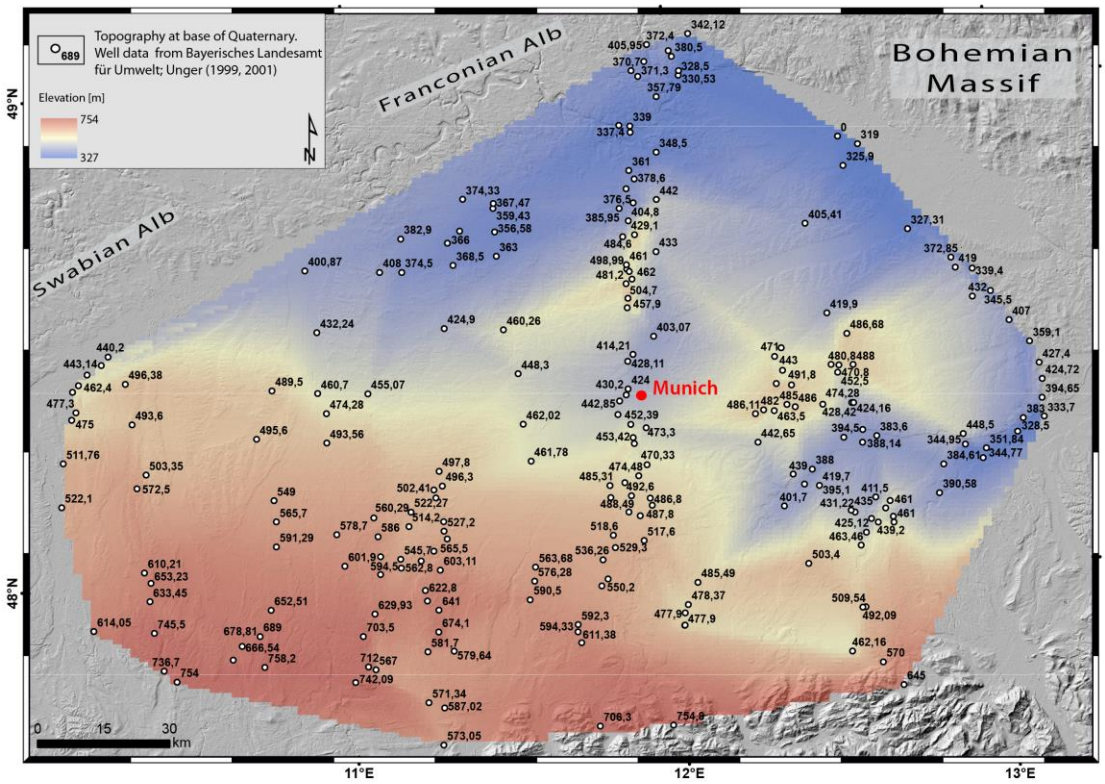

Fig. 4.13: Map showing the base of the Quaternary across the central Northern Alpine Foreland. Background ASTER DEM 1 arc sec. The elevation data of the Quaternary are given in m a.sl. The data are interpolated to a Paleo-DEM indicating the topography at base of the Quaternary (red-blue surface). Note: The moving window for Paleo-DEM interpolation is 1 km^2.

With less than 5 m on average, the thinnest Quaternary cover is found along an east-west-striking, up to 40 km wide, oval-shaped corridor, in the center of the basin (Fig. 4.14). Towards the Alpine range front, the sediment thickness increases locally up to ~ 200 m in over-deepened glacial, paleo valleys, representing the maximum thicknesses of Quaternary sediments preserved in this part of the basin (Fig. 4.14). Across the basin, the overall Quaternary thickness decreases from west to east and south to north (Fig. 4.15).

In the area between Altötting and Marktl am Inn, the thickness of sediments changes by almost 150 m within a few kilometers across the river from north to south (Fig. 4.16). This decrease of Quaternary sediments coincides with the surface exposure of Miocene sediments from the older series of OSM, in direct contact with Holocene fluvial terraces (Fig. 4.9b).

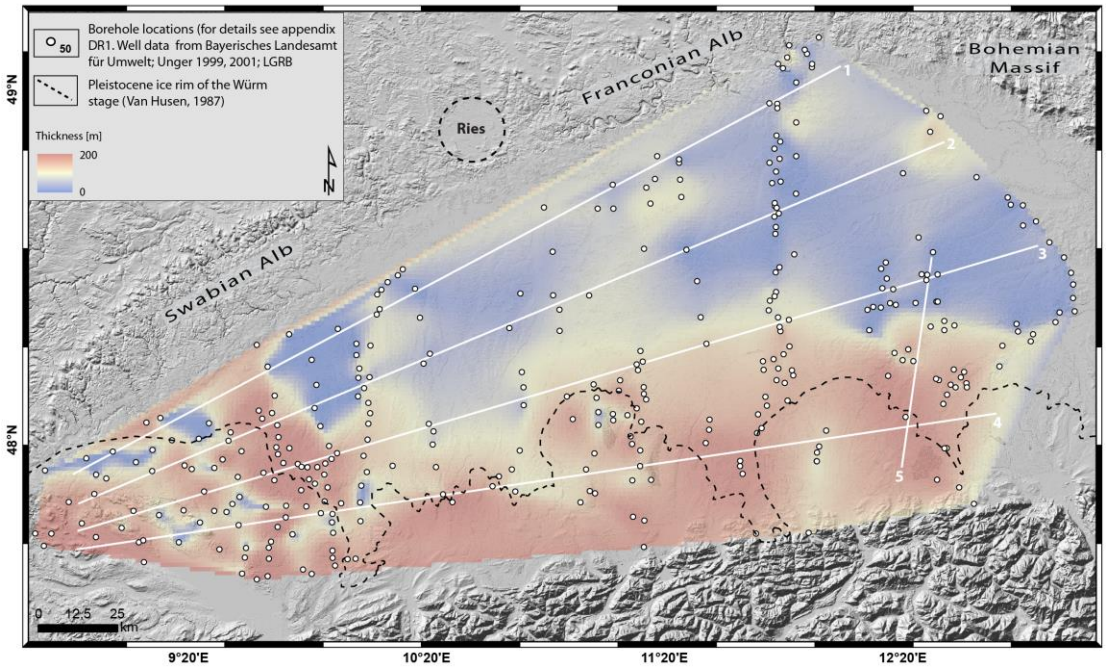

Fig. 4.14: Map showing the thickness of Quaternary sediments across the central Northern Alpine Foreland. Background TanDEM-X digital elevation model, resolution 12 m/pixel. The data are interpolated to a paleo-DEM indicating the topography of the Quaternary (red-blue surface). White lines depict profiles in Fig. 4.15, 4.16.

In the area of Mühldorf am Inn, sharp bounded unconformal contacts occur between the youngest fluvial units from the latest Pleistocene (Würm stage) and Pliocene/ Miocene sand and gravel deposits (Fig. 4.9b). At the sites (a) and (b) in Fig. 4.9, the hiatuses cover ~ 4.9 Ma. The unconformity correlates with the strike of normal faults in a depth of about ~ 1 km that are identified from geophysical data (Fig. 4.9a). Across a set of normal faults about 12 km north of Waldkraiburg, we detect a 3 m offset of Quaternary sediments above a basement normal fault system (Fig. 4.9a). Pliocene sediments are partly preserved in the east underlying the thin Quaternary cover. The preservation of Pliocene sediments is slightly larger in the eastern basin. The Quaternary pattern shows the opposite. Average values are < 10 m in the east and up to 40 m in the west.

The distribution of Holocene cut and fill terraces is generally greater along the Inn, near Marktl. The next older terrace unit of late Pleistocene age (Würm) is widely deposited along the Inn, Alz and Salzach, but almost no terraces occur along the Isen river. East of Waldkraiburg, a set of Riss terraces is sharply cut on their northern margin. The early Pleistocene (Mindel) terraces occur as a large patch west of Waldkraiburg on top of Pliocene sand and marls. To the south, they are bound by the younger Riss gravel deposits. East of this location, no Mindel deposits are preserved. The oldest unit that can be found, are early Pleistocene (Günz) terraces. Two small isolated patches occur about 7 km south of Marktl, deposited on top of Miocene sand and marls. Towards the north, the distribution of Pleistocene and Holocene fluvial deposits ends along the east - west striking boundary of the Tertiary Hills. Northwest of this boundary, a thin cover of Pliocene sand and marl is exposed. To the east, the sediments pinch out and older Miocene sand and marl units are exposed. Here, also several documented basement normal faults are located in depth of ~ 1 km – 1.5 km (Fig. 4.9a).

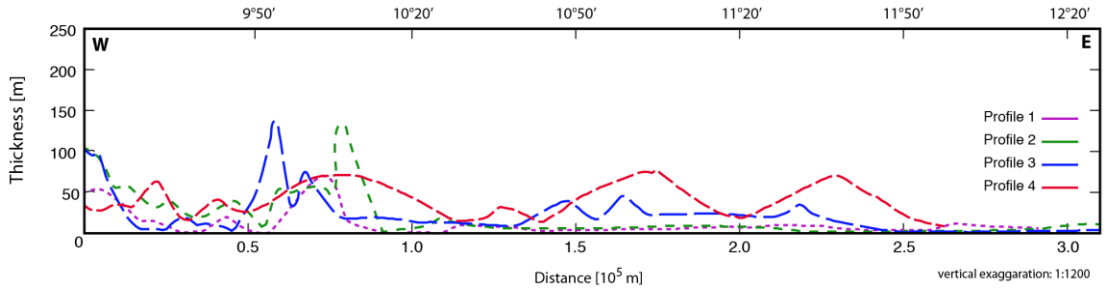

Fig. 4.15: Profiles indicating the thickness of Quaternary sediments along the east-west axis of the NAFB. For location of profiles see Fig. 4.14.

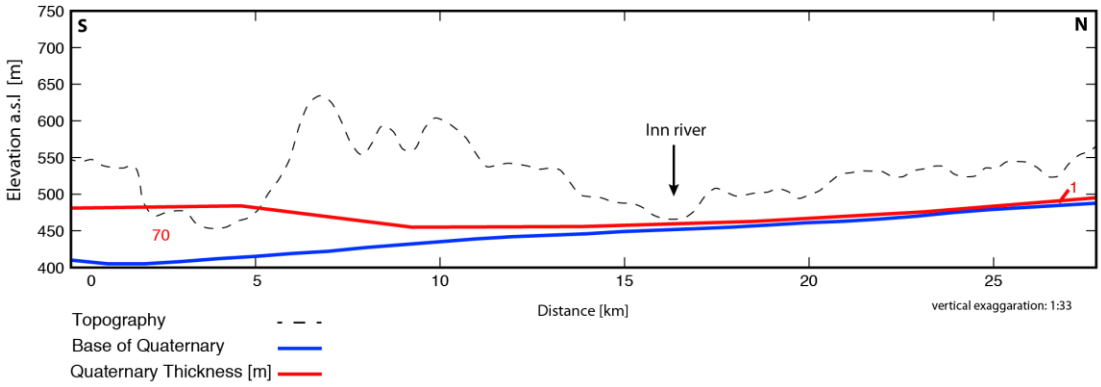

Fig. 4.16: N-S thickness plot of Quaternary sediments between the northern Alpine range front and the Tertiary Hills. For location of profile line (no. 5) see Fig. 4.14. The red numbers indicate the thickness of Quaternary sediments in meters.

5.5. Basin erosion contour lines

The erosion contour lines are constructed (Fig. 4.17; Tab. 4.2.1 – 4.2.3). The pattern of the ≤ 500 m erosion contour line follows the outer basin area in the west and extends along the Landshut-Neuötting normal fault (strike NW-SE) in the eastern portion.

In general, the erosion contour lines run parallel to the Alpine front. In the Inn – Salzach area, east of Munich, we observe an increase in erosion, expressed by a distinct steepening of the contour lines, where they reach the southern margin of the Tertiary Hills. Towards the west, they follow the same pattern up to the area of Memmingen. Here, the sediments are thicker and the ≤ 500 m erosion contour line terminates. North of lake Constance, the contours form an isolated patch, indicating locally increased Quaternary sediment thickness up to 190 m in over deepened glacial valleys. The average thickness of sediments in the western basin is higher compared to eastern portion.

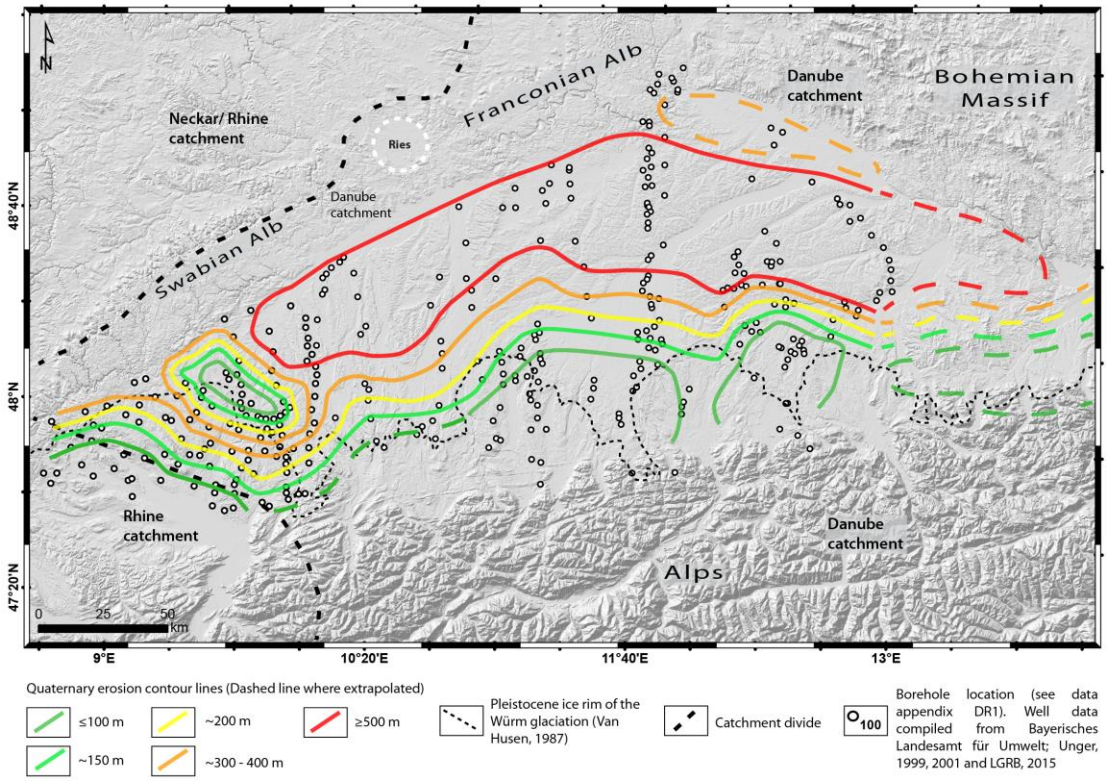

Fig. 4.17: Map showing the erosion pattern of Quaternary sediments in the NAFB along isopatch lines (German part). The numbers are based on averaging accumulation over the last 2.5 Ma. The average sediment flux is related to Hinderer (2001), assuming that on the first order the material from the related catchments has been stored in the basin and exclusively eroded from there. We also compared thicknesses of Quaternary sediments from the Rhine Graben and the Po Basin to assume a reasonable minimum amount of material. See text for discussion.

6. Interpretation

During the Quaternary, a significant amount of sediments has been eroded from the NAFB (Fig. 4.17; Tab. 4.4 – 4.10). The thinnest Quaternary cover might represent an increased erosion along a basin axis parallel zone. We attribute this pattern to an ongoing basin inversion, as a result from flexural uplift that most likely continues the "Resthebung" since ~ 5 Ma (Lemcke, 1974). To explain the observed thicker Quaternary cover in the western basin, we suggest a time dependent signal that migrated from west to east. This process has likely started during the Pliocene and continues today.

According to the geometry of fluvial networks, the western basin seems to be controlled by erosional uplift of the Alps, which results in transversal drainages

transporting material into the basin, and presumably this effect has almost paced out the increased erosion from basin inversion.

The observed change in erosion pattern can be linked to the change in sediment transport direction in the basin, reflecting a lithospheric control (Fig. 4.18). If the change to an inverting basin originated in the western basin during the Pliocene and later migrated eastward, this could explain the increased Pliocene erosion rates in the west, while the Quaternary rates show the opposite.

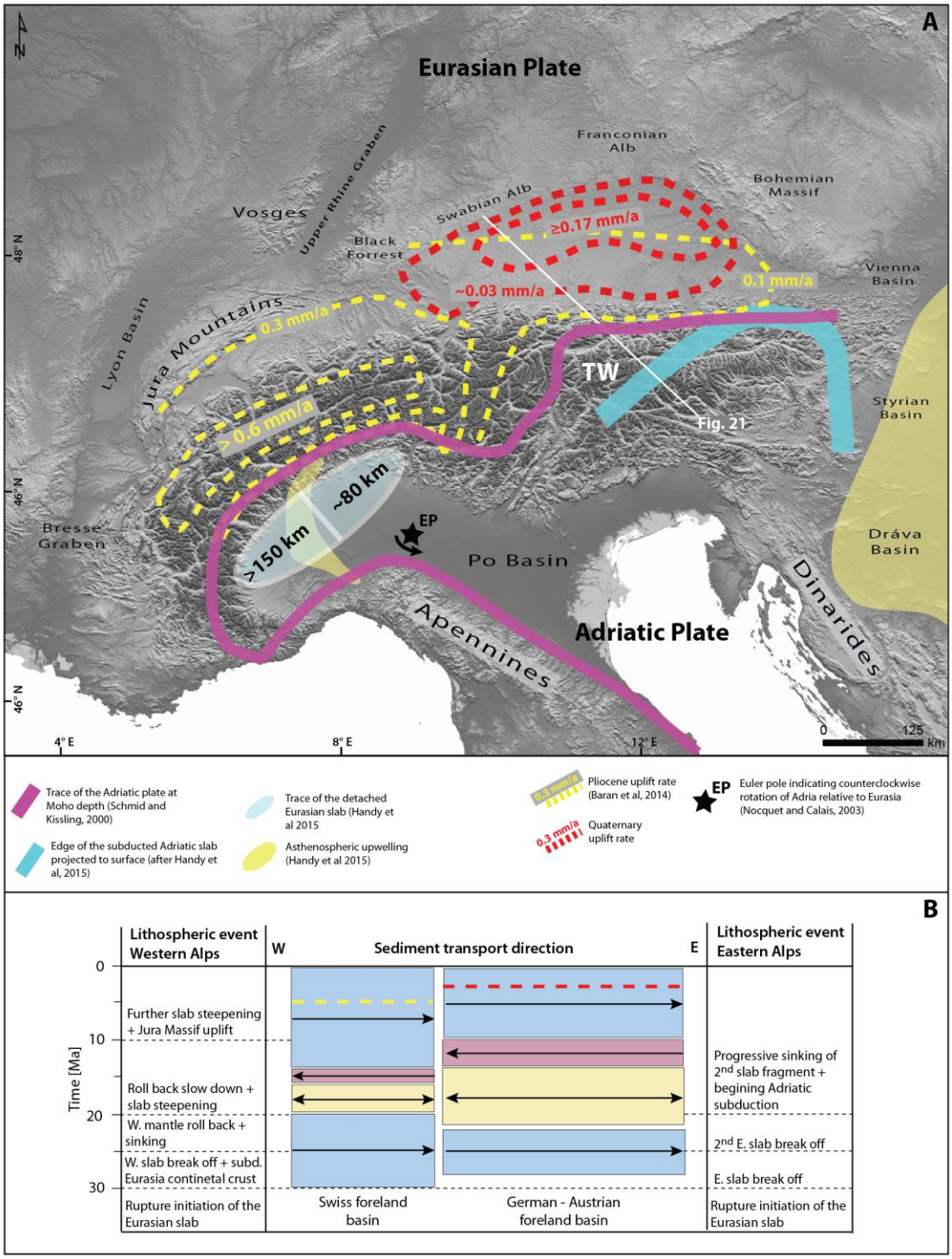

Fig. 4.18: Previous page: Shaded relief map showing the Alpine region with main observables from Pliocene-Quaternary erosion pattern. A) Erosion rates and present-day plate geometry along the Eurasia - Adriatic collision. B) Basin-axial transport direction of sediment in the NAFB through time linked to major lithospheric events. TW = Tauern Window. Data of the Swiss Molasse basin compiled from Schlunegger (1999) and Schlunegger et al. (2007), and those of the German-Austrian Molasse basin taken from Lemcke (1984), Kuhlemann et al. (2006) and Handy et al. (2015).

On the medium time scale, river steepness indices (*KSN*) for several rivers in the eastern NAFB suggest disequilibrium, possibly caused by uplift (Fig. 4.10, 4.12). Similar observations come from the northern Alpine margin, in the area of the Inn river, where high steepness values cluster at the river segment near Waldkraiburg and along the Tertiary Hill front (Fig. 4.11). In contrast, in the western basin steepness values are generally lower and for example the rivers Iller and Riss show very minor steepened segments. The river Lech flows along the boundary between the eastern and the western drainage network, and shows a steepened segment between the Alpine front and the city of Augsburg.

The observed change in river morphology across the Tertiary Hills suggests an ongoing surface uplift increasing from east to west. This corresponds to significant river path changes during the Pleistocene, where head-ward erosion in the Tertiary Hills captured western rivers like the river Paar (Scheuenpflug, 1978). The N-S striking drainage divide was located east of Augsburg and moved westward during the Pleistocene (Scheuenpflug, 1991). This is in agreement with the reported westward migration of the Rott headwaters. The perpendicular contact between the head ward erosion of rivers in the eastern basin and the drainage orientation in the west comprises a N-S lineament following the present-day Lech river.

The recent orientation of the Inn, Vils and Rott rivers (strike 45° - 80° NE) in the eastern basin is interpreted as a transient stage between the ceasing of tectonic loading along the eastern Alps, and the sedimentary control of fluvial networks in a beginning basin inversion. In contrast, we observe clear transversal river morphology in the western basin. Here, rivers run almost straight N-S, perpendicular to the basin axis and the range front. This suggests uplift by inversion, potentially supported by the slow thrust front at convergence rates of ~ 0.5 mm/a – 1.0 mm/a (Tesauro et al., 2005). The fluvial pattern is also controlled by enhanced sediment supply from accelerated erosion of the mountain range (Burbank, 1992).

Furthermore, the pattern of fluvial terraces in the eastern basin implies that rivers respond to uplift. In the area of Altötting and Marktl, the Inn reaches the southwestern most extend of the Tertiary Hills, bound by the tail of the LNH normal fault system. At this point, the river gets deflected ~ 120° towards the southeast, (Fig. 4.9). This deflection appears to be younger than late Pleistocene, as indicated by cut terraces on the abandoned riverbank north of the present-day river path. The observed contact

between young Holocene terraces of the Inn and Isen river, and Miocene sand deposits at the margin of the Tertiary Hills can be explained by uplift of the area, which is compensated by enhanced river incision cutting down the younger terrace levels. The maximum age is estimated to be mid-Pliocene, when the rivers started to occupy this area by northward migration (Bader, 1982a; Tillmanns, 1980).
The width of the late Pleistocene to Holocene terraces decreased remarkably where the rivers Isen and Inn reach the Tertiary Hills. Along all rivers in the area investigated, we observe contacts between the youngest Holocene fluvial deposits and the underlying Miocene sediments, indicating incision.

North of the Inn river, the asymmetric pattern of the rivers Vils and Rott (Fig. 4.7, Fig. 4.12) most likely reflects sequential uplift of the region that is expressed by the fluvial asymmetry (Burbank and Anderson, 2001; Schumm, 1986). The homogeneous loess and loess loam deposits in the area have a low resistance to erosion, and therefore morphologic disequilibrium will be balanced quickly. This suggests, that asymmetric tributary networks are controlled by uplift and possibly local tectonics. Furthermore, the stream capture of Vils headwaters by the Rott river (Fig. 4.12) shows a northwestward drainage migration of the Rott. This is interpreted to reflect the northward steepening of the Rott drainage area, causing stream capture. The boundary conditions of precipitation and base level of the main discharge system are assumed to be constant over the timescale of stream reorganization. Since the pattern is distributed, it cannot be linked to a single fault, because the basement structures have no clear surface expression, and there are no shallow high-resolution geophysical data available.

7. Discussion

The comparison of the eastern and western NAFB demonstrates that the Tertiary Hills and local fluvial systems are significantly asymmetric, which is not a result from lithology and climate alone. Both areas are covered with poorly consolidated Quaternary sediments from the last glacial and interglacial periods. Though, this cover is minor, compared to neighboring basins (Fig. 4.19).

The evolution of the young drainage networks in the Tertiary Hills has been so far explained by simple climatic organization of fluvial channels (Wende, 1995). But results show, that differences of stream features occur at small spatial scales, where a climatic control is expected to provide similar features across a region. Therefore, we propose that the Pleistocene and Holocene drainage evolution is the result of active uplift and local faulting, where rivers react to reach steady-state conditions.

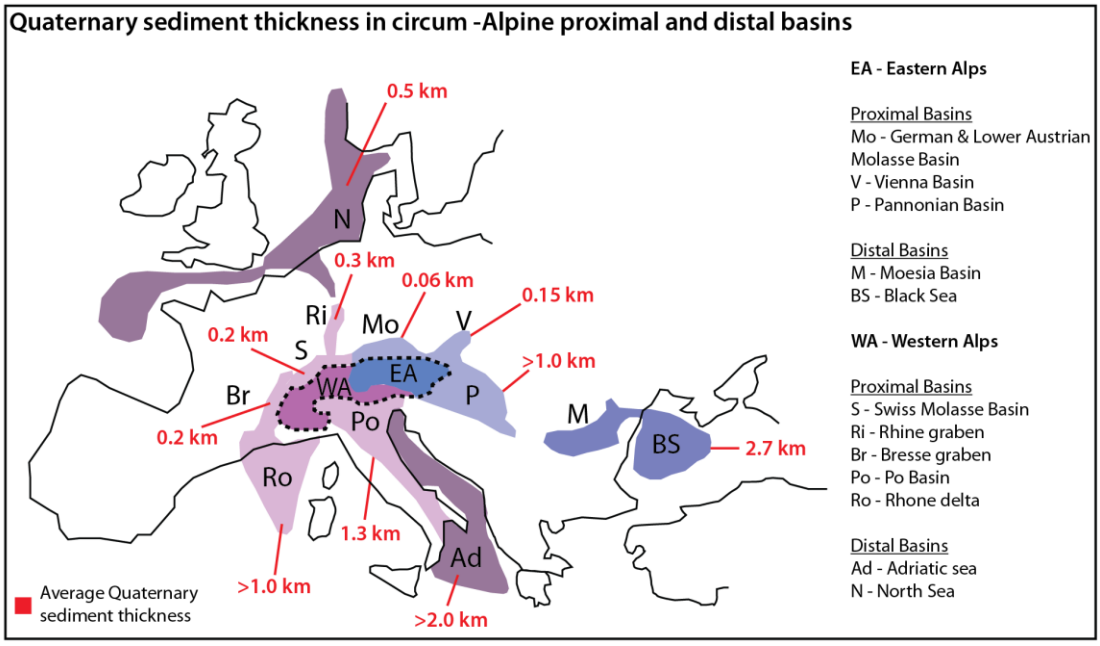

Fig. 4.19: Schematic map of proximal and distal basins for the Alpine erosion area with average thickness of Quaternary for each basin. Geologic data compiled from Nikishin et al (2003), Horvath and Cloething (1996), Bartz (1974), Ori and Friend (1984), Kooi et al (1991), Phillipe et al (1998). Data for the NAFB data from this study.

The *KSN* results indicate non-steady-state conditions in the NAFB, which could be explained by inversion and tectonics. The largest rivers in the southeastern basin (Isar, Inn and Salzach) show a uniform pattern of steep segments a few kilometers north of the Alpine front. We attribute this pattern to active uplift that is compensated by the ongoing incision of the fluvial systems. In several places, the rivers have incised into Pleistocene terrace deposits and the underlying Miocene sediments. In the case of the river Isar, this incision is about 60 m between the terraces from the LGM and the recent alluvium.

A general consideration for the *KSN* results is the anthropogenic overprint. In the NAFB, most of the rivers are modified (Bayerisches Wasserwirtschaftsamt). Especially artificial gravel filling, carried out to reduce depth erosion of rivers, has to be considered (e.g., Isar at Bad Tölz and Wasserburg am Inn). This changes the steepness values of individual segments, leading to a potential overestimation. Also the Sylvenstein dam upstream in the Alps influences the river Isar. Since the dam establishment in 1959, it mainly controls water discharge and sediment load. Further anthropogenic influence is provided by river embankments, which may lead to observing biased signals. However, the spatial distribution of river modification is larger compared to the localized steepness pattern we observe. Therefore, even an overestimation of the absolute values does not limit the significance of the overall pattern.

In this context, the generally observed high *KSN* values exceeding 2,000 are significantly larger than for example in active mountainous regions, like the Himalayas (Topal et al., 2016; Whipple and Tucker, 1999). We attribute this to the intensively alluviated valleys and fans in the NAFB. The method shows limitations, when extracting a narrow channel from wide areas of equally low topography. Similar problems occur for stream analysis on large alluvial fans in the Himalayas (pers. comm. Bufe, A., 2016). When translating the *KSN* values into zones of uplift, this problem reduces the reliability of the absolute values. However, the numbers itself do not affect the pattern along streams and tributaries.

Therefore, we assume the *KSN* results to actually reflect active river response, possibly caused by regional and local uplift. In general, the fact that a river system shows steep channel gradients and active incision on its downstream part indicates a tectonically controlled process (Wobus et al., 2010). The river maintains a higher stream power and transport capacity, compared to the amount of sediments supplied

in the headwater area. If active uplift occurs on the downstream channel, the river starts to incise upstream (Wobus et al., 2010). This is observed independently on modified rivers emerging from the Alps (e.g., Isar, Inn) and rivers originating in the Tertiary Hills (e.g., Vils, Rott), where no dams and embankments control the water discharge.

If climate would be the main driving factor of basin erosion and deposition pattern, it should be reflected by along-stream erosion and deposition (e.g., Schumm, 1986). Climate is expected to affect regions over several hundreds of kilometers (e.g., Hijmans et al., 2005) and therefore control all catchments of a region at the same time. However, tectonically induced changes would control individual catchments, starting with the largest and progressively affecting the smaller ones.

Our study shows that the highest amounts of erosion in the central NAFB do not follow a river system that has reworked the area. During the Quaternary, the Danube has occupied the region along the tip of the Swabian Alb. But so far, there is no evidence that it ran along the central E-W basin axis (Bader, 1982a; Tillmanns, 1980; Villinger, 1986, 1989). Indeed, the river systems in the NAFB have changed several times throughout the entire evolution of the basin (Brügel, 1998; Kuhlemann and Kempf, 2002; Unger, 1999c). Besides some uncertainties for the Quaternary, there is good knowledge on the drainage organization, based on provenance analyses of fluvial terraces (Jerz, 1993; Scheuenpflug, 1978; Unger, 1999c). Still, the age of most of the deposits has not been determined by radiometric methods like cosmogenic nuclide dating, which could resolve the exposure age of the sediments as e.g., terraces. Age constraints have been derived from provenance analysis based on the assumption that the lithological composition reflects source area and transport path. Further, it is assumed that material remained unmixed and mineral weathering, causing preferential sorting, can be neglected (Brügel, 1998; Penck, 1922). In summary, the climatically controlled Quaternary paleo river network was most likely not the main driver of the east-west erosion pattern.

However, an additional climatic contribution, which emphasized local asymmetric topography and enhanced local erosion by fluvial incision, cannot be ruled out.

The observed stream capture affecting the Vils river (Fig. 4.13), indicates the active migration of the catchment. This is likely a result of local surface uplift, forcing the Rott to compensate by head ward incision. Alternatively, this can be explained by base level.

The Vils drains into the Danube – Black Sea system. A base level drop could result in the observed enhanced incision (e.g., Schumm, 1986; Willett et al., 2014). In this context, changes in Black Sea base level of several tens of meters have been reported for Pleistocene (e.g., Constantinescu et al., 2015). However, along the c. 1,600 km distance between the Black Sea and the Vils/ Rott drainage basins, also the Vienna Basin influences fluvial systems. Therefore, the changes on this order of magnitude are likely too insignificant to maintain a continuous stream capture by head ward erosion in the Vils-Rott tributaries. Further, the spatial pattern of the detected stream piracy is restricted to the capturing of the Vils, while a similar mechanism has not been observed for the neighboring rivers. Therefore, we explain the capture of Vils tributaries by uplift at the southeastern most tip of the Tertiary Hills.

The first attempt to identify Quaternary faulting in the central NAFB using river network pattern in the Tertiary Hills has been carried out based on aerial photography (Mühlfeld, 1968). The results indicate a correlation of basement fault orientation with local asymmetric drainage pattern. In principle, our results confirm these observations, which indicate potential vertical motion on the Landshut-Neuötting normal faults in the Tertiary Hills. However, this indications are only robust for activity during a time interval on which those river systems existed, and their age is not well constrained. Most likely the systems exist since the Pliocene, as inferred from gravel provenance studies (Bader, 1982a; Tillmanns, 1980). Further, the rivers might be affected by local tectonics, which does not necessarily reflect basin wide signals of deformation.

To detect a basin inversion, long-term geologic records provide suitable data.

For the long timescale analysis, we calculated Quaternary sediment budgets and converted those to a time averaged erosion rate for the German portion of the NAFB. The results are compared to the six other proximal sedimentary basins surrounding the Alps (Fig. 4.19). These basins have been receiving sediments from the Alps during the Pliocene and Quaternary (for a compilation on sediment yields, see Baran, 2012; Baran et al., 2014). The observed present-day Quaternary thickness in the NAFB (0 m- 300 m, average: 60 m), is up to six times smaller compared to the Po Basin (500 m – 2000 m) (Ori and Friend, 1984), and still about half of the Rhine Graben yield (200 m - 400 m) (Bartz, 1974). However, the Quaternary denudation rates in the Alpine catchment areas have been found to be quite similar for the Quaternary (Hinderer, 2001). Furthermore, the other basin systems have also been

exposed to reworking and erosion, but they do not show rates and pattern similar to the NAFB.

For example, the Rhine Graben sink became connected to the Rhine headwaters from the Alps at the Pliocene/ Pleistocene boundary (Hagedorn, 2004). During the Quaternary, the Rhine river has reworked and eroded parts of the previously stored sediments. In the Po Basin, the youngest observed phase of erosion happened during the Messinian salinity crisis, when the basin lost up to 200 m of latest Miocene sediments (Preusser et al., 2010).

In the NAFB, a hiatus occurred during the Pliocene. Apatite fission track data and subsidence analyses have revealed between 0.3 km and 2.0 km of Pliocene erosion across the Alpine foreland (Cederbom et al., 2004; Genser et al., 2007). Conceptually, the amount of sediments stored in the proximal basins corresponds to the sediment influx, if the basin constantly subsides and creates accommodation space (e.g., Busby and Ingersoll, 1995).

The rate of proximal basin erosion is ~ 0.1 mm/a, while the rate of material flux from the Alpine range into the basin is ~ 0.4 mm/a (Hinderer, 2001), resulting in a positive net mass balance. The material that is removed from the Alpine range (in the catchments draining to the NAFB) is temporarily deposited in the proximal basins, and only later becomes eroded and transported to distal basin systems. As Baran (2012) and Baran et al. (2014) pointed out, the Alpine denudation rates during the last 5 Ma (Champagnac et al., 2007; Kuhlemann and Kempf, 2002) have previously been overestimated. Therefore we based our calculation on the lower rates introduced by Baran (2012).

Besides the wide erosion of Quaternary sediments, abundant deposits occur along the northern Alpine range front in over-deepened, post-glacial lake valleys. The formation of these sinks results in a temporary disconnection of the upstream source area from the downstream depositional area (Hinderer, 2012). This has locally resulted in sediment accumulation of > 300 m (Krömer, E., pers. comm., 2016). We therefore attribute the enhanced Quaternary thicknesses near the Ammer lake, Chiem lake and the Allgäu region, as exceptions.

The estimation of bulk sediment budgets and inferred erosion rates utilized in this study contains several sources of error. For the mean sediment yield, given by (Kuhlemann et al., 2001; Kuhlemann and Kempf, 2002), the typical error is 50%, which has been confirmed in similar studies for the outer Alps and the foreland

(Hinderer, 2001). Our main results are based on the well data, for which we have to rely on the correct documentation of Quaternary sediments. However, uncertainties arise from the lithological similarities of sediments of the latest Pliocene and the earliest Quaternary, especially if no radiometric ages were determined.
The estimates of Quaternary thicknesses of over deepened glacial valleys, like the Lake Constance area and the former Lake Rosenheim, are on the order of 130 m - 150 m (Hinderer, 2001). In the area of Neubeuern, thicknesses > 300 m are observed (pers. comm. Ernst Krömer, LfU, Bavaria, 2016). In our erosion estimates, we have considered a general increased thickness along the Alpine front, expressed by the shape of the erosion contour lines. When converting the sediment volume of an area into the erosion rate, usually the mass of shallow sediments is overestimated, because bulk densities vary with facies and burial depth. As we observe compaction of sediments in outcrops in the Ulm region, as well as for gravel deposits in the Tertiary Hills, several hundred meters of sedimentary overburden are realistic. The total error from the compaction uncertainty does not exceed 15% (Hinderer, 2001) but nevertheless, for this type of erosion estimates, an overall uncertainty of 50 % has to be accepted. Though, the conclusions drawn from the data are related to pattern after all. Therefore a change in the absolute values does not deny the overall result.

The observed pattern of Quaternary erosion is most likely the result from an ongoing basin inversion that started in the Pliocene, focused in the western basin (Baran et al., 2014; Lemcke, 1974). Comparison of uplift rates across three time scales, at several sites across the basin, supports this assumption.
Between 30 Ma and 5 Ma, we observe a switch from subsidence to inversion across the basin, as suggested by Lemcke (1974). The 5 Ma uplift rate is on the order of 0.1 mm/a – 0.5 mm/a, while the signal on the Quaternary timescale turns out to be generally smaller, with rates of 0.03 mm/a – 0.1 mm/a. Yet, this is still ranging in the same order of magnitude within errors. On the short timescale (c. 6,000 a – 7,000 a), the rate of 0.25 mm/a – 0.33 mm/a, is higher than the average Pliocene and Quaternary rates, and also exceeds the 30 Ma - 5 Ma average.
The highest rates on the 30 Ma time scale are observed in the western basin, while for the Quaternary we found the highest values in the eastern basin (Tertiary Hills). This region also shows the highest rates on the short-term timescale.

The cumulative plot of the uplift data from the three time scales shows an increasing trend from the basin formation at 30 Ma until today. We further observe a saturation effect for the average uplift rate since the last 5 Ma, which is indicative for the ongoing basin inversion that maintains the high topographic elevation and the erosional relief of the basin (Fig, 4.21, Fig. 4.22).

The apparent increasing rates in the Holocene are an effect of the time dependent ratio between the signals, also known as the "*Sadler"* effect (Sadler, 1981). The comparison of the three time bins shows the typical spikes of the shorter 2nd and 3rd order processes (Fig. 4.1), while the moving average matches the long-term signal estimates (Fig. 4.20).

Fig. 4.20: Next page: Uplift rates for the three time intervals and the cumulative signal of basin uplift analyzed in this study.

1st order
long-term
40 Ma - 5 Ma

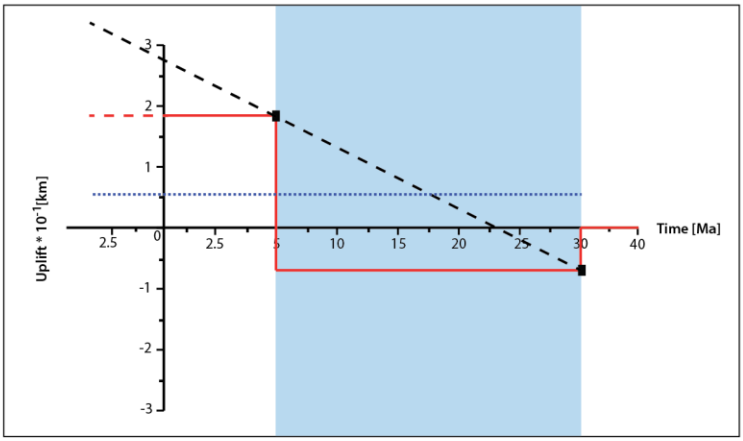

2nd order
medium-term
5 Ma - 3 Ma

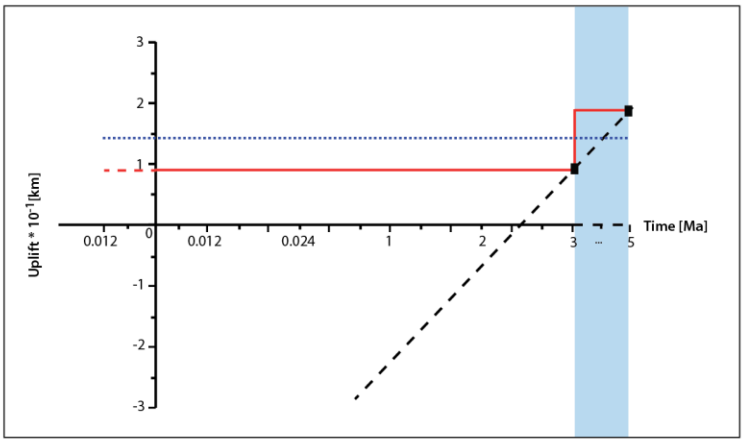

3rd order
short-term
3 Ma - present

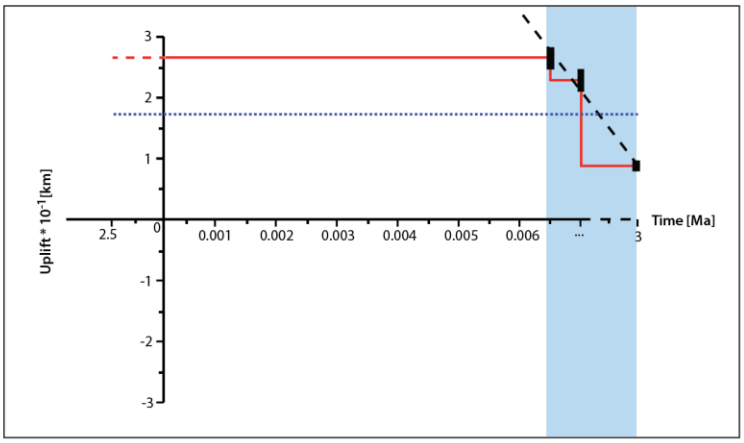

cumulative
results
40 Ma - present

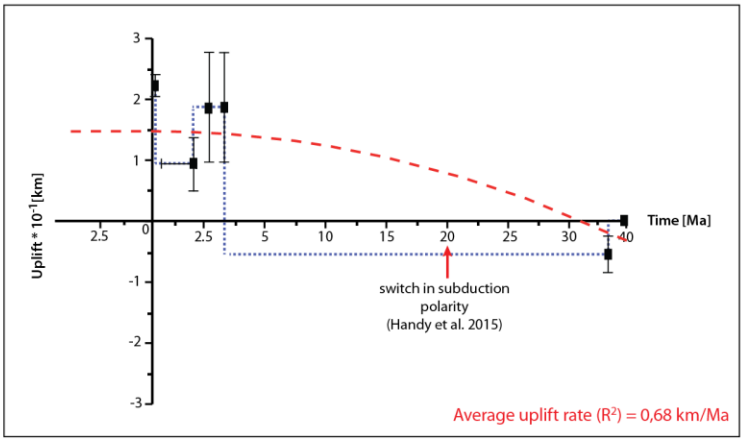

linear average error range

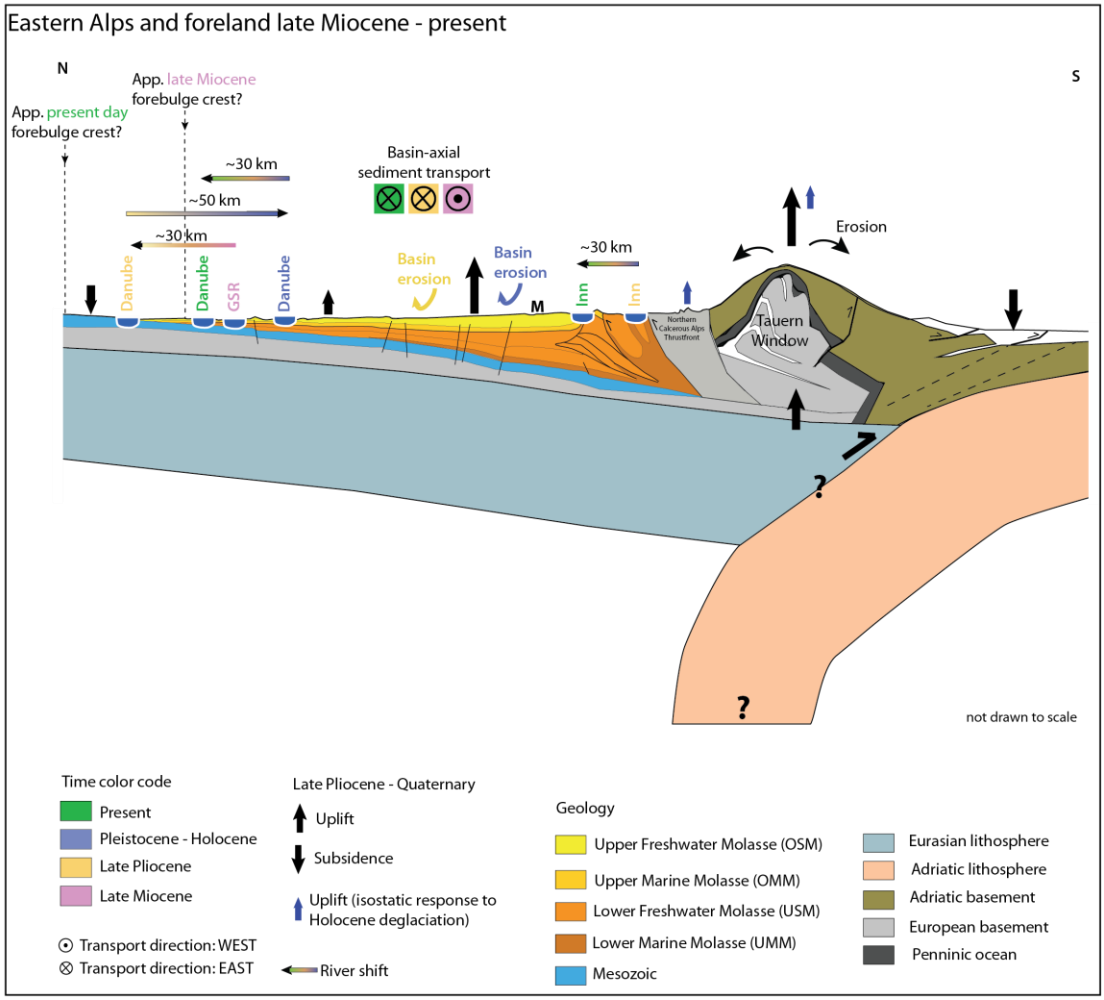

Fig. 4.21: Schematic cross section of the eastern Alps and the northern foreland basin. M = München. GSR = Graupensandrinne. For profile location see Fig. 4.18. Data compiled from Bayerisches Geologisches Landesamt (1996), Kuhlemann and Kempf (2002), Rosenberg et al (1998), Handy et al (2015), Reichenbacher (2008), Gutscher (1995). For discussion of the forebulge position see chapter III of this thesis.

8. Conclusions

In the low strain NAFB, active deformation is detected on timescales from 10^3 a to 10^6 a. According to our results, the basin has been active during the Quaternary by ongoing inversion. The timing for the shift from subsidence to uplift in the late Pliocene – early Quaternary is in agreement with previous Pliocene estimates based on long-term proto-backstripping (Lemcke, 1974). Increased uplift rates on the short timescale suggest contributions from local faulting in the Tertiary Hills (see also chapter II, Hoffmann M. et al., 2016a).

The erosional relief of the NAFB reflects the basins uplift, and the asymmetric topography of Tertiary Hills turned out to be tectonically influenced of being simply controlled by lithology and climate. Especially the local occurrence of tectono-geomorphic features contradicts a basin wide climatic driver.

Detected river asymmetries and steepened segments can be explained by young basin uplift and potential tectonic surface modification, which has mainly affected the eastern portion of the NAFB. Another indicator of active uplift comes from our study on Quaternary erosion rates. We identified a remarkable erosion of Quaternary sediments in the NAFB, whose pattern depict a basin axis parallel oval shape. This indicates a basin wide inversion, instead of simple fluvial transport. The same signal of uplift has also been detected on shorter time sales from local archeology in the Tertiary Hills.

Based on our results, we suggest that the basin inversion has not stopped by the end of the Pliocene, but ceased and pursued at lower rates. However, the inferred NAFB inversion of c. 0.5 km since the late Pliocene, covering a region of several hundreds of kilometers, can also result from underlying mantle processes, namely dynamic topography. In order to detect possible contributions from those processes, additional far-field studies are required. Further research in this direction will help to detect potential contemporaneous events of erosion and uplift outside the NAFB, which could be related to mantle processes.

9. Acknowledgements

MH acknowledges salary from the Helmholtz Alliance Project - HGF, Remote sensing and Earth System Dynamics, WPG9 – Geological context of tectonically active but seismically inactive regions, awarded to AMF.

10. References

Allen, P. A., and Homewood, P., 1986, Foreland basins, Oxford, Blackwell Scientific Publications, Spec. Publ. Int. Ass. Sediment., p. 3–228.

Andeweg, B., and Cloetingh, S., 1998, Flexure and 'unflexure' of the North Alpine German-Austrian Molasse Basin: constraints from forward tectonic modelling: Geological Society, London, Special Publications, v. 134, no. 1, p. 403–422.

Bachmann, G. H., Dohr, G., and Müller, M., 1982, Exploration in a Classic Thrust Belt and Its Foreland: Bavarian Alps, Germany: AAPG Bulletin, v. 66, no. 12, p. 2529–2542.

Bachmann, G. H., and Müller, M., 1991, The Molasse basin, Germany: evolution of a classic petroliferous foreland basin: Generation, accumulation, and production of Europe's hydrocarbons (ed. A.M. Spencer, Special Publication of the European Association of Petroleum Geoscientists, Oxford University Press, v. 1, p. 273–276.

Bachu, S., 1995, Synthesis and Model of Formation-Water Flow, Alberta Basin, Canada: AAPG Bulletin, v. 79, no. 8, p. 1159–1178.

Bader, K., 1982a, Die Verbauung von Ur-Isartälern durch die Vorlandvergletscherung als Teilursache der anomalen Schichtung des Quartärs in der Münchener Ebene.: Mittl.Geograph.Ges. München, v. 67, p. 5–20.

Baran, R., 2012, Quantification of Landscape Evolution on Multiple Time-Scales: Applications of High-Resolution 3-D Laser Scanning and Erosion Measurements to Tectonic and Geomorphological Questions. Ph.D. Thesis, Ludwig-Maximilians-Universität, p. 103–142.

Baran, R., Friedrich, A. M., and Schlunegger, F., 2014, The late Miocene to Holocene erosion pattern of the Alpine foreland basin reflects Eurasian slab unloading beneath the western Alps rather than global climate change: Lithosphere, v. 6.2, p. 124–131.

Bartz, J., 1974, Die Mächtigkeit des Quartärs im Oberrheingraben: Approaches to Taphrogenesis, v. 8, p. 78–87.

Beaumont, C., Fullsack, P., and Hamilton, J., 1992, Erosional control of active compressional orogens, Thrust tectonics, Springer Netherlands, p. 1–18.

Bernet, M., Brandon, M., Garver, J., Balestieri, M. L., Ventura, B., and Zattin, M., 2009, Exhuming the Alps through time: clues from detrital zircon fission-track thermochronology: Basin Research, v. 21, p. 781–798.

Böhme, M., Ilg, A., and Winklhofer, M., 2008, Late Miocene "washhouse" climate in Europe: Earth and Planetary Science Letters, v. 275, no. 3–4, p. 393–401.

Brügel, A., 1998, Provenances of alluvial conglomerates from the East Alpine foreland: Oligo-Miocene denudation history and drainage evolution of the Eastern Alps: Tüb. Geowiss. Arb., A. Geol. Paläont.. Stratigr., v. 40, p. 1–168.

Burbank, D., 1992, Causes of recent Himalayan uplift deduced from deposited patterns in the Ganges basin: Nature, v. 357, p. 680–683.

Burbank, D., and Anderson, R., 2001, Tectonic Geomorphology, p. 159–241

Burbank, D., Beck, R. A., and Mulder, T., 1996, 9 The Himalayan foreland basin, p. 149–190.

Busby, C. J., and Ingersoll, R. V., 1995, Tectonics of sedimentary basins, p. 1–113.

Cederbom, C. E., Sinclair, H. D., Schlunegger, F., and Rahn, M. K., 2004, Climate-induced rebound and exhumation of the European Alps: Geology, v. 32, no. 8, p. 709.

Cederbom, C. E., van der Beek, P., Schlunegger, F., Sinclair, H. D., and Oncken, O., 2011, Rapid extensive erosion of the North Alpine foreland basin at 5-4 Ma: Basin Research, v. 23, no. 5, p. 528–550.

Champagnac, J. D., Molnar, P., Anderson, R. S., Sue, C., and Delacou, B., 2007, Quaternary erosion-induced isostatic rebound in the western Alps: Geology, v. 35, no. 3, p. 195.

Constantinescu, A. M., Toucanne, S., Dennielou, B., Jorry, S. J., Mulder, T., and Lericolais, G., 2015, Evolution of the Danube Deep-Sea Fan since the Last Glacial Maximum: new insights into Black Sea water-level fluctuations: Marine Geology, v. 367, p. 50–68.

D'Agostino, N., Avallone, A., Cheloni, D., D'anastasio, E., Mantenuto, S., and Selvaggi, G., 2008, Active tectonics of the Adriatic region from GPS and earthquake slip vectors: Journal of Geophysical Research: Solid Earth, v. 113, no. B12, p. 1–19.

Davies, J. H., and von Blanckenburg, F., 1995, Slab breakoff: a model of lithosphere detachment and its test in the magmatism and deformation of collisional orogens: Earth and Planetary Science Letters, v. 129, no. 1, p. 85–102.

DeCelles, P. G., 2004, Late Jurassic to Eocene evolution of the Cordilleran thrust belt and foreland basin system, western USA: American Journal of Science, v. 304, no. 2, p. 105–168.

DeCelles, P. G., and Giles, K. A., 1996, Foreland Basin Systems: Basin Research, v. 8.2, p. 105–123.

Devoti, R., Riguzzi, F., Cuffaro, M., and Doglioni, C., 2008, New GPS constraints on the kinematics of the Apennines subduction: Earth and Planetary Science Letters, v. 273, no. 1–2, p. 163–174.

Doppler, G., 1989, Zur Stratigraphie der nördlichen Vorlandmolasse in Bayerisch-Schwaben: Geologica Bavarica, v. 94, p. 83–133.

Doppler, G., and Schwerd, K., 1996, Faltenmolasse, Aufgerichtete Molasse und westliche Vorlandmolasse, *in* Freudenberger, W., and Schwerd, K., eds., Erläuterungen zur Geologischen Karte von Baysrn 1: 500,000, Volume 4: München, Bayersiches Geologisches Landesamt, p. 150–168.

Ellwanger, D., 2015, Lithostratigraphische Entwicklung des baden-württembergischen Rheingletschersgebiets – Übertiefte Becken- und Moränenlandschaft, LGRB-Fachbericht, v. 4, Freiburg im Breisgau, p. 1–86.

Füchtbauer, H., 1964, Sedimentpetrographische Untersuchungen in der älteren Molasse der Alpen.: Eclogae geol. Helv. Basel, v. 57, p. 157–298.

Ganss, O., 1968, Erläuterungen zur Geologischen Karte von Bayern, 1:25k, Blatt Traunstein: Bayersiches Geologisches Landesamt.

Gebrande, H., Castellarin, A., Lüschen, E., Millahn, K., Neubauer, F., and Nicolich, R., 2006, TRANSALP—A transect through a young collisional orogen: Introduction: Tectonophysics, v. 414, no. 1–4, p. 1–7.

Genser, J., Cloething, S. A. P. L., and Neubauer, F., 2007, Late orogenic rebound and oblique Alpine convergence: New constraints from subsidence analysis of the Austrian Molasse basin: Global and Planetary Change, v. 58, p. 214–223.

Hagedorn, E., 2004, Sedimentpetrographie und Lithofazies der jungtertiären und quartären Sedimente im Oberrheingebiet: Köln. Ph.D. Thesis Universität Köln, 248 p.

Handy, M. R., Ustaszewski, K., and Kissling, E., 2014, Reconstructing the Alps–Carpathians–Dinarides as a key to understanding switches in subduction polarity, slab gaps and surface motion: International Journal of Earth Sciences, v. 104, no. 1, p. 1–26.

Hay, W. W., Wold, C. N., and Herzog, J. M., 1992, Preliminary mass-balanced 3D reconstructions of the Alps and surrounding areas during the Miocene, in Pfl ug, R., and Harbaugh, J.W., eds., Computer graphics in geology, three-dimensional computer graphics in modeling geologic structures and simulating geologic processes: Lecture Notes in Earth Sciences, v. 41, p. 99–100.

Heermann, O., 1954, Erdölgeologische Grundlagen der Aufschlussarbeiten im Ostbayerischen Molassebecken: Bull. Ver. Schweiz. Petrol.-Geol. u. Ing., v. 21, no. 60, p. 5–22.

Heidbach, O., Tingay, M., Barth, A., Reinecker, J., Kurfeß, D., and Müller, B., 2008, The World Stress Map database release 2008: GFZ Potsdam, p. 3–15.

Herman, F., Seward, D., Valla, P. G., Carter, A., Kohn, B., Willett, S. D., and Ehlers, T. A., 2013, Worldwide acceleration of mountain erosion under a cooling climate: Nature, v. 504, p. 423–426.

Hesse, R., 1975, Turbiditic and non-turbiditic mudstone of Cretaceous flysch sections of the East Alps and other: Sedimentology, v. 22, p. 387–416.

Hijmans, R. J., Cameron, S. E., Parra, J. L., Jones, P. G., and Jarvis, A., 2005, Very high resolution interpolated climate surfaces for global land areas: International Journal of Climatology, v. 25, no. 15, p. 1965–1978.

Hinderer, M., 2001, Late Quaternary denudation of the Alps, valley and lake fillings and modern river loads: Geodinamica Acta, v. 14, no. 4, p. 231–263.

Hinderer, M., 2012, From gullies to mountain belts: A review of sediment budgets at various scales: Sedimentary Geology, v. 280, p. 21–59.

Hüttner, R., 1969, Bunte Trümmermassen und Suevit: Geologica Bavarica, v. 61, p. 142–200.

Jerz, H., 1979, Das Wolfratshausener Becken: seine glaziale Anlage und Übertiefung, p. 63–70.

-, 1993, Das Eiszeitalter in Bayern - Erdgeschichte, Gesteine, Wasser, Boden, Stuttgart, E. Schweizerbart'sche Verlangsbuchhandlung, Geologie von Bayern II, p. 1–243.

Jin, J., Aigner, T., Luterbacher, H. P., Bachmann, G. H., and Müller, M., 1995, Sequence stratigraphy and depositional history in the south-eastern German Molasse Basin: Marine and Petroleum Geology, v. 12, no. 8, p. 929–940.

Kirby, E., and Whipple, K. X., 2012, Expression of active tectonics in erosional landscapes: Journal of Structural Geology, v. 44, p. 54–75.

Knödel, K., Krummel, H., and Lange, G., 2013, Handbuch zur Erkundung des Untergrundes von Deponien und Altlasten, Springer-Verlag, p. 425–726.

Konyuhov, A. I., and Maleki, B., 2006, The Persian Gulf Basin: Geological history, sedimentary formations, and petroleum potential: Lithology and Mineral Resources, v. 41, no. 4, p. 344–361.

Kraus, L., 1969, Erdöl- und Erdgaslagerstätten im ostbayerischen Molassebecken: Erdoel-Erdgas-Zeitschrift, v. 85, p. 442–454.

Kuhlemann, J., Dunkl, I., Brügel, A., Spiegel, C., and Frisch, W., 2006, From source terrains of the Eastern Alps to the Molasse Basin: Detrital record of non-steady-state exhumation: Tectonophysics, v. 413, no. 3–4, p. 301–316.

Kuhlemann, J., Frisch, W., Dunkl, I., and Székely, B., 2001, Quantifying tectonic versus erosive denudation by the sediment budget: the Miocene core complexes of the Alps: Tectonophysics, v. 330, p. 1–23.

Kuhlemann, J., and Kempf, O., 2002, Post-Eocene evolution of the North Alpine Foreland Basin and its response to Alpine tectonics: Sedimentary Geology, v. 152, p. 45–78.

Lemcke, K., 1974, Vetikalbewegungen des vormesozoischen Sockels im nördlichen Alpenvorland Perm bis zur Gegenwart?: Eclogae Geologicae Helvetiae, v. 67, no. 1.

-, 1984, Geologische Vorgänge in den Alpen ab Obereozän im Spiegel vor allem der deutschen Molasse: Geologische Rundschau, v. 73, p. 371–398.

-, 1988, Das bayerische Alpenvorland vor der Eiszeit, p. 5–134.

Leydecker, G., 2011, Erdbebenkatalog für Deutschland mit Randgebieten für die Jahre 800 bis 2008, Geologisches Jahrbuch Reihe E, Volume Band E59, p. 1–198.

Lindner, H., 2011, Flussgeschichte der Donau, 28 p.

Lóczy, D., 2007, The Danube: morphology, evolution and environmental issues, *in* Gupta, A., ed., Large rivers: geomorphology and management., John Wiley & Sons, p. 235–260.

Lucchi, F. R., 1986, The Oligocene to Recent foreland basins of the northern Apennines, Foreland Basins, Volume 8, Special Publication of the International Association of Sedimentologists, p. 105–139.

Lüschen, E., Borrini, D., Gebrande, H., Lammerer, B., Millahn, K., Neubauer, F., and Nicolich, R., 2006, TRANSALP—deep crustal Vibroseis and explosive seismic profiling in the Eastern Alps: Tectonophysics, v. 414, no. 1–4, p. 9–38.

Lüschen, E., Lammerer, B., Gebrande, H., Millahn, K., and Nicolich, R., 2004, Orogenic structure of the Eastern Alps, Europe, from TRANSALP deep seismic reflection profiling: Tectonophysics, v. 388, no. 1–4, p. 85–102.

Mayr, M., 1957, Geologische Untersuchungen in der ungefalteten Molasse im Bereich des unteren Inn (Positionsblätter Simbach a. Inn 653 und Julbach 652 / Ostteil. Beihefte zum Geologischen Jahrbuch 26, p. 309–370.

Mazurek, M., Hurford, A. J., and Leu, W., 2006, Unravelling the multi-stage burial history of the Swiss Molasse Basin: integration of apatite fission track, vitrinite reflectance and biomarker isomerisation analysis: Basin Research, v. 18, p. 27–50.

Mühlfeld, R., 1968, Photogeologische Beobachtungen zum Sedimentaufbau und zur Tektonik im ostbayerischen Molassebecken zwischen Landshut und Eggenfelden: Geol. Jb., v. 85, p. 285–298.

Nikishin, A. M., Korotaev, M. V., Ershov, A. V., and Brunet, M. F., 2003, The Black Sea basin: tectonic history and Neogene–Quaternary rapid subsidence modelling: Sedimentary Geology, v. 156, no. 1, p. 149–168.

Norton, K. P., and Hampel, A., 2010, Postglacial rebound promotes glacial re-advances - a case study from the European Alps: Terra Nova, p. 297–302.

Oeltzschner, H., 1965, Geologische und sedimentpetrographische Untersuchungen auf Blatt Vilsbiburg 7540 (Niederbayern): Univ. München, 101 S., 139 Abb. p. 1–101.

Ori, G. G., and Friend, P. F., 1984, Sedimentary basins formed and carried piggyback on active thrust sheets: Geology, v. 12, no. 475–478.

Penck, A., 1922, Ablagerungen und Schichtstörungen der letzten Interglazialzeit in den nördlichen Alpen: Verlag der Akad. der Wiss, p. 1–214.

Pfiffner, O. A., 1986, Evolution of the north Alpine foreland basin in the Central Alps: In Foreland basins. Spec. Publ. Int. Ass. Sediment., v. 8, p. 219–228.

Preusser, F., Reitner, J. M., and Schlüchter, C., 2010, Distribution, geometry, age and origin of overdeepened valleys and basins in the Alps and their foreland: Swiss Journal of Geosciences, v. 103, no. 3, p. 407–426.

Prinz, H., and Strauß, R., 2012, Ingenieurgeologie, Springer Verlag, 650 p.

Quinlan, G. M., and Beaumont, C., 1984, Appalachian thrusting, lithospheric flexure, and the Paleozoic stratigraphy of the Eastern Interior of North America: Canadian Journal of Earth Sciences, v. 21, no. 9, p. 973–996.

Regard, V., Faccenna, C., Bellier, O., and Martinod, J., 2008, Laboratory experiments of slab break-off and slab dip reversal: insight into the Alpine Oligocene reorganization: Terra Nova, v. 20, p. 267–273.

Reichenbacher, B., Böttcher, R., Bracher, H., Doppler, G., von Engelhardt, W., Gregor, H. J., Heissig, K., Heizmann, E. P., Hofmann, F., Kälin, D., and Lemcke, K., 1998, Graupensandrinne–Ries-Impakt: Zur Stratigraphie der Grimmelfinger Schichten, Kirchberger Schichten und Oberen Süßwassermolasse (nördliche Vorlandmolasse, Süddeutschland): Zeitschrift der deutschen geologischen Gesellschaft, v. 149, no. 1, p. 127–161.

Reicherter, K., Froitzheim, N., Jarosinski, M., Badura, J., Franzke, H. J., Hansen, M., and Stackebrandt, W., 2008, Alpine tectonics north of the Alps: The Geology of Central Europe. Volume 2: Mesozoic and Cenozoic, p. 1233–1285.

Royden, L., Patacca, E., and Scandone, P., 1987, Segmentation and configuration of subducted lithosphere in Italy: an important control on thrust-belt and foredeep-basin evolution: Geology, v. 15, no. 8, p. 714–717.

Rutte, E., 1987, Rhein, Main, Donau: Wie, wann, warum sie wurden; eine geologische Geschichte, Thorbecke, p. 15–140.

Sadler, P. M., 1981, Sediment accumulation rates and the completeness of stratigraphic sections: The Journal of Geology, p. 569–584.

Scheuenpflug, L., 1978, Zur Flußgeschichte der Paar südöstlich Augsburg (Bayerisches Alpenvorland), p. 14–21..

-, 1991, Die frühpleistozäne Augsburger Altwasserscheide am Ostrand der Iller-Lech-Platte (süddeutsches Alpenvorland, Bayern). Beiträge zur Quartär und Landesforschung. Festschrift zum 60.Geburtstag von Julius Fink. Wien, p. 47–55.

Schlunegger, F., Jordan, T. E., and Klaper, E. M., 1997, Controls of erosional denudation in the orogen on foreland basin evolution: The Oligocene central Swiss Molasse Basin as an example: Tectonics, v. 16, no. 5, p. 823–840.

Schlunegger, F., and Kissling, E., 2015, Slab rollback orogeny in the Alps and evolution of the Swiss Molasse basin: Nat Commun, v. 6, p. 8605.

Schlunegger, F., Melzer, J., and Tucker, G., 2001, Climate, exposed source-rock lithologies, crustal uplift and surface erosion: a theoretical analysis calibrated with data from the Alps/North Alpine Foreland Basin system: International Journal of Earth Sciences, v. 90, no. 3, p. 484–499.

Schlunegger, F., and Simpson, G., 2002, Possible erosional control on lateral growth of the European Central Alps: Geology, v. 30, no. 10, p. 907–910.

Schmid, S. M., and Kissling, E., 2000, The arc of the western Alps in the light of geophysical data on deep crustal structure: Tectonics, v. 191, no. 1, p. 62–85.

Schmid, S. M., Pfiffner, O. A., Froitzheim, N., Schönborn, G., and Kissling, E., 1996, Geophysical-geological transect and tectonic evolution of the Swiss-Italian Alps: Tectonics, v. 15, p. 1036–1064.

Schmidt-Thomé, P., 1955, Zur Frage quartärer Krustenbewegungen im Alpen-und Voralpengebiet des Isartalbereichs: Geologische Rundschau, v. 43, no. 1, p. 144–158.

Schumm, S. A., 1986, Alluvial river response to active tectonics, p. 80–94.

Schwanghart, W., and Scherler, D., 2014, Short Communication: TopoToolbox 2-MATLAB-based software for topographic analysis and modeling in Earth surface sciences: Earth Surface Dynamics, v. 2, no. 1., p. 1–7.

Sella, G. F., Dixon, T. H., and Mao, A., 2002, REVEL: A model for Recent plate velocities from space geodesy: Journal of Geophysical Research: Solid Earth, v. 107, no. B4, p. ETG 11-11–ETG 11-30.

Sinclair, H. D., 1997, Tectonostratigraphic model for underfilled peripheral foreland basins: An Alpine perpective: GSA Bulletin, v. 109, no. 3, p. 324–346.

Stocchi, P., Spada, G., and Cianetti, S., 2005, Isostatic rebound following the Alpine deglaciation: impact on the sea level variations and vertical movements in the Mediterranean region: Geophysical Journal International, v. 162, no. 1, p. 137–147.

Strahler, A. N., 1957a, Quantitative Analysis of Watershed Geomorphology, Transactions. American Geophysical Union, v. 38, no. 6, p. 913–920.

Strasser, M., 2011, Höhlen der Schwäbischen Alb als Pegelschreiber für Flussgeschichte und Tektonik in Südwestdeutschland seit dem Miozän [Ph.D. Dissertation]: Universtität Stuttgart, 109 p.

Strasser, M., Strasser, A., Pelz, K., and Seyfried, H., 2009, A mid Miocene to early Pleistocene multi-level cave as a gauge for tectonic uplift of the Swabian Alb (Southwest Germany): Geomorphology, v. 106, no. 1–2, p. 130–141.

Tesauro, M., Hollenstein, C., Egli, R., Geiger, A., and Kahle, H.-G., 2005, Continuous GPS and broad-scale deformation across the Rhine Graben and the Alps: International Journal of Earth Sciences, v. 94, no. 4, p. 525–537.

Tillmanns, 1980, Zur plio-pleistozänen Flu0geschichte von Donau und Main in Nordostbayern.: Jber. Mitt. oberrhein. geol. Ver., N.F., v. 62, p. 199–205.

Topal, S., Keller, E., Bufe, A., and Koçyiğit, A., 2016, Tectonic geomorphology of a large normal fault: Akşehir fault, SW Turkey: Geomorphology, v. 259, p. 55–69.

Trauth, M. H., Gebbers, R., Marwan, N., and Sillmann, E., 2007, MATLAB recipes for earth sciences, Berlin, Springer, p. 311–312.

Trümpy, R., 1973, The timing of orogenic events in the Central Alps: Gravity and tectonics, p. 229–251.

Tucker, G. E., and Slingerland, R., 1997, Drainage basin responses to climate change: Water Resources Research, v. 33, no. 8, p. 2031–2047.

Unger, H. J., 1978a, Erläuterungen zur Geologischen Karte von Bayern 1:50 000, Blatt L7740 Mühldorf a. Inn - 184: Bayerisches Geologisches Landesamt, ,184 p.

-, 1978b, Geologische Karten von Bayern Blatt L7740 Mühldorf a. Inn: Bayerisches Geologisches Landesamt, scale 1:50 000.

-, 1999a, Die tektonischen Strukturen der bayerischen Molasse: Documenta naturae, v. 125, p. 1–16.

-, 1999c, Die Geisenfeld-Abfolge. Gedanken zur pliozänen ENtwässerung der bayerischen Molasse.: Documenta naturae, v. 125, no. 57–97.

Unger, H. J., and Schwarzmeier, J., 1982, Die Tektonik im tieferen Untergrund Ostniederbayerns: Bayerisches Geologisches Landesamt.

-, 1987, Bemerkungen zum tektonischen Werdegang Südostbayerns: Geol. Jb., v. A105, p. 3–23.

Villinger, E., 1986, Untersuchungen zur Flussgeschichte von Aare-Donau/Alpenrhein und zur Entwicklung des Malm-Karsts in Südwestdeutschland: Jh. geol. Landesamt Baden-Württemberg, Freiburg, v. 28, p. 297–362.

-, 1989, Zur Fluss-und Landschaftsgeschichte im Gebiet von Aare–Donau und Alpenrhein: Jahresh. Ges. Naturkd. Württembergs, v. 144, p. 5–27.

von Guembel, C. W., 1861, Geognostische Beschreibung des bayerischen Alpengebirges und seines Vorlandes: J. Perthes, v. 1, p. 1–440.

Vrabec, M., Preseren, P. P., and Stopar, B. O. J. A. N., 2006, GPS study (1996–2002) of active deformation along the Periadriatic fault system in northeastern Slovenia: tectonic model: GEOLOGICA CARPATHICA-BRATISLAVA, v. 57/1, p. 57.

Wagner, L. R., 1998, Tectono-stratigraphy and hydrocarbons in the Molasse Foredeep of Salzburg, Upper and Lower Austria - in: Mascle, A. et al (eds.): Cenozoic Foreland Basins of Western Europe: Geological Society of London, Special Publication, v. 134, p. 339–369.

Wende, R., 1995, Drainage and valley asymmetry in the Tertiary Hills of Lower Bavaria, Germany: Geomorphology, v. 14, p. 255–265.

Wesnousky, S. G., Kumar, S., Mohindra, R., and Thakur, V. C., 1999, Uplift and convergence along the Himalayan Frontal Thrust of India: Tectonics, v. 18, no. 6, p. 967–976.

Whipple, K. X., and Tucker, G. E., 1999, Dynamics of the stream ‐ power river incision model: Implications for height limits of mountain ranges, landscape response timescales, and research needs: Journal of Geophysical Research: Solid Earth, v. 104, no. B8, p. 17661–17674.

Willett, S. D., McCoy, S. W., Perron, J. T., Goren, L., and Chen, C.-Y., 2014, Dynamic Reorganization of River Basins: Science, v. 343, p. 1117–1126.

Wobus, C. W., Tucker, G. E., and Anderson, R. S., 2010, Does climate change create distinctive patterns of landscape incision?: Journal of Geophysical Research, v. 115, no. F4.

Zhang, P., Molnar, P., and Downs, W. R., 2001, Increased sedimentation rates and grain sizes 2-4 Myr ago due to the infl uence of climate change on erosion rates: Nature, v. 410, p. 891–897.

Ziegler, P. A., 1990, Geological Atlas of Western and Central Europe Shell Int. Petrol. Maatschap: Geological Society of London, 239 p.

Zöbelein, H. K., 1995, Die jungtertiäre Graupensandrinne in der V orlandmolasse Südwestdeutschlands (For- schungsgeschichte, Verlauf, Entstehung, Füllung und Beziehungen zur Umrandung): Doc. nat. München, v. 91, p. 1–108.

11. Appendices

11.1. Calculation steps of Quaternary sediment budget analysis

Step 1:

Based on mapping results from the high-resolution digital elevation models, we consider the surface areas of the German and lower Austrian Molasse basin (Tab. 4.4) 34,500 km^2, the Alpine catchments that contribute material to the basin, 36.305 km^2, and the Swabian-Frankonian Alb and Bohemian Massif catchments 25,167 km^2 (Fig. 4.17). In order to estimate the sediment yield that is transported and temporarily stored in the NAFB, we then multiply the catchment areas with the average bulk erosion rates for the area adopted from (Hinderer, 2001; Kuhlemann et al., 2001; Kuhlemann and Kempf, 2002) (Table 4.4). The erosion rates exhibit an error of up to ±50%, which is related to the original datasets of Kuhlemann et al (2001 and 2002).

Step 2:

The continuous erosion from the basin into distal catchments limits the amount of material stored in the basin. We therefore calculate the sediments stored by multiplying the average proximal basin erosion rate adopted from Baran (2012) with the total storage area. The result is subtracted from the total sediment yield (step 1). The final average sediment thickness accumulated in the basin is then calculated by dividing the new sediment yield by the total storage area. The residual amount of material reflects the minimum thickness left in the basin sink.

Step 3:

To derive the amount of eroded Quaternary sediments, we subtract the present day Quaternary thickness extracted from borehole data. For the region along the Alpine front several glaciations resulted in over deepened valleys, and therefore locally, significantly increased Quaternary thicknesses of up to 300 m. However, these values do not represent realistic average thicknesses for the basin. To prepare the final regional erosion contour lines, we added data by hand to adjust for the locally increased values of sediments (Jerz, 1979, 1993; Penck, 1922; Preusser et al., 2010).

Step 4:

For datasets, where errors are published, we have included those. Our results are compared to published erosion data for the western foreland basin (Mazurek et al., 2006), the eastern foreland basin (Genser et al., 2007), and the entire Alpine system (Baran et al., 2014). We find that our estimates within the error range of ≥ 10% are consistent with previous estimates on different time scales.

Table 4-4: Calculation of sediment yield in the NAFB contributed from surrounding catchment areas of the eastern Alps (EA), the Swabian Alb (SA) and the Bohemian Massif (BM).

(A) Time [Ma]	(B) Sediment yield EA [km^3/Ma][3]	(C) Sediment yield EA [km^3/Ma][2,3,5]	(D) Total sediment yield (EA, SA, BM) [km^3/Ma][1,2,5]	(E) Average thickness proximal basins [km][1]	(F) Sediment yield SA, BM [km^3]	(G) Erosion rate Alps[1]
0	20,500	11,254	4,564.17	0.13	251.67	0.125
0.012	-	-	2,164.67	0.63	251.67	0.62
0.024	20,500	11,254	60,971.67	1.77	251.67	1.76
1	15,500	8,350	13,706.67	0.40	251.67	0.39
2	11,000	5,808	13,706.67	0.40	251.67	0.39
3	10,000	5,546	6,806.67	0.20	251.67	0.19
Average	-	-	20,232.92	0.59	251.67	0.58

1: Erosion rate from Hinderer, 2001; 2: Area based on mapping in this study; 3: Kuhlemann et al, 2001, 2002; 4: Erosion rate from Baran, 2012; 5: This study

Column D): Calculation of the sediment yield by adding the catchment areas (EA, SA, BM) and multiplying the total area by the erosion rate (G)

Column E): Calculation of the average thickness by dividing the total area yield (D) by the basin area of 34,500 km^2

Table 4-5: Calculation of residual sediment yield in the NAFB and resulting thicknesses

Time [Ma]	(H) Total sediment yield proximal basin[4, 3] [km]	(I) Erosion rate Alps[3] [km/Ma]	(J) Erosion rate proximal basin[4]	(K) Sediment yield eroded from NAFB[4, 3] [km]	(L) Calculated residual sediment yield[3] [km]	(M) Calculated thickness [km]
0	13,800	0.31	0.1	3,450	1,114.17	0.03
0.012	13,800	0.31	0.10	3,450	18,191.67	0.53
0.024	13,800	0.31	0.10	3,450	57,521.67	1.67
1	10,100	0.23	0.08	2,760	10,946.67	0.32
2	7,000	0.16	0.05	1,725	11,981.67	0.35
3	6,600	0.15	0.05	1,725	5,081.67	0.15
Average	10,850	0.245	0.08	2,760	17,472.92	0.51

1: Erosion rate from Hinderer, 2001; 2: Area based on mapping in this study; 3: Kuhlemann et al, 2001, 2002; 4: Erosion rate from Baran, 2012; 5: This study

Column K): Calculation of the sediment yield eroded from the basin by multiplying the area by the erosion rate (column J)

Column L): The residual is calculated by subtracting the amount of eroded sediment from the total sediment yield (column D)

Column M): Calculation of the total thickness by multiplying the residual sediment yield (column L) by the area of 34,500 km^2

Table 4-6: Calculation of eroded sediment thicknesses in the NAFB based on the observed Quaternary sediment thickness from borehole data

Time [Ma]	(N) Measured average sediment thickness[5] [km]	(O) Measured average sediment thickness along central basin axis[5] [km]	(P) Eroded sediment thickness (minimum)[5] [km]	(Q) Eroded sediment yield (maximum)[5] [km]
0	0.06	0.005	0.028	-0.027
0.012	0.06	0.005	-0.467	-0.522
0.024	0.06	0.005	-1.607	-1.662
1	0.06	0.005	-0.257	-0.312
2	0.06	0.005	-0.287	-0.342
3	0.06	0.005	-0.087	-0.142
Average	0.06	0.005	-0.45	-0.50

1: Erosion rate from Hinderer, 2001; 2: Area based on mapping in this study; 3: Kuhlemann et al, 2001, 2002; 4: Erosion rate from Baran, 2012; 5: This study

Column P): The minimum amount of sediment eroded during the last 3 Ma is calculated from subtracting the calculated residual thickness (column M) from the observed thickness (column N, O, for min and max values). The negative result in column (P, Q) represents the amount of missing Quaternary sediments against the expected thickness from the depositional parameters.

Table 4-7: Long-term uplift rates for the NAFB from backstripping curves, Lemcke (1974)

No.	Site	Eroded thickness [m]	Erosion rate 0-5 Ma [mm/a]	Subsidence 30-5 Ma [m]	Erosion rate 30-5 Ma [mm/a]	Time scale [Ma]	Method	Reference
1	Essertines	2,500	0.5	2,100	-0.08	5/ 25	Backstripping, subsidence analysis and "Resthebung"	Lemcke, 1974
2	Courton	1,600	0.32	2,000	-0.08			
3	Paffnau	1,620	0.32	1,550	-0.06			
4	Lindau	560	0.11	1,700	-0.07			
5	Berlingen	670	0.13	1,420	-0.06			
6	Dingelsdorf	730	0.14	1,150	-0.05			
7	Pfullendorf	870	0.17	620	-0.02			
8	Heimertingen	620	0.12	1,450	-0.06			
9	Scherstetten	660	0.13	1,350	-0.05			
10	Anzing	630	0.13	2,300	-0.09			
11	Gendorf	530	0.11	1,820	-0.07			
12	Füssing	510	0.10	700	-0.03			
13	Schwanenstadt	480	0.10	1,850	-0.07			

Table 4-8: Long-term uplift rates for two caves along the Swabian Alb.

Site	Eroded thickness [m]	Erosion rate [mm/a]	Subsidence 30-5 Ma [m]	Erosion rate 5-30 Ma [mm/a]	Time scale [Ma]	Method	Reference
Sonnenbühl	-	0.013	-	-	9	Time averaged cave level evolution	Strasser, 2009, 2011
Laichingen	-	0.013	-	-			

Table 4-9: Long-term uplift rates for the NAFB and the two sites along the Swabian Alb from this study

Site	Eroded thickness [m]	Erosion rate [mm/a]	Subsidence 30-5 Ma [m]	Erosion rate 5-30 Ma [mm/a]	Time scale [Ma]	Method	Reference
Ravensburg	100	0.03	-	-	3	Quaternary sediment budget	This study; Hüttner, 1969; Hinderer, 2001; Baran, 2012
Kaufbeuren	100	0.03	-	-			
Augsburg	400	0.13	-	-			
Pfaffenhofen a.d.I.	490	0.16	-	-			
Chiem	100	0.03	-	-			
Marktl a.I.	490	0.16	-	-			
Heldenfingen	250	0.05	-	-	17.5	Time averaged coastline uplift	
Burgmagerbein	250	0.03	-	-			

Table 4-10: Short-term uplift rate from depth estimates of bronze age graves in the Tertiary Hills region

No.	Site	Eroded thickness [m]	Erosion rate [mm/a]	Subsidence 30-5 Ma [m]	Erosion rate 5-30 Ma [mm/a]	Time scale [Ka]	Method	Reference
1	Baierbach	1.5	0.21 - 0.25	-	-	6,500 – 7,000	Time averaged erosion rate based on archeological data	Bayerisches Landesamt für Denkmalpflege
2	Reut	1.8	0.26 - 0.28	-	-			

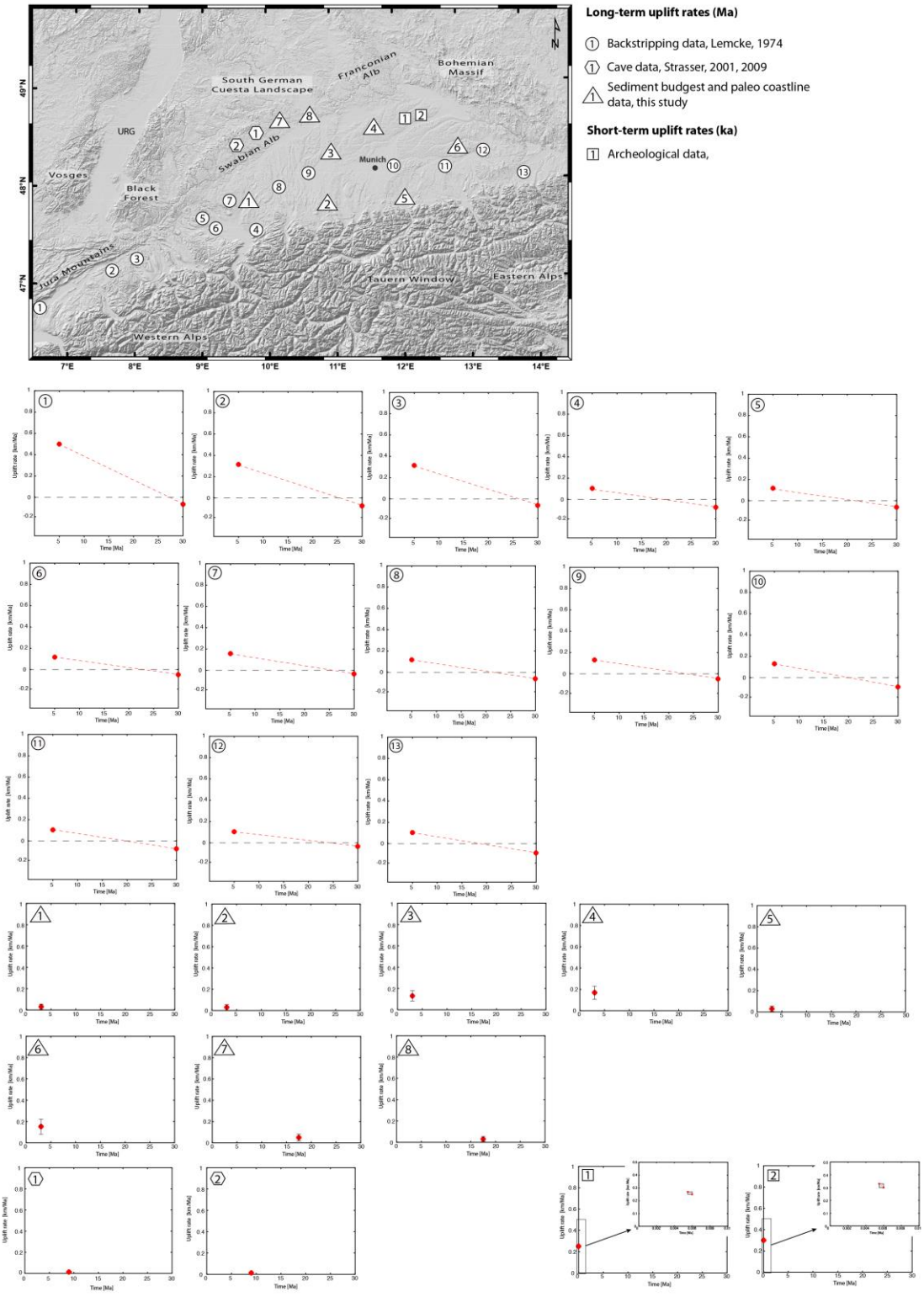

Fig. 4.22: Compilation of erosion rates on long, medium, and short timescales across the NAFB. The DEM inset indicates the locations of the spatial individual datasets. The calculation of Quaternary uplift rates can be followed in tables 4.4 – 4.10.

11.2. Processing of geomorphic directions from valleys in the Tertiary Hills:

A) Calculating the orientation of the line features using the code:

```
360 + math.degrees(math.atan2((!Shape.lastpoint.X! -
!Shape.firstpoint.X!),(!Shape.lastpoint.Y! - !Shape.firstpoint.Y!))) if
math.degrees(math.atan2((!Shape.lastpoint.X! -
!Shape.firstpoint.X!),(!Shape.lastpoint.Y! - !Shape.firstpoint.Y!))) < 0 else
math.degrees(math.atan2((!Shape.lastpoint.X! -
!Shape.firstpoint.X!),(!Shape.lastpoint.Y! - !Shape.firstpoint.Y!)))
```

B) Plotting the vector directions of the lines features with MatLab. Converting the degree values into radians (Trauth et al., 2007):

```
load directions2.txt; % read data
directions2 = pi*directions2/180;
%# data and angular histogram
theta = directions2(:,1)
%x = rand(400,1) .* 2*pi;
rose(theta,36)          %# this does not generate a plot
%# set plot's max radial ticks
%figure
%rMax = 50;
%h = polar(0, rMax);
%delete(h)
%set(gca, 'Nextplot','add')
set(gca,'View',[-90 90],'YDir','reverse');
%# draw patches instead of lines: polar(t,r)
%[x,y] = pol2cart(t,r);
%h = patch(reshape(x,4,[]), reshape(y,4,[]), 'b');
%alpha(h, 0.5)      %# note: this switches to OpenGL renderer
```

11.3. Data repository

Table DR1: List of borehole data derived from the website of Landesamt für Umwelt, Bayern. Extracted on the www.bis.bayern.de website, June 2016 and Ellwanger, 2015 (mbh: mapped by hand).

No	Object-Id	Lat	Long	Thickness (m)	No	Object-Id	Lat	Long	Thickness (m)
1	7141BG015213	48,883921	12,534333	5,0	173	7933BG015018	48,048981	11,205711	4,3
2	7141BG015212	48,86657	12,594731	15,0	174	7833BG015030	48,119744	11,171422	51,0
3	7342BG000704	48,688516	12,736824	6,5	175	7833BG000125	48,14913	11,178589	29,0
4	7343BG000144	48,626085	12,866149	3,0	176	7333BG000190	48,639018	11,170778	6,5
5	7343BG000105	48,605354	12,878015	1,0	177	7233BG000939	48,707146	11,170692	4,1
6	7343BG000121	48,601466	12,9302	3,8	178	7332BG000217	48,640359	11,1028	9,0
7	7443BG000049	48,553822	12,982728	2,5	179	7632BG000001	48,393292	11,05628	9,3
8	7443BG000126	48,544383	12,926059	4,0	180	7832BG015008	48,139385	11,064692	15,3
9	7544BG000153	48,492427	13,035171	7,0	181	7832BG015101	48,101004	11,075935	18,0
10	7544BG000067	48,447101	13,094437	1,0	182	7932BG000016	48,059939	11,082115	1,5
11	7544BG015019	48,402275	13,12083	4,6	183	7932BG015142	48,023671	11,080399	4,5
12	7644BG000144	48,368962	13,127278	2,5	184	7932BG015141	48,035618	11,144557	25,2
13	7644BG000104	48,330455	13,123877	6,4	185	7932BG015152	48,053665	11,143398	12,3
14	7744BG000100	48,291352	13,063195	1,0	186	8032BG015105	47,943105	11,060271	27,5
15	7744BG000106	48,292212	13,127471	4,3	187	8132BG015080	47,897972	11,023149	16,0
16	7744BG000121	48,264351	13,043615	10,0	188	8132BG015423	47,835736	11,036668	28,0
17	7743BG015022	48,213913	12,933762	14,0	189	8132BG015424	47,829225	11,058812	38,0
18	7743BG000080	48,233584	12,945349	10,3	190	8131BG015221	47,804413	10,996199	18,6
19	7842BG015138	48,146914	12,795435	7,8	191	7931BG015035	48,042382	10,972509	56,1
20	7841BG015272	48,135928	12,643611	44,4	192	7831BG000002	48,107137	10,949936	26,0
21	7841BG000014	48,144405	12,600181	43,0	193	7731BG015084	48,294998	10,926247	8,6
22	7841BG015120	48,101204	12,584045	48,5	194	7631BG016473	48,354872	10,927663	9,3
23	7941BG015276	48,093036	12,604344	10,1	195	7631BG015698	48,396369	10,9023	6,3
24	7941BG015275	48,073569	12,566535	52,0	196	7431BG015097	48,520795	10,904188	5,0
25	7941BG015285	48,047755	12,548683	45,0	197	7331BG015054	48,647469	10,872087	9,3
26	7743BG000090	48,265109	12,876577	1,5	198	7530BG015119	48,403928	10,761967	3,5
27	7743BG015171	48,243617	12,881663	5,1	199	7630BG015014	48,305941	10,711412	4,4
28	7742BG000126	48,205383	12,812419	20,4	200	7830BG015021	48,179843	10,760636	11,0

29	7841BG015001	48,103554	12,651207	62,5	201	7830BG015061	48,136386	10,766172	9,3
30	7841BG015144	48,12109	12,628763	44,0	202	7930BG000009	48,085152	10,764713	5,7
31	7841BG000011	48,115704	12,534907	39,0	203	8030BG015099	47,956126	10,743985	13,1
32	7841BG015121	48,120022	12,523341	48,0	204	8030BG015111	47,902871	10,708923	18,2
33	7941BG015377	48,091607	12,65227	38,0	205	8130BG015068	47,839703	10,721197	7,8
34	8236BG015065	47,700039	11,734267	33,7	206	8129BG015061	47,883506	10,65352	28,5
35	8141BG015212	47,832617	12,507977	65,4	207	8129BG015034	47,856005	10,62541	37,6
36	8141BG015226	47,807662	12,599902	22,0	208	8128BG000002	47,813233	10,453749	103,0
37	8241BG015017	47,759254	12,658975	9,0	209	8128BG015037	47,836131	10,414867	15,8
38	8041BG015272	47,921367	12,554862	48,2	210	8028BG015040	47,913967	10,387487	27,3
39	8041BG015283	47,921215	12,5454	50,0	211	8028BG015022	47,978625	10,375428	7,5
40	7940BG000019	48,015383	12,386849	78,7	212	7928BG000016	48,016015	10,379934	8,0
41	7839BG015054	48,134553	12,319708	75,1	213	7928BG015070	48,037369	10,360279	9,0
42	7840BG015118	48,17756	12,384585	8,0	214	7728BG015014	48,209824	10,34204	5,5
43	7840BG015117	48,173433	12,429528	17,3	215	7728BG015006	48,237329	10,370407	4,7
44	7740BG015110	48,207307	12,410302	46,0	216	7627BG000021	48,340611	10,330195	8,4
45	7840BG015111	48,198783	12,350993	13,0	217	7527BG015540	48,423387	10,311549	0,2
46	7741BG000036	48,257333	12,567286	12,7	218	7527BG015176	48,479887	10,260222	8,3
47	7639BG000112	48,329856	12,301512	2,0	219	7527BG015309	48,462773	10,2387	5,5
48	7639BG000081	48,332485	12,268703	1,0	220	7527BG000036	48,443603	10,194604	2,2
49	7639BG000078	48,325148	12,243619	4,0	221	7527BG015389	48,422329	10,167718	9,8
50	7739BG000023	48,266961	12,247438	0,6	222	7526BG000005	48,408734	10,148964	12,4
51	7741BG015050	48,283346	12,569733	13,0	223	7626BG000067	48,366877	10,15862	8,7
52	7640BG000035	48,341557	12,341273	5,0	224	7626BG015095	48,351735	10,145187	9,0
53	7741BG015059	48,269251	12,510531	12,8	225	7726BG015233	48,263247	10,117078	12,4
54	7741BG015010	48,269581	12,611961	11,4	226	7826BG015147	48,173548	10,110512	4,8
55	7641BG000078	48,33947	12,539821	3,2	227	8027BG015305	47,919777	10,203209	20,0
56	7540BG000189	48,411453	12,332003	3,0	228	mbh	48,26899	10,05657	1,0
57	7640BG000040	48,380707	12,357602	7,0	229	mbh	48,23682	10,05591	0,0
58	7641BG000079	48,339185	12,545528	0,2	230	mbh	48,19868	10,06825	20,0
59	7539BG000706	48,457547	12,33108	2,8	231	mbh	48,17182	10,06332	0,0
60	7541BG000075	48,402503	12,501411	3,5	232	mbh	48,14234	10,08718	15,0
61	7540BG000233	48,419196	12,481885	6,2	233	mbh	48,11919	10,06048	0,0

62	7541BG000040	48,416861	12,549691	2,0	234	mbh	48,10006	10,10463	20,0
63	7541BG000071	48,417288	12,505875	1,2	235	mbh	48,07075	10,11099	20,0
64	7541BG000046	48,480851	12,534499	1,0	236	mbh	48,04054	10,10334	20,0
65	7440BG000042	48,524687	12,476285	7,1	237	mbh	47,99535	10,09883	25,0
66	7640BG015050	48,3385	12,450986	2,0	238	mbh	47,94934	10,08084	25,0
67	7639BG000230	48,384807	12,311211	2,2	239	mbh	47,90303	10,09404	20,0
68	7640BG015002	48,335766	12,366014	2,0	240	mbh	47,86470	10,06918	0,0
69	7539BG000600	48,440411	12,30988	2,0	241	mbh	47,81619	10,06323	0,0
70	7240BG000040	48,709278	12,42146	5,8	242	mbh	47,76334	10,06357	20,0
71	7141BG000081	48,823839	12,546601	23,2	243	mbh	47,65642	10,04096	40,0
72	6838BG000420	49,106402	12,082815	7,5	244	mbh	47,65529	10,00711	50,0
73	6937BG000013	49,087351	12,953211	7,6	245	mbh	47,63765	9,95393	50,0
74	8038BG015216	47,986151	12,046766	19,6	246	mbh	47,65963	9,94447	95,0
75	8038BG015011	47,941581	12,014794	21,1	247	mbh	47,68011	9,94413	90,0
76	8038BG015008	47,924703	12,004666	21,2	248	mbh	47,73102	9,94787	15,0
77	8038BG015007	47,899591	12,001705	10,1	249	mbh	47,76106	9,94348	0,0
78	8337BG015005	47,696807	11,956043	17,2	250	mbh	47,78484	9,94603	20,0
79	8038BG015007	47,899871	12,002563	10,1	251	mbh	47,81500	9,98333	50,0
80	7937BG015094	48,075576	11,887894	40,4	252	mbh	47,82082	9,91345	35,0
81	7837BG015003	48,126325	11,878452	35,3	253	mbh	47,86071	9,92618	100,0
82	7837BG015199	48,161661	11,911411	28,6	254	mbh	47,89747	9,91338	20,0
83	7837BG015168	48,146888	11,916475	36,2	255	mbh	47,91866	9,88330	150,0
84	7837BG015004	48,134954	11,844249	37,5	256	mbh	47,92886	9,91748	50,0
85	7837BG015164	48,167823	11,854162	27,2	257	mbh	47,94150	9,94463	100,0
86	7837BG015078	48,195236	11,835365	44,7	258	mbh	47,95796	9,96832	50,0
87	7737BG015001	48,208165	11,878667	18,0	259	mbh	47,97872	9,93467	20,0
88	7737BG015039	48,230039	11,904974	32,1	260	mbh	48,03566	9,89879	0,0
89	7737BG015073	48,274209	11,868582	39,5	261	mbh	48,08773	9,87553	0,0
90	7637BG015067	48,305598	11,906691	13,8	262	mbh	48,15337	9,88377	0,0
91	7537BG000085	48,491574	11,940379	6,6	263	mbh	48,22493	9,86505	0,0
92	7337BG000108	48,609914	11,880512	3,2	264	mbh	48,20667	9,67671	0,0
93	7337BG000117	48,630624	11,865664	0,6	265	mbh	48,12366	9,70548	20,0
94	7337BG000078	48,664089	11,957717	2,0	266	mbh	48,03980	9,71570	50,0

95	7237BG000192	48,70022	11,89373	0,4	267	mbh	48,00549	9,72019	155,0
96	7237BG015017	48,7706	11,965227	2,0	268	mbh	47,97377	9,76654	170,0
97	7137BG000036	48,866844	11,970377	13,5	269	mbh	47,85346	9,81428	170,0
98	7037BG000111	48,922314	11,891584	8,0	270	mbh	47,97651	9,71057	5,0
99	7037BG015043	48,980483	11,977243	1,0	271	mbh	47,93157	9,73971	110,0
100	6938BG000404	49,022075	12,047753	8,5	272	mbh	47,92830	9,80129	70,0
101	6938BG015028	49,031389	12,049341	4,2	273	mbh	47,92010	9,81675	0,0
102	6938BG015759	49,061177	12,029343	1,7	274	mbh	47,91849	9,84222	50,0
103	6938BG015757	49,073015	12,020202	3,1	275	mbh	47,88278	9,70079	160,0
104	6937BG000027	49,053134	11,942954	17,8	276	mbh	47,80962	9,74999	2,0
105	6937BG000010	49,03543	11,902077	7,5	277	mbh	47,77630	9,74810	105,0
106	6937BG000017	49,022883	11,922054	2,7	278	mbh	47,74939	9,71312	180,0
107	7037BG000130	48,909377	11,891627	6,6	279	mbh	47,70766	9,68504	30,0
108	7037BG000074	48,924578	11,857767	5,9	280	mbh	47,69058	9,67494	45,0
109	7137BG000020	48,831806	11,88343	5,0	281	mbh	47,65915	9,67524	110,0
110	7137BG000118	48,814091	11,898923		282	mbh	47,60041	9,62309	120,0
111	7237BG000024	48,794559	11,872444	1,4	283	mbh	47,61739	9,56133	0,0
112	7237BG000013	48,76529	11,893086	6,1	284	mbh	47,69015	9,57903	0,0
113	7237BG000216	48,755134	11,849184	4,5	285	mbh	47,66304	9,57380	40,0
114	7237BG000127	48,729174	11,875534	2,2	286	mbh	47,80729	9,66444	0,0
115	7337BG000110	48,69695	11,856737	3,5	287	mbh	47,87160	9,87330	0,0
116	7337BG000068	48,639586	11,864719	4,0	288	mbh	47,72803	9,77563	0,0
117	7337BG000109	48,625781	11,872873	3,9	289	mbh	47,80713	9,83547	40,0
118	7337BG000046	48,601125	11,861458	4,9	290	mbh	47,90399	9,65576	100,0
119	7437BG000078	48,571253	11,865749	0,3	291	mbh	47,75553	9,54798	20,0
120	7437BG000056	48,551891	11,862402	1,3	292	mbh	47,68685	9,46688	60,0
121	7537BG000685	48,456266	11,875019	3,9	293	mbh	47,89314	9,54589	20,0
122	7537BG000541	48,442404	11,858068	3,0	294	mbh	47,96638	9,56297	50,0
123	7637BG015631	48,386167	11,85605	8,5	295	mbh	47,94342	9,48194	85,0
124	7637BG015652	48,374139	11,849442	9,0	296	mbh	47,91880	9,44701	0,0
125	7636BG017013	48,362278	11,828499	13,3	297	mbh	48,00236	9,38175	0,0
126	7636BG016476	48,334506	11,821718	7,5	298	mbh	47,99839	9,26751	20,0
127	7637BG015356	48,313668	11,860256	9,7	299	mbh	47,91628	9,35137	10,0

128	7737BG000001	48,286318	11,865749	16,0	300	mbh	47,79830	9,31595	30,0
129	7836BG015017	48,190336	11,789618	20,2	301	mbh	47,79645	9,44525	30,0
130	7836BG015007	48,165783	11,790648	23,4	302	mbh	47,70742	9,29494	0,0
131	7936BG000033	48,088707	11,794596	33,4	303	mbh	47,78521	9,21132	0,0
132	7936BG000047	48,063266	11,799145	37,7	304	mbh	47,76381	9,38495	0,0
133	7936BG015163	48,03934	11,760006	38,1	305	mbh	47,79338	9,49751	0,0
134	7936BG015150	47,999727	11,773653	42,2	306	mbh	47,99615	9,50797	0,0
135	8036BG015150	47,986323	11,753612	48,5	307	mbh	47,81612	9,52247	15,0
136	8036BG015084	47,908913	11,677608	81,7	308	mbh	47,83597	9,55307	0,0
137	8136BG015020	47,894059	11,676235	64,2	309	mbh	47,97094	9,18442	0,0
138	8136BG015018	47,87161	11,686277	83,8	310	mbh	47,91096	9,18279	20,0
139	8035BG000008	47,9629	11,5341	77,5	311	mbh	47,79726	9,10325	45,0
140	7935BG015440	48,000683	11,549807	52,4	312	mbh	47,70773	9,12635	110,0
141	7935BG015438	48,029395	11,553669	34,1	313	mbh	47,71342	9,14471	70,0
142	7735BG015373	48,245817	11,550837	21,5	314	mbh	47,72255	8,94505	165,0
143	7635BG015001	48,321866	11,530108	7,0	315	mbh	47,65105	9,14736	75,0
144	7535BG000233	48,425063	11,519809	3,7	316	mbh	47,89015	8,98876	20,0
145	7434BG000518	48,515658	11,478953	1,0	317	mbh	47,84538	8,93785	45,0
146	7334BG000525	48,666187	11,464148	12,0	318	mbh	47,82242	8,82971	65,0
147	7234BG001591	48,715763	11,461358	10,5	319	mbh	47,94725	8,90371	0,0
148	7234BG000607	48,764038	11,458912	4,7	320	mbh	47,96681	9,01639	0,0
149	7234BG000821	48,773945	11,460071	2,7	321	mbh	48,06230	9,21813	0,0
150	7234BG000511	48,784607	11,3657	9,1	322	mbh	48,04906	9,15914	65,0
151	7234BG000736	48,719982	11,353426	7,5	323	mbh	47,92636	9,32098	65,0
152	7333BG000244	48,6961	11,314631	9,0	324	mbh	47,85183	9,40257	70,0
153	7333BG000205	48,650531	11,329994	13,5	325	mbh	47,91269	8,72885	0,0
154	7433BG000158	48,521989	11,296778	8,6	326	mbh	47,90061	8,94557	0,0
155	7733BG015019	48,231011	11,268325	10,2	327	mbh	47,73230	8,75660	105,0
156	7733BG015194	48,200614	11,27665	20,0	328	mbh	47,69700	8,72503	100,0
157	7833BG015119	48,193148	11,250515	25,0	329	mbh	47,76202	8,88498	25,0
158	7833BG015523	48,176631	11,25582	15,5	330	mbh	47,74873	9,05374	0,0
159	7833BG015009	48,1277	11,277637	23,4	331	mbh	48,04648	9,42539	0,0
160	7833BG015027	48,108389	11,277809	29,8	332	mbh	48,08168	9,63741	130,0

161	7933BG015016	48,092462	11,286821	24,0	333	mbh	48,05875	9,65204	60,0
162	7933BG015001	48,068092	11,245022	50,5	334	mbh	48,07421	9,69415	20,0
163	7933BG015112	48,029182	11,263046	32,0	335	mbh	48,01992	9,51672	40,0
164	8133BG000007	47,862742	11,297722	25,3	336	mbh	47,73261	8,68815	70,0
165	8233BG015232	47,747561	11,264248	60,0	337	mbh	47,62751	9,81852	20,0
166	8333BG000021	47,671787	11,258411	57,4	338	mbh	47,61438	9,85528	60,0
167	8233BG015078	47,759254	11,216912	79,0	339	mbh	47,60919	9,66932	110,0
168	8133BG015034	47,862915	11,218243	8,4	340	mbh	47,88440	9,84804	140,0
169	8033BG015092	47,903015	11,253047	22,2	341	mbh	47,95671	9,71738	170,0
170	8033BG015093	47,947676	11,255407	22,0	342	mbh	47,78762	9,89627	10,0
171	8033BG015089	47,966816	11,221161	73,6	343	mbh	48,26911	9,63136	40,0
172	8033BG015114	47,988467	11,215947	50,6	344	mbh	48,29861	9,76997	0,0
					345	mbh	48,31250	9,97894	0,0
					346	mbh	47,93633	9,11451	0,0

Chapter 5

Conclusions and Outlook

The focus of this thesis was to find evidence for recent vertical tectonic activity and basin potential inversion in the Northern Alpine Foreland Basin (NAFB). This is addressed by studying the landscape evolution across the NAFB.

In order to analyze the geomorphology, the availability of new high-resolution digital elevation data from the TanDEM-X mission (DLR) has improved remote sensing mapping. The data also enabled the detection of surface lineaments and geomorphic features in greater detail. Geomorphic data linked with subsurface information show that the NAFB landscape has been shaped by local-scale tectonics and lithospheric-scale uplift. Additional climatic drivers are mainly responsible for a secondary overprint. Especially the local occurrence of tectono-geomorphic features contradicts a simple basin wide climatic driver.

The young active deformation detected in the low strain NAFB appears to be higher in the eastern portion and along its northern margin. In the northeastern basin, the Tertiary Hills region, we found numerous geomorphic features, which formed by a combination of tectonic and climatically-induced processes. In this area, surface lineaments match the geometry of basement faults, and the subsurface offsets we detected at the study sites *Paindlkofen* and *Tunzenberg* can be linked to inferred faults by the similar geometry. Therefore, the dominating mechanism shaping the late Quaternary landscape evolution in the Tertiary Hills is likely tectonics.

Further, along the basin's marginal area at the boundary to the Swabian Alb, remnants of a mid-Miocene cliff can be used to characterize a wider coastal area. This zone has recorded local displacement bound to the individual history of coastal outcrops, but also underlying process, like dynamic topography. A combination of these mechanisms has uplifted the Swabian Alb region since the mid-Miocene. Most of this late Miocene and Pliocene vertical motion is likely caused by a northward migration of the NAFB forebulge, supplemented by the additional uniform uplift signal on a lithospheric scale.

In summary, the present-day erosional relief of the NAFB is mostly controlled by regional-scale uplift, which has been set up during the Pliocene. Further, the distribution of Quaternary sediments implies an ongoing basin inversion that is most

prominent in the eastern portion of the basin. Here, also geomorphic indicators like river orientations suggest a continuous shift of the region from subsidence, controlled by the Eurasia-Adriatic convergence, to uplift. This inversion is likely a result of ceased convergence potentially supported by the unflexing of the Eurasian lithosphere.

In addition, the identified Quaternary erosion in the NAFB, whose pattern depicts a basin axis parallel shape, is likely caused by the ongoing inversion, instead of simple fluvial transport. Most likely the uplift continued beyond the Pliocene and is still ongoing today at lower rates. Therefore, the NAFB is suggested to be an active basin system.

In order to quantify the contributions from the individual processes analyzed in this thesis, additional far-field studies are required. Further research in this direction will help to detect potential contemporaneous events of erosion and uplift outside the NAFB, which could be related to mantle processes. Regarding the basin's earthquake history, paleoseismic trenching would significantly improve the data basis in order to better understand the recurrence intervals of large events. Clearly more mapping, synthesis and seismic campaigns are needed – unless industry-based data, recently compiled in GeoMol (2015), provide further information.

Appendix

Installation of the New Geodetic Southeast Iran – Makran Backbone Array (SIMBAR) – Concepts, Challenges and First Results

Authors
Markus Hoffmann[1]*, Amir M. Abolghasem[1], Abbas Bahroudi[2],
Mohammad A. Sharifi[3], Anke M. Friedrich[1]

Affiliations
1. Department of Earth and Environmental Sciences, Geology, Ludwig-Maximilians University of Munich, Germany, 2. Mining Engineering Department, University of Tehran, Iran, 3. Department of Geomatics Engineering, University of Tehran, Iran.

*Corresponding author
(e-mail: ma.hoffmann@lmu.de)

1. Abstract

The Makran subduction zone defines a 1000 km-long, active segment of the Arabia – Eurasia plate boundary. Eastern Makran experienced the 1945 M_w 8.1 Balochistan earthquake with up to 4,000 casualities reported from India, Pakistan and Iran. In contrast, western Makran has been fairly quiescent over the past centuries. Recent GPS and seismic data imply a serious seismic hazard potential along this portion of the subduction zone. In particular, since the recent lessons learned from the 2004 Sumatra and the 2011 Tohoku-Fukushima earthquakes, where apparently silent segments of these subduction zones broke, resulting in devastating earthquakes and substantial economic losses. Therefore, even a currently silent subduction zone may be subject to contemporary strain accumulation, depending on the locking rate of the boundary interface. A well-distributed GPS network and elastic block models provide a first-order image of the strain field and its spatial and temporal variations. However, the existing regional GPS network is not dense and widespread enough to monitor distributed and transient deformation across the Makran subduction zone. A collaborative research project of LMU Munich Geology and University of Tehran

Geomatics Institute has formed in early 2014 to improve the monitoring of the W-Makran subduction zone by installing the first GPS backbone array.

We have run a GPS site selection in November 2015, including a geologic field mapping campaign and a telemetric survey. Between April and June 2016, seven new permanent GPS stations have been installed and brought online in the districts of Kerman, Hormozgan and Sistan-Balochistan, forming the new *Southeast-Iran-Makran Backbone-Array (**SIMBAR**)*. Two additional stations are currently under construction. A specialized design has been developed individually for all sites. The site selection and monumentation were following UNAVCO and Munich Geology standards. The final sites chosen are school buildings providing excellent security and monument stability at low costs. The team of authors of this paper has carried out the complete installation of all sites. Stations are in full operating mode since June 20th, 2016 recording dynamic positions at 1 Hz. In the second phase of this project we will further expand and densify the network including campaign and semi-permanent observations. In addition, we plan to include substantial geology field mapping, gravity field measurements, and tiltmetry in future. A combination of these disciplines will enable us to analyze strain accumulation and the potential of a strong earthquake in the near future.

2. Introduction

The subaerial part of the Makran subduction zone is a 1000 km long and 250 km wide coastal strip covering parts of Iran and Pakistan along the Gulf of Oman. Here, the Oman Sea subducts underneath continental Eurasia since the Early Cretaceous (Berberian and King, 1981) forming the world's largest accretionary prism. In comparison to global convergent plate boundaries, at Makran an incipient continent-continent collision can be observed today, similar to the Alps 35 Ma ago, or the Himalaya 20 Ma ago.

The N-13° directed shortening across the Arabia-Eurasia collision is mainly accommodated by the Makran subduction zone with about 2 cm/a and the Kopeh-Dag fault belt with about 0.7 cm/a (Vernant et al., 2004). The recent global plate velocity model REVEL indicates a NNE-ward motion of the Arabic plate of 2.6 cm/a at the latitude of southern Iran (Sella et al., 2002). Over the past 3 Ma, an even higher convergence of ~ 4 cm/a has been observed (DeMets et al., 1990; Kopp et al., 2000). The horizontal motions on geologic and geodetic timescales indicate the active nature of the Makran subduction zone and adjacent continental Iran and Pakistan.

Seismically, the western portion of the plate boundary, between the straight of Hormoz and the bay of Gwadar, has been fairly quiescence. One large historic event in the year 1483 A.D. is documented. However, the epicenter and the related fault system remain unknown (Byrne and Sykes, 1992). The hazardous nature of the eastern half of Markan (Pakistan), from the bay of Gwadar to Karatschi is mostly associated with 4 major earthquakes in 1765, M_S VIII; 1851 and 1865, M_S VII-VIII and 1945, M_W. 8.1 (Quittenmeyer and Jacob, 1979).

In order to understand the apparent silence of western Makran, new regional kinematic models based on new permanent GPS data are desired. With this data, current plate motion and distributed deformation from shortening on upper crustal structures can be analyzed.

Important steps when installing a new permanent geodetic network in infrastructural and political challenging areas are (1) selecting a proper location and designing an adequate monument in order to serve for the scientific aim, (2) ensuring the safety and stability of each site to record suitable data, (3) acquiring all necessary permissions and (4) planning of logistics.

The first phase of our project has started with preliminary defining locations for the anticipated eight new antennas. In order to monitor deformation across the active Makran Subduction zone, GPS stations have to be distributed between the subduction front and the adjacent stable continent to allow near- and far-field observations. Therefore, we selected eight future sites across the districts of Kerman, Hormozgan and Sistan-Balochistan in SE-Iran (Fig. A.1).

With our new backbone array we will gain a better understanding of the Makran subduction zone and the associated hazard potential. The new high-resolution monitoring of shortening rates across the subduction zone will significantly improve the analysis of current strain accumulation. On the first order the strain accumulation is based on a conventional model assuming a locked upper plate interface and continuous slip at the long-term convergence rate at depth (Savage, 1983). From the horizontal GPS motion the direction of maximum contraction and the min. and max. principal strain rate are calculated (Murray, 2000). Besides the long-term geologic record, monitoring and understanding horizontal GPS velocity fields is essential in seismic hazard risk analyses. Previous authors have indicated a possible segmentation of the Makran subduction zone (Barnhart et al., 2014; Byrne and Sykes, 1992; Kukowski et al., 2000). However, these constraints are limited to rupture plane estimates from historic earthquake magnitudes and upper crustal faults, which are believed to separate the subducting plate. The size and dip of one or more rupture surfaces of the subduction interface have to be studied in more detail.

In the past centuries, the Makran has been a sparsely populated, remote area. Since the last two decades, several urban areas have evolved. The city of Chabahar in Iran with its free trade zone is one of the fastest growing urban areas in Iran with about 80,000 residents. The city recently received several millions of dollars of investments and represents the main port connecting Iran to trade partners such as India and U.A.E. This emphasizes the significance of a comprehensive hazard analysis for this costal region based on new data.

3. Methods

3.1. Site Selection

The thorough investigation of future sites for permanent GPS stations is one of the key tasks during the installation of geodetic backbone arrays. The quality of recorded position data depends significantly on the stability of the monument and the knowledge of local error sources e.g. faults, joints, soft sediments, subsurface structures and infrastructural limitations as well as signal obstacles causing multipath. For our new SE-Iran permanent geodetic network we have visited 13 potential antenna locations in November and December 2015, including one possible campaign site (Fig. A.1). These target locations, mainly school buildings, are documented and verified in table A.11. Our field-based recon-survey included assessment of local geology, building quality, urban infrastructure, general site safety, support by landowners and general logistics.

Prior to the field campaign, the sites had been selected based on (1) existing GPS horizontal velocity gradients published for the area to verify the geodetic significance and (2) a remote sensing study according to UNAVCO standards to investigate the technical suitability (Tab. A.11). Finally, we successfully selected seven sites suitable for the installation of permanent GPS antennas within SIMBAR (Fig. A.1).

3.2. Permissions

The installation of specialized radio transmitter equipment in official state buildings such as schools is strongly tied to permissions from Iranian governmental administration. This process is usually time consuming and was therefore started immediately after the final sites had been identified. The research group from the University of Tehran has contacted the heads of school administration for the districts of Kerman, Hormuzgan and Sistan-Balochestan, and permissions have been issued for all sites. To ensure the uninterrupted data transfer, additional telephone lines had to be requested and installed.

3.3. Installation of GPS stations

A team of scientists and local collaborators has carried out the installations in the field. Three, several-weeks-long trips were necessary to finish the first set of the array including the sites BDJA, ZRBD, BERI and IRNS (Tab. A.11). Operations in general benefitted from the support of local workers and companies engaged with lightning protections and outside cabling. All sites have been equipped with a lightning protection. The system consists of a catcher pole at the roof in a distance of 3 m – 4 m from the antenna. Height of the pole is 3 m. The antenna pole is grounded with a wire connection. The grounding is carried out as an underground contact in ~ 2.5 m depth at the base of the building.

3.4. Monument design

The most suitable monument type for the installation on building rooftops turned out to be a modified concrete-pin type (Fig. A.2). The monuments are constructed of a stainless steel pole, 25 cm long and 2.5 cm in diameter with a 0.4 inch standard thread and six rills in the lower half, three vertical rills in 120° offset and a drill hole with 4 mm diameter in the lower 5 cm of the pole (Fig. A.4). The rills are 5 mm deep to maximize the contact surface between the steel pole and the Hilti-Epoxy® used for cementation. This ensures strong mechanical coupling inside the borehole. The pole is installed in a drill hole, 28 cm deep and 2.8 cm wide. First, the hole is drilled vertical with a Hilti TE 6-A36® power drill. Subsequently, the hole is filled with Hilti-Epoxy® to ~ 85% to stimulate outflow at the top and ensure filling of small side holes from the surrounding bricks. The pole is inserted in the hole while the vertical orientation is constantly checked with a level temporary attached to the pole. The Epoxy hardens after ~ 7 min under prevailing temperature conditions of > 45° C and > 90 % humidity. The antenna pole has been kept leveled while inserting into the liquid Epoxy. A potential later deviation from the vertical is corrected by installing the adjustable SECO 2072-33® monument mount.

3.5. Error sources and data quality

Stabilizing a geodetic monument is a general challenge researchers face when carrying out measurements at permanent GPS sites (e.g., Langbein, 1995; Wyatt et al., 1989). There are three main sources of errors: (1) a time independent caused by the technique of measurement, (2) a time depending from seasonal variations affecting also the construction material used and (3) a long-term monument-related error due to the ground specifications, resulting in a random-monument-walk described with the Brownian Motion (Langbein, 1995). In order to filter the data from all known error sources, the monument design and the local conditions have to be described and recorded with the highest possible accuracy. The common, short-term error source from bidirectional shear forces for single pole monuments can simply be described by

$$\gamma_{xy} = \gamma_{yx} = \frac{\partial v}{\partial x} + \frac{\partial u}{\partial y} \quad (1)$$

Where x, y are the initial object length, u, v are the deformations in x-, y-direction and γ is the dimensionless shear (Tipler, 2003). For the *SIBA* sites this effect mainly appears during strong wind with velocities of > 60 km/h which has an influence on the stability of the choke ring antenna, especially because of its own weight of about 8.2 kg, plus the 2.3 kg weight of the adjustable monument and the large working surface of the radome (0.64 m^2).

Another common error source is the thermal length expansion of the stainless steel pole, simply be described as:

$$\Delta L = L0\ \alpha\ (T1 - T0) \quad (2)$$

Where ΔL is the change of the object length, $L0$ is the initial length of the object, α is the specific thermal expansion coefficient, $T0$ is the initial temperature and $T1$ is the final temperature (Tipler, 2003). Depending on the steel alloy, the variation in length can be on the order of > 1.0 mm. The local, average daily temperatures (shade) range from 25° C in winter (October to March) up to > 55°C in summer (May to September), while night temperatures are below 30° C and 35° C, respectively. The

coastal stations on average experience lower temperatures with about 16° C during winter and about 45° C in summer.

4. The SIMBAR GPS Network

Seven operating permanent GPS sites comprise the base array of the SIMBAR network, spanning about 1,200 km from the Strait of Hormuz region to the eastern side of the Sistan Suture Zone near the Iran-Afghanistan border (Fig. A.1). Another four sites are under construction at the moment (December 2016). All sites are installed and equipped with similar specifications. The sites profit from excellent sky view and a general low level of atmospheric water vapor. They are based on short, steel-pole concrete monuments and each site has a grounded lightning protection. Data are transferred three times a day in 50 MB chunks via direct landline connection by push-to-FTP. With the exception of the site BDJA all sites are mounted on school buildings under the consideration of site safety.

The previous investigation of local buildings and infrastructure revealed that school buildings are the most reliable and best accessible sites in SE-Iran for our purposes. They are mainly made of steel-reinforced brick walls with flat rooftops and monuments reaching up to 2 m depth. Most schools have been build by the Iranian navy in the 1980s to 1990s. The only exception is the station BDJA that is located on the property of a weather observation facility. At this site, we are using a two meter high concrete pillar. One important issue to consider is the site safety. Remote stations are a likely subject to vandalism and thievery, especially in the poor regions of SE-Iran. The installation of remote sites has therefore been ruled out for the first phase of the project. All selected school buildings are protected with up to four meter high walls and full time present janitors or technical staff being. The antennas are not visible from the surrounding streets and students have no access to the sites.

The antennas are installed at or close to stabilized corners at the rooftop. Stability is increased since the corners are supported with a column underneath (Fig. A.3). The utility housing mounted inside the buildings, is made of a rugged metal box containing receiver, backup batteries and an Ethernet connection via landline (Fig. A.2). The antenna cables are stringed on the walls wrapped in a special protection plastic tube. All permanent stations are equipped with Leica® AR25 and AR20 choke-

ring antennas mounted on a SECO 2072-33® adjustable tilt monument mount. Receivers are Leica® GRX 1200+ and GR10 with dual power supply including a specialized emergency lithium battery in automatic charge mode. A direct telephone/ internet connection realizes the data transfer. Data are transmitted to the University of Tehran in eight-hour intervals. The network build up was carried out in two main steps: Preparation phase from December 2015 until February 2016 and technical installation from May to June 2016.

4.1. Site Bandar-e-Jask (BDJA)

The site BDJA is located in the town of Jask on the western end of the Iranian Oman Sea coast, east of the Zendan-Minab-Fault system (Fig. A.1). This strike-slip system defines the transition between the Arabia – Eurasia subduction along the Makran and the Arabia – Eurasia collision at the Zagros orogenic belt. The local geology is composed of Quaternary marine beach rock terraces covered with reworked fine-grained sandstones and marls. The site is equipped with a Leica AR25 choke ring antenna installed on a two meter high concrete pillar. It is located on the property of the local weather station giving excellent security. Previously published velocity vectors from the National Cartographic Center of Iran (NCC) suggest a northward trend of the area at about 14.8 mm/a (Vernant et al., 2004). Given a motion rate of this magnitude, we expect minor influence from local instabilities relating back to the relative soft ground composition covering the beach terraces. However, data analyses of the first baseline results are required to confirm this assumption.

4.2. Site Zarabad (ZRBD)

The site ZRBD is located about 15 km landward from the Oman Sea coast half along the way between Jask and Chabahar (Fig. A.1). Zarabad is sitting on several tens of meters thick older wash deposits of Holocene age. They consist of silt and clay eroded from Flysch deposits exposed along the cost. The AR25 GNSS antenna is installed on the roof of a single-story school building, inside a protected schoolyard ensuring the site security. The Leica GRX receiver records the position data. For this part of the subduction zone, no permanent, semi-permanent or campaign velocities have been published before. The relative position of ZRBD will provide new data to identify the

gradient between the fast moving western end (at BDJA) and the velocity half as much at the eastern branch of the Iranian part of Makran at NCC site CHBR.

4.3. Site Beris (BERI)

The station BERI is situated in the central part of the Markran subduction zone ~ 50 km from the Iran-Pakistan border and ~ 60 km east of the harbor city of Chabahar. The town is build on Quaternary marine beach rock terraces covered with reworked fine grained sandstones and marls. The AR25 GNSS antenna is mounted on the roof of a single-story school building in the center of Beris. The surrounding schoolyard is well protected by a 3 m high wall. The nearest published velocity vector of about 8 mm/a comes from a permanent NCC site at Chabahar ~ 60 west of Beris (Vernant et al., 2004).

4.4. Site Iranshar (IRNS)

The site IRNS is located on the eastern end of the Jaz-Murian backarc basin, a part of the inner Makran sequence. The location can be found 340 km land inward from the active Makran subduction front. Also the southeastern most extend of the proposed Lut block and its southeastern bounding fault, the Daman fault, are located at the latitude of Iranshar. The Saravan thrust systems is located east of the site (Fig. A.1). The town is build on Quaternary basin fill composed of reworked fine-grained sandstones and marls. The GNSS antenna, model AR25, is mounted on the roof of a three-story school building (Fig. 5) at the northeastern end of the city. The surrounding schoolyard is well protected by a 2.5 m high wall.

5. Discussion and Outlook

With the installation of the SIMBAR array, the first step towards monitoring active, distributed deformation at the Makran subduction zone has been taken. Additional new GPS data will improve the understanding of ongoing deformation along the plate interface and the associated hazard potential. In order to accomplish this goal, the technical implementation of our new geodetic network provides the fundamental base for data of scientific quality according to UNAVCO standards.

The monument design has been developed taking the main time dependent and time independent error sources into account, and minimizing them (Langbein, 1995). After collecting several reports from scientists and local authorities in Iran, the installation of remote stations using, e.g., SDBM monuments similar to the LMU Geology site at Brac (BRAC) (Croatia) was not an option. The risk of thievery has been rated as too high. School buildings are the adequate alternative.

The direct monument anchor depth is limited because of the location at building rooftops. The indirect monument stability is provided by depth of the building foundation of up to 2 m and the area of the foundation exceeding 100 m^2. This will level out small instabilities. However, signal errors and disturbances due to internal deformation of the building, such as small cracks and localized subsidence, cannot be ruled out. The initial documentation of the buildings and the maintenance reports from local people in charge does still provide a measure to track building related errors. For future monitoring, we will install additional survey points to track those with terrestrial laser scanner and camera-based photogrammetry methods. The estimated reliability of the horizontal velocity data recorded relate to the previously expected velocities. In contrast to permanent networks like BARGEN (Basin and Range Geodetic Network, USA), where rates on the order of < (2.0 ±0.25) mm/a on average are observed (Davis et al., 2003), the velocities across the Makran exceed (10.0 ± 1.0) mm/a (Vernant et al., 2004). In both cases the uncertainty falls within the 10 % – 15 % range. Even in case of enhanced disturbance by the foundation, the overall results persist.

The occurrence of possible large-scale error sources, like local subsidence and heavy meteorological events, have been addressed by our geological study and the continuous weather and atmospheric monitoring carried out by the meteorological service of Iran. Especially at site IRNS, substantial groundwater extraction by farmers

has already caused local subsidence in the town. Therefore, we expect to identify this signal of vertical motion in our data. The sites SIRK, BDJA, ZRBD, BERI and QUES are built on medium consolidated coastal marine terraces and clay rich wash sediments. A monotonous seasonal effect is not expected, since the region does not experience frequent precipitation. Sporadic thunderstorm events resulting in large flash floods are the main weather related disturbance leading to swelling of clay minerals. With respect to such weather events, we expect to recognize vertical effects in the data. The individual amplitude of swelling and shrinking at each site can therefore shed light on sediment composition, thickness and local aquifer structures. This will later improve our correction algorithms. Finally, during the data processing, using the software package GAMIT (King and Bock, 1999), we will apply necessary filters and corrections to address the above mentioned uncertainties.

6. Conclusions

We have developed the SIMBAR network to improve studies on active deformation of the Makran subduction zone and the adjacent intracontinent. Now seven new permanent GNSS stations are operating in southeast Iran. The geometric distribution of the stations enables us to record transient deformation from the Makran to the continental interior up to the latitude of Zabol (Fig. A.1). The results from our site selection campaign revealed the suitability of school buildings as prime locations for the GNSS antennas taking all boundary conditions into account. The new design for the stainless steel pole concrete monuments is simple to install and provides enhanced stability for the heavy equipment with choke ring antennas and adjustable mounts, with 10.5 kg in total. The simple concept also facilitates the application of error corrections. The concept of a site installation, practically involving an entire building, is not among the common workflows in permanent geodetic arrays. Our results document this specialized backbone array installation for the first time.

Even though the permission procedures for technical installations and additional data communication are complex, we were able to install all anticipated sites. Our approach provides a new workflow and conceptional approach to install permanent geodetic networks in regions with significantly restricted access and very limited infrastructural conditions.

7. Acknowledgements

The authors acknowledge funding from the University of Tehran, Research Institute of Geotechnical Engineering, awarded to MAS and the Helmholtz Alliance Project - HGF, Remote sensing and Earth System Dynamics, WPG9 – Geological context of tectonically active but seismically inactive regions, awarded to AMF.

8. References

Barnhart, W. D., Hayes, G. P., Samsonov, S. V., Fielding, E. J., and Seidman, L. E., 2014, Breaking the oceanic lithosphere of a subducting slab: The 2013 Khash, Iran earthquake: Geophysical Research Letters, v. 41, no. 1, p. 32-36.

Berberian, M., and King, G. C. P., 1981, Towards a paleogeography and tectonic evolution of Iran: Canadian Journal of Earth Science, v. 18, p. 210-265.

Byrne, D. E., and Sykes, L. R., 1992, Great Thrust Earthquakes and Aseismic Slip Along the Plate Boundary of the Makran Subduction Zone: Journal of Geophysical Research, v. 97, no. B1, p. 449-478.

Davis, J. L., Bennett, R. A., and Wernicke, B. P., 2003, Assessment of GPS velocity accuracy for the Basin and Range Geodetic Network (BARGEN): Geophysical Research Letters, v. 30, no. 7.

DeMets, C., Gordon, R. G., Argus, D. F., and Stein, S., 1990, Current plate motions: Geophysical Journal International, v. 101, p. 425-478.

Ide, S., Baltay, A., and Beroza, G. C., 2011, Shallow dynamic overshoot and energetic deep rupture in the 2011 Mw 9.0 Tohoku-Oki earthquake: Science, v. 332, no. 6036, p. 1426-1429.

King, R. W., and Bock, Y., 1999, Documentation for the GAMIT GPS analysis software: Mass. Inst. of Technol., Cambridge Mass.

Kopp, C., Fruehn, J., Flueh, E. R., Reichert, C., Kukowski, N., Bialas, J., and Klaeschen, D., 2000, Structure of the Makran subduction zone from wide-angle and reflection seismic data: Tectonophysics, v. 329, p. 171-191.

Kukowski, N., Schillhorn, T., Flueh, E. R., and Huhn, K., 2000, Newly identified strike-slip plate boundary in the notheastern Arabian Sea: Geology, v. 28, no. 4, p. 355-358.

Langbein, J. W., Frank; Johnson, Hadley Hamann, Duane; Zimmer, Paul, 1995, Improved stability of a deeply anchored geodetic monument for deformation monitoring: Geophysical Research Letters, v. 22, no. 24, p. 3533-3536.

Murray, M. H., Lisowski, M., 2000, Strain accumulation along the Cascadia subduction zone: Geophysical Research Letters, v. 27, no. 22.

Quittenmeyer, R. C., and Jacob, K. H., 1979, Historical and Modern Seismicity of Pakistan, Afghanistan, Northwestern India, and Southeastern Iran: Bulletin of the Seismological Society of America, v. 69, no. 3, p. 773-823.

Savage, J. C., 1983, A dislocation model of strain accumulation and release at a subduction zone: Journal of Geophysical Research, v. 88, no. B6, p. 4984 - 4996.

Sella, G. F., Dixon, T. H., and Mao, A., 2002, REVEL: A model for Recent plate velocities from space geodesy: Journal of Geophysical Research: Solid Earth, v. 107, no. B4, p. ETG 11-11-ETG 11-30.

Tipler, P. A., Mosca, G. P., 2003, Physics for scientists and engineers, W. H. Freeman.

Vernant, P., Nilforoushan, F., Hatzfeld, D., Abbassi, M. R., Vigny, C., Masson, F., Nankali, H., Martinod, J., Ashtiani, A., Bayer, R., Tavakoli, F., and Chéry, J., 2004, Present-day crustal deformation and plate kinematics in the Middle East constrained by GPS measurements in Iran and northern Oman: Geophysical Journal International, v. 157, no. 1, p. 381-398.

Wyatt, F. K., Bolton, H., Bralla, S., and Agnew, D. C., 1989, New designs of geodetic monuments for use with GPS.: Eos Transactions AGU, v. 70, p. 1054-1055.

9. *Figures and Tables*

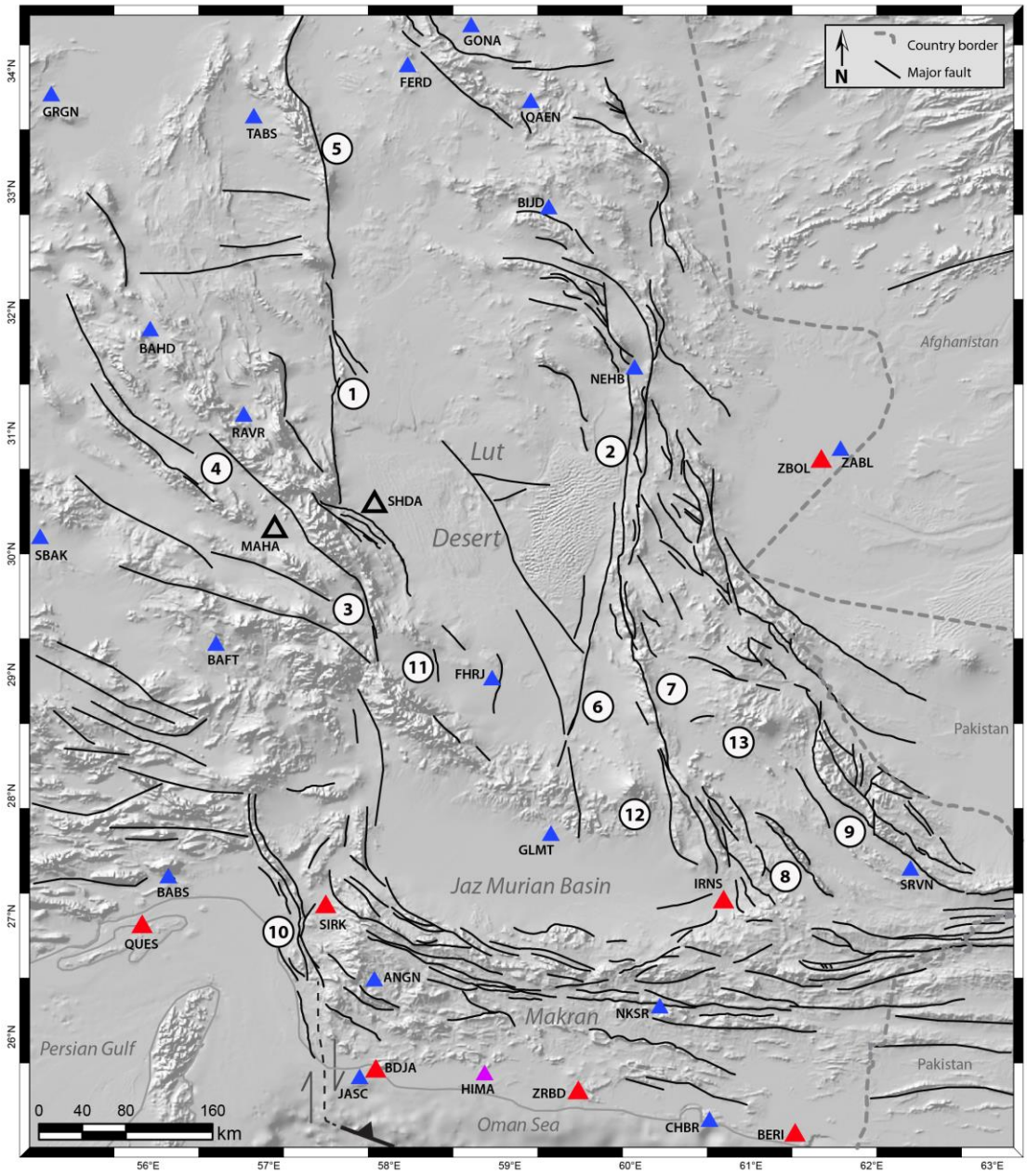

Fig. A.1: Map of the major fault systems and permanent geodetic stations in southeast Iran. Background SRTM 1 arc second. Blue triangle = National Cartographic Center of Iran permanent GPS station (NCC). Purple triangle = anticipated campaign site, this study. Red triangle = SIBA station, active. Open triangle = SIBA station under construction. Major faults: 1) Nayband Fault, 2) Sistan Suture Zone, 3) Gowk Fault, 4) Kuhbanan Fault, 5) Tabas Fault, 6) Kahurak Fault, 7) Daman Fault, 8) Birg Fault, 9) Saravan Fault, 10) Zendan-Minab-Palami Fault System, 11) Bam Fault.

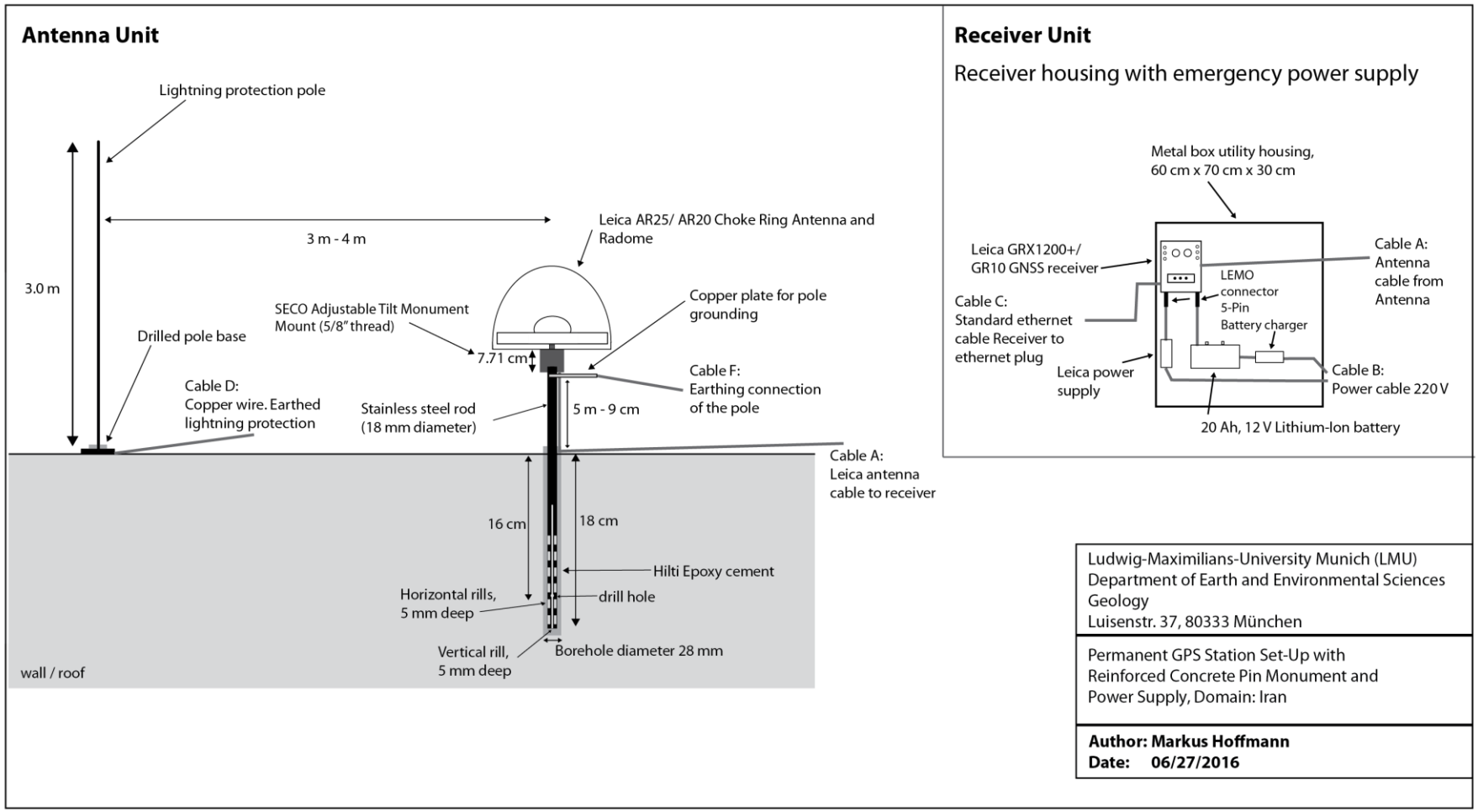

Fig. A.2: Blueprint of the SIMBAR site construction, except BDJA. Not drawn to scale, details are simplified.

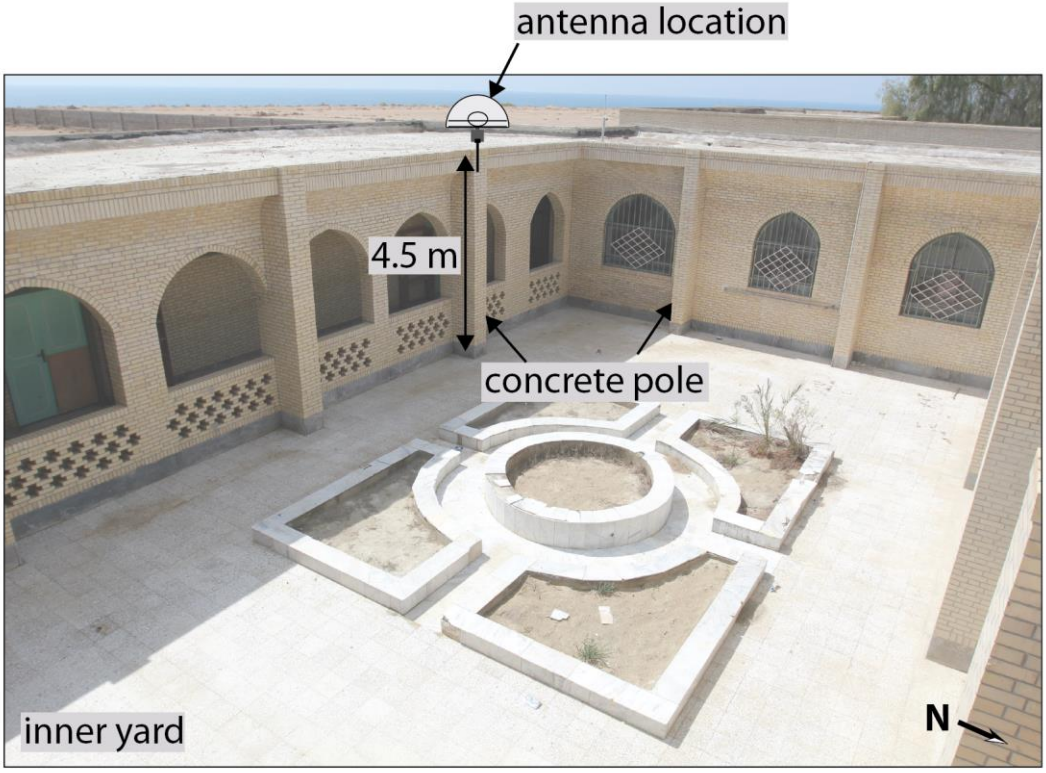

Fig. A.3: Photo from the site BERI with antenna position and building structure. The concrete pole construction with brick walls is almost identical at all school sites.

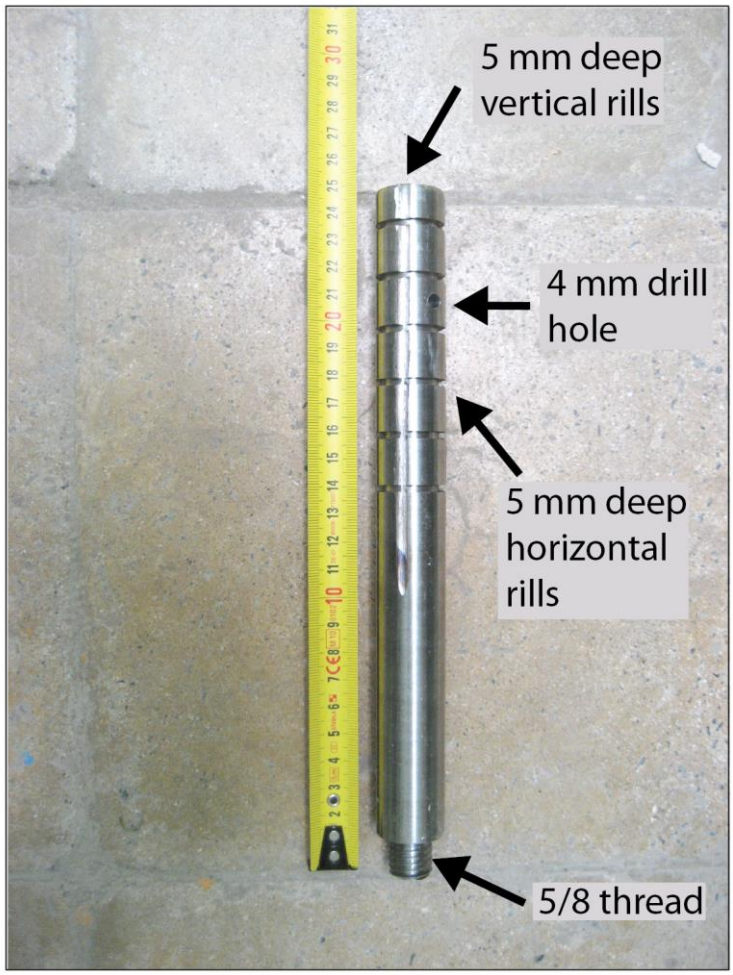

Fig. A.4: Photo of the stainless steel antenna pole. The rills are 5 mm deep in equal distance. The thread is a 5/8 inch standard for GPS equipment.

Table A-1: Remote sensing site selection criteria applied for 2015 recon-survey. Note, value 0 refers to “not true/ no data”. Due to differences in individual relevance, the criteria 1, 2, 4, 5, 8 and 9 have been weighted by a factor of 2, criteria 6 by a factor of 0.5, since these are less important in comparison. The percent value of ‘100’ represents the ideal location. For the detailed description of the individual stations see appendix of this chapter.

Criteria for site selection	Remote sensing	Recon survey	Importance	**DESC**	**DESC2**	**SIRI**	**BDJA**	**HIMA**	**ZRBD**	**BERI**	**BERI2**	**IRNS**	**ISWS**	**QUES**	**HMUN**
No steep unstable slope (< 20°)	X	**X**	high	2	2	2	2	0	2	2	2	2	2	2	2
No active faults (radius 20 km)	X	**X**	high	0	0	2	2	2	2	2	2	0	0	0	2
No joints	-	**X**	medium	0	0	0	0	0	1	1	1	1	1	0	1
Stable bedrock ground	X	X	high	0	0	0	0	0	0	0	0	0	0	0	0
Geodetically significant location	**X**	-	high	2	2	0	2	2	2	2	2	2	2	2	2
Close to facility, urban area	**X**	X	low	0,5	0,5	0,5	0,5	0	0,5	0,5	0,5	0,5	0,5	0,5	0,5
Good accessibility (roads)	**X**	X	medium	1	1	1	1	0	1	1	1	1	1	1	1
Skyview > 70 %	X	**X**	high	2	2	2	2	2	2	2	2	2	2	2	1
No high voltage power line wihtin 50 m	-	**X**	high	2	2	2	2	2	2	2	2	2	0	2	0
Match				**66%**	**66%**	**66%**	**79%**	**55%**	**86%**	**86%**	**86%**	**72%**	**59%**	**66%**	**66%**

10. Appendix

Site documentation

The four sites presented here have been installed until mid-2016. The additional sites, mentioned in text, have been installed after the field campaign documented here.

Site BDJA

Photo of the site BDJA looking southwest. Taken June 21, 2016.

Coordinates:

Antenna height on pole: 1.97 m

Distance from lightning pole: 17.50 m

Cell phone signal strength: 81 dB

Horizon profile:

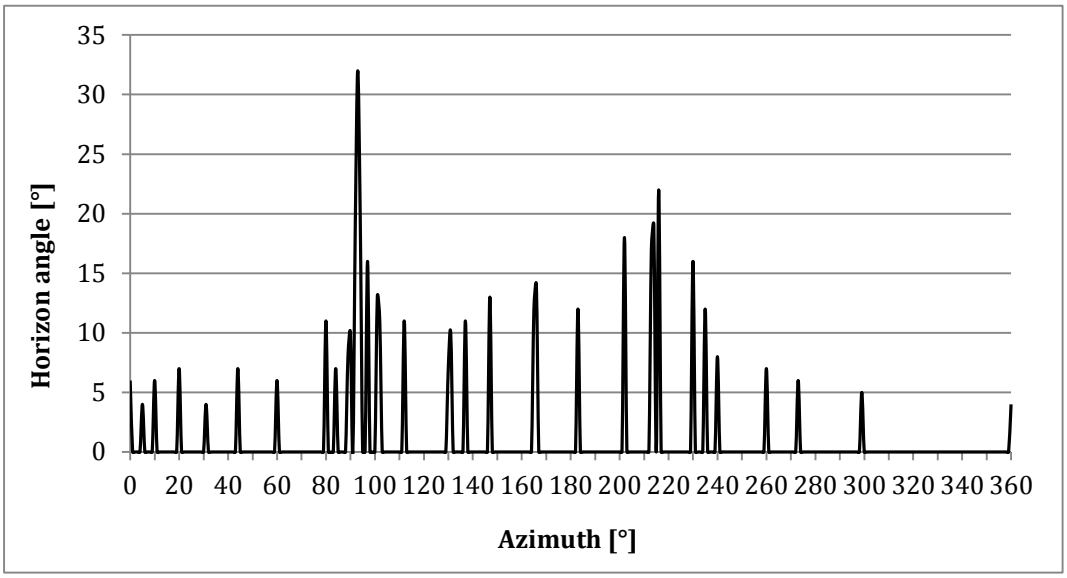

Horizon profile at BDJA. The signal cutoff is below 15° horizon angle.

Site ZRBD

Photo of the site ZRBD looking south. Taken June 20, 2016.

Coordinates:

Antenna height on pole: 16.71 cm

Distance from lightning pole: 2.93 m

Cell phone signal strength: 78 dB

Horizon profile:

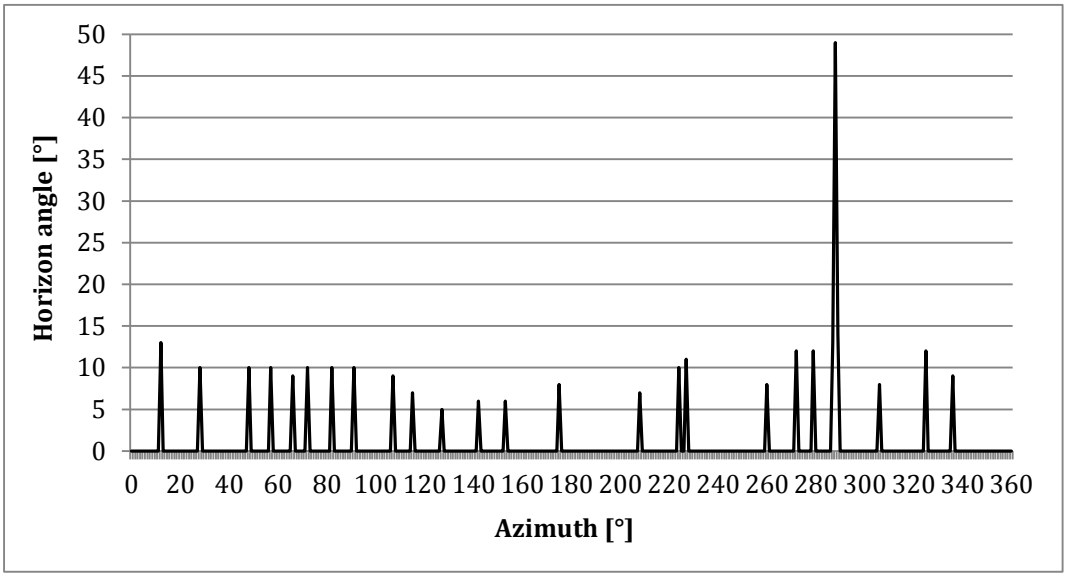

Horizon profile at ZRBD. The signal cutoff is below 15° horizon angle.

Site BERI

Photo of the site BERI looking southeast. Taken June 19, 2016.

Coordinates:

Antenna height on pole: 14.60 cm

Distance from lightning pole: 4.39 m

Cell phone signal strength: 90 dB

Horizon profile:

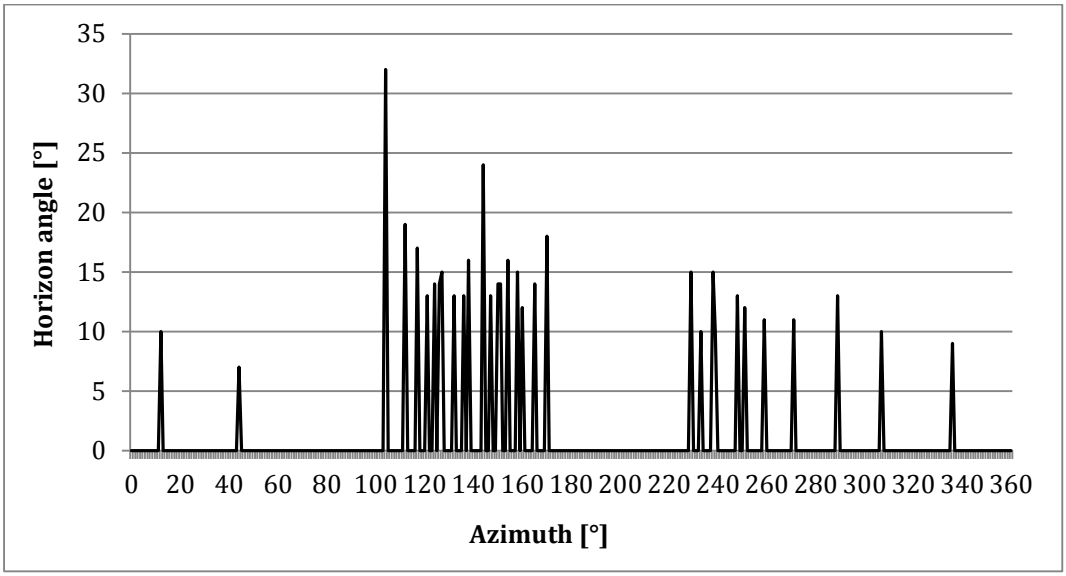

Fig. 6: Horizon profile at BERI. The signal cutoff is below 15° horizon angle.

Site IRNS

Photo of the site IRNS looking north. Taken June 19, 2016.

Coordinates:
Antenna height on pole: 12.71 cm
Distance from lightning pole: 8.83 m
Cell phone signal strength: 88 dB

Horizon profile:

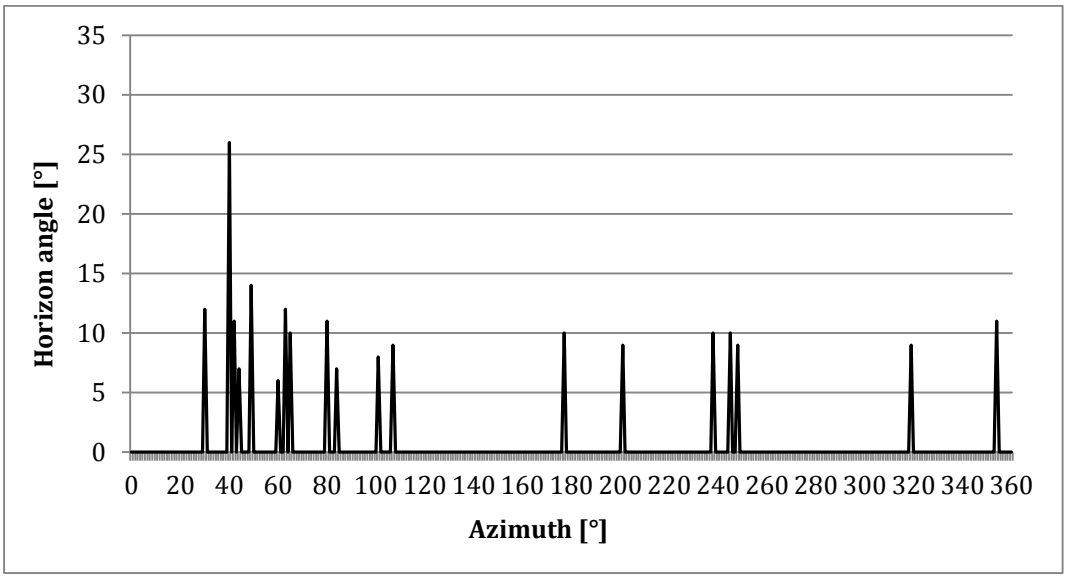

Horizon profile at IRNS. The signal cutoff is below 15° horizon angle.